

Hunting for the wavefront: investigation of somite boundary positioning in zebrafish

Présentée le 28 octobre 2022

Faculté des sciences de la vie
Unité provisoire pour le Prof. Oates
Programme doctoral en biotechnologie et génie biologique

pour l'obtention du grade de Docteur ès Sciences

par

Arianne BERCOWSKY RAMA

Acceptée sur proposition du jury

Prof. F. Naef, président du jury
Prof. A. C. Oates, directeur de thèse
Prof. A. Aulehla, rapporteur
Prof. P. Tomancak, rapporteur
Prof. D. Duboule, rapporteur

How you do anything is how you do everything.
— Martha Beck

To hope,

For an ideal world with no Covid, no racism, no climate change, no war.

Acknowledgments

I am very grateful to you, Andy, from the moment you let me into the lab, to today as we end this journey. You are one of the kindest, warmest, smartest people I know and a great person to talk to about research and life. Thank you for all the trust you put in me, the independence to pursue my own ideas and all the advice during these four years. I told you once and I will say it again, you are a very good boss.

Thank you Laurel, you are an important part of this thesis and these last few years. You were the toughest one who interviewed me when I wanted to join the lab. You have taught me everything I know about embryology, you have advised me every step of the way, you read all my reports and corrected my Spanglish and you always do it with a smile. Thank you for the best trips to Paris, for those cocktail evenings and above all, for being my good friend.

I would like to thank the members of my jury committee: Profesor Pavel Tomancak, Professor Alexander Aulehla and Professor Denis Duboule. Your work has been an inspiration during my PhD and I am honoured to have you read, evaluate and later discuss this thesis. I would also like to thank Professor Felix Naef for agreeing to preside this defense. You were present during my candidacy exam and now you will accompany me on my last step, so thank you.

Thank you Professor Alexandre Persat, you were a great mentor and I enjoyed our yearly meetings. I would also like to thank the Persat lab, our lab neighbours, for sharing reagents, snacks and beers.

I was lucky enough to join the Oaties, the best lab in the world if you ask me. I am really grateful to all my colleagues for making my life in and out of the lab so wonderful during these four years. That is why I want to take the time to thank them one by one:

Olivier, we were the only PhD students for a long time, you have always been there for me and I have learned a lot from you. Thank you for all the good times in the in situ bench, in the SPIM room, in the fish facility but also in Holy Cow, Sattelite (oh, I will miss the Lupulus beer!), summer dinners, and many more moments. I am happy that

you introduced us to Margaux, she is truly wonderful!

Chloé, you have been the best friend one could wish for. I have had so many good times and you have helped and taught me so much, in and out of the lab. You and Julien have become very important people in my life. You were a huge support in the Covid days. We've had so much fun in all those board game nights, beach volleyball and barbecues, escape games, weddings and trips. These four years have been wonderful and it has been largely thanks to you and Julien, so thank you.

Pablo, desde el momento en el que te conocí sabia que nos llevaríamos bien. Lo que no sabia era que te acabarías convirtiendo en un amigo tan especial. Gracias por siempre estar ahí para hacer *cafesitos*, barbacoas, comentar el football, mi compañero de happy hour y por enseñarme tanto de biología molecular! Espero no perdamos nunca el contacto ya que tanto Joan como yo te tenemos un gran aprecio, y a Anastasia también!

Guillaume, even if you are not an official member of the lab, you feel like one of us. Thanks for all the help, I know how to do the best in situs and cell transplants thanks to you. You have been a great friend and beer partner at Holy Cow. I am going to miss watching Real Madrid win with you. Oh, and see PSG loose.

Sundar, Pryam and the new member, **Arshika**, thank you for always being so kind, for the great brunches and summer hikes. I wish you all the best in your new adventure in India, we will come to visit you. Thank you Sundar for your constant feedback, you will be a great supervisor.

Ece, you are my busiest friend, but still an amazing friend. Thank you for always being so nice with me, always with a smile on your face. I wish you all the best in your last year of your PhD and hope to see you more after you are done.

Virginie, you have been my *cafesito* partner for four years, no matter if we are in the cafeteria or in the stinky room, I always enjoy our morning talks. Thank you for all your help and for being my morning friend in the lab.

Jose, Gala, Andrea y Cristina, gracias por ser tan maravillosos y tan agradables con nosotros. Nos encantó tenerlos en la boda y nos encanta cuando nos visitan y hacemos galletas con Gala. Gracias Jose por toda la ayuda en el trabajo y por siempre estar tan pendiente de mí.

Cristina, me alegra mucho de que formes parte del lab, con quien sino puedo discutir los partidos de tenis. Seguro que el PhD te va genial y seguro que llegarás lejos.

Vania, you have been so helpful and always looking after me. You are like a mom to the lab.

Paula, llegaste hace poco pero que bien que te haya conocido. Has hecho que este último año en el lab sea aun mejor, gracias por estar siempre tan alegre y contagiarnos a todos.

Last but not least, I want to thank **Daniele**, for teaching me so much in so little time (like dechorionating unfertilised embryos) and **Rachna** for taking me in so kindly during my first year.

Almost all of my work was carried out using a Viventis light-sheet. The microscope is great, but the people behind it are even better - Andrea, Petr and Camille. Thank you for being really helpful all of these years and for always being there when I needed you. I look forward to seeing what new ideas you come up with next. Another big part of my work was in the fish facility. Thanks for all the help during these years with my fish but also for always making me feel at home when I go to see my fish. Special thanks to Florian.

Thank You Jean-Yves for allowing us to visit Paris and all your help with Mastodon. Thank you BIOP - Romain, Olivier, Nicolas and Arne - you have been truly helpful and I have learned a lot from you. Thank you also NEUBIAS, for allowing me to be part of the image analysis community, I enjoyed and learned a lot during the meetings. Thanks Nicolas Barrier, for all the support and help with all of our IT problems. Special thanks to Olaf, for always being there when we needed help with the HIVEs. It has been a pleasure to work with you, I have learned a lot.

I have met amazing people along the way with whom I've had the pleasure to work with. JiSoo Park, Pierre Osteil, Alexandre Mayran, Yinan Wan. I would also like to thank all of my students for letting me supervise their work for the summer and allowing me to learn so much from them: Charline, Quentin, Tim, Valeria and Clara. I also want to thank Daniel Sage and all the team of the image processing course - Pol, Yan, Kay, Alejandro. It has been an honour and a pleasure to teach this wonderful subject with you.

Quiero agradecer a Jordi García Ojalvo y Alfonso Martínez Arias, mis mentores y a quienes debo casi todo lo que s'e. Gracias por enseñarme tanto.

Esta tesis espero sea un reflejo de todo lo que me enseñaron, papa y mama. Ustedes me decían que las cosas o se hacen bien, o no se hacen. Este ha sido mi lema durante la carrera, el doctorado y mi día a día. Andresito, estoy muy orgullosa de ti, estoy segura de que serás muy exitoso en todo lo que hagas. Gracias a los tres por ser un apoyo incondicional, no lo habría logrado sin ustedes. Gracias por todo lo que hacen por mí.

Joan, esta tesis es tan mía como tuya. Has sido mi gran apoyo, mi compañero de discusiones (te podrías sacar otra tesis en Zebrafish), con la persona que quería celebrar los logros pero también que me consolara en los momentos difíciles. Esta es la tercera tesis que escribimos juntos y espero sea la última. Estoy muy emocionada por la nueva aventura que nos espera. Gracias por todo.

Lausanne, September 29, 2022

Arianne Bercowsky Rama

Abstract

Somitogenesis is the rhythmic and sequential formation of somites, which are tissue blocks that give rise to segmented adult body structures including the vertebrae and associated muscle. Somite formation is controlled by the segmentation clock, a population of genetic oscillators that are coordinated by an interplay of cell-intrinsic and -extrinsic spatiotemporal information. Disruption of the segmentation clock can lead to misplaced or defective somite boundaries, and consequently results in deformed adult structures (e.g., congenital scoliosis). Despite decades of research into how the segmentation clock pattern is established, and how it acts to position somite boundaries within the pre-segmental mesoderm (PSM), many open questions remain. The position where the somite boundary is set along the anteroposterior axis of the PSM has been named the “determination front”. Questions still remain as to the mechanism and location of the determination front, and what spatiotemporal information is instructive. Here I present three studies that tackle this question by advancing imaging and analysis tools such that questions that have persisted for decades can be directly addressed. My work contributed significantly to obtaining a better picture of how somite boundaries are precisely formed.

Keywords: Somitogenesis, cell-tracking, clock, microscopy, python, zebrafish.

Résumé

La somitogenèse est la formation rythmique et séquentielle des somites, qui sont des blocs de tissus donnant naissance à des structures adultes segmentées, notamment les vertèbres et les muscles associés. La formation des somites est contrôlée par l'horloge de la segmentation, une population d'oscillateurs génétiques qui sont coordonnés par une combinaison d'informations spatio-temporelles intrinsèques et extrinsèques aux cellules. La perturbation de l'horloge de la segmentation peut conduire à des délimitations de somites mal placées ou défectueuses, et par conséquent à des structures adultes déformées (par exemple, une scoliose congénitale). Malgré des décennies de recherche sur la façon dont l'horloge de la segmentation est établie, et comment elle agit pour positionner les délimitations des somites dans le mésoderme pré-somitique (PSM), de nombreuses questions restent ouvertes. La position où la delimitation des somites est fixée le long de l'axe antéro-postérieur du PSM a été appelée "front de détermination". De nombreuses questions subsistent quant au mécanisme et à la localisation du front de détermination, et quant à l'identité des informations spatio-temporelles qui sont instructives. Je présente ici trois études qui s'attaquent à cette question en faisant progresser les outils d'imagerie et d'analyse afin de pouvoir répondre aux questions qui persistent depuis des décennies. Mes travaux ont contribué de manière significative à obtenir une meilleure compréhension de la manière dont les délimitations des somites sont précisément formées.

Mots-clés : Somitogenèse, suivi des cellules, horloge, microscopie, python, poisson zèbre.

Contents

Acknowledgments	1
Abstract (English/Français)	4
Introduction	8
0.1 Chronicles of embryo imaging	10
0.1.1 Whole mounts and scanning electron microscopy	10
0.1.2 The arrival of GFP	11
0.1.3 Live imaging of embryo development	12
0.1.4 Imaging with cellular resolution	13
0.1.5 Image and data analysis of big data	14
0.2 Zebrafish embryo somitogenesis	15
0.2.1 Zebrafish as our model organism	16
0.2.2 Nomenclature during somitogenesis	16
0.3 Precision and accuracy in pattern formation	16
0.4 Somitogenesis in the late 20th century	19
0.4.1 Clock and wavefront model	19
0.4.2 First evidence of positional determination	21
0.4.3 Segmentation genes	22
0.5 Molecular nature of the wavefront	26
0.5.1 Opposing morphogen gradients	26
0.5.2 Determination front	30
0.5.3 Positional information in somite boundary formation	31
0.6 Dynamics of the segmentation clock	33
0.6.1 Clock core circuit	33
0.6.2 Live reporters of the segmentation clock	35
0.6.3 <i>In vitro</i> dynamics of the segmentation clock	36
0.7 The arrest of the segmentation program	37
0.7.1 Role of T-box transcription factors	37
0.7.2 The Ripply family	38
0.8 Research questions	39

1	Image analysis pipeline and Paleontologist	42
2	Hunting for the determination front	82
2.1	FGF signalling gradient modifies the accuracy but not the precision of somite boundary formation	84
2.1.1	Effect on somite length during SU5402 inhibition	84
2.1.2	dpERK spatial profile during longer somite formation	89
2.2	Changes in the clock and maturation during FGF signalling perturbations	93
2.2.1	The temporal dynamics of the clock gene <i>her1</i> are not affected in FGF perturbations	93
2.2.2	Elongation is affected in addition to maturation when FGF is highly reduced	96
2.3	S-IV does not have a constant position on the dpERK curve throughout segmentation	98
3	Cell autonomous generation of the wave pattern	103
4	Clock, wavefront and timer model	160
4.1	<i>tbx6</i> and <i>rippy1/2</i> are good molecular candidates for a timer mechanism	161
4.2	Can <i>Tbx6</i> be influenced by FGF in the embryo?	162
4.3	<i>Tbx6</i> modulates the maximal expression of the clock gene <i>her1</i> in a relative dosage form	164
4.4	How is the timer information translated into somite boundary formation?	168
	Outlook	179
	Materials and Methods	180
5.1	Antibody Staining	180
5.1.1	Reagents used	180
5.2	Zeiss Movies	180
5.2.1	Acquisition	180
5.2.2	Analysis	181
5.3	Image Analysis	182
5.3.1	SPIM Movies	182
5.4	Transgenic lines	184
	Bibliography	186

Introduction

Observing embryonic development, one can appreciate life in its full form; a single cell gives rise to the mechanisms, pathways and material necessary to make a fully patterned multi-cellular embryo. Due to the obvious complexity spanning genetic to tissue scales, Developmental Biology as a field has had to evolve hand in hand with experimental techniques, such as the microscopy and computational tools that I developed in my thesis. Here I present work directly addressing long-standing questions about how the vertebrate body plan is precisely segmented. Segmentation is controlled by a molecular oscillator in presomitic mesoderm cells called the segmentation clock. Individual cells turn on and off gene expression in a synchronised manner resulting in a wave of expression at the tissue level. This clock rhythmicity is then translated into spatial periodicity by a wavefront controlled by a timing gradient to position the somite boundaries. Although this oscillating system is rapid and highly dynamic, the use of live imaging with cellular resolution allows us to understand how the patterns emerge. Visualising the spatiotemporal dynamics of the cells, combined with gene expression, allows us to better understand how segments are formed. Specifically, I want to explore how spatial information is provided to the cells to form a somite boundary in the right place and time. To set my work in context, this introduction will take you dear reader on a journey through time that links the evolution of research into segmentation with the development of experimental methods, imaging hardware and data analysis tools (Figure 1). Hopefully, this perspective will help you appreciate the advances made over the years in the face of many constraints. In later chapters, I describe how I overcame present day limitations by creating an imaging pipeline to capture long-term time-lapse movies and developing novel analysis tools to describe the captured spatiotemporal dynamics at cellular resolution.

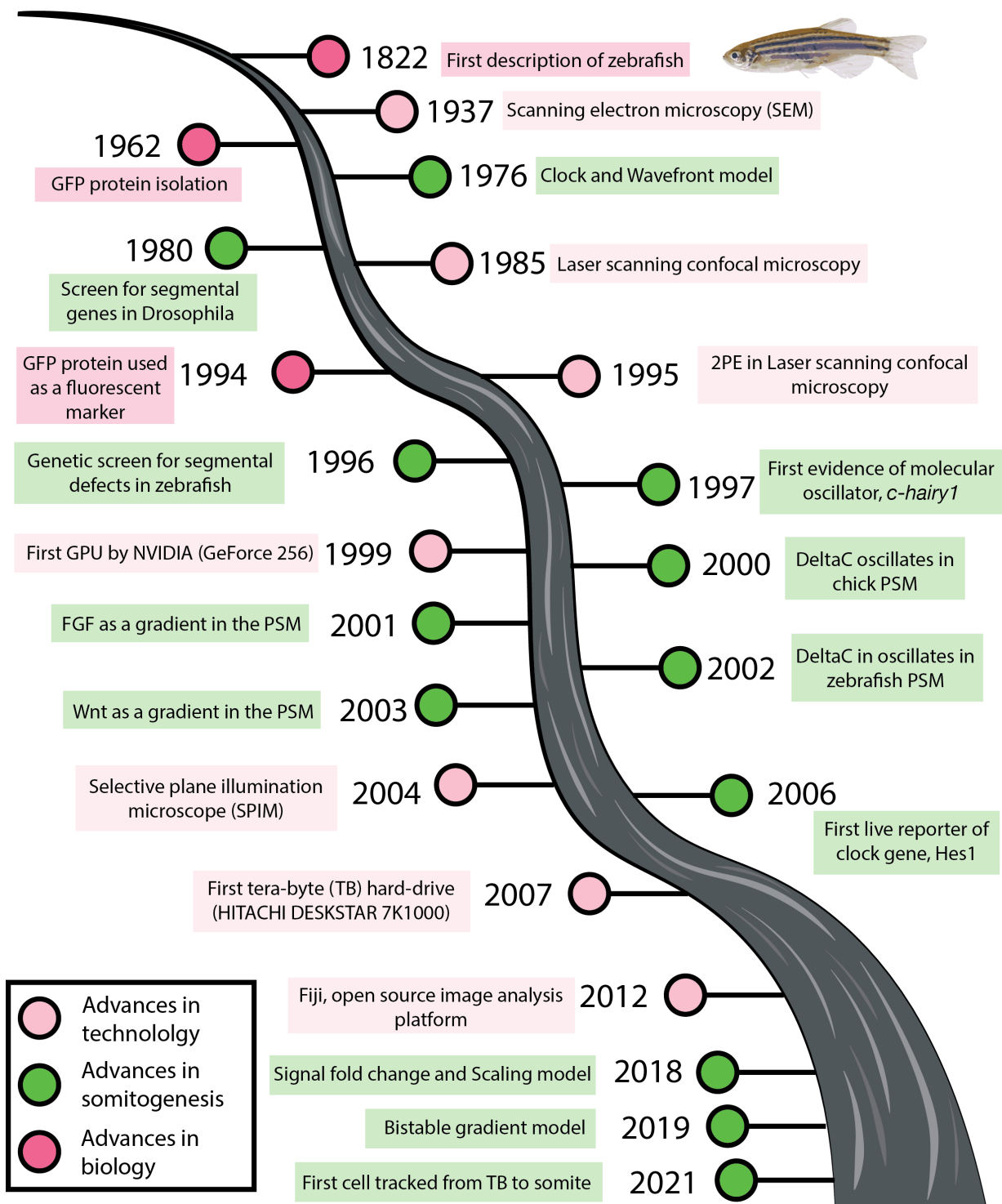


Figure 1: **Timeline cascade.** Important events that have shaped the somitogenesis field and which have lead to our understanding of how somites form nowadays. The cascade represents how it started as a narrow field then evolved in combination with new technologies and techniques.

0.1 Chronicles of embryo imaging

One of the goals in Developmental Biology is to understand cellular behaviours as well as the molecular mechanisms underlying the complex morphogenetic process of shaping a multicellular organism such as the embryo (Nowotschin and Hadjantonakis, 2014). *In vivo* imaging with good spatiotemporal resolution is crucial for understanding cell dynamics during different developmental processes such as segmentation. Intrinsic cell behaviour is not only determined by gene expression, but also by intercellular interactions between cells. This section summarises how imaging of developing embryos has progressed from the second half of the 20th century to the present day. We place special emphasis on the main findings and contributions to understanding segmentation.

Microscopy techniques and analysis tools have evolved mainly during the last two decades, leading to new discoveries in the field of developmental biology, but also to new challenges. From the use of an analog camera to image embryonic tissue to the *in toto* cell tracking of an entire developing embryo, this section covers the evolution of the field up to the current state of the art.

0.1.1 Whole mounts and scanning electron microscopy

In the second half of the 20th century, most studies of embryonic development visualised dead embryos at single timepoints to reveal general morphological characteristics. The dynamics and sequence of events were deduced by analysing multiple sequentially staged embryos.

The two main imaging techniques during this period were whole-tissue photo-negatives and scanning electron microscopy. The former was performed by mounting a film camera directly over the eyepiece of the microscope, with the camera objective focused at infinity (Mollring, 1965). The tissue of interest was placed on a microscope slide with a dark slide behind it for contrast. Finally, the photo-negatives were captured. This practice has evolved over time with the use of genetic stains and improved microscopy techniques, but is still commonly used in laboratories. The latter, scanning electron microscopy, was created in 1937 by a German researcher and applied physicist, Manfred von Ardenne. This microscopy technique allows high resolution by scanning the surface with a focused electron beam. These imaging techniques provided insight into tissue structure and some obvious phenotypes (which could not be related to genotype due to the lack of techniques available at the time). These static images provide excellent spatial resolution, but are not optimal for capturing changes in rapid cyclic gene expression,

such as the segmentation clock.

0.1.2 The arrival of GFP

In the 60's, Osamu Shimomura first isolated green fluorescent protein (GFP) from the jellyfish *Aequorea Victoria* (Shimomura, F. H. Johnson, and Saiga, 1962). However, it was not until three decades later when Chalfie et al., 1994 showed that GFP could be expressed and fluoresce outside the jellyfish. They used bacteria and *c-elegans* to show GFP expression. They incorporated GFP into the promoter for a gene encoding β -tubulin and showed that it could serve as a marker for expression levels. GFP attracted attention because of its stability over a wide pH and temperature range and also because it does not need a cofactor to fluoresce (Bokman and Ward, 1981). In 2008, Osamu Shimomura, Martin Chalfie and Roger Tsien received the Nobel prize in Chemistry for the discovery and development of GFP. This major accomplishment was followed by the discovery of spectrally different fluorescent proteins that allowed multi-channel fluorescence imaging. This opened a new way to study the interactions between different fluorescently labeled proteins (Matz et al., 1999; Shaner et al., 2004).

Early work with fluorescent proteins expressed GFP on the same promoter as another gene to monitor expression levels. However, this widespread expression of native fluorescent proteins did not provide the desired cellular resolution for imaging or the dynamics and interactions of the proteins of interest. A big breakthrough was the optimisation of a method to fuse the genes of a protein of interest with a fluorescent protein and express this in a cell — thus leaving the cell relatively unperturbed. This was first demonstrated by the fusion of GFP fusion to *bicoid* (*bdc*), a transcription factor in *Drosophila* by Wang and Hazelrigg, 1994. The fusion of GFP with a protein of interest made it possible to visualise their location, movement, turnover and the time passed from protein synthesis (Chudakov et al., 2010). A common use of protein fusions are histone fusions that mark the cell nucleus. The ability to observe individual cells and follow their dynamics over time is very promising, as will be shown in this thesis.

These advances in genetics pushed the field towards the use of fluorescence imaging to record the dynamics of labelled proteins, DNA, mRNAs, etc. Fluorescent microscopy therefore became the imaging technique of choice used to visualise dynamics at the cellular level but also at the tissue level. All these advances have led to the current situation in the field of imaging and have allowed us to better understand how embryonic patterns emerge.

0.1.3 Live imaging of embryo development

In conventional fluorescence microscopy, the entire sample is illuminated and the emitted light collected. Much of the light collected comes from parts of the sample that are out of focus. To overcome this problem, Marvin Minsky patented the first confocal microscope in 1961 (Wollman et al., 2015). In confocal microscopy, a pinhole is placed after the light source and before the detector. This way, all the sample is illuminated and only focused light is collected. As a result, the background of the fluorescent image is reduced and allows deeper imaging of the sample by optical sectioning. This technique was later improved by Wilke, 1985, who introduced laser scanning confocal microscopy, which achieved better fluorescent contrast. However, the depth of the sample image was still limited due to scattering of incident light from the sample creating a fluorescent background. This was particularly problematic when imaging developing embryos. One solution was to use fluorophores with longer wavelengths, but there are very few available for single photon excitation.

In traditional fluorescence microscopy, the excitation wavelength is shorter than the emission wavelength. However, Göppert, 1931 theorised that two photons with half the energy needed can excite the emission of one photon whose energy was the sum of the two in a very narrow window of absorption time (around 10^{-18} s) (Wollman et al., 2015). Therefore, the probability of two photon-excitation (2PE) occurring in a sample was very low due to the small coincidental time for the two photons. Denk, Piston, and W. W. Webb, 1995 used 2PE laser scanning microscopy to observe live cultured pig kidney cells. Since then, this has become an important tool to image molecular processes in live tissue. However, confocal microscopy has the disadvantage that it needs a lot of light to penetrate the tissue. This increases the chances of photo-bleaching, photo-toxicity and slows acquisition. Despite the drawbacks, it is still a great tool for optical sectioning and cellular resolution.

The combination of these new imaging tools and the ability to create transgenic lines with fluorescently labelled genes was a major game changer in the early 2000s (Goldman et al., 2001; Lawson and Weinstein, 2002). A new era in the study of embryonic developmental dynamics began. The field is constantly advancing towards better spatiotemporal resolution, larger fields of view and higher signal-to-noise ratios.

0.1.4 Imaging with cellular resolution

To overcome the disadvantages of confocal imaging of live embryos, [Voie, Burns, and Spelman, 1993](#) developed an imaging technique called orthogonal-plane fluorescence optical sectioning (OPFOS) to image the internal architecture of the the guinea-pig cochlea. In this technique, the sample is only illuminated through the plane that is in focus. This is achieved by illuminating with a flat excitation beam perpendicular to the imaging optics. Stacks of sample slices can be assembled to produce a 3D reconstruction of the imaged tissue. Ernst Stelzer then further developed this technique to develop what is called *selective plane illumination microscopy* (SPIM). They showed this technique by imaging GFP-labeled muscle tissue in transgenic Medaka (*Oryzias latipes*) embryos ([Huisken et al., 2004](#)). They also demonstrated SPIM by imaging 17 hours of *Drosophila* embryogenesis without damaging the sample.

SPIM only illuminates the section that is being imaged, therefore the sample is exposed to orders of magnitude lower light dose than in laser-scanning confocal microscopy. This allows faster imaging (due to the lower exposure times), less photobleaching of the fluorophores, and less photo-toxicity of the biological sample. This imaging technique marked the beginning of a new way of acquiring long time-lapse movies without damaging the sample. For example, it is now possible to image the first 24 hours of zebrafish development with enough spatiotemporal resolution to follow single nuclei ([Keller et al., 2008](#)). Moreover, it is also feasible to image different types of organoids ([Medeiros et al., 2021](#); [He et al., 2022](#)) in order to track and record cell lineages.

With the popularity of SPIM, variations on this technique also emerged to address specific questions. For instance, to overcome the challenge of light scattering and absorption when imaging opaque specimens, sample rotation during imaging has been employed ([Verveer et al., 2007](#); [Preibisch, Saalfeld, et al., 2010](#)). In this case, although some problems were solved (such as improved image quality due to reduced light scattering), two main challenges were created: (1) the output images suffered from misalignment and (2) the rotation was slower than the biological process that needed to be captured. To address these new challenges, [Krzic et al., 2012](#) developed a new optical configuration called multi-view SPIM (MuVi-SPIM), which allows for rapid imaging of large fluorescent organisms from multiple directions without the need to rotate the sample.

As demonstrated so far, the field has been moving towards longer movies with better spatiotemporal resolution, which is exactly what a SPIM provides. However, commercial solutions are not an option for many labs. For this reason, an open-source community was created to allow scientists without prior knowledge in building optical systems to

make their own SPIM. This open access platform is called OpenSpim (Pitrone et al., 2013) and contains the set of instructions and the software needed to get your imaging working. Moreover, startups, such as Viventis whose SPIM instrument is used in my work, have entered into the expanding light-sheet microscopy community.

0.1.5 Image and data analysis of big data

It is clear that microscopy techniques have come a long way and, with them, the massive datasets acquired in state-of-the-art set-ups are often beyond the scale of accessible visualisation or, worse, manipulation and analysis. Now the real question is, are computing technologies, storage and analysis systems up to the challenge? Currently, extra processing or quantification steps are required to extract meaningful features. Software such as Fiji (Schindelin et al., 2012), which is fully open source, has greatly transformed image processing. It is now possible to perform registration (Preibisch, Saalfeld, et al., 2010), deconvolution (Preibisch, Amat, et al., 2014), cell tracking (Tinevez et al., 2017; Wolff et al., 2018) and many more other types of analysis thanks to the great open-source imaging community that has been created over the past years. Together, these techniques and tools accelerate the study of developmental biology. As will be seen later in the chapters, we can now perform classical experiments, but study individual cell dynamics in the context of developing tissue.

The field has made incredible discoveries (such as those we will see in next sections) with the available imaging and genetic techniques. By fixing embryos to infer the dynamics of molecular processes, the first molecular evidence of the segmentation clock was found (Palmeirim et al., 1997). With advances in microscopy and fluorescence proteins, this oscillator was imaged over time revealing a tissue level wave pattern (Masamizu et al., 2006; Aulehla, Wiegraebe, et al., 2008; Soroldoni, Jörg, et al., 2014). Today, we have the possibility to image this pattern at cellular resolution, including the embryonic context, over long periods of time (Rohde et al., 2021). The aim is to understand the cellular behaviour and molecular mechanisms underlying the complex morphogenetic process of somite formation. Specifically, in my thesis I want to try to understand how somite boundaries are precisely formed, i.e. what are the mechanisms that drive positional information so that cells know where and when to place a somite boundary, since a defective or misplaced boundary leads to malformations. To do this, I use light-sheet microscopy, cell tracking and a novel analysis tool, all described in Chapter 1 .

Chapter 1 explains how we use light-sheet microscopy and the image analysis workflow we developed. Additionally, I introduce a novel tool I created in python – called Paleontologist - that aids the analysis of the data from single tracked cells that is output

by our pipeline. Hopefully, our cell tracking pipeline and Paleontologist will help others in the field to answer the question “*But, what are the cells doing?*”.

0.2 Zebrafish embryo somitogenesis

All vertebrate species have a segmented body that is established during somitogenesis in early embryonic development. Somitogenesis is the sequential formation of epithelialised blocks of tissue called somites, which are the precursors of segmented bone and muscle. Genetic defects that disrupt somitogenesis lead to abnormal skeletal morphologies, such as scoliosis in humans (Guo, Ikegawa, and Shukunami, 2018). My thesis addresses how are somite boundaries precisely formed. Specifically, when, where and how is positional information generated and used to form somite boundaries in the right place and at the right time?

Somites form rhythmically and sequentially starting at the anterior end of the pre-somitic mesoderm (PSM). The PSM is located bilaterally along the anteroposterior (AP) axis, starting posterior to the head and continuing to the tailbud (TB). As cells are incorporated into somites at the anteriormost end of the PSM, cells from the TB enter the posterior PSM while the embryo elongates. In most vertebrates, PSM length gradually grows in early embryogenesis, then shortens as somite formation in the anterior removes more cells than are added posteriorly (Gomez et al., 2008). The number of somites and somite length is typical and precise for each individual species. For instance, mice (*Mus musculus*) have 65 somites, chicken (*Gallus gallus*) have 55, zebrafish (*Danio rerio*) have 31, humans have 33 and corn snakes (*Pantherophis guttatus*) have 315. Moreover, the period of somite formation is also species dependent: 30 minutes in the zebrafish, 90 minutes in both the chick and Xenopus, 2 hours in the mouse embryos and 6-8 hours in humans (Gomez et al., 2008).

Although somite length varies between species, the rhythmicity that controls periodic somite formation is driven by the segmentation clock, a molecular oscillator that acts in PSM cells (Cooke and Zeeman, 1976) which has been studied in several model organisms (Oates, Morelli, and Ares, 2012; Hubaud and Pourquié, 2014). Individual cells synchronously switch gene expression on and off to give rise to a wave of expression at the tissue level. This oscillating system is rapid and highly dynamic, involving transcriptional oscillations (Soroldoni and Oates, 2011). Taken together, live imaging is crucial to understand the dynamics of the segmentation clock and how they are related to the precise formation of somite boundaries. As described in the next section, Zebrafish is a good system for studying somitogenesis.

0.2.1 Zebrafish as our model organism

We study segmentation using Zebrafish (*Danio rerio*), a major model system for vertebrate developmental studies (Figure 2 A). Although first described in 1822 by the Briton Francis Hamilton (Bradbury, 2004), zebrafish did not become widely used until the 1980's (Kimmel, 1989). Zebrafish are relatively easy to maintain compared to other vertebrate model systems, produce many embryos with each breeding, and are amenable to genetic manipulation. Importantly, the embryos are transparent and rapidly develop, allowing real-time visualisation of segmentation during the first day of development (Figure 2 B). In zebrafish, 31 pairs of somites form, starting at 10 hours post fertilisation (hpf), with a pair forming every 30 minutes at 24°C (Schröter, Herrgen, et al., 2008). The rate of segmentation is temperature dependent, with slower/faster segmentation at lower/higher temperatures (Figure 2 C). In addition to temperature sensitivity being an experimental tool, it adds to the practicality of the model system.

0.2.2 Nomenclature during somitogenesis

A unified nomenclature for embryonic segmentation between species was adopted decades ago (Pourquié and Tam, 2001; Ordahl and Le Douarin, 1992). Somites are numbered from cranial to caudal. Thus, when the first somite is formed, it would be staged as S1 or somite stage (ss) 1. However, to compare somites according to their position in relation to the most recently formed somite, Roman numerals are used: I, II, III, etc. Therefore, the first somite forming the posterior and anterior boundaries is called SI followed anteriorly by SII. In addition, the prospective somites are also numbered: S0 is the somite formed more posterior than SI and still lacking the posterior boundary. The PSM is then subdivided into S0, S-I, S-II, etc (Figure 2 D).

0.3 Precision and accuracy in pattern formation

During zebrafish somitogenesis, the periodicity of somite formation, the length of somites and the final number of segments have a variance (Schröter, Herrgen, et al., 2008; Schröter and Oates, 2010). This intrinsic variability was calculated comparing embryos under the same experimental conditions at the tissue level. Furthermore, when observing somite formation at the cellular level, it can be seen that the cells at the somite boundary form a straight row of cells perpendicular to the notochord, creating a sharp boundary (Figure 3 A). The consequences of having an abnormal number of segments,

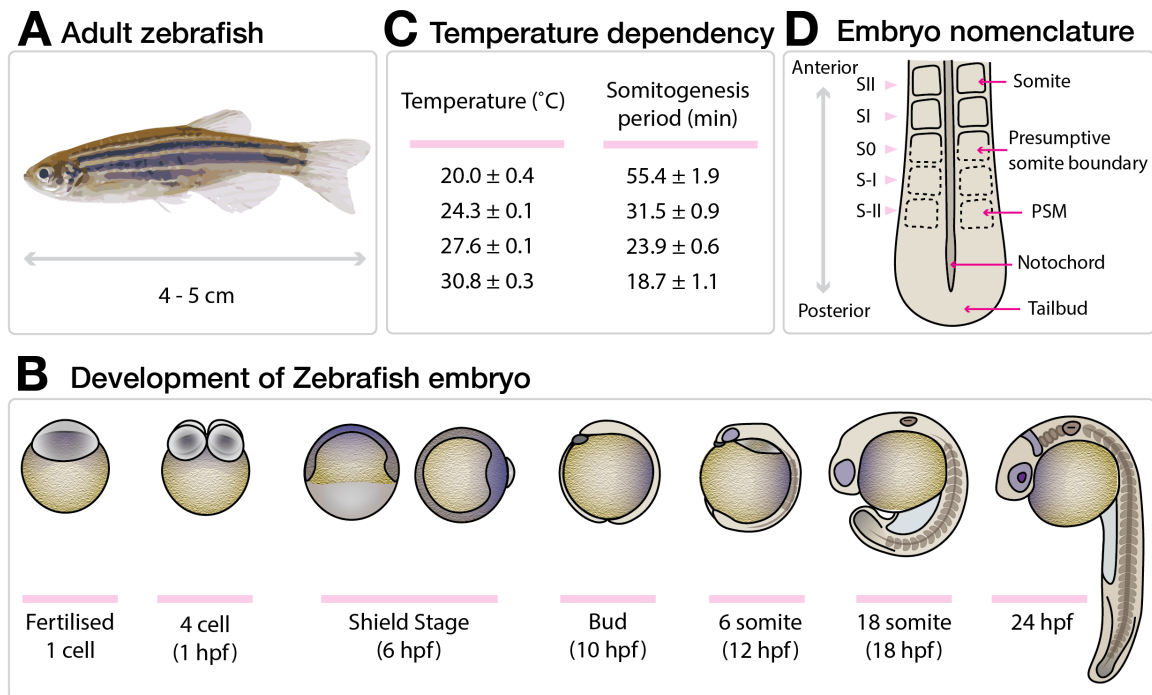


Figure 2: Zebrafish embryo development. **A.** Adult zebrafish can reach a size of 4-5 cm (ZF-HEALTH - Zebrafish Regulomics for Human Health). **B.** Development of the zebrafish embryo from 1 fertilised cell until the end of somitogenesis at 24 hours post-fertilisation (hpf), at 28.5°C. Illustrations inspired from [Kimmel et al., 1995](#). **C.** Period of somite formation is temperature dependent and it has been calculated by [Schröter, Herrgen, et al., 2008](#). **D.** Embryo nomenclature which is used in the somitogenesis field. Because somite formation is repetitive, at any given time-point in development, somites are named with roman numerals with reference to the most recently formed somite (SI, S0, S-I, ...); and the S0 corresponds to the somite which formed the anterior but not the posterior boundary. The ordinal somite number along the axis is demarcated with Arabic numerals (S1, S2, etc).

somite lengths or a skewed somite boundary can be developmental defects ([Schröter and Oates, 2010](#); [Liao, Jörg, and Oates, 2016](#); [Harima et al., 2013](#); [Herrgen et al., 2010](#); [Kim et al., 2011](#)). In humans, when somitogenesis goes awry, a group of vertebral disorders arise, including the generation of skeletal and muscular deformities ([Turnpenny et al., 2007](#); [Sparrow et al., 2006](#)). In my thesis work I focus on the mechanism responsible for precisely positioning a somite boundary such as in Figure 3 A. To study this, we first need to define what we mean by precision and accuracy.

Precision and accuracy are two measures of observational error, i.e. the difference between a measured value and its true value (or ground truth). Precision is a measure of the closeness or dispersion of observations. Accuracy is a measure of how close or far a given set of observations is from its true value. In other words, given a certain distribution

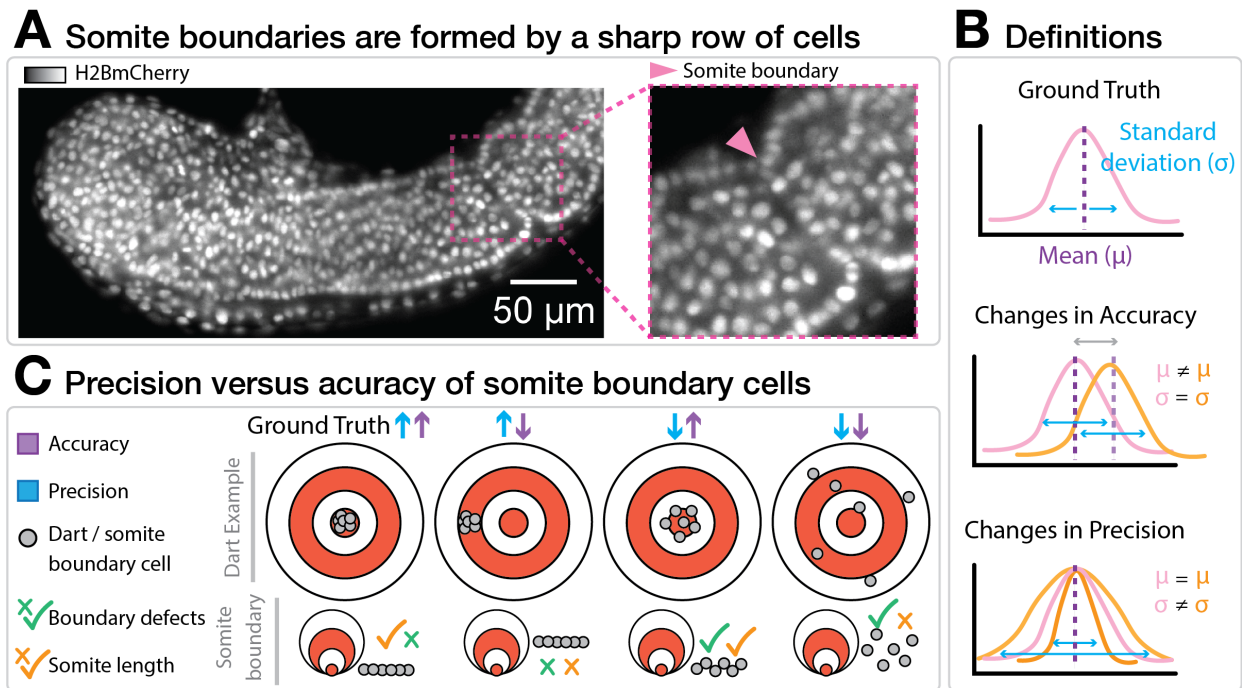


Figure 3: Precision and accuracy in somite boundary formation. **A.** Single slice of a light-sheet microscopy image of an embryo carrying H2B::mCherry at 15ss. The pink triangle points at a row of cells that forms the somite boundary. **B.** Illustrations of the definition of ground truth distribution and what happens when changes in accuracy and precision occur. **C.** Example of accuracy and precision with a dart case and translating this idea to somite boundary formation.

(assumed to be the true value), any variation in the mean is considered a change in accuracy, while variations in variance are changes in precision (Figure 3 B). The game of darts is an excellent way to illustrate accuracy and precision as shown in Figure 3 C. From left to right, in the best case, the hits are accurate and precise (the innermost red circle is the target). In the second case, the hits are precise (all in a given circle) but not accurate as they are far from the centre (the target). The third case is the opposite, the hits are distributed around the centre but in a more dispersed way, so it is accurate but less precise. Finally, the fourth case loses its precision and accuracy as the hits are spread all over the board and away from the centre. This analogy can be transferred to the formation of somite boundaries (Figure 3 C). We can imagine that the centre (the target) is the case where the row of cells forming the somite boundary is in the correct (accurate) position and forms a sharp (precise) boundary. Thus, this would result in the correct somite length and the absence of segmental defects, respectively. Following this line of thought, in chapters 2 and 4 we study extrinsic and intrinsic mechanisms that contribute to providing positional information to form a somite boundary correctly in space and time.

The question of precision and accuracy of positional information during developmental patterning has been previously investigated. [Houchmandzadeh, Wieschaus, and Leibler, 2002](#) studied how positional information in *Drosophila* is precise due to a noise-filtration mechanism. In this study, the intrinsic variability of the given patterns at the tissue level was studied. Later studies characterised the precision in reading morphogen gradients ([Gregor et al., 2007](#); [Morton de Lachapelle and Bergmann, 2010](#)). Inspired by these studies, later in Chapter 4 we recapitulate similar behaviour in one of the patterns that could lead to the basis of precision during somite boundary formation.

Quantification of precision and accuracy is relative to the resolution offered by the measuring instrument. Thanks to advances in imaging and analysis tools, such as those proposed in Chapter 1, we can define and characterise precision and accuracy at the cellular and tissue level. In Chapter 2 we will explore how extrinsic signals can affect positional information along the PSM by perturbing the accuracy of somite formation. In Chapter 3 we show that cells in culture can recapitulate dynamics observed in the embryo but with a lower level of precision. Finally, in Chapter 4 we show by tracking single cells that a molecular candidate for a time-keeping mechanism could drive to the basis of precision during somite boundary formation.

0.4 Somitogenesis in the late 20th century

0.4.1 Clock and wavefront model

In the mid 20th century, the lack of today's genetic and microscopy techniques hindered the collection of quantitative data. This limited research on tissue patterning to purely empirical data. One well-known hypothesis on tissue patterning from this period is the theoretical description provided by Alan Turing in *The chemical basis of morphogenesis* ([Turing, 1952](#)), in which he describes a mathematical model of the growing embryo. His model includes two or three morphogens (chemical substances) that react together and diffuse through a tissue to create a pattern. Turing's model was given new life in the 1970s in the context of Gierer and Meinhardt's theoretical description of pattern formation by morphogen activator-inhibitor systems ([Gierer and Meinhardt, 1972](#)).

Until the 1970s, these reaction-diffusion systems were considered the best explanation as to how spatially periodic pre-patterns – such as those that were hypothesised to prefigure somites – could be generated. However, in 1976 there was a shift in thought about the mechanism controlling rhythmic and sequential segmentation when Jonathan

Cooke, a biologist, and Christopher Zeeman, a mathematician, published *The clock and wavefront model* (Cooke and Zeeman, 1976). Their model rejected the idea of a repeating pre-pattern of the Turing class. Instead, they provided a conceptual description that to this day dominates the field and spawns many experimentally testable hypotheses.

Cooke and Zeeman, 1976 proposed a theory to explain the observed degree of constancy for the number of somites in individuals of a given species. Although they do not explicitly mention the words precision and accuracy, their description of the mechanisms of how somites are formed connotes these measures. They postulated that cells in the PSM behave as a clock, which they defined as a population of smooth intracellular oscillators that drive the periodicity of somite formation (Figure 4). In the clock and wavefront model, the position of a somite boundary is precisely and accurately positioned when a posteriorly moving wavefront of cellular change (e.g. maturation) coincides with a particular oscillatory phase. Clock periodicity thus sets the rhythm of boundary formation by modulating the effect of the wavefront as it progresses, and the wavefront sets the position of the boundary. The oscillators in the clock were imagined to be phase entrained such that neighbouring cells are determined by the wavefront to be boundary cells at the same time. Although not specified in the manuscript, the fact that neighbour cells become a boundary at the same time suggests a high level of precision (low variability between neighbours) and accuracy (all boundary cells are determined at the correct time).

In the clock and wavefront model, a rate or timing gradient across the PSM was proposed to control the wavefront. The local value of the gradient could be perceived by the cells to determine when to differentiate into a somite. In the model, perturbations in the gradient profile resulted in misplaced somite boundaries and abnormal somite length. Furthermore, this gradient was assumed to be involved in controlling the wavelength, which in turn was supposed to determine the precise number of somites. These gradients controlling the wavefront suggest a global modulation of the positioning of the somite boundaries, i.e. accuracy. The lack of molecular evidence for the wavefront made it impossible, from the description by Cooke and Zeeman, 1976, to distinguish between an intrinsic and/or extrinsic mechanism underlying this maturation process.

As I will discuss in following sections, some of the ideas from the clock and wavefront model have been reinforced by later experimental finding and this model still looms large in the field.

Clock and wavefront model

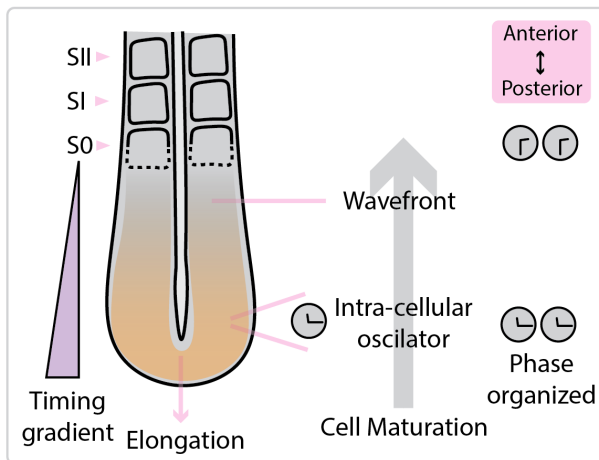


Figure 4: **Clock and wavefront model in vertebrate segmentation.** The Clock is comprised by molecular oscillators in the PSM (orange). The Wavefront is a posteriorly moving front of cell maturation controlled by a timing gradient (purple). The oscillators are phase organised, e.g., when the wavefront passes, they are determined to be boundary cells at the same time. The caudal tissue elongates as new segments form in the anterior.

0.4.2 First evidence of positional determination

"...cells enter a phase of rapid alteration in locomotory and/or adhesive properties at successively later times according to anterior-posterior body position." Page 455, [Cooke and Zeeman, 1976](#).

Segmental determination occurs in the posterior PSM

Active research into the mechanisms underlying vertebrate segmentation started in the second half of the 20th century, and was mostly carried out in chicken and amphibian embryos ([Pourquié, 2022](#)). The field was greatly influenced by the clock and wavefront model ([Cooke and Zeeman, 1976](#)). One particular prediction of the model was that at some point along the AP axis, unsegmented PSM cells change their locomotor-adhesive behaviour to differentiate into a somite.

This idea was reinforced by [Elsdale, Pearson, and Whitehead, 1976](#), who performed heat shock experiments in *Xenopus* during somitogenesis and observed that there was a substantial delay between the heat shock and the appearance of segment abnormalities. This delay suggested that instructions to become a somite are provided to the cells hours before somite formation. Tantalisingly, they proposed that the AP location where segments are first determined may be linked back to where the PSM cells in the first abnormal somite were located at the time of the heat shock. [Roger J Keynes and Claudio D Stern, 1984](#) further tried to address this question about the location of segmental determination. Their experiments included the inversion of fragments of the PSM along the anteroposterior axis. When inverted, the PSM fragments retained

their original schedule of development, showing that segmentation has a high degree of tissue autonomy.

Combined, this foundational experimental embryology was consistent with segmental determination occurring prior to morphological boundary formation.

0.4.3 Segmentation genes

"It is then proposed that all the cells are also coupled oscillators with respect to an unknown "clock" or limit cycle in the embryo, periodically modulating the effect of the wavefront as the latter progresses." Page 460, [Cooke and Zeeman, 1976](#).

During the 1980s, traditional genetics, experimental embryology and new molecular techniques were combined to piece together a picture of developmental mechanisms in the fruit-fly (*Drosophila melanogaster*) ([Peter Anthony Lawrence, 1992](#)). Tools and techniques had advanced at such a fast rate that Peter Lawrence mentioned in his book (The making of a fly), that *"the molecular analysis of new genes is being reported at the rate of one a week and rising"*. Mutations found in the large-scale systematic mutant screen in *Drosophila* by [Nüsslein-Volhard and Wieschaus, 1980](#) made it possible to identify loci required for segmental patterning. One of the loss-of-function phenotypes discovered was the deletion of alternating segments. Mutants in this category were named the pair-rule mutants. Molecular and biochemical studies of the pair-rule mutants helped to explain how segments are generated along the anteroposterior axis during *Drosophila* embryogenesis. For instance, pair-rule genes, are initially expressed in alternating segments, with some being expressed in odd segments, and some in even (Figure 5 A). Importantly, descriptions of the mechanisms regulating segmentation in *Drosophila* then served as a reference to understand segmentation in other insects, and even in vertebrates.

Hairy

"In the model, the smooth intracellular oscillator itself interacts with the possibility of the rapid primary change or its transmission within cells, thereby gating rhythmically the slow progress of the wavefront." Page 455, [Cooke and Zeeman, 1976](#).

Molecular characterisation of the fly segmentation pathway, using new advances in gene cloning, drove the identification of vertebrate homologs. Hand in hand, technical improvements allowed images to be captured of whole-mounted tissue stained for spe-

cific gene expression. This technique, still used in labs today, is called *in situ hybridisation* (ISH). In an important step forward, [M. v. Muller, Weizsacker, and J. Campos-Ortega, 1996](#) used primers directed to conserved regions of the *Drosophila hairy* gene, a pair-rule gene encoding a bHLH protein, to clone zebrafish *her1*. They found its expression pattern in zebrafish embryos to be similar to the pair-rule stripes observed in *Drosophila* and *Tribolium*. Influenced by the known mechanisms of *Drosophila* segmentation, they interpreted the striped pattern of *her1* as static - with each stripe corresponding to a distinct segment - and proposed that *her1* operates similarly to pair-rule genes in zebrafish segmentation.

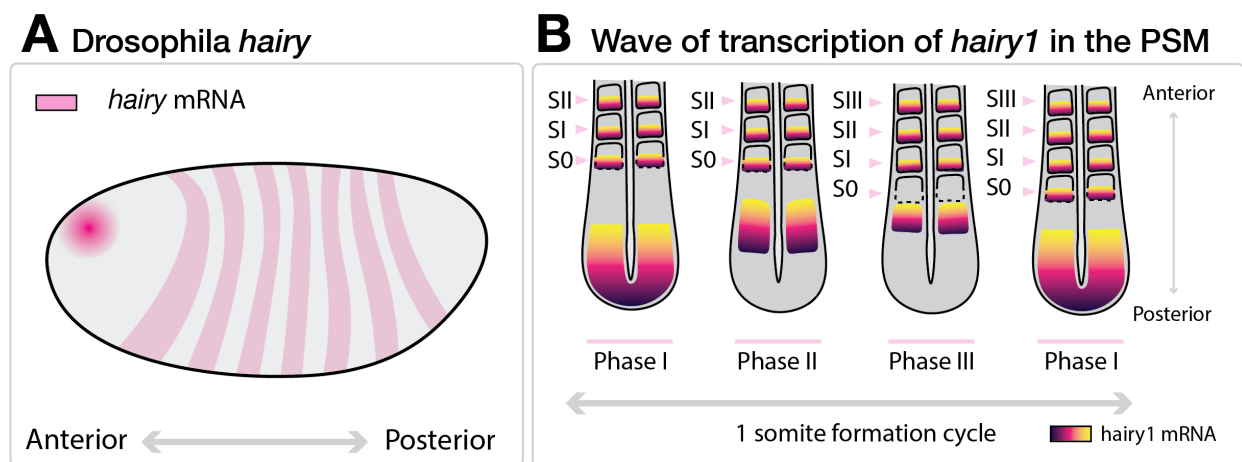


Figure 5: ***Drosophila hairy* versus chick *c-hairy1*** **A.** Cartoon showing the *Drosophila hairy* expression. Each gene expression stripe marks out one specific segment. **B.** Illustration of the results of the experiment conducted by [Palmeirim et al., 1997](#) to observe the dynamics of *c-hairy* in chick embryos. Each gene expression stripe is a moving wave that sweeps across multiple pre-segment domains in the posterior before coming to rest.

One year later, [Palmeirim et al., 1997](#) published a similar ISH analysis in the chick embryo with a *hairy* homologue, *c-hairy1*. They observed that within groups of tightly staged embryos, both *hairy1* and *hairy2* showed a range of expression patterns during segmentation that could be reconstructed into a dynamic sequence (Figure 5 B). Moreover, this expression pattern repeated with the formation of each somite. They concluded that rather than a static pattern of expression, *hairy1* and *hairy2* are expressed as periodic waves traveling along the PSM during the formation of each somite. [Palmeirim et al., 1997](#) thus provided the first evidence of the molecular oscillator, as predicted by the clock and wavefront model. Indeed, this indirect approach of inferring dynamics from fixed samples is still taken today, whenever live imaging is not possible, despite the limitations it places on quantitative analysis. This breakthrough in the field came about by increasing the temporal resolution of the acquired images. It demonstrates how sometimes, with the use of more precise analysis measured, the same experimental

result can be reinterpreted.

The discovery of oscillating segmentation genes in the chick ignited the hunt for others, leading to the discovery of *hairy*-related basic helix–loop–helix (bHLH) genes in mouse (*Hes1*, *Hes5*, *Hes7* and *Hey2*) and zebrafish (*her1* and *her7*) (Henry et al., 2002; Oates and Ho, 2002; Sawada, Fritz, et al., 2000). Lunatic Fringe (*Lfng*), a glycosyltransferase, was also identified as a cyclic gene, oscillating in phase with *hairy1* (Aulehla and R. L. Johnson, 1999; McGrew et al., 1998) in chick and mouse, but not in zebrafish. Disruption of these oscillating genes resulted in defective somite boundaries, with defects dependent on the particular gene and species. Deficient *her1* and *her7* zebrafish embryos, for example, displayed a high loss of boundary integrity and produced variably sized somites. The number of segments affected and the frequency and severity of boundary defects were higher than when each gene was affected individually (Oates and Ho, 2002).

Notch

"..an oscillator, shared by all the pre-somite cells, with respect to which they are an entrained and closely phase-organized population, because of intercellular communication." - lines 5-7, Page 467, Cooke and Zeeman, 1976

In parallel to the work on segmentation, researchers were also asking how is cell fate determined, i.e. how are diverse cell types generated from initially homogeneous precursor cells? One hypothesis was that developmental decisions depend on cell-cell communication. Research in *Drosophila* that focused on neurogenic progenitor cells, in which cell-cell interactions specifying cell fate, had identified a requirement for Notch (Jose A Campos-Ortega, 1988). Motivated by this work, Coffman, Harris, and Kintner, 1990 identified the first vertebrate Notch gene in *Xenopus*, Xotch. Comparing the structure and expression patterns of Xotch and Notch, they concluded that Xotch and *Drosophila* Notch may have equivalent functions and that mechanisms of cell specification may be conserved. However, as Notch was expressed in regions of cell differentiation in the nervous system, this study only explored the expression of Xotch in the retina because there were differentiated and pluripotent cells.

Reaume et al., 1992 was the first to report the expression pattern of a mammalian Notch homolog, Motch. Its expression in the PSM and the forming somites in mouse suggested a role in segmentation. However, it was not until a few years later (Conlon, Reaume, and Rossant, 1995) that Notch was shown to be required for somitogenesis when *Notch1* knock-out resulted in somite size and alignment defects. They concluded

that *Notch1* plays a role in coordinating somite formation, independent of cell-type specification and somite maturation.

In the 90s a series of genetic screens for segmentation defects in zebrafish embryo were published (Van Eeden et al., 1996a; Solnica-Krezel et al., 1996). The names of the mutants were then chosen according to the phenotype observed, e.g. *no tail (ntl)* has a non-differentiated notochord and reduced tail, and *spade tail (spt)* has too many cells in the tail due to an early convergence defect. Van Eeden et al., 1996b identified the mutations *after eight (aei)*, *deadly seven (des)* and *white tail (wit)*, all of which produce a series of normal somites in the anterior body followed by irregular somite boundary formation. Cloning of the genes responsible for these phenotypes showed that most of them were part of the Delta family (Delta -A, -B, -C and -D), acting as ligands for Notch (Holley, Geisler, and Nüsslein-Volhard, 2000; Smithers et al., 2000). Also that year, Jiang et al., 2000 performed the same assay as Palmeirim et al., 1997, allowing them to reveal a sequence of *DeltaC* expression corresponding to temporal oscillation in the PSM. Additionally, they showed that mutations in the zebrafish Notch pathway lead to salt and pepper expression of *DeltaC*. Consistent with these results and with the help of theoretical models, Özbudak and Lewis, 2008, Riedel-Kruse, C. Muller, and Oates, 2007 and Lewis, 2003 proposed that the essential function of Notch signalling in somite formation is to synchronise oscillations of neighbouring PSM cells. This was later confirmed using live imaging and a fluorescent reporter of the clock gene *her1* that allowed cell tracking and comparison of the oscillatory dynamics of neighbouring cells (Delaune et al., 2012). Similar in mouse, the role of Notch was proposed to be to synchronise the segmentation clock (Okubo et al., 2012). This statement was later confirmed and further studied using a live imaging and a fluorescent reporter of the clock gene *Hes7* (Yoshioka-Kobayashi et al., 2020).

Notch is known to be a cell-cell communication pathway (Venzin and Oates, 2020), so this idea of synchronisation through Notch signalling alludes to the control of local precision between neighbouring cells, the lack of which leads to salt-and-pepper patterns and segmental defects. This type of precision control is not studied in this thesis, however, it is important to understand its role in order to rule out its possible contribution to other types of precision and accuracy modulation.

What was known until the 2000s?

At the end of the 20th century, there was strong evidence supporting the following:

1. Positional information is being read in the posterior PSM that determines the

somite boundary position.

2. Segmentation mechanisms may not be conserved between invertebrate and vertebrates.
3. Vertebrate segmentation involves a molecular oscillator that drives the periodicity of somite formation.
4. The Notch pathway is required to synchronise the segmentation clock.

However, many questions remained (Dale and Pourquié, 2000):

1. What is the molecular nature of the wavefront / segment positioning?
2. What drives the segmentation clock?
3. What is the role of the segmentation clock during somitogenesis?
4. What regulates the arrest of the clock in the forming somite?

The rest of the introduction is organised along these questions, which will provide the necessary background for understanding Chapters 2, 3 and 4. A summary of what somitogenesis looked like in the early 2000s is shown in Figure 7 (spoiler alert), which gathers the information from the following sections.

0.5 Molecular nature of the wavefront

"There will thus be a rate gradient, or timing gradient along these columns, and we shall assume a fixed monotonic (not necessarily linear) relation between rate of an intracellular evolution or development process, and local p.i. value experienced by a cell at the time of setting that rate." Pages 464-465, Cooke and Zeeman, 1976.

0.5.1 Opposing morphogen gradients

A lot of progress had been made by the end of 20th century regarding the molecular dynamics behind the segmentation clock. However, besides the initial experiments from the 70's (Elsdale, Pearson, and Whitehead, 1976; Roger J Keynes and Claudio D Stern,

1984), little was known about what could be gating the spatial response of PSM cells to the clock signal to ensure the sequential production of somites. In other words, what could be the molecular identity of the wavefront postulated by [Cooke and Zeeman, 1976](#)? The formulation proposed in their study did not distinguish whether the time gradient was driven by an extrinsic and/or intrinsic mechanism. However, in the early 2000s there was evidence to support that signalling gradients (i.e. the extrinsic mechanism) influenced the spatial positioning of somite boundaries. These studies involved three molecules - Wnt, FGF and RA - that show graded signalling along the PSM.

Wnt and FGF are expressed at high levels in the posterior of the extending axis, where PSM precursors arise ([Dubrulle and Pourquié, 2004](#); [Aulehla, Wehrle, et al., 2003](#)). *fgf8* mRNA is then progressively degraded as PSM cells flow anteriorly, forming an mRNA gradient across the PSM ([Dubrulle, McGrew, and Pourquié, 2001](#); [Dubrulle and Pourquié, 2004](#)). Expression of *axin2*, a Wnt pathway target, was also found to be graded along the PSM, with higher levels in the TB ([Aulehla, Wehrle, et al., 2003](#)), suggesting a gradient of Wnt/ β -catenin signalling along the PSM. RA is synthesised in the differentiating PSM and somites as indicated by the expression of RA-synthesising enzyme (Raldh2) ([Swindell et al., 1999](#)), with the highest levels detected in the somites ([Maden et al., 1998](#); [Moreno and Kintner, 2004](#)). Together, these studies paint a picture of opposing gradients of signalling molecules that, as we will see next, provide positional information in the PSM.

According to the clock and wavefront model ([Cooke and Zeeman, 1976](#)), the gradient determines the positional information for each cell to go through the process of segmental differentiation. Although not mentioned in the study, this spatial gradient may be responsible for providing global precision and accuracy in the positioning of the somite boundary. To better understand the role of this gradient, in the following sections I explain the molecular candidates proposed to generate the wavefront acting as signalling gradients.

Fibroblast Growth Factor (FGF)

Members of the fibroblast growth factor (FGF) family of signalling molecules and their receptors had been shown to be capable of playing roles in mesoderm induction and patterning ([Kimelman and Maas, 1992](#)). Following this, [Yamaguchi, Conlon, and Rossant, 1992](#) in mice and [Sawada, Fritz, et al., 2000](#) in zebrafish, showed that Fgfr1 (Fgf receptor mediated signalling 1) was expressed in the PSM and the rostral half of somites. One of the downstream targets of activated receptor kinase (RTK), including Fgfrs, is doubly phosphorylated ERK (dpERK) ([Gotoh and Nishida, 1996](#)) (Figure 6 A). The expression

pattern of dpERK was found to closely resemble that of *fgf8* and at least of one of the Fgfrs, *Fgfr1*, in the PSM and forming somites (Sawada, Shinya, et al., 2001; Dubrulle, McGrew, and Pourquié, 2001). Taken together, dpERK is a good readout of FGF signalling in the TB and PSM.

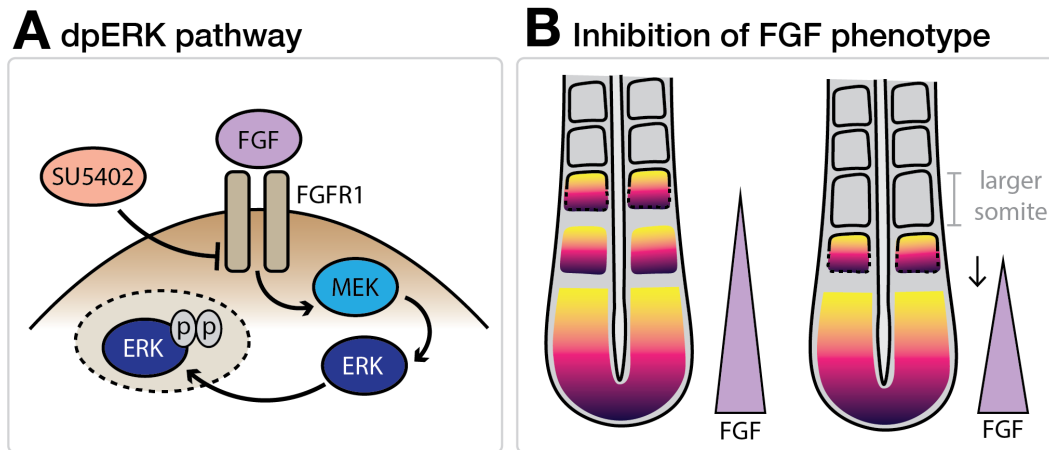


Figure 6: **SU5402 inhibition of the FGF signalling pathway results in longer somites.** **A.** dpERK signalling pathway. SU5402 acts by inhibiting the tyrosine kinase activity of FGFR. Thus, signal transmission by sequential phosphorylation of downstream kinases does not occur. When ERK is doubly phosphorylated (dpERK) it can translocate to the nucleus. **B.** A longer somite is formed due to SU5402 inhibition of the FGF signalling gradient.

Sawada, Shinya, et al., 2001 – using zebrafish embryos – showed that perturbation of the FGF/MAPK signalling pathway resulted in abnormal somite length (Figure 6 B). Treatment at the two-somite stage with SU5402 (kinase inhibitor specific to FGF receptor 1, Mohammadi et al., 1997) for 8 minutes produced a longer somite after a delay of four to five normal length somites, after which normal somite formation resumed. dpERK staining is rapidly and greatly reduced and within 3 hours, ERK activation is gradually recovered (shown using Western Blot in Sawada, Shinya, et al., 2001). When a longer somite was formed, *her1* cyclic expression, as assessed by in situ hybridisation, terminated prematurely in the PSM. Interestingly, posterior PSM expression patterns in the treated embryos suggested cyclic expression was present. Moreover, pre-patterning of segment polarity occurred as shown by *mesp* and *papc* expression. The authors concluded that the longer somite produced by SU5402 treatment arises from a transient posterior shift in boundary formation, owing to acceleration of maturation or wavefront progression in the PSM. They also performed the reverse experiment, in which an FGF8-soaked bead was transplanted into the embryo. In this case, the segment border was anteriorly displaced and shorter somites formed in the region anterior to the FGF bead.

Similarly, Dubrulle, McGrew, and Pourquié, 2001 - in the chick embryo - implanted

beads soaked in FGF8 which resulted in the formation of smaller somites. In both cases, the changes in size were caused by a reduction in the number of cells in the somite and not due to increased cell death or decreased cell division. Taking these studies together, we can conclude that FGF is involved in the positioning of somite boundaries and its role seems to be conserved among vertebrate species. Below, in Chapter 2, I will investigate the role of FGF during somite boundary positioning in more detail.

Wnt

Canonical Wnt signalling was already well known for its role in the formation and elongation of posterior body structures, including the PSM (Greco et al., 1996), making it a perfect candidate to play a role in segmentation. Similar to the studies performed with FGF, Aulehla, Wehrle, et al., 2003 perturbed the Wnt signalling pathway. They generated transgenic mouse embryos mis-expressing the Wnt inhibitor, *Axin2*, under the control of a PSM-specific promoter. This resulted in longer somites. To test the opposite effect, they implanted micro-carrier beads covered with cells (NIH3T3) expressing *Wnt3a* into the posterior PSM of chick embryos. This induced shorter somites and an anterior shift of segment boundaries. Experiments in zebrafish (Bajard et al., 2014) using a heat-shock *Dkk1* transgene to inhibit the Wnt/ β -catenin pathway also resulted in longer somites post-heat shock, while similar expression of *Wnt8* reduced somite length. In addition, there was a delay of four to five somites between the time when Wnt signalling was reduced and the time when the largest somite was formed. Together, these experiments show that Wnt signalling acts similarly to FGF, suggesting that it also has a role in somite boundary positioning.

Retinoic Acid (RA)

RA, a biologically active derivative of Vitamin A, is synthesised in the anterior PSM and somites as detected by expression of the RA-synthesising enzyme *Raldh2* (Swindell et al., 1999). Work by Corral et al., 2003 showed in chick that FGF and RA are mutually inhibitory, as FGF8-soaked beads repressed *Raldh2*. Furthermore, Vermot and Pourquié, 2005 also demonstrated in chick that blockade of RA with disulphiram resulted in smaller somites as a result of a gain of function of FGF shifting the determination front anteriorly. Overall, these studies suggest opposing gradients of FGF and RA. When Moreno and Kintner, 2004 treated *Xenopus* embryos with RA, 2 to 4 somites of double the cell number formed after a 4 hour delay. When they repressed RA signalling using a dominant-negative RA receptor, the result was severely disrupted somite boundaries. This indi-

cated, therefore, that an opposing RA gradient could also alter the positioning of somite boundaries in a manner opposite to FGF and Wnt.

Despite being performed across different species, these studies on FGF, WNT and RA supported the hypothesis that positional information to place the somite boundary is provided in the posterior PSM. Opposing gradients of signalling molecules (Wnt, Fgf, RA) looked key to play a role in PSM maturation and somite boundary positioning (Aulehla and Pourquié, 2010). However, there was a lack of consensus at this time (and still today) regarding the mechanism of somite boundary positioning and somite scaling. In Chapter 2 I focus on FGF to try to understand how this signalling gradient drives positional information which in turn lead to somite boundary formation in an accurate and precise way.

0.5.2 Determination front

Cells in the TB are thought to be maintained as undifferentiated by high levels of FGF signalling, then initiate their differentiation program only when an appropriate threshold of FGF activity has been reached in the anterior TB (Vasiliauskas and Claudio D Stern, 2001). Dubrulle and Pourquié, 2004 showed that *fgf8* mRNA is restricted to the growing tailbud and is progressively degraded in the newly formed tissue, thus creating an *fgf8* mRNA gradient as it decays. This “gradient by decay” was thought to account for the tight control between tissue differentiation and tissue elongation. Moreover, this was different to the mechanism in *Drosophila* by which molecular signalling gradients supply positional information during simultaneous subdivision of the body into fixed sized segments. Thus, the question raised at the time was *where is the positional information from the gradients being read?*

Dubrulle, McGrew, and Pourquié, 2001 performed anteroposterior (AP) inversions of somite-length regions of the PSM in chick embryos then examined after 3 to 24 hours of reincubation. To evaluate the effect on segmental organisation, they checked somite boundary formation and the expression of the Notch ligand *Delta1*, whose expression is restricted to the caudal somite half. Inversion of somite-length fragments of somite 0 or somite -I, resulted in a somite exhibiting boundaries properly positioned but with reversed polarity. Contrary to this result, inversions of somites -II to -IV resulted in ectopic boundaries and abnormal anteroposterior subdivision in the graft. Finally, inversion of somite-length fragments in the region from somite -V to somite -XII led to a normal segmentation pattern. The authors suggested that these results reveal that the posterior two-thirds of the PSM are undetermined with regard to segmentation, whereas the anterior regions is either fully determined or labile. Dubrulle and Pourquié,

2004 suggested that pre-somite -V could be the position at which the level of Fgf/MAPK activation drops below a threshold, rendering the cells receptive to maturation signals.

Together, these studies suggested that the somite boundaries are determined around somite -IV in the PSM. Notably this corresponded approximately to the zone of sensitivity to heat shock (Primmatt, C. Stern, and R. Keynes, 1988), and corresponds also to the time-delay after which FGF, Wnt and RA-induced segment-length changes are seen. "Because this position is not fixed, but regresses along the AP axis as somitogenesis proceeds, we term this PSM level the determination front" (Dubrulle, McGrew, and Pourquié, 2001).

0.5.3 Positional information in somite boundary formation

As mentioned above, the fact that somite size and number is so tightly regulated within species, suggests the existence of a mechanism controlling the precise and accurate positioning of the somite boundaries (Gomez et al., 2008). A long-lasting question in the field has thus been how cells integrate positional information within an elongating body axis. For decades, somite formation has been interpreted in the framework of the clock and wavefront model, in which the cellular oscillator sets the frequency of somite formation while the wavefront, encoded by a timing (or maturation) gradient, translates the temporal information into the spatial periodic pattern (Boareto, Tomka, and Iber, 2021; Oates, Morelli, and Ares, 2012). When Cooke and Zeeman, 1976 described the model, there was no molecular evidence for the clock or the wavefront. Thus, the timing gradient that controls maturation along the body axis may be driven by an extrinsic and/or intrinsic mechanism. However, in the early 2000s, a group of studies showing that signalling gradients (i.e. extrinsic mechanism) (Sawada, Shinya, et al., 2001; Dubrulle, McGrew, and Pourquié, 2001; Aulehla, Wehrle, et al., 2003; Moreno and Kintner, 2004) could shift the position of somite boundaries, diverted the attention from the idea of the intrinsic mechanism as a timing gradient for several years. Thus, most recent models explaining how cells read positional information include FGF signalling gradient. I describe these models here in some detail as I will evaluate them experimentally in Chapter 2.

Scaling Gradient

J. Cooke, 1975, showed decades ago in *Xenopus* how removing blastulae cells lead to the development to abnormally smaller embryos and somites but no change in the number

of somites formed. Similarly, and 43 years later, using both surgically size-reduced and normally developing zebrafish embryos, in combination with mathematical modelling and live imaging, [Ishimatsu et al., 2018](#) proposed the *clock and scaled gradient model*. In this scheme, the somite boundaries are set by a dynamically scaling signal gradient across the PSM. As expected, the sized-reduced embryos made the same number of somites but of reduced length. They also found that while the clock period, axis elongation speed and the wavelength of *her1* traveling waves all did not scale with the PSM length, the gradient of FGF activity (shown by dpERK) did scale. Their model thus predicts that in order to form a somite boundary (1) the clock needs to reach a certain value and (2) the gradient needs to exceed a certain threshold.

Thus, this type of linear phase gradient model suggests that accuracy in somite boundary positioning is controlled by reaching a certain threshold of the gradient. Furthermore, precision would be provided by the fact that all cells that have crossed that threshold are closely synchronised and pass through a certain clock phase to form a sharp somite boundary.

Bistable Gradient

[Akiyama et al., 2014](#) proposed that the anterior limit of dpERK at S-V is the first detectable sign of a future somite boundary. They observed that the *fgf8a* mRNA expression domain continuously moves posteriorward as would be expected of a regressing wavefront. However, dpERK was observed to regress in a clock-dependent step-wise manner. They proposed that the anterior limit of dpERK corresponds to the *signal integration spot* between the clock and the wavefront. This study was later supported by time-lapse imaging using a FRET sensor for dpERK dynamics ([Sari et al., 2018](#); [Wong et al., 2018](#)). Both studies showed that without proper clock function, the stepwise regression of dpERK activity occurs at an irregular timing.

Inspired by these results, [Naoki et al., 2019](#) proposed a mathematical model for ERK-mediated somitogenesis. In this model, bistable ERK activity is regulated by an FGF gradient, cell-cell communication, and the segmentation clock, subject to intrinsic noise. Contrary to the continuous phase mapping idea of the clock and wavefront model ([Cooke and Zeeman, 1976](#)), they proposed a saltatory mechanism for the positioning of the somite boundary. Similar to [Ishimatsu et al., 2018](#), the signalling gradient of FGF controls the accuracy with which the somite boundaries are positioned. But in this model, cells at a certain dpERK threshold (called the intermediate state) suppress the ERK activity of their neighbours. Thus, cell-cell interaction plays an important role. Therefore, in this case it is the gradient that controls not only the accuracy but also

the precision of somite boundary positioning. The clock in this model also plays an important role, but it is more related to the reduction of the inherent irregularity of somite boundaries observed in clock-deficient embryos.

Signal fold change

Quantification of the mechanism encoding the determination front can be challenging because the posterior of the embryo elongates while the signalling gradients regress. Moreover, there are multiple signalling pathways acting in the PSM (Wnt, Fgf, RA) making it difficult to untangle the different effects of each signalling gradient. To overcome these challenges, [Simsek and Özbudak, 2018](#) used a 3D zebrafish tail explant model, which recapitulates the same scaling in somite size as in the embryo. They developed a mathematical spatial gradient model to account for how positional information is precisely translated. This was done by computing the signal fold change (SFC) between two neighbouring cells, then designating this as how positional information is delivered. When the SFC exceeds a threshold, the presumptive somite boundary is placed. This type of model proposes that the positional signal is read by a non-linear threshold of the FGF target dpERK.

These three hypothesis - linear gradient, bistable gradient and SFC - have all been theoretically proposed with supporting experimental evidence. In Chapter 2, I show results that cannot be explained by these models, and suggest a fourth hypothesis.

0.6 Dynamics of the segmentation clock

0.6.1 Clock core circuit

The existence of an oscillator as described by [Cooke and Zeeman, 1976](#) was already shown by [Palmeirim et al., 1997](#). The role of such oscillator in the model is to generate temporal periodicity that can be translated into the formation of somite boundaries. Furthermore, additional genes referred to as “cyclic” or “core segmentation clock” genes, have since been identified: *Hairy1* and *Lnfg* in chick; *Hes7*, *Lnfg*, *Dll1* among others, in mouse; *her7*, *her1* and *deltaC* in zebrafish (summarised in [Oates, Morelli, and Ares, 2012](#)). The core of the oscillating genetic network exhibits similar spatial patterns and has been described in mouse, frog, fish and chick embryos ([Pourquié, 2003](#)). However, even though many components of the segmentation clock had been identified, the way

they interact to produce oscillations remains unclear. Proposing a hypothesis, Lewis, 2003 formulated a mathematical model of transcriptional oscillation based on a delayed negative feedback loop. These delays are caused by the time it takes to splice mRNA and import the protein into the nucleus. Initially, this model was established with zebrafish *Her* genes in mind, but was then extended to *Hes7* in mouse (Harima et al., 2013). Later experiments both in mouse and fish suggested that the segmentation clock is a more complex oscillating genetic network.

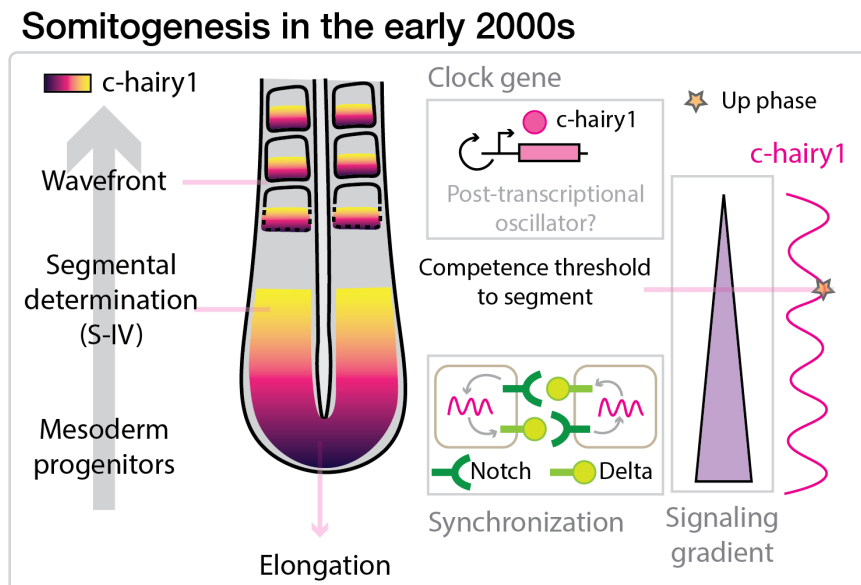


Figure 7: **Vertebrate segmentation at the beginning of the century.** Cyclic changes in molecules of the oscillator mechanism (in pink) change the expression of *deltaC* in each cell which in turn changes Notch in its neighbour. This was the mechanism proposed to keep oscillations in adjacent cells synchronised. Segmental determination is achieved when a threshold of the gradient (in purple) is crossed and at a certain clock phase (shown as an orange star). Factors that drive *c-hairy* oscillations can be periodically activated post-transcriptionally.

Dequéant et al., 2006 performed microarray studies in mouse PSM transcriptomes. They showed the network of cyclic genes of the notch, FGF, and Wnt pathways underlying the mouse segmentation clock. Moreover, Hirata et al., 2002 and Bessho and Kageyama, 2003 showed that *Hes1* and *Hes7*, respectively, are regulated by a negative feedback loop. In zebrafish, Brend and Holley, 2009a were the first to identify binding sites for *Her* proteins, showing the existence of direct negative auto-regulation of the *her* genes. This negative feedback loop is what gives rise to the oscillatory dynamics. Moreover, they also found binding sites for Tbx6 (a T-box transcription factor) and Suppressor of Hairless proteins (DNA-binding protein component of the Notch signalling pathway), which are required for the activation of *her1* expression. However the full core pace-making circuit in zebrafish was not experimentally shown until the parallel work by Schröter, Ares, et al.,

2012 and Trofka et al., 2012. They showed that there are two redundant negative feedback loops, Her1:Her1 homo-dimers and Her7:Hes6 hetero-dimers, operating in parallel with strong DNA binding activity. They then concluded that even though Hes/Her proteins can dimerise promiscuously, they do not all have strong DNA binding activity.

0.6.2 Live reporters of the segmentation clock

For many years, segmentation clock dynamics had been deduced from spatial expression patterns of cyclic genes in fixed embryos. Pioneering work by Masamizu et al., 2006, generated a transgenic reporter that included a luciferase driven by the *Hes1* promoter. Using *ex vivo* cultures of mouse embryos, they were the first to observe live oscillations of a cyclic gene reporter. Moreover, they confirmed that the rhythm of somite formation is accompanied by travelling waves of gene expression, which sweep from the tailbud to the anterior end of the PSM. Aulehla, Wiegraebe, et al., 2008 later engineered a transgenic mouse line expressing a highly destabilised Venus reporter under the control of the *lunatic fringe* (*Lfng*) promoter. The reporter line was called LuVeLu and has been widely used ever since. Performing 2PE time-lapse imaging, they showed periodic waves of *Lfng* expression. These studies opened the door to new discoveries and analyses that could be made thanks to the improved temporal resolution provided by live imaging. Before these papers, it was a matter of inferring dynamics from fixed samples, now the field was moving towards a more quantitative era of segmentation clock dynamics.

Live reporters were a huge leap forward in understanding clock dynamics. For example, prior to live imaging it was believed that the segmentation clock had a single, well-defined period. In other words, both the onset and arrest of the kinematic wave happened with the same period. Soroldoni, Jörg, et al., 2014 made a systematic assay in which they simultaneously time-lapsed 20 embryos carrying a transgene they created to report *her1* dynamics (Looping). They observed that multiple kinematic waves travel through the PSM at a given time and importantly they concluded: (1) Reporter arrest in the anterior coincides with the formation of a new somite; (2) Oscillations in the TB are different than those in the anterior PSM; (3) Anterior oscillations match the periodicity of somite formation. Crucially, they showed that the segmentation rhythm is influenced by a Doppler effect arising from waves of gene expression in a shortening embryonic tissue. They were only able to reach the latter conclusion thanks to live imaging of the fluorescent transgene.

Although real-time reporters have provided a tissue-level picture of the segmentation across the PSM, technical challenges have frustrated analysis at the level of the oscillating PSM cells. Delaune et al., 2012 was the first to visualise the dynamics of individual PSM

cells *in vivo*. Similarly, [Shih et al., 2015](#) followed the single cell oscillatory dynamics of future somite boundary cells. This analysis was limited to the PSM, and they found that cells in the anterior PSM increased intensity and slowed oscillations by about 1.5 times compared to more posterior PSM cells. These results confirmed the tissue level dynamics observed by [Soroldoni, Jörg, et al., 2014](#). Although this was not fully addressed, the level of resolution and analysis performed were the first steps in trying to understand how the dynamics of the molecular oscillator play a role during somite boundary formation.

0.6.3 *In vitro* dynamics of the segmentation clock

As clock dynamics were explored in live embryos with advances of imaging techniques, the subsequent move in the field was the development of *in vitro* models of the clock owing to two main motivations: 1) some model systems, such as mice, were exceptionally challenging for *in vivo* experimentation and imaging, and 2) much could be learned from deconstructing the clock. [Lauschke et al., 2013](#) showed pioneering progress when culturing mouse tailbud explants from the LuVeLu reporter line. They showed that these explants could recapitulate oscillatory and differentiation dynamics observed in the intact embryo. Later, [Hubaud, Regev, et al., 2017](#) used a similar system to engineer stable oscillatory dynamics by maintaining cells in a medium that prevented differentiation. Using cultures of different cell number, they concluded that rather than a cell-autonomous property, oscillations are a collective property of PSM cells. Moreover, they proposed that the segmentation clock behaves as an excitable system triggered by mechano-signalling controlling Notch oscillations.

Using a deconstruction approach in the zebrafish, [A. B. Webb et al., 2016](#) dissociated single tailbud cells from embryos carrying *her1:YFP* (Looping). They observed persistent oscillations in these cells, suggesting that cells of the zebrafish segmentation clock behave as self-sustained, autonomous oscillators with noisy dynamics. As with [Hubaud, Regev, et al., 2017](#), cells in this culture were thought to be maintained in an undifferentiated state by growth factors, serum and BSA (Bovine serum albumin) in the culture medium.

Recently, we isolated PSM cells *in vitro*, in the absence of cell-cell interactions and added signalling morphogens ([Rohde et al., 2021](#)). This study revealed that when PSM cells are allowed to differentiate, they have the intrinsic ability to slow oscillations and arrest coincident with the expression of the segmental polarity marker, *Mesp*. Pairing this work with *in vivo* cell tracking, revealed that a cell's behaviour along the anteroposterior axis of the PSM can be recapitulated solely with information carried by the cell. This intrinsic program suggested that PSM cells *in vivo* use differentiation time as a spatial

reference to generate the segmentation clock pattern and set arrest. However, we also found the arrest time *in vitro* to be noisier, suggesting that extrinsic spatiotemporal cues globally modify the intrinsic timer. Furthermore, this also suggests that extrinsic signals in the embryo play an important role in providing the level of precision observed *in vivo*. This study is shown in Chapter 3.

0.7 The arrest of the segmentation program

0.7.1 Role of T-box transcription factors

As mentioned in section 0.4.3, previous studies performed a large-scale screen looking for mutations that would lead to somite boundary defects in zebrafish embryos (Solnica-Krezel et al., 1996; Van Eeden et al., 1996b). Characterised initially by their phenotype, three of these mutants were shown to belong to the family of T-box genes, *no tail (ntl)*, *spade tail (spt)* and *fused somites (fss)* (Herrmann et al., 1990; Griffin et al., 1998; Nikaido et al., 2002). T-box genes encode transcriptional activators and repressors that contain a conserved DNA-binding domain called the T-box. These transcription factors play an important role during somitogenesis, as we will see in the following paragraphs.

The *ntl* mutant lacks a differentiated notochord and the caudal region of their body axis (Schulte-Merker et al., 1994). Moreover, *ntl* is the zebrafish ortholog of mouse *Brachyury*, a T-domain transcription factor and the first T-box gene to be molecularly identified (Herrmann et al., 1990). *ntl* is expressed in the notochord and in the tailbud. Interestingly, *ntl* has been shown to directly regulate *deltaD (dld)* in the posterior tailbud and *tbx6* (a T-box transcription factor) (Garnett et al., 2009). The *her* genes, being repressors, need activators in order to show expression and Brend and Holley, 2009a showed that *her1* gene has binding sites in an enhancer region driving expression in the anterior PSM for Tbx6 and Suppressor of Hairless proteins, a DNA-binding protein component of the Notch signalling pathway (Bray and Furriols, 2001). Thus, in the tailbud, *ntl* acts as a regulator of the *her1* gene.

The *spt* mutant lacks PSM in the trunk, and consequently somites, however tail somites appear normal. These anterior defects are due to defective convergent extension caused in part by the failure to express downstream targets such as *protocadherin (papc)*, a protein involved in cell-cell adhesion (Yamamoto et al., 1998). *spt* was later shown to be encoded by Tbx16 (Griffin et al., 1998), expressed in the TB and posterior PSM. Moreover, it interacts with FGF (Warga et al., 2013), Wnt and RA (Mueller, Huang, and

Ho, 2010). As *ntl*, it has been shown that *spt* directly regulates *dld* and *tbx6*, making it another key regulator of *her1* in the tailbud and posterior PSM. Moreover, in the absence of *tbx16* and *ntl*, *her1* is not expressed, suggesting that PSM development is abolished in their absence (Amacher et al., 2002).

The *fss* mutant was given its name due to the absence of distinct segments. The anterior most stripe of *her1* (Holley, Geisler, and Nüsslein-Volhard, 2000) and anterior markers including *mesp-a* (Durbin et al., 2000; Oates, Rohde, and Ho, 2005) were also missing in *fss* embryos. Subsequently, Nikaido et al., 2002 showed that *fss* encodes the T-box transcription factor *tbx6*, which is expressed in a restricted AP domain within the PSM. Moreover, as mentioned before, *her1* has binding sites for *tbx6*, making it a direct activator of this clock gene (Brend and Holley, 2009b). Chapman and Papaioannou, 1998 identified mouse *tbx6*, finding it an indispensable component for PSM differentiation and segmentation.

Taken this information together, *no tail (ntl)*, *spade tail (spt)* and *fussed somites (fss)* operate as a network of interacting genes to regulate region-specific gene expression and developmental fate (Goering et al., 2003). More specifically, given this evidence and the fact that *tbx6* can bind to *her1* (Brend and Holley, 2009a), this T-box gene network has been thought to be the machinery driving segmentation clock gene expression.

Due to the strong *fss* phenotype, *tbx6* has received a lot of attention. Several studies reported that both in mouse and zebrafish, Tbx6 protein exhibits a step boundary in the position corresponding to the presumptive somite boundary in the PSM (Oginuma et al., 2008; Wanglar et al., 2014; Zhao et al., 2015). Moreover, it has been shown that Tbx6 expression is maintained by transcriptional auto-regulation (Ban et al., 2019). Because *tbx6* is the anterior-most t-box gene expressed and can bind to *her1*, this means it is potentially the last input given to *her1*. The question is then, what shuts down *tbx6* in order to arrest the cyclic gene expression? In other words, what is the molecular mechanism behind the arrest of the segmentation clock?

Although *tbx6* has been widely studied, little is known about the dynamics during somitogenesis. In Chapter 4 we show preliminary results in the role of *tbx6* and how it contributes to the precise positioning of somite boundaries.

0.7.2 The Ripply family

Great advances have been made in describing the molecular mechanism and dynamics of the segmentation clock. However the molecular mechanisms as well as the biological

significance of the arrest has remained unclear. In zebrafish, three structural homologs of *rippy* genes were identified (Kawamura et al., 2005). Of them, *rippy1* and *rippy2* show overlapping expression in the anterior region of the PSM whereas only *rippy1* is expressed more broadly in several newly formed somites. These genes became of interest when Kawamura et al., 2005 showed that *rippy1* is essential for somite boundary formation when knock-down experiments resulted in fused somite boundaries. Moreno, Jappelli, et al., 2008 and Wanglar et al., 2014 performed knockdown experiments and showed that *rippy1* and 2 function redundantly in somite segmentation. No apparent morphological defects are observed in homozygous *rippy2* mutants (Kinoshita et al., 2018; Moreno, Jappelli, et al., 2008) and down-regulation using morpholinos caused no apparent defect in somite formation (Kawamura et al., 2005). Performing a detailed analysis of gene expression in the PSM, these studies showed that *rippy1* has two main roles: (1) termination of the segmental program and, (2) maintenance of rostra-caudal polarity. *rippy1* knockdown results in ectopic anterior expansion of *her1* into the somites. In zebrafish *rippy1* and *rippy2* are a transcriptional targets of *Tbx6* and are also regulated via Notch signalling. This was the first evidence of a molecular mechanism that could lead to the arrest of the segmentation program. Further evidence followed when Wanglar et al., 2014, using antibody staining for *Tbx6* showed how the anterior border of *Tbx6* domain coincided with the presumptive somite boundary in zebrafish. Moreover, they reported this boundary shifted during 1 cycle of somite formation. This suggests that *tbx6* may be involved in the mechanism of translating the temporal rhythmicity of the clock into positional information to give rise to the somite boundary.

Finally, it has been shown that the relative gene dosage between *rippy1/2* and *tbx6* is crucial for somite boundary formation. *rippy1*^{-/-};*tbx6*^{+/+} show defective segments. However, this phenotype can be recovered by reducing the copy number of *tbx6*: *rippy1*^{-/-};*tbx6*^{+/-} (Kinoshita et al., 2018). Thus, there is a tight control between *rippy* and *tbx6* to arrest the clock. All these studies were performed on fixed samples. In chapter 4 we show how this network of *rippy* and *tbx6* can be involved not only in arresting the clock but in doing so with the level of precision needed to form a sharp somite boundary.

0.8 Research questions

I am interested in how the vertebrate body plan is precisely segmented, specifically, how positional information is provided to cells to know where and when to form a somite boundary. Hopefully, this introduction has put you in context for a better understanding of the next chapters. Some of the research questions proposed can only be answered using live imaging. As mentioned above, the field is advancing hand in hand

with microscopy techniques, analysis tools and experimental approaches.

Figure 8 shows a summary of the main events that occur during somitogenesis in zebrafish and that have been explained throughout this section. Now that we are all on the same page, I will define the 4 main research questions that I have been working on during my thesis:

State of the art of somitogenesis in zebrafish

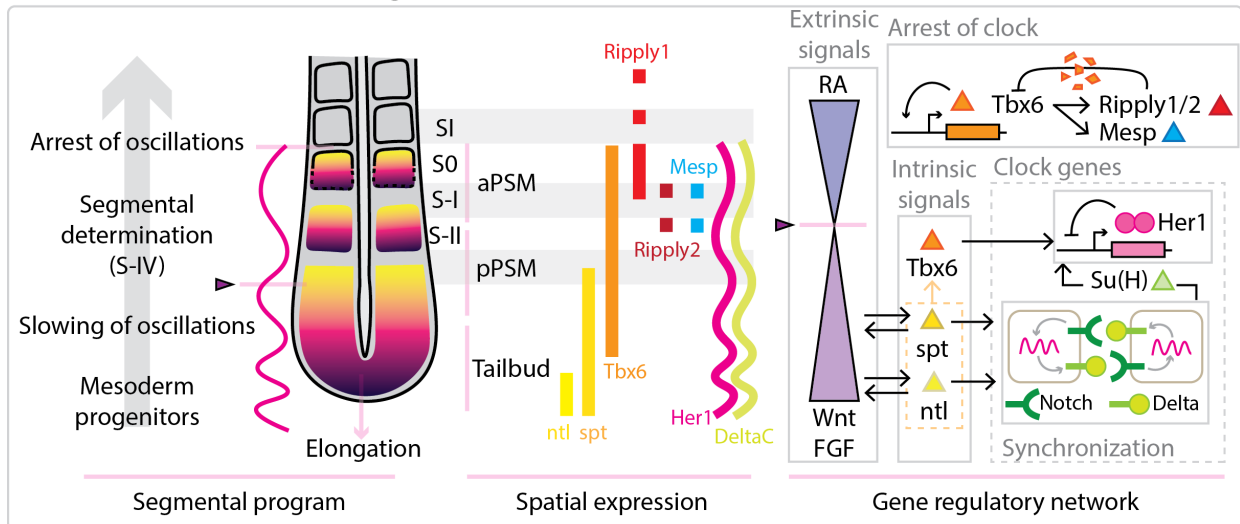


Figure 8: **Summary of the state of the art of somitogenesis in zebrafish.** The segmental program category includes the global events occurring during somite formation as the cells progress from the TB to the PSM. The spatial expression includes the mRNA expression shown by the studies mentioned in this section. The gene regulatory network category includes the overall interactions between the main players during the segmental program. Lines with arrowheads mean activation whereas lines with flatheads mean inhibitions or degradations.

Chapter 1

In Chapter 1 I show the image analysis pipeline that we have developed and I used in the following chapters. In addition, you will also find a tool I developed called Paleontologist. This is an open source Python package that allows the quantification of single cell traces. With this pipeline and tool we were able, in the other chapters, to study how, when and where is positional information read by the cells and what are the mechanisms that lead to the precise formation of somite boundaries.

Chapter 2

As I am interested in what mechanisms provide positional information to precisely form a somite boundary, the starting point of my work was to explore the FGF signalling gradient. As mentioned earlier in the introduction, FGF has been implicated in somite boundary positioning by establishing the position in the PSM where somite boundary determination occurs. Thus, in Chapter 2 I study the effects of FGF on somite boundary formation, clock and wavefront dynamics. In addition, by tracking single cells we can get a better picture of where the positional information read by the cells is located in the PSM.

Chapter 3

After studying how an extrinsic signal plays a role in providing positional information to form somite boundaries in the correct position, the next question I addressed was whether intrinsic signals can play a role. More specifically, can the segmental programme function autonomously? In Chapter 3 you will see our study called *Cell-autonomous generation of the wave pattern within the vertebrate segmentation clock*.

Chapter 4

In Chapter 3 we proposed that the segmentation clock integrates an intrinsic timer mechanism underlying the arrest of the program. Thus, in chapter 4 I show preliminary results on molecular candidates for the timer: Tbx6 and Ripply, and how this mechanism may be involved in the precise formation of somite boundaries.

Chapter 1

Image analysis pipeline and Paleontologist

There are indications (Dubrulle, McGrew, and Pourquié, 2001; Bajard et al., 2014) that spatiotemporal information determining boundary position is delivered earlier, in the posterior PSM. Investigation of this “determination front” and mechanisms regulating its precision requires that we first have a quantitative description of cellular-level clock and differentiation dynamics across a cell’s entire trajectory from Tailbud (TB), PSM to Somite. Although real-time reporters of the segmentation clock exist in zebrafish (Delaune et al., 2012; Soroldoni, Jörg, et al., 2014) and other systems (Aulehla, Wieggraabe, et al., 2008), limitations in imaging cellular-level dynamics over long developmental periods in the growing tailbud and PSM have prevented the creation of this *in toto* map of the segmentation program. Moreover, much of our understanding of TB and PSM cell differentiation to date comes from fixed samples, thus lacking temporal resolution. Here, to address my thesis questions (section 2, 3 and 4), we have established a standardised light-sheet microscopy imaging protocol and developed an open source data analysis tool for data collected. The resulting dataset and analysis has already revealed previously unknown dynamic patterns possibly related to the precise and accurate somite boundary positioning.

This chapter includes two manuscripts in preparation for submission:

- But, what are the cells doing? Image analysis pipeline to follow single cells in the zebrafish embryo
- Paleontologist, a modular python package for single cell tracking analysis

Title: But, what are the cells doing? Image Analysis pipeline to follow single cells in the zebrafish embryo

Authors:

5 **Ariane Bercowsky-Rama**^{1,†}, Olivier F. Venzin^{1,†}, Laurel A. Rohde¹, Nicolas Chiaruttini², Andrew C. Oates^{1,*}

Affiliations:

¹Institute of Bioengineering, École Polytechnique Fédérale de Lausanne; Lausanne, CH

10 ²BioImaging and Optics Core Facility, École Polytechnique Fédérale de Lausanne; Lausanne, CH

†Equal contribution

*Corresponding author. Email: andrew.oates@epfl.ch

One-sentence Summary

User friendly cell-tracking pipeline that connects from image acquisition through to data
15 analysis of cellular dynamics in multicellular systems.

Abstract

Microscopy has rapidly evolved at pace with live markers to enable higher spatiotemporal resolution of multicellular dynamics within bigger fields of view. Consequently, we are now in the era of widespread production of terabyte (TB)-sized timelapse movies of experimental
20 model systems, including developing embryos and organoids. Working with these large datasets has brought a new set of challenges and, as of yet, standardized open-source pipelines for acquiring, handling and analyzing data are still lacking. Moreover, although tracking cells throughout an entire biological process, for example vertebrate segmentation, is key to revealing underlying cellular dynamics, this has proven elusive to many researchers. To
25 specifically address the question “But, what are the cells doing?”, we created an image analysis pipeline optimized to track single cells in light-sheet acquired datasets (1 TB sized timelapse, 8h of imaging, 30 min genetic oscillatory cycle, speed cell movement ($\mu\text{m}/\text{minute}$), 200-400

µm tissue depth). Our modular pipeline optimizes and connects the following: image acquisition parameters to improve tracking feasibility; hardware specifications; data handling and compression tools; pre-processing steps; connections to state-of-the-art cell tracking tools (Mastodon, Elephant, MaMuT) and a novel open-source/ python-based tool (Paleontologist) to
5 analyze spatiotemporal dynamics of the tracked cells. Importantly, our pipeline is adaptable to a variety of experimental systems and accessible to researchers regardless of expertise in coding and image analysis.

Introduction

10 Live imaging of multicellular systems for the purpose of describing tissue and cellular spatiotemporal dynamics has become practice in many labs ([Attardi et al., 2018](#); [McDole et al., 2018](#); [Shah et al., 2019](#)). We have also recently used this approach to understand the cellular-level dynamics underlying the segmentation clock wave pattern in the developing zebrafish embryo ([Rohde et al., 2021](#); [Soroldoni et al., 2014](#)). Here we detail the pipeline we created to
15 facilitate imaging, cell-tracking and data analysis of rapid oscillatory dynamics (30 minute gene expression cycles) and cell movements of individual cells throughout the hours-long timeframe of segmentation. This pipeline is modular and adaptable to similar challenging systems including organoids in which researchers wish to track spot-like structures.

20 When imaging a tissue at cellular resolution, the ultimate goal is usually to quantify spatiotemporal dynamics of tracked cells. There are two main approaches to cell tracking, the first of which is *in toto* cell tracking, such as performed by [McDole et al., 2018](#), and [Shah et al., 2019](#), in mouse and zebrafish embryos, respectively. These *in toto* approaches relied on automatic algorithms, including TGMM (Tracking with gaussian mixture model, [Amat et al.,
25 2014](#)), to generate the cell tracks in the order of many thousands, a scale that renders manual

curation unrealistic. Automated tracking accuracy exponentially decays over trajectory length, thus limiting analysis to short tracks as in [Shah et al., 2019](#), cell tracks of 10 frames, 20 minutes), or requiring custom statistical analysis to infer the dynamics as in [McDole et al. 2018](#) (less than 30 time points over a 2-hour period improved by a factor of 3.1) The second cell-tracking approach relies on manual or semi-automatic cell tracking ([Delaune et al., 2012](#); [Shih et al., 2015](#); [Rohde et al., 2021](#)), in which the user selects cells within a region of interest then manually curates the tracks. Although the number of tracks obtained is relatively lower, in the order of many hundreds, this approach produces reliable trajectories that run considerably longer (100 frames, 150 min, [Rohde et al., 2021](#) using Mastodon). Selection of one of these two approaches will depend on the question being asked and the accuracy required to answer it. Here, our pipeline takes a semi-automatic tracking approach, but includes optimized parameters for both imaging and processing steps to reduce the burden of manual curation.

Despite examples of successful cell tracking and analysis at various scales and timeframes, it remains out-of-reach for many labs due to lack of expertise. A diverse set of skills is required across the many steps of the process, including the following: preparing and mounting live samples ([Kleinhans and Lecaudey, 2019](#); [Hirsinger and Steventon, 2017](#)); adjusting microscopy setups to produce high resolution and low photo-toxicity ([Garcia et al., 2011](#); [McConnell et al., 2016](#)); modifying imaging software and hardware ([Mc Dole et al., 2018](#)); post-processing of the acquired data, e.g. deconvolution ([Sage, et al., 2017](#); [Preibisch et al., 2014](#)) and registration ([Preibisch et al., 2010](#)); assembling efficient processing and analysis computing hardware ([Roger et al., 2016](#)); segmenting and/or tracking cells in 3D over time ([Schmidt, et al. 2018](#); [Weigert et al., 2020](#)) ([Tinevez et al., 2017](#)); and finally, writing bespoke code to analyze the dynamics of the tracked cells ([de Medeiros et al., 2021](#); [Zhisong et al., 2020](#)). Thus, without standardized pipelines in place, analysis of spatiotemporal cell dynamics

can be a daunting task. Keeping increased accessibility as a goal, here we provide a user-friendly cell-tracking pipeline accompanied by guidance, open-source code and novel analysis software.

5 In this paper we first give an overview of each of the modules in the pipeline, explaining the main goals and concepts of the process, as well as their application and limitations. In the Materials section, we give the concentrations, parameters and settings that we have optimized specifically for study of the segmentation clock in zebrafish. In the Procedure section, we go into detail of each of the steps in all four modules, also pointing out where, how and why the
10 concentrations, parameters and settings can be modified for application to other samples.

Pipeline Overview, Application and Limitations

The pipeline has 4 main modules (Figure 1): 1) a time-lapse of a live sample is acquired; 2) the time-lapse is processed to facilitate data handling and further analysis; 3) spots are detected
15 and cells are tracked within the timelapse and 4) spatiotemporal features are extracted from the cell tracks and analyzed.

Here we demonstrate the step-by-step application of our pipeline as we follow individual cells throughout segmentation of the developing zebrafish embryo. The segmentation clock is a
20 multi-cellular patterning system that translates the rhythm of cellular genetic oscillations into the successive and periodic formation of blocks of tissue in the trunk and tail called somites. Clock activity produces tissue-level waves of gene expression in presomitic mesoderm (PSM) that travel anteriorward until arrest at the position of the newly forming somite (Aulehla et al.,
2008; Delaune et al., 2012; Masamizu et al., 2006; Palmeirim et al., 1997; Soroldoni et al.,
25 2014). Historically, rapid cellular-level clock oscillations and ongoing tissue morphogenesis

have made it difficult to describe the full picture of cellular dynamics underlying the clock pattern in zebrafish and other model systems (Delaune et al., 2012; Morelli et al., 2009; Shih et al., 2015; Yoshioka-Kobayashi et al., 2020). In creating the cell tracking pipeline our motivation was thus two-fold, first to directly answer questions about cellular clock dynamics, and second, to standardized a pipeline that makes this level of analysis accessible to a broader range of researchers and model systems.

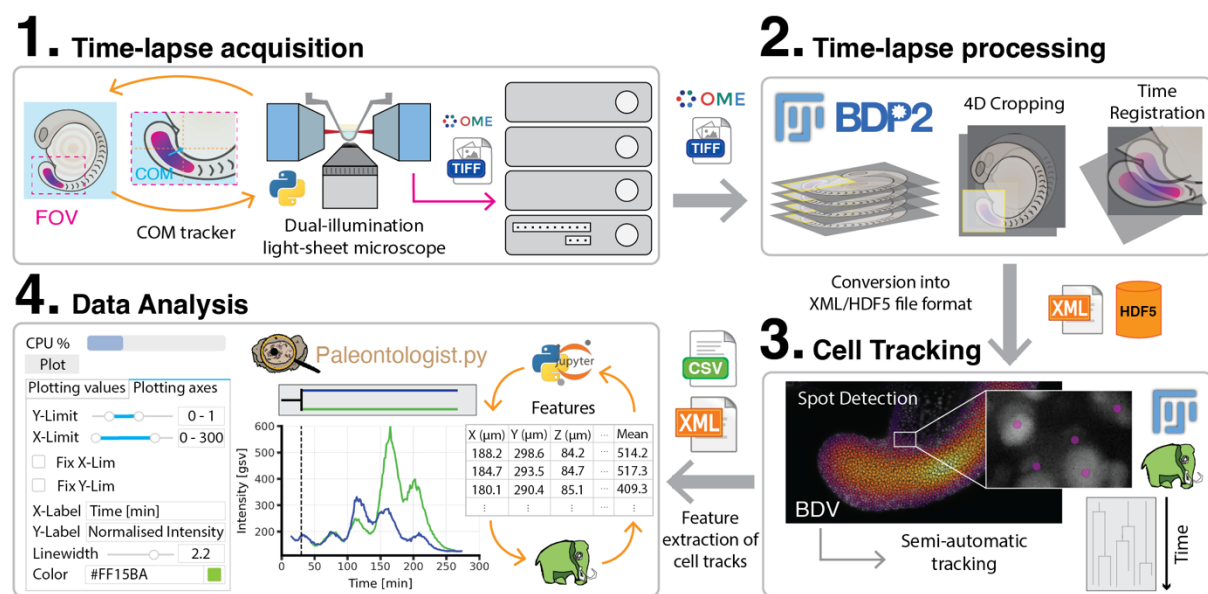


Figure 1. Cell tracking pipeline overview. 1) Cellular resolution time-lapse acquisition using, for example, light-sheet microscopy. To keep the region of interest inside the field of view (FOV), Python-based centre of mass (COM) tracking is implemented. Resulting OME-TIFF data is saved into a centralized workstation. 2) The 5D time-lapse data cropping, drift correction and time-registration to facilitate later cell tracking. Processed time-lapses are saved in XML-HDF5 file format to allow interaction between the visualization and analysis tools. 3) Tracking is done using Mastodon, a Fiji plugin. Mastodon outputs all the features from the cell tracks (XYZ cell coordinates, intensities, velocities, etc.) as an XML or CSV file. 4) Data analysis of the features is made easy in Paleontologist, a modular python package that was built in our lab to interactively analyze tracked cells and output publication quality figures. Features from Mastodon can be iteratively plotted and edited in Paleontologist, then re-checked in Mastodon for cell visualization in the context of the embryo.

1. Acquisition: Cell-tracking in our system relies on a fluorescent nuclear marker, however the pipeline could also be adapted to track intra- or inter-cellular spot-like structures, for example tracking centrioles (Erpf et al., 2020). Feasibility is in large part determined by the quality of the acquired data; thus, it is an important first step to consider sample-dependent
5 limitations including constraint-free mounting of the live sample, photo-bleaching, photo-toxicity, and spatiotemporal resolution relative to the dynamics of interest. Each experimental system will present unique limitations that require troubleshooting.

Depending on the sample size and microscopy hardware, the field of view (FOV) required to image at cellular resolution may fail to cover the entire region of interest (ROI). Particularly
10 challenging is that the ROI itself may simply move out of the FOV due to growth and morphogenesis, a limitation we faced in the extending tail of the zebrafish. Happily, FOV problems can be resolved using short scripts of code to communicate with the microscope software controlling the camera and stage movement. For example, to enable long-term imaging of the segmentation clock, we designed a center of mass tracker in Python that keeps
15 the fluorescent clock signal inside the FOV as the embryo extends its tail. Our tracking script included here can easily be translated into other microscope systems that allow custom scripts. As microscopy has evolved, so has the level of automation enabled by these scripts which allow adaptive imaging (Roger et al., 2016). Von Wangenheim et al., 2017 developed custom software – TipTracker – to automatically track diverse moving objects on various microscope
20 setups.

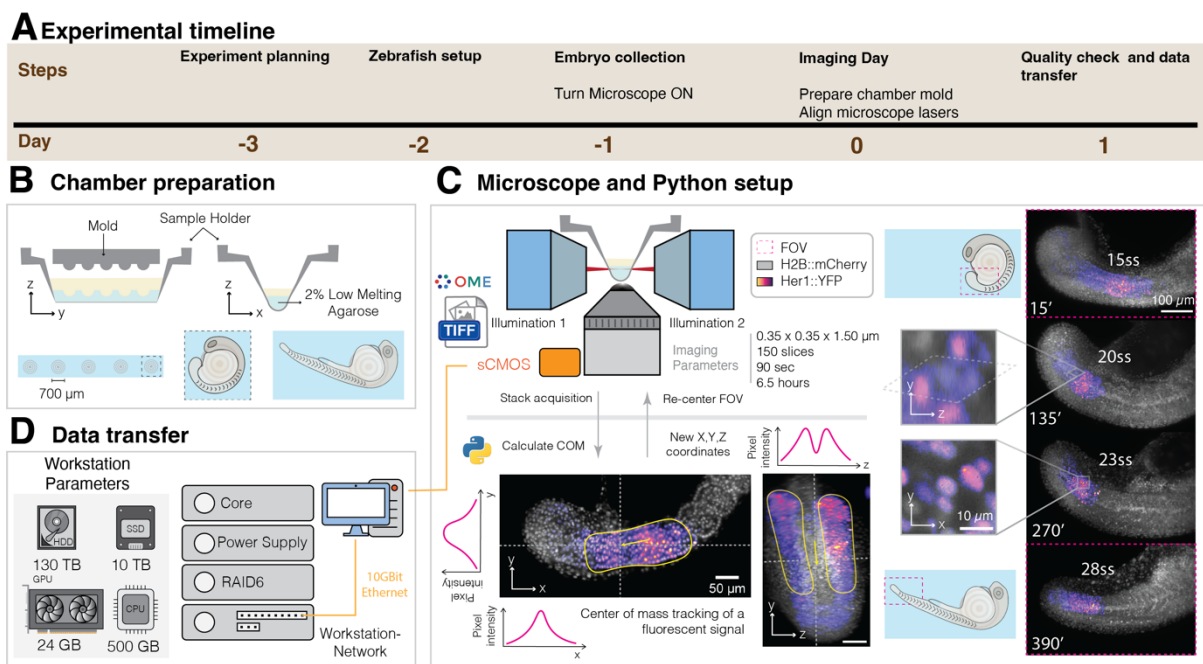
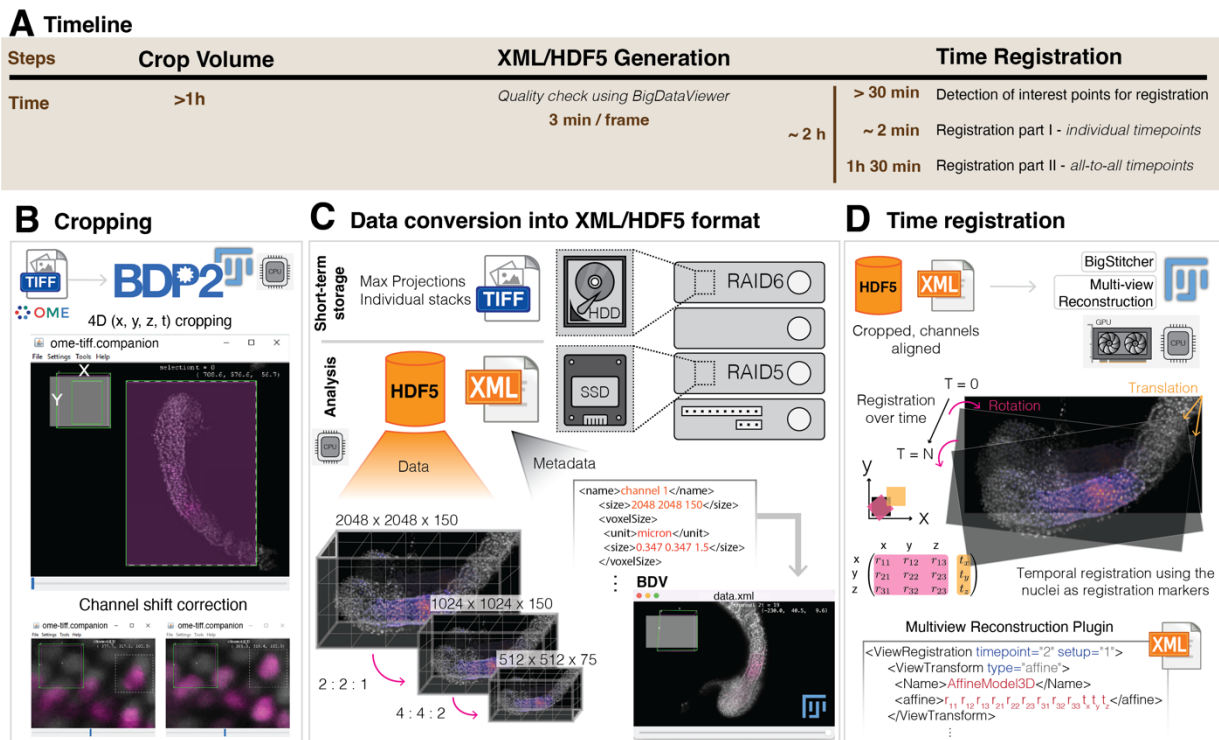


Figure 2. Time-lapse acquisition of zebrafish embryonic segmentation. **A)** Timeline to acquire a timelapse of a zebrafish embryo. **B)** Preparation of the imaging chamber and mounting embryo. A 3D-printed sample holder is glued to a transparent filament sheet, creating a trough. Low-melting point agarose is added to the trough, then a 3D printed mold is used to create depressions into which the yolk of the embryo sits. **C)** We use a dual-illumination light-sheet microscope to acquire 5D time-lapse movies of 0.35 μm in X-Y and 1.5 μm in Z, 150 slices, 90 seconds time-step and at least 6.5 h of imaging. Data is saved as an OME-TIFF file. During acquisition, the center of mass (COM) of the signal of interest (Magenta), is tracked to instruct the microscope to re-center the field of view (FOV) in XYZ. **D)** Acquired data is transferred from the imaging computer to an image processing station equipped with 24 GB of GPU, 500 GB of RAM, 10 TB of SSD and 130 TB of HD storage.

2. Processing: Following the acquisition of a TB-sized time-lapse movie, even the initial visualization can be problematic without the correct tools (software and hardware) due to the limitations of a standard computer's RAM. To guide users over this hurdle, we detail pre-processing steps that convert the timelapse into a manageable, ready-to-be tracked format. We cover cropping to reduce size in all dimensions XYZT, conversion to HDF5 files, and time registration to reduce sample movement and drift. Our pipeline consolidates and smooths the workflow through pre-processing steps that have been published as stand-alone operations

(cropping, registration, chromatic aberration corrections), custom built for a specific project (tracking of all the cells in a developing mouse embryo, [McDole et al., 2018](#)) or available as a commercial product (Imaris (Bitplane), Arivis). The tools we recommend for pre-processing are mainly open-source (although we propose the equivalent commercial solutions), tested in multiple systems, and include a user-friendly interface (Fiji as open source and Imaris (Bitplane), Arivis as commercial). To facilitate the movement and storage of the TB-sized datasets, we recommend data compression systems (Lempel-Ziv-Welch (LZW), Deflate compression as open source and Jetraw (Dotphoton) as commercial).



10

Figure 3. Pre-processing the Time-lapse. **A)** Timeline of pre-processing using the specified memory parameters from Figure 2B. **B)** Cropping and channel shift correction using BigDataProcessor2. After loading the OME-TIFF files, the user interface allows a choice of transformations to apply (affine transformed viewing, cropping, binning, bit-depth conversion, drift correction and channel alignment). **C)** The transformed and cropped data is saved into XML-HDF5 file format, while the OME-TIFF raw data is stored in HDD as backup. The XML-HDF5 is saved in the SSD to speed future read-write processes. HDF5 data is organized in a pyramidal structure that enables interactivity when opened in BigDataViewer. **D)** To correct for embryo movement or drift, time registration is applied using the

15

nuclei as registration markers. This step can be performed in CPU or GPU, with the resulting registration matrices for each timepoint stored in the XML.

3. Cell Tracking: Pre-processing results in files that are easily opened and viewed in the cell-tracking tool Mastodon – a large-scale tracking and track-editing framework for large, multi-view images (<https://github.com/mastodon-sc/mastodon>). Although automation of the cell tracking within Mastodon is limited by timelapse quality, we will cover how tracking parameters can be tuned for particular spot size, signal intensity, cell density, movement, etc. Manual tracking and editing are also user-friendly. Features including mean intensity, XYZ coordinates, number of links, and velocities can be extracted from the tracks and saved in CSV (comma separated values) files for later analysis.

4. Data Analysis: To explore features extracted from the cell tracks we created Paleontologist (<https://github.com/bercowskya/paleontologist>), a novel open-source analytical tool that requires no coding experience, but allows custom scripting. Paleontologist has been designed to interactively aid in quantitative and qualitative analysis of spatiotemporal features for single or multiple cell tracks of interest. The user can move back and forth between Paleontologist and Mastodon to investigate, correct and refine cells or groups of cells of interest. After using the data exploration interface, users can output their results as publication-quality figures.

20

We were motivated to develop Paleontologist due to the limited tools available to analyze spatiotemporal dynamics, especially those from individual cell tracks. Louveaux and Rochette developed an R package `mamt2r` (<https://marionlouveaux.github.io/mamt2r/>), which imports and visualizes xml files from MaMuT, a Fiji Plugin pre-cursor to Mastodon (Carsten et al., 2018). However, besides custom-built scripts for specific purposes, no open-source tool exists to perform similar tasks for Mastodon. Mastodon outputs large CSV files that include the

25

necessary information to reconstruct cell tracks, however the reconstruction process can be a challenge in the presence of cell division. Paleontologist solves these issues and returns arrays of tracks already reconstructed and including an ID for cell division to keep track of daughter cells. Moreover, spatiotemporal analysis can be complicated due to the large amount of data and the need to consider data pre-processing. For example, if registration was performed, then coordinates provided by Mastodon must also be registered. Paleontologist allows you to undo the registration if needed.

Materials

1. Zebrafish

Transgenic (Tg) fish were maintained according to standard procedures in École Polytechnique fédérale de Lausanne (EPFL, Lausanne, CH). Embryos were produced by natural pairwise spawning. We used double Tg embryos heterozygous for a real-time segmentation clock reporter *Tg(her1:her1-yfp)* (Soroldoni et al., 2014) and the nuclear marker *Tg(Xla.Eef1a1:H2BmCherry)* (Recher et al., 2013). Embryos were incubated at 28.5°C in facility water until shield stage, then incubated at 19.5°C until the 8 to 10 somite stage when they were returned to 28.5°C until imaging at the 15-somite stage. Embryos for experiments were dechorionated manually prior to imaging, then immersed in facility water with 0.02% Tricaine (Sigma) for the rest of the experiment to avoid muscle twitching.

2. Microscope

We used a LightSheet Microscope LS1 (Viventis Microscopy Sàrl, Switzerland) with the following configuration: Andor Zyla 4.2 sCOMS camera; 515 nm laser to image YFP; 561 nm

laser to image mCherry; CFI75 Apochromat 25X, NA 1.1 detection objective (Nikon); scanned gaussian beam light sheet with thickness (FWHM) of 2.2 μm .

3. Imaging

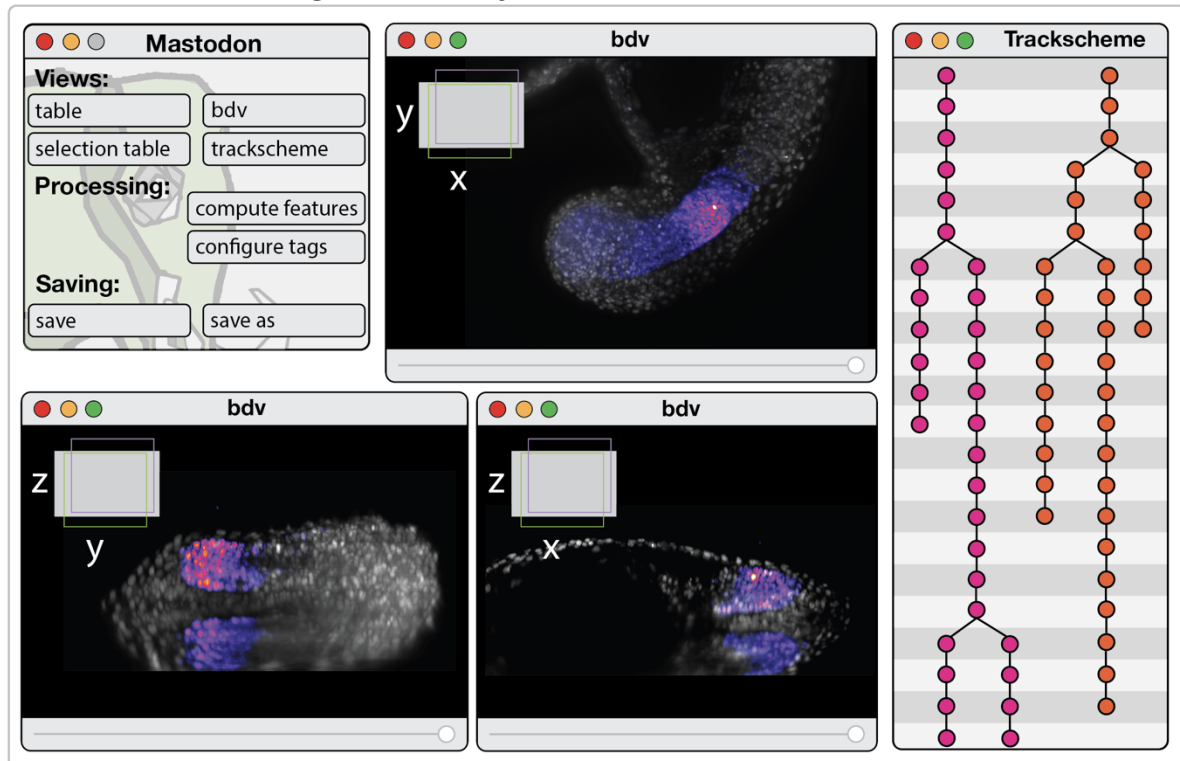
3.1 Mounting

5 Whole embryos were mounted in an imaging chamber that reliably holds them in a lateral orientation, ideal for illuminating the segmenting trunk and tail. To make our molds, we first glue a thin membrane to the bottom of a 3D-printed chamber to make a trough (Viventis Microscopy Sàrl, Switzerland). 2% LMP Agarose (Sigma, in E3 medium) is then added in stages to the trough along with a 3D-printed counter mold of 5 to 10 small protruding semi-
10 circles (750 μm in diameter) such that depressions are created to hold the embryo's yolk while allowing unhindered extension of the tail and body (Herrgen L., Schröter C., Bajard L., Oates A.C., 2009) (Figure 2B). Embryos were added to the chamber after removing the mold and filling the trough with facility water plus 0.02% tricaine (Sigma). Our region of interest, the trunk and tail, lay flat in a lateral view along the thin agarose surface (Figure 2B). Temperature
15 was kept at 28.5°C using a recirculating air heating system (Cube 2, Life Imaging Services, Switzerland).

3.2 Imaging parameters

To track cells, we relied on a non-oscillating nuclear marker *Tg(Xla.Eef1a1:H2BmCherry)* (Recher et al., 2013). Cells in the segmenting region of the zebrafish embryo have a nucleus of
20 7-10 μm , requiring z-planes every 1.5 μm to produce spatial resolution suitable for tracking. We took stacks of 150 z-planes to span the depth of one entire side (right or left) of the bilaterally segmenting tissue at 15 somite stage and older. Younger embryos require more z-planes to compensate for greater depth of the segmenting tissue. To follow individual cells

A Mastodon tracking windows layout



B Analysis workflow with Paleontologist

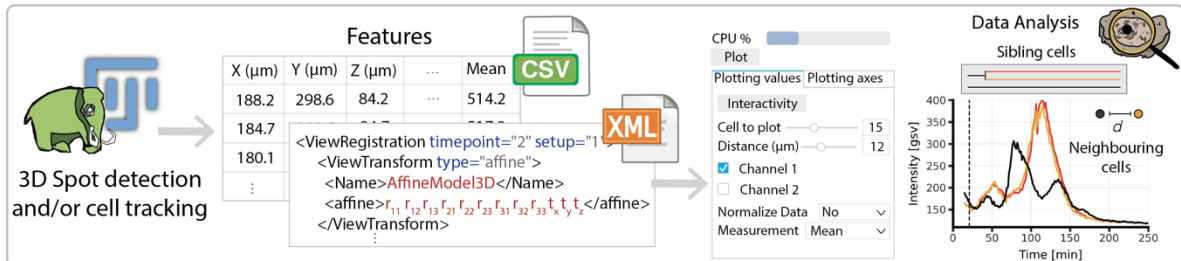


Figure 4. Cell tracking with Mastodon and analysis of tracks with Paleontologist. **A)** Layout we recommend for 3D tracking using Mastodon. Three BigDataViewer (BDV) windows are opened, each displaying a different view of the sample (XY, XZ and YZ). These views are also locked (using the lock symbol at the top left of the BDV window) so they all move synchronously through time while tracking. The track-scheme is also opened in one side and it is also locked so that the tracks can be easily and jointly inspected with the BDV windows. The Mastodon menu is also useful to have in hand since it is used to adjust tracking parameters, tags and sub-tags, to save, etc. **B)** Once tracking is done, we compute features (using the *compute features* button from Mastodon Menu, see A) and we obtain the comma-separated (csv) file with all the information needed for analysis. Paleontologist can then read this file and the XML file obtained when converting to HDF5 and use them to perform spatiotemporal analysis and cell track inspection with a user interface.

semi-automatically, we needed to acquire images every 90-120 seconds due to cell movement / mixing in the segmenting tissue.

Our timelapse movies run at least 6 hours (240 time points), with 90 sec intervals, a bit depth of 16, X-Y dimensions of 2048x2048 pixels, two channels, and 150 planes. A movie with these
5 parameters has the following size:

Time Lapse movie size = [240 x 16 x 2048 x 2048 x 2 x 150] bits x 1 byte/8 bites = 6 x 10¹¹
bytes = 600 GB

3.3 Center of mass tracking

To keep the segmenting tissue in the FOV, we automatically track the center of mass (COM)
10 of the Her1-YFP signal while acquiring the time-lapse (Figure 2C). COM detection was performed using a python environment that directly communicates updated coordinates to the microscope control system. To find the COM in our channel of interest, YFP, we use a cropped region (Figure S1A) of a single timepoint that has been XYZ max-projected in the YFP channel (Figure S1B). These projections are processed using a median filter and a gaussian blur to
15 smooth the signal, resulting in a filtered max projection that we binarized using an Otsu thresholding method (Figure S1C). COM is then calculated using this binary mask, and an offset value is produced corresponding to the XYZ distance that the FOV needs to shift when re-centering (Figure S1D). To prevent abrupt shifts, we set the movement to be maximum of 5µm per interval (Figure S1E). The following additional parameters can be adjusted: filter size
20 applied (Gaussian and Median); use of the entire field of view or a cropped section (in XYZ); start of tracking while imaging; and COM as a binary mask, in which the center of pixels is used, or an intensity mask, in which the brightest area acts as the COM.

3.4 Data compression

The resulting four-dimensional (XYZT) for each channel is saved as an OME-TIFF (Leigh et al., 2017; Besson et al., 2019) (Figure 2C), a standardized format that is read by most open-
5 source and commercial software. To make data easier to handle, during moving, processing and storage, we recommend compressing data during acquisition so that the output is a compressed ome.tiff file, which is easily read in Fiji. LZW (Lempel–Ziv–Welch) is an open-
10 source universal lossless data compression algorithm that is easy to implement. In the case of our timelapse movies, we obtain a reduction factor of 1:4, and can compress the data during acquisition if the imaging parameters permit this in terms of speed. If the compression speed is too low to run during acquisition or a better reduction factor is desired, a commercial solution, Jetraw (Dotphoton SA) allows for a 1:8 compression ratio at acquisition speed.

3.5 Quality Check

15 To avoid saving poor quality timelapse data, e.g., a movie in which the sample degrades, we perform a quality check in parallel to acquisition by saving a maximum-intensity projection for each timepoint as a tiff file (Figure S2) (see Table 1). The max projections are viewed throughout acquisition (using Fiji) without the memory and speed problems that would
20 otherwise be caused if trying to view the virtual stack.

3.6 Time registration

In order to stabilize the time-lapse images in time to improve the cell tracking, we registered
25 the 3D volumes from all timepoints using the first timepoint as the frame of reference.

Parameters can be tuned according to the sample and imaging parameters. We show the steps and the parameters we use in Figure S3 which can be used as a starting point.

4. Computing Hardware

Image processing and data handling was done using a HIVE (Acquifer Imaging), a powerful
5 centralized workstation for big-data storage and higher performance computing. Our HIVE is
equipped with a 24 GB Graphics Processing Unit (GPU), 500 GB of Random-access memory
(RAM), 10 TB Solid-state drive (SSD) (RAID5) and 130 TB Hard Drive Disk (HDD)
(RAID6). Data is stored in SSD while processing, then moved to the HDD for short-term
10 storage. The microscope computer where the data is saved during acquisition is connected
through a 10 Gbit cable to the HIVE to allow rapid transfer.

5. Software

Our main software platform was Fiji ([Schindelin et al., 2012](#)), which can be installed in
Windows, Max OS and Linux operating systems. Users requiring more than 2GB of RAM in
Fiji should run on a 64-bit operating system due to limitations in Java memory management on
15 32-bit systems ([Arganda-Carreras and Philippe, 2017](#)). The core functionality of Fiji can be
extended using plugins specified in the protocol. Fiji and its plugins used here can be found
along with installation instructions at the imagej.net website.

Paleontologist runs on Python 3.6 or above and installation instructions are on the GitHub
webpage (<https://github.com/bercowskya/paleontologist>). Install Anaconda Distribution
20 (Anaconda Inc, 2020) to include interactivity and the user interface.

Procedure

Sample preparation and Image Acquisition

1. REQUIRED: Image your sample on a light-sheet or confocal microscope with resolution parameters that enable cell tracking (our parameters are shown in Figure 2C).
5 Cell tracking works best in timelapses acquired at high temporal and spatial resolution relative to cell movement/mixing. The rule of thumb we use is that if you cannot follow the cell by eye, the automatic tracking will not be able to track it either.
TROUBLESHOOTING: Explore the range of spatiotemporal resolution in which tracking is feasible by acquiring short timelapses using various parameters, then view
10 as described in step 2 to see if you can visually follow the nuclei. Balance this acquisition rate against potential photo-toxicity and the projected file size over the time interval of interest.
2. OPTIONAL: Use a COM tracker (or other method than enables automated detection
15 of the ROI) to keep your ROI in the FOV (Figure 2C, S1).
3. OPTIONAL: We highly recommend data compression during or after acquisition (LZW, Jetraw).

20 Quality check of timelapses and data transfer

4. REQUIRED: Download the free, open-source image processing software Fiji (<https://imagej.net/software/fiji/#downloads>)(Schindelin 2012). Note that there are commercial and other open-source solutions for big image data inspection including Imaris (Oxford Instruments), Arivis Vision 4D (Arivis AG), Vaa3D (Bria, et al., 2015)

and TDat (Li, et al., 2017). However, since we use Fiji for our pipeline, we will mainly describe the processing and tracking plugins using this software.

5. REQUIRED: Generate a maximum-intensity projection of the timelapse (Table 1) using your image processing software of choice, then check the following to assess timelapse quality:

a. Visually check for photo-bleaching of the signal over time. A severe intensity decay could obscure the dynamics of interest, as well as interrupt cell tracking (Figure S2A).

10 TROUBLESHOOTING: Either alter the imaging parameters when possible (reduce exposure time, laser intensity, the frame rate) or correct using a tool like for example: Correction for photo-bleaching from Miura, 2021.

b. Using the re-slice tool from Fiji (Table 1), check whether the z-resolution is high enough so that the cells look like spot-like structures (Figure S2B). If the resolution is too low, the cells will appear almost like lines and the spot detection during cell tracking will not work.

15 TROUBLESHOOTING: Alter imaging parameters by reducing the pixel size in the z-axis.

20 6. REQUIRED: Transfer the checked timelapse to an image processing station. The specifications vary according to the size of the data and the desired waiting time between the processes. Because all of the tools we propose here can handle big data, the amount of RAM or the availability of a GPU will only improve the speed of the processing and the interactivity during the cell tracking. BigDataViwer (BDV) adapts

25

the size of the cache to the available memory (Pietzsch et al., 2015) and BigDataProcessor2 uses lazy loading and processing (Tischer, et al., 2021).

Data conversion

- 5 7. OPTIONAL: Crop the timelapse in XYZT to reduce file size (Figure 3B) using BigDataProcessor2 (BDP2, Tischer, et al., 2021), a Fiji plugin for processing n-dimensional big data images. Install by activating the *BigDataProcessor* Fiji update, then access using the graphical user interface or a Fiji macro. The timelapse OME-TIFF is loaded and displayed using BigDataViewer (BDV, Pietzsch et al., 2015), which
10 allows efficient lazy loading of raw data such that all processing steps are applied and then re-saved only once. When cropping, confirm that the sample remains inside the bounding cropping box by checking the initial, an intermediate and the last timepoint.

- 15 8. OPTIONAL: Detect chromatic shifts by looking for small XYZ shifts in normally overlapping signals (e.g., a nuclear marker and nuclear localized signal). Correction for shifts can be applied uniformly throughout the timelapse in BDP2.

- 20 9. REQUIRED: Convert the timelapse to HDF5 format (The HDF Group, 1997-2019) using BigDataViewer (Pietzsch, Tobias, et al., 2015). The HDF5 is associated with an XML file containing the metadata and all future registrations, etc. applied to the data. The XML-HDF5 should be stored in an SSD for fast reading and writing operations. When the conversion starts, the HDF5 and the XML are automatically created at the same time. All subsequent steps use HDF5/XML files.
25 TROUBLESHOOTING: The XML file and the HDF5 need to be in the same folder since the XML file has the path of the HDF5 which was used when it was created.

Therefore, if the XML or the HDF5 are separated in different folders, a reading error will appear when trying to open the data.

Time registration

5 10. REQUIRED: During extended time-lapse imaging, the sample might drift due to
growth or technical issues. This can make the cell tracking harder or sometimes not
possible. To compensate for this drift, the nuclei are used as markers to register
individual time-points to each other. We select a timepoint, usually the first, then use it
as a reference. To perform time registration, we propose Fiji Plugins Multiview-
10 Reconstruction ([Preibisch et al., 2010](#)) or BigStitcher ([Hörl et al., 2019](#)) as both are
compatible with the XML-HDF5 file format. An alternative to Fiji would be Elastix
([Klein et al., 2009](#); [Shamonin et al., 2014](#)), a toolbox for intensity-based medical image
registration. If the imaging setup allows it, for instance when performing multi-view
imaging, beads can be added and then used as registration markers ([Preibisch et al.,](#)
15 [2010](#)).

TROUBLESHOOTING: The registrations are not actually applied to the data, but
rather the matrices applied are saved for each timepoint in the XML (Figure 3D). This
is useful since backup XML files (saved as `~.xml`) are created in the process so that in
case the registration fails, you can go back to the unregistered XML file and try various
20 parameters without having to re-convert the data into XML-HDF5. However, this
should be taken into account because the cell tracking coordinates will be outputted in
the registered space.

a. Detect nuclei using the feature “Detect interest points”. We recommend using
the detection method “Difference of Gaussian (DoG)”. Two parameters need to
25 be defined for detection of interest points, an intensity threshold and a radius.
These parameters can be tested on a single timepoint before running the

detection for the whole timelapse. If the nuclear signal varies over time (for example in the case of photobleaching), we recommend tuning the detection parameters using a timepoint where the signal is weak.

- 5 b. Perform a first round of registration using the method “Fast description based” (rotation invariant) registration in which timepoints are registered individually. Moreover, all the views are compared to each other and the first time-point is fixed so that the rest of the time-points can map-back to it using the translational invariant model. The transformation is rigid affine. Figure S3A shows the parameters we apply to our segmentation clock timelapses, which can be used
10 as a starting point to tune parameters for other systems.
- c. Perform a second round of registration using the method. “Fast description based” translational invariant. In this case, because all timepoints are registered,
15 we need to perform group-wise optimization by reasonable global optimization to “all-to-all” time-points with range. As before, the first view is fixed and the rest map-backed using a translational model. The parameters we used (Figure S3B) will require fine tuning for each independent dataset, but it is a good start.
- 20 d. Using the Fiji plugin “Multiview reconstruction”, duplicate the transformation obtained using BigStitcher for the “nuclear marker” channel to the other channels. Multiview Reconstruction > Batch processing > Tools > Duplicate transformations.
- 25 e. Apply transformation of “One channel to other channels”.

TROUBLESHOOTING: Registration usually fails due to the poor alignment of the registration markers (nuclei or beads) over time. This can be corrected by improving the temporal resolution. Bright objects in the FOV that are not within the sample, for example lint or debris, can also disrupt registration.

- 5 TROUBLESHOOTING: Automatic registration can sometimes fail because of the sample ‘jumping’ or rotating significantly in a few timepoints during the acquisition (the embryo might fall on the side and adopt a new equilibrium position). The resulting discontinuities may prevent automatic tracking. It is possible to correct big discontinuities manually with a set of tools from the BigDataViewer-Playground library
- 10 (<https://imagej.net/plugins/bdv/playground-manual-registration>).

Spot detection and cell tracking

11. REQUIRED: The dataset is now ready for cell tracking using the Fiji plugin
- 15 “Mastodon”. Set up three BDV windows with orthogonal views. Synchronize the windows by locking each of them on view 1 by clicking on the first lock (Figure 4A). Select the channel corresponding to the nuclear marker, which will be used for tracking.
12. Set up the TrackScheme window and synchronize it with the BDV windows by locking each of them on view 1 by clicking on the first lock.
- 20 13. Familiarize yourself with the actions and their corresponding keyboard shortcuts. They can be found, and modified, in Mastodon > File > Preferences > Keymap.
14. Set up semi-automatic tracking (Mastodon > Plugins > Tracking > Configure semi-automatic tracker...) with the following parameters (information about the parameters is displayed by placing the cursor over a given parameter):

- a. Setup ID: Select the channel corresponding to the nuclear marker. This is the channel that will be used for tracking.
- b. Quality factor: This parameter depends on the dataset and needs to be empirically determined. A value of 0.5 is a reasonable starting point.
- 5 c. Distance factor: This parameter depends on the dataset, especially on how much cells move between time frames, and needs to be empirically determined. A value of 1.5 is a reasonable starting point.
- d. N time-points: This parameter specifies how many time-points can be processed at most. It does not affect the quality of tracking itself and can therefore be set
10 at a large number (e.g., 40).
- e. Tracking direction selection: Forward and back tracking in time can be performed.
- f. Untick “Allow linking to an existing spot” if performing semi-automatic tracking since if you already curated a track, it will stop the new track to start
15 following previously tracked cells.
- g. Tick “Run detection if existing spot cannot be found”

15. Place the cursor on one cell of interest and hit “A” to add a new Spot.

16. Adjust the size of the Spot to make it fit the nucleus by making the Spot smaller (“Q”) or bigger (“E”).

20 17. Click on the cell of interest, place the cursor inside the Spot added in step 14 and start semi-automatic tracking (Mastodon > Plugins > Tracking > Semi-automatic tracking or Ctrl + T).

TROUBLESHOOTING: If semi-automatic tracking fails, adjust tracking parameters.

If it still does not work, try a different timelapse with improved registration and adjusted
25 imaging settings.

18. Curate the track by visually inspection. Check that the cell of interest is followed through the entire track. Portions of a track can be deleted onwards from the timeframe where an error is made. OPTIONAL: tag the track with a label.
19. Save the Mastodon project regularly to avoid losing tracking data in case of software crash (“Save” button in the Mastodon window or Mastodon > File > Save project)
20. Repeat steps 17 to 19 until the cell of interest has been tracked for the desired duration.
21. Repeat steps 15 to 20 for each cell that needs to be tracked.
22. Compute the features of interest (“compute features” button in the Mastodon window).
23. Generate a results table (“table” button in the Mastodon window).
24. Export the table as a CSV file (Table window > File > Export to CSV).
25. To use Paleontologist, you need to load the CSV and the XML files. To see the details on how to use the documentation visit <https://github.com/bercowskya/paleontologist>.

FIJI PLUGIN NAME	USAGE	URL FOR WIKI	PROCEDURE STEPS
Z-FUNCTIONS	Max Intensity Projection	https://imagej.net/imagaging/z-functions	Image > Stacks > Z-Project Projection type: Max Intensity
Z-FUNCTIONS	R-Slice	https://imagej.net/imagaging/z-functions	Image > Stacks > Reslice
BIGDATAVIEWER	Convert into XML-HDF5	https://imagej.net/plugins/bdv/	1. Open time-lapse (as a virtual stack) 2. Export current image as XML/HDF5
BIGSTITCHER	Time registration	https://imagej.net/plugins/bigstitcher/	See Figure S3 for steps
MULTIVIEW RECONSTRUCTION	Duplicate Transformations to other channels	https://imagej.net/plugins/multiview-reconstruction	
MASTODON	Cell tracking	https://github.com/mastodon-sc/mastodon	

Table 1. Fiji Plugins name, usage, link to wiki and procedure steps.

5 References

- Amat, Fernando, et al. "Fast, accurate reconstruction of cell lineages from large-scale fluorescence microscopy data." *Nature methods* 11.9 (2014): 951-958.
- 10 Anaconda Software Distribution. "Anaconda Documentation." (2020).
- Arganda-Carreras, Ignacio, and Philippe Andrey. "Designing image analysis pipelines in light microscopy: a rational approach." *Light Microscopy*. Humana Press, New York, NY, 2017. 185-207.

- Attardi, Andrea, et al. "Neuromesodermal progenitors are a conserved source of spinal cord with divergent growth dynamics." *Development* 145.21 (2018): dev166728.
- 5 Besson, Sébastien, et al. "Bringing open data to whole slide imaging." *European Congress on Digital Pathology*. Springer, Cham, 2019.
- Bria, Alessandro, Giulio Iannello, and Hanchuan Peng. "An open-source VAA3D plugin for real-time 3D visualization of terabyte-sized volumetric images." *2015 IEEE 12th International Symposium on Biomedical Imaging (ISBI)*. IEEE, 2015.
- 10 de Medeiros, Gustavo, et al. "Multiscale light-sheet organoid imaging framework." bioRxiv (2021).
- Delaune, Emilie A., et al. "Single-cell-resolution imaging of the impact of Notch signaling and mitosis on segmentation clock dynamics." *Developmental cell* 23.5 (2012): 995-1005.
- 15 Erpf, Anna C., and Tamara Mikeladze-Dvali. "Tracking of centriole inheritance in *C. elegans*." *microPublication Biology2020* (2020).
- 20 Garcia, Monica D., et al. "Live imaging of mouse embryos." *Cold Spring Harbor Protocols* 2011.4 (2011): pdb-top104.
- Guo, Long, Shiro Ikegawa, and Chisa Shukunami. "Emergence of Zebrafish as a Model System for Understanding Human Scoliosis." *Zebrafish, Medaka, and Other Small Fishes*. Springer, Singapore, 2018. 217-234.
- 25 He, Zhisong, et al. "Lineage recording reveals dynamics of cerebral organoid regionalization." bioRxiv (2020).
- 30 Hirsinger, Estelle, and Ben Steventon. "A versatile mounting method for long term imaging of zebrafish development." *JoVE (Journal of Visualized Experiments)* 119 (2017): e55210.
- Hörl, David, et al. "BigStitcher: reconstructing high-resolution image datasets of cleared and expanded samples." *Nature Methods* 16.9 (2019): 870-874.

- Klein, Stefan, et al. "Elastix: a toolbox for intensity-based medical image registration." *IEEE transactions on medical imaging* 29.1 (2009): 196-205.
- 5 Kleinhans, David Simon, and Virginie Lecaudey. "Standardized mounting method of (zebrafish) embryos using a 3D-printed stamp for high-content, semi-automated confocal imaging." *BMC biotechnology* 19.1 (2019): 1-10.
- Kluyver, Thomas, et al. *Jupyter Notebooks-a publishing format for reproducible computational workflows*. Vol. 2016. 2016.
- 10 Leigh, Roger, et al. "OME Files-An open source reference library for the OME-XML metadata model and the OME-TIFF file format." *BioRxiv* (2017): 088740.
- Li, Yuxin, et al. "TDat: an efficient platform for processing petabyte-scale whole-brain volumetric images." *Frontiers in neural circuits* 11 (2017): 51.
- 15 Maroto, Miguel, Robert A. Bone, and J. Kim Dale. "Somitogenesis." *Development* 139.14 (2012): 2453-2456.
- 20 McConnell, Gail, et al. "A novel optical microscope for imaging large embryos and tissue volumes with sub-cellular resolution throughout." *Elife* 5 (2016): e18659.
- McDole, Katie, et al. "In toto imaging and reconstruction of post-implantation mouse development at the single-cell level." *Cell* 175.3 (2018): 859-876.
- 25 Miura, Kota. "Bleach correction ImageJ plugin for compensating the photobleaching of time-lapse sequences." *F1000Research* 9 (2020).
- Morelli, Luis G., et al. "Delayed coupling theory of vertebrate segmentation." *HFSP journal* 3.1 (2009): 55-66.
- 30 Oates, Andrew C., Luis G. Morelli, and Saúl Ares. "Patterning embryos with oscillations: structure, function and dynamics of the vertebrate segmentation clock." *Development* 139.4 (2012): 625-639.

- Pietzsch, Tobias, et al. "BigDataViewer: visualization and processing for large image data sets." *Nature methods* 12.6 (2015): 481-483.
- 5 Preibisch, Stephan, et al. "Efficient Bayesian-based multiview deconvolution." *Nature methods* 11.6 (2014): 645-648.
- Preibisch, Stephan, et al. "Software for bead-based registration of selective plane illumination microscopy data." *Nature methods* 7.6 (2010): 418-419.
- 10 Recher, Gaëlle, et al. "Zebrafish midbrain slow-amplifying progenitors exhibit high levels of transcripts for nucleotide and ribosome biogenesis." *Development* 140.24 (2013): 4860-4869.
- Rohde, Laurel A., et al. "Cell-autonomous generation of the wave pattern within the vertebrate segmentation clock." *bioRxiv* (2021).
- 15
- Royer, Loïc A., et al. "Adaptive light-sheet microscopy for long-term, high-resolution imaging in living organisms." *Nature biotechnology* 34.12 (2016): 1267-1278.
- Sage, Daniel, et al. "DeconvolutionLab2: An open-source software for deconvolution microscopy." *Methods* 115 (2017): 28-41.
- 20
- Sawada, Atsushi, et al. "Fgf/MAPK signalling is a crucial positional cue in somite boundary formation." (2001): 4873-4880.
- 25 Schindelin, Johannes, et al. "Fiji: an open-source platform for biological-image analysis." *Nature methods* 9.7 (2012): 676-682.
- Schmidt, Uwe, et al. "Cell detection with star-convex polygons." *International Conference on Medical Image Computing and Computer-Assisted Intervention*. Springer, Cham, 2018.
- 30
- Shah, Gopi, et al. "Multi-scale imaging and analysis identify pan-embryo cell dynamics of germlayer formation in zebrafish." *Nature communications* 10.1 (2019): 1-12.

- Shamonin, Denis P., et al. "Fast parallel image registration on CPU and GPU for diagnostic classification of Alzheimer's disease." *Frontiers in neuroinformatics* 7 (2014): 50.
- 5 Shih, Nathan P., et al. "Dynamics of the slowing segmentation clock reveal alternating two-segment periodicity." *Development* 142.10 (2015): 1785-1793.
- Soroldoni, Daniele, et al. "A Doppler effect in embryonic pattern formation." *Science* 345.6193 (2014): 222-225.
- 10 Tinevez, Jean-Yves, et al. "TrackMate: An open and extensible platform for single-particle tracking." *Methods* 115 (2017): 80-90.
- Tischer, Christian, et al. "BigDataProcessor2: A free and open-source Fiji plugin for inspection and processing of TB sized image data." *Bioinformatics* 37.18 (2021): 3079-3081.
- 15 Von Wangenheim, Daniel, et al. "Live tracking of moving samples in confocal microscopy for vertically grown roots." *Elife* 6 (2017): e26792.
- Weigert, Martin, et al. "Star-convex polyhedra for 3d object detection and segmentation in microscopy." *Proceedings of the IEEE/CVF Winter Conference on Applications of Computer Vision*. 2020.
- 20 Wen, Chentao, et al. "3DeeCellTracker, a deep learning-based pipeline for segmenting and tracking cells in 3D time lapse images." *Elife* 10 (2021): e59187.
- 25 Wolff, Carsten, et al. "Multi-view light-sheet imaging and tracking with the MaMuT software reveals the cell lineage of a direct developing arthropod limb." *Elife* 7 (2018): e34410.
- 30 Yoshioka-Kobayashi, Kumiko, et al. "Coupling delay controls synchronized oscillation in the segmentation clock." *Nature* 580.7801 (2020): 119-123.

Acknowledgements: We thank JiSoo Park, Pierre Osteil, Alexandre Mayran for testing the pipeline and generating feedback, J-Y Tinevez and T. Pietzsch for Mastodon assistance, EPFL's fish facility and Bioimaging and Optics Platform, P. Strnad and A. Boni for imaging help.

5

Supplementary Materials:

Figures S1 to S3

Supplementary Materials for

Title: **But, what are the cells doing? Image Analysis pipeline to follow single cells in the zebrafish embryo**

5

Authors:

Arianne Bercowsky-Rama^{1,†}, Olivier F. Venzin^{1,†}, Laurel A. Rohde¹, Nicolas Chiaruttini², Andrew C. Oates^{1,*}

Affiliations:

10 ¹Institute of Bioengineering, École Polytechnique Fédérale de Lausanne; Lausanne, CH

²BioImaging and Optics Core Facility, École Polytechnique Fédérale de Lausanne; Lausanne, CH

†Equal contribution

*Corresponding author. Email: andrew.oates@epfl.ch

15

This PDF file includes:

Page 2-4: Figures S1 – S3

20

25

30

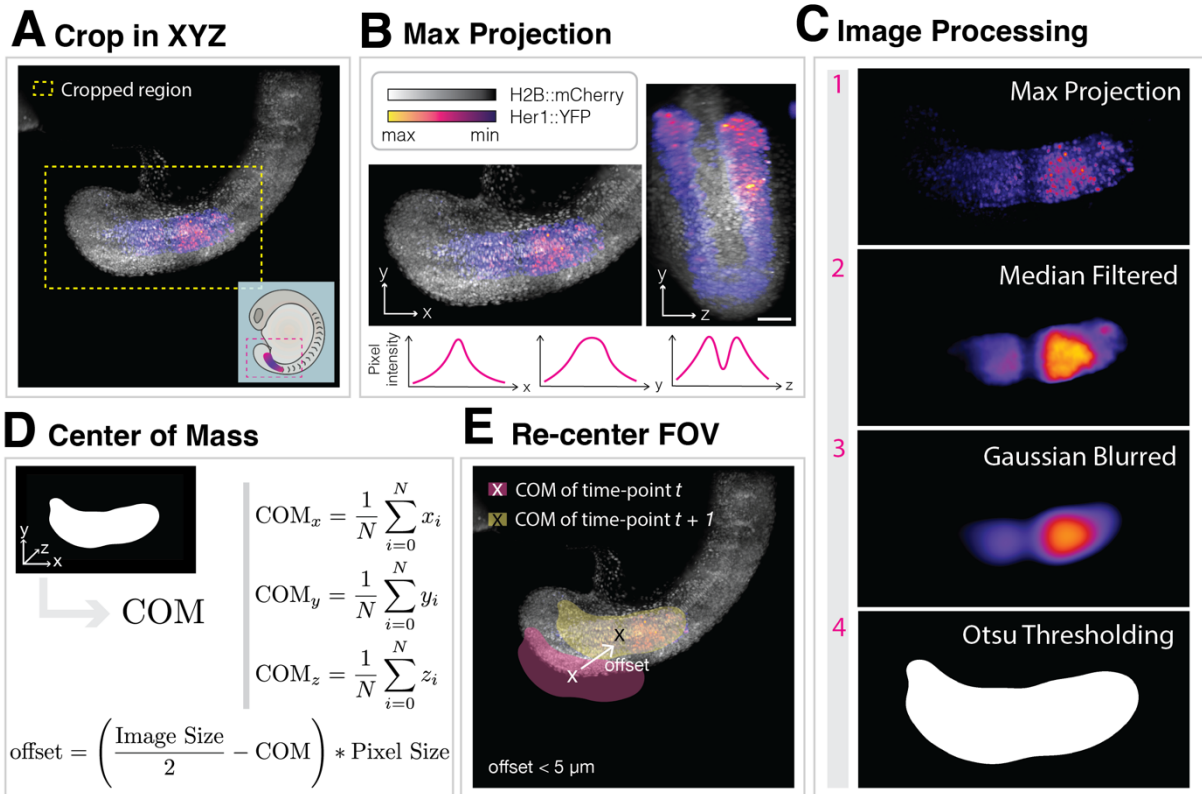
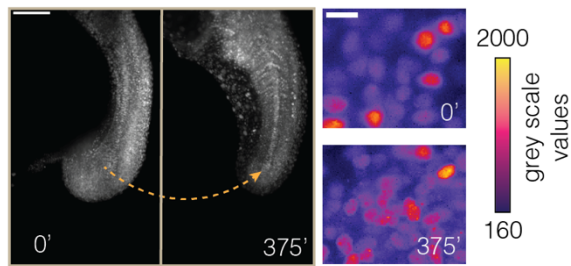


Figure S1. Centre of Mass calculation to re-centre the field of view. **A)** The first step is to crop the data in XYZ in order to only process the region of interest. **B)** Perform max projection of the cropped volume and of the desired channel to perform the COM tracking. **C)** Perform image processing steps to make it easier to obtain the COM. First, apply a median filter (filter size = 40 in this case), apply a gaussian blur ($\sigma = 40$). Finally, apply an Otsu threshold to binarize the images. **D)** Calculate the centre of mass (COM) from the binary image. This is done by performing the sum of all the coordinates (xyz) where the binary mask is equal to 1 and dividing by the number of pixels where the mask is equal to 1. **E)** The offset, as long as it is not greater than $5 \mu\text{m}$, apply to the next time-point in order to re-centre the field of view.

A Max Projection Quality Check

1) Max projection shows the quality of the signal and whether the COM tracker worked



B Re-slice Quality Check

2) Re-slice one timepoint to check Z-step size

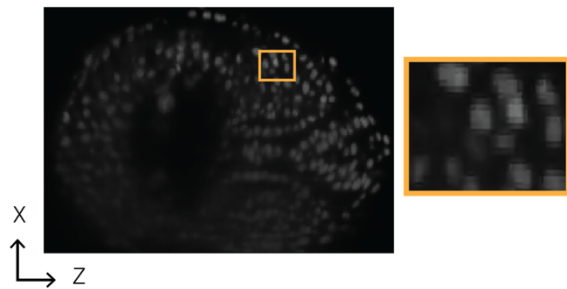


Figure S2. Quality checks. **A)** Once the acquisition is over, the first thing to check is whether the COM tracker worked and if there was any photo-bleaching or bleed-through. This can be checked using the maximum projection of the channels over time and observing whether the intensities have changed from the beginning to the end of the movie. A histogram can be displayed in Fiji by pressing the letter “h” (<https://imagej.nih.gov/ij/docs/menus/analyze.html#hist>). Error bars displayed (left to right) are 100 μm and 10 μm . **B)** Using Fiji, there is a re-slice option so that we can now change the view to observe whether the z-step size is good enough in order to observe blob-like structures. Otherwise, tracking will be more challenging. For example, these nuclei have a diameter of 10 μm and the z-resolution is of 1.5 μm .

A Registration part I - individual timepoints

Basic Registration Parameters

Registration algorithm: Fast descriptor-based (rotation invariant)

Registration over time: Register timepoints individually

Registration in between views: Compare all views against each other

Interest points: nuclei

Group Channels

Register: Register timepoints individually

Fix views: Fix first view

Map back views: Map back to first view using translational model

Algorithm parameters [Fast descriptor-based (rotation invariant)]

Transformation model: Afine

Regularize Model

Redundancy for descriptor matching: 3

Significance required for a descriptor match: 5

Parameters for robust model-based outlier removal (RANSAC)

Allowed error for RANSAC (px): 10

Number of RANSAC iterations: Normal

Regularization Parameters

Model to regularize with: Rigid

Lambda: 0.10

Select interest point grouping

Interpoint Grouping: Do not group interest points, compute views independently

Interest point merge distance: 5

B Registration part II - all-to-all timepoints

Basic Registration Parameters

Registration algorithm: Fast descriptor-based (translation invariant)

Registration over time: All-to-all timepoints matching with range ('reasonable' global optimization)

Registration in between views: Only compare overlapping views (according to current transformations)

Interest points: nuclei

Group Channels

Register: All-to-all timepoints matching with range

Range for all-to-all timepoint matching: 5

Consider each timepoint as rigid unit

Fix views: Fix first view

Map back views: Map back to first view using translational model

Algorithm parameters [Fast descriptor-based (translation invariant)]

Transformation model: Afine

Regularize Model

Redundancy for descriptor matching: 3

Significance required for a descriptor match: 10

Parameters for robust model-based outlier removal (RANSAC)

Allowed error for RANSAC (px): 5

Inlier factor (minimal amount of inliers): 3

Number of RANSAC iterations: Normal

Select interest point grouping

Interpoint Grouping: Group interest points (simply combine all in one virtual view)

Interest point merge distance: 5

Figure S3. Time Registration step-by-step. A) Load the XML file and the user interface will show. The first step is to perform registration on the timepoints individually using rotation invariant registration. B) As a second round of registration, load the XML file again and the user interface will again show. This time, the registration will be translation invariant and it will be applied to all timepoints matching with range.

Title: Paleontologist – Modular python package for spatiotemporal analysis of single cell tracks in a tissue context

Authors:

5 **Arianne Bercowsky-Rama**¹ and Andrew C. Oates^{1,*}

Affiliations:

¹Institute of Bioengineering, École Polytechnique Fédérale de Lausanne; Lausanne, CH

*Corresponding author. Email: andrew.oates@epfl.ch

10 **GitHub Repository**

<https://github.com/bercowskya/paleontologist>

Summary

The last step of most image analysis pipelines is the quantification and analysis of the obtained data to draw conclusions and produce figures. However, few tools exist to perform coding-free
15 useful plots. In particular, analysis of cells' behaviors in time-lapse imaging of developing tissues is a challenge. For this reason, we developed Paleontologist, a modular python package which enables publication-ready plots without prior coding experience. Paleontologist integrates seamlessly and interactively with the Fiji cell-tracking plugin Mastodon (<https://github.com/mastodon-sc/mastodon>). It is built by combining a group of Jupyter
20 Notebooks (Kluyver et al., 2016), which allow for temporal and spatial analysis merging the dynamics at the single cell scale with the tissue-level scale. This multi-scale analysis will be relevant for any application where cell behavior in the tissue context is important, for example in development or regeneration in organoids or embryos.

Statement of Need

The field of imaging large living biological specimens has expanded rapidly since the development of selective plane illumination microscopy (Huisken et al., 2004). This imaging technique allows the acquisition of multidimensional images of samples of a few millimeters in size with cellular resolution. As a result, the acquired time-lapse movies are on the order of hundreds of Giga-bytes (GBs) to Tera-bytes (TBs) and require dedicated processing and analysis tools. One of the main goals in acquiring this type of data is to understand the spatiotemporal dynamics of cells. Thus, 3D cell tracking has become a widely used technique and several tools have been developed in recent years for this purpose (Wolff et al., 2018; Tinevez et al., 2017; Amat et al., 2015). Mastodon, by Jean-Yves Tinevez and Tobias Pietzsch is a large-scale tracking and track-editing framework for multi-view big data. It is an open-source plugin from Fiji (Schindelin et al., 2012) that allows combining big-data visualization, with 3D cell tracking over time and includes a user interface that makes it very easy to use. After tracking the cells, Mastodon provides as output a large comma-separated (csv) file with many features of the cell traces, such as time-frames, coordinates (XYZ), average intensity, among others. Therefore, the challenge is how to reconstruct the tracks and cell divisions from the csv files and, moreover, how to easily process data for further analysis. So far, only custom codes have been reported for analyzing Mastodon cell tracks (de Medeiros et al., 2021; He, Zhisong et al., 2020). A generalised tool that simplifies the visualisation of temporal traces and allows easy and user-friendly interactivity with the resulting data is lacking.

Paleontologist is our new bioimage analysis software designed to meet the growing need for a user-friendly, extensible, open-source solution for cell tracking and whole sample image analysis. It is a modular open-source Python package that allows the visualization and sorting of individual cell traces obtained from Mastodon. The package is modular because it supports

different types of analysis (temporal, spatial and combined) and can be used by experienced users (calling functions and classes) or by users with no coding experience (via the user interface). This set of scripts also includes a group of Jupyter Notebooks (Kluyver et al., 2016) with interactive features and examples of how to perform different types of analysis.

5

Each notebook contains the interactive layout created with *ipywidgets* (<https://ipywidgets.readthedocs.io/>) so that the user can inspect the cell tracks in a simple and interactive way. Each notebook serves a different purpose and at the end of them there is a section explaining how the user can start coding their own project.

10

To use Paleontologist the first steps are to have the data ready for cell tracking with Mastodon. The time-lapse needs to be in a specific file format (XML-HDF5) to be used with Mastodon. Once the cell tracking is done, a csv file is exported with all the chosen features. Paleontologist then performs the analysis chosen by the user (Figure 1A). In addition, Paleontologist can edit the files obtained by Mastodon, e.g., exclude cells according to some features, and then open this edited file in Mastodon for visualization of the remaining traces. To label regions of the sample in 3D in a simple way, the Fiji plugin LABKIT (Arzt et al., 2022) can be used. As a result, these labeled regions can be used by Paleontologist to label, select or delete cell tracks.

15

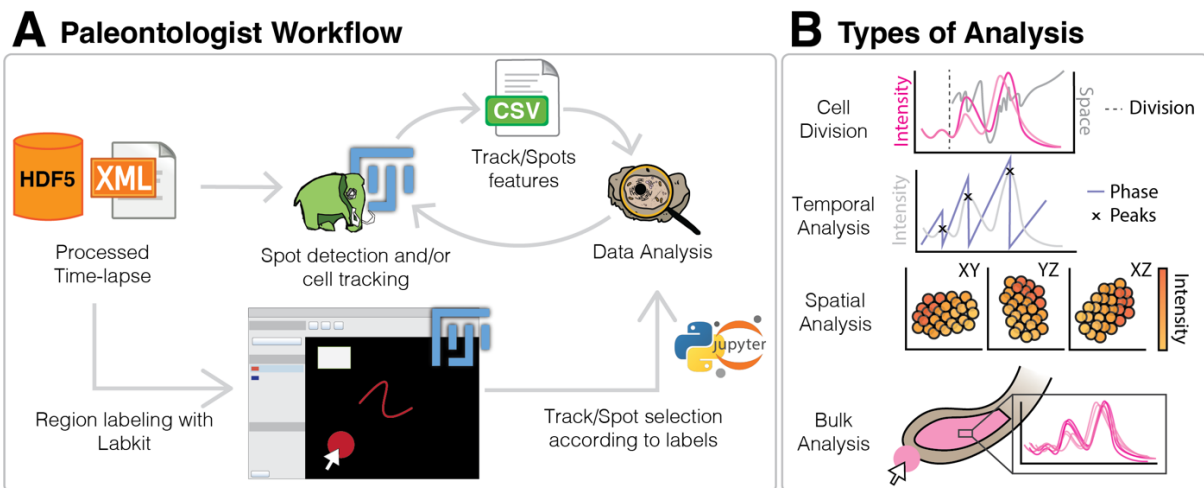
20

The package includes a Jupyter Notebook for example analysis and a user interface to perform (1) spatiotemporal cell division and cell neighborhood analysis, (2) temporal analysis such as peak detection and phase calculation of time traces, (3) spatial analysis using cell centroid coordinates and (4) bulk analysis, which allows the user to edit the Mastodon file using LABKIT labeled regions (Figure 1B).

25

Community impact

Paleontologist has been successfully employed in research articles (Rohde et al., 2021; Ozelci et al., 2022) and it is part of several ongoing projects.



5

Figure 1. Summary of Paleontologist workflow and main analysis.

Aknowldegments

10 We thank Yinan Wan, Ece Özelçi, Joan Rué-Queralt and Romain Guiet for the feedback and discussions on Paleontologist. We also thank Cristina Loureiro for making the beautiful logo.

References

15 Amat, Fernando, et al. "Efficient processing and analysis of large-scale light-sheet microscopy data." *Nature protocols* 10.11 (2015): 1679-1696.

Arzt, Matthias, et al. "LABKIT: labeling and segmentation toolkit for big image data." *Frontiers in Computer Science* (2022): 10.

20

de Medeiros, Gustavo, et al. "Multiscale light-sheet organoid imaging framework." *bioRxiv* (2021).

25 He, Zhisong, et al. "Lineage recording reveals dynamics of cerebral organoid regionalization." *bioRxiv* (2020).

<https://github.com/mastodon-sc/mastodon>

30 Huiskens, Jan, et al. "Optical sectioning deep inside live embryos by selective plane illumination microscopy." *Science* 305.5686 (2004): 1007-1009.

Kluyver, Thomas, et al. *Jupyter Notebooks-a publishing format for reproducible computational workflows*. Vol. 2016. 2016.

5 Ozelci, Ece, et al. "Deconstructing body axis morphogenesis in zebrafish embryos using robot-assisted tissue micromanipulation." *bioRxiv* (2022).

Rohde, Laurel A., et al. "Cell-autonomous generation of the wave pattern within the vertebrate segmentation clock." *BioRxiv*(2021).

10

Schindelin, Johannes, et al. "Fiji: an open-source platform for biological-image analysis." *Nature methods* 9.7 (2012): 676-682.

15

Tinevez, Jean-Yves, et al. "TrackMate: An open and extensible platform for single-particle tracking." *Methods* 115 (2017): 80-90.

Wolff, Carsten, et al. "Multi-view light-sheet imaging and tracking with the MaMuT software reveals the cell lineage of a direct developing arthropod limb." *Elife* 7 (2018): e34410.

20

Summary Chapter 1

In this chapter we have shown the standardised light-sheet microscopy imaging protocol used to acquire and process time-lapse movies to prepare them for single cell tracking. We acquire long movies, on the order of TBs, which need to be pre-processed to make them suitable for cell tracking, but also to facilitate data handling, transfer and storage. This protocol encompasses the knowledge we have gathered over the last few years on imaging, processing and analysis of light-sheet microscopy data. We hope that this protocol can help the community by showing the right set of software, hardware and advice needed to start acquiring big data to perform cell tracking. In addition, I have developed an open source data analysis tool called Paleontologist. It is a modular Python package that allows for spatiotemporal analysis of the cellular traces obtained.

This pipeline and Paleontologist have been used in chapters 2, 3 and 4 to reveal previously unknown dynamic patterns during somitogenesis, related to boundary positioning and precision mechanisms.

Chapter 2

Hunting for the determination front

The point along the AP axis where the somite boundary position is determined prior to morphological boundary formation is called the “determination front” (section 0.5.2). Amazingly, the determination front and the mechanism that established it remains elusive. According to the clock and wavefront model (Cooke and Zeeman, 1976), a gradient of timing (or maturation) controlled the wavefront where the clock interacts to create a segment-sized groups of cells (Figure 4, Introduction 0.4.1). In this model, the wavefront velocity in combination with the frequency of the segmentation clock controls where a boundary will be determined. In other words, each segment length (S) can be mathematically described at the steady state as being the product of the velocity of the wavefront (v) and the period of the clock (T), $S = vT$ (Oates, Morelli, and Ares, 2012). In this section we will explore how the somite length can be perturbed and how this affects the clock and the wavefront. In addition, we will explore the proposals of different models that suggest where and how positional information is read to make a somite boundary.

When Cooke and Zeeman, 1976 defined the model, there was no molecular evidence for the clock or what the timing gradient might be, only that the latter controlled maturation. Two decades later, the first molecular evidence of the clock came when Palmeirim et al., 1997 described *c-hairy* as a molecular oscillator in the chick PSM. This study showed that the oscillator arrested and that it so in spatial register with the somite boundaries, suggesting that the arrest might be important. It was subsequently proposed, based on studies of the *tbx6* mutant (*fss*), that as PSM cells mature along the AP axis, they acquire a wavefront activity that arrests cyclic gene expression and initiates somite formation (Holley, Geisler, and Nüsslein-Volhard, 2000). Therefore, a change in wavefront velocity (v) would be expected to result in an accelerated or delayed maturation of the PSM, which in turn leads to an alteration of the somite length (S).

This scenario could be the result of an extrinsic and/or intrinsic mechanism acting as the timing gradient. However, in the early 2000s, a group of studies demonstrated that perturbations in the FGF, Wnt and RA signalling gradients modified segment length (Sawada, Shinya, et al., 2001; Dubrulle, McGrew, and Pourquié, 2001; Aulehla, Wehrle, et al., 2003; Moreno and Kintner, 2004). Thus, signalling gradients (i.e. an extrinsic mechanism) became good candidates for the timing gradient-controlled wavefront, leaving the idea of an intrinsic mechanism playing a role unresolved.

FGF and Wnt signalling show long spatial gradients, with the highest levels being in the posterior of the embryo (Dubrulle, McGrew, and Pourquié, 2001; Sawada, Shinya, et al., 2001; Dubrulle and Pourquié, 2004; Aulehla, Wehrle, et al., 2003). As the tailbud elongates due to growth, gradients subsequently travel through the PSM, implying a decay of mRNA (Dubrulle and Pourquié, 2004). Prevailing models support the idea that these morphogen gradients maintain the oscillations and that the arrest occurs once signalling drops below a certain level. In the case of the zebrafish, these conclusions have been drawn mainly from fixed samples of early embryonic stages (up to 8ss), as at this stage, the embryos can be de-yolked and easily imaged. With modern acquisition techniques, we can now perform similar experiments as before, but across different stages of development, with live imaging (given the probes available for the molecule working *in vivo*) and good spatiotemporal resolution.

To investigate how, when and where spatial information is read by the cells to precisely and accurately form a somite boundary, I decided to start by examining perturbations of somite length by changes in the FGF signalling gradient. The reason is that there is a large body of literature on FGF perturbations and theoretical models describing attempts to understand how, when and where positional information is read by the cells (Ishimatsu et al., 2018; Naoki et al., 2019; Simsek and Özbudak, 2018). However, there is still no consensus on the role of the FGF signalling gradient during somitogenesis.

In this chapter I will focus on the following questions:

1. What is the relationship between different transient FGF inhibitions and the resulting longer somite? Is there an upper size limit for a somite?
2. We know that FGF is involved in the accuracy of somite boundary positioning, but does it also affect precision? When the FGF gradient is perturbed, the somites are larger/smaller, but what is the variability?
3. How is the spatial expression of dpERK, an FGF readout, during these inhibitions? Is there any relation between the observed phenotype (the longer somite) and the spatial expression of dpERK?

4. Can the FGF gradient alter the dynamics of the segmentation clock? As mentioned before, somite length can be affected by the velocity of the wavefront and the period of the clock ($S = vT$). [Sawada, Shinya, et al., 2001](#) showed using in situ hybridisation that at early stages, the last *her1* stripe was missing after transient inhibition of dpERK. They concluded that accelerated maturation caused this loss of the *her1* stripe, would live imaging of the Her1 signal support this proposal?
5. Where do cells read positional information? It has been hypothesised that somite - IV (S-IV) is the last region of the PSM where cells can respond to signalling gradients such as FGF. Furthermore, this region has been correlated with a threshold of the FGF readout, dpERK. However, these studies have been performed at very restricted developmental times. How does S-IV change with respect to the spatial profile of dpERK during development?

To answer these questions, I will perform a series of experiments with an inhibitor of the FGF receptor (FGFr), SU5402 ([Mohammadi et al., 1997](#)) using live imaging and antibody staining. This drug has been previously used to perturb the FGF signalling gradient to record changes in somite length ([Sawada, Shinya, et al., 2001](#); [Dubrulle and Pourquié, 2004](#); [Simsek and Özbudak, 2018](#)). In addition, to observe the effects of this inhibition on FGF pathway targets, we will use antibody staining for doubly phosphorylated ERK (dpERK) and observe the relationship between the resulting altered somite size and the down-regulation of the dpERK spatial profile. We will also analyse the effect of this perturbation on the dynamics of one of the clock genes, *her1*. Finally, we will use cell tracking to quantify the distance from the newly formed somite (SI) to the suspected position of the determination front, S-IV, and check how the spatial profiles of dpERK changes along the different developmental stages.

2.1 FGF signalling gradient modifies the accuracy but not the precision of somite boundary formation

2.1.1 Effect on somite length during SU5402 inhibition

One way to look at how FGF contributes to fixing the accuracy of somite boundary positioning is to perturb it. For this, previous work has relied extensively on the FGF receptor inhibitor, SU5402 ([Sawada, Shinya, et al., 2001](#); [Dubrulle and Pourquié, 2004](#); [Simsek and Özbudak, 2018](#)), used to inhibit FGFr1, the only FGF receptor detected in the PSM ([Sawada, Fritz, et al., 2000](#); [Yamaguchi, Conlon, and Rossant, 1992](#)). However, the

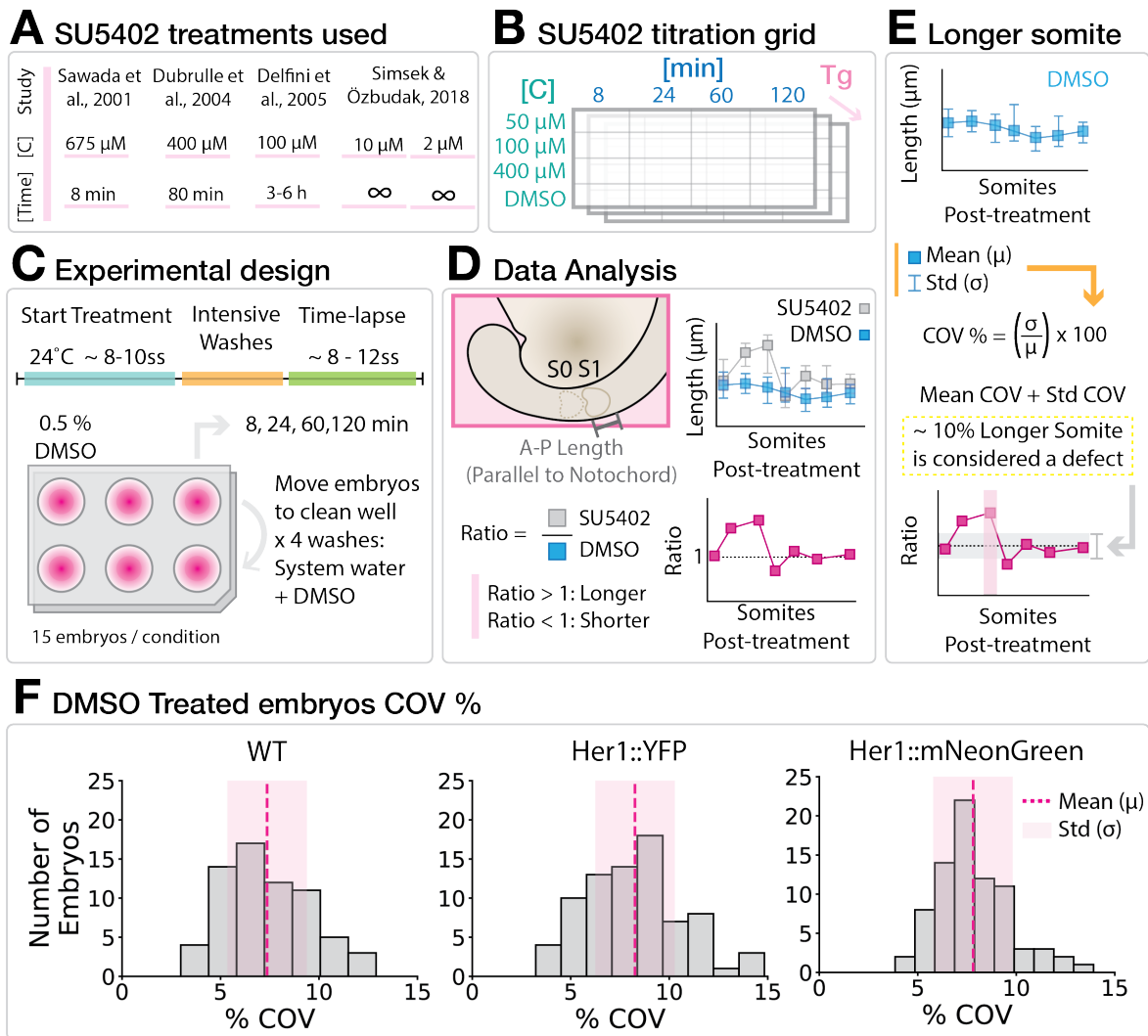


Figure 2.1: SU5402 Titration experimental design and analysis. **A.** Examples of concentrations for SU5402 found in the literature. The infinity symbol represents continuous treatment (no wash-out). **B.** The titration grid consisted of 4 different pulse durations, 3 concentrations of SU5402 with 0.5 % DMSO as a control and 3 different zebrafish lines (wild-type, Her1::YFP and Her1::mNeonGreen). **C.** Treatment was initiated around the 8 to 10-somite stage (ss) and was performed at room temperature (around 24°C). Using a 6-well plate coated with 2 % low-melting point agarose, the dechorionated embryos were treated with 0.5 % DMSO or SU5402 (Sigma). After completion of the treatment pulse, embryos were transferred to another coated well with system water plus 0.5 % DMSO, then washed with system water plus 0.5 % DMSO. Finally, the embryos were time-lapsed with a Zeiss Wide-field microscope in 2 % low-melting agarose coated wells with 0.02 % of Tricaine (Sigma) and E3 medium. **D.** Data was analysed by drawing a line parallel to the notochord in the anteroposterior (AP) direction for each somite post-treatment and for all embryos imaged. The mean and standard deviation for each treatment were then plotted as a function of length versus somite post-treatment. To assess whether the somites changed in size with respect to the control (DMSO), a ratio between the mean somite lengths of each treatment was plotted against the DMSO case. As a result, we obtained a somite length ratio for each post-treatment somite.

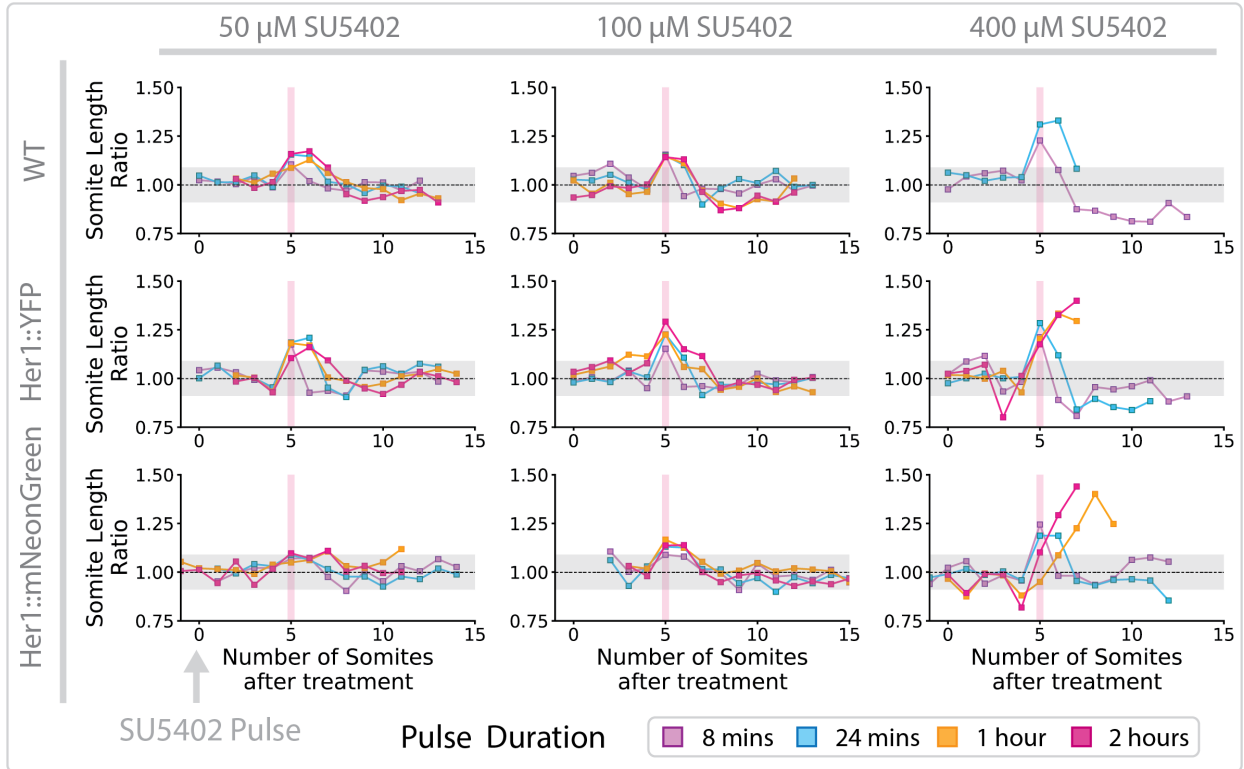
Figure 2.1: (Previous page) **E.** What is the criteria to define a longer somite? For each control experiment, the coefficient of variation (COV) of all post-treatment somites was calculated. The mean and standard deviation of this resulting COV was calculated. The critical percentage was then chosen using the sum of the mean COV plus the standard deviation of the COV. Any ratio showing a 10 % difference was defined as a change in somite length caused by the treatment. **F.** Percentage of COV for all somites of all embryos in the DMSO cases. The pink dashed line shows the mean and the shaded region shows the standard deviation plus-minus the mean.

concentration and pulse duration of this treatment vary many-fold between each study, making it difficult to compare and evaluate the conclusions (Figure 2.1 A). To better understand how the FGF signalling gradient affects somitogenesis, I titrated 4 different pulse durations (8, 24, 60, 120 minutes) and 3 different concentrations of SU5402 (50, 100, 400 μ M) using 0.5% of DMSO as a control. In addition, 3 different types of embryos (at 8ss) were used: 2 transgenic lines (Her1::YFP and Her1::mNeonGreen) and 1 WT line (Figure 2.1 B). These transgenic lines are included in this experiment because they will be used later to analyse the clock dynamics (to know more about these lines see Figure 5.11 B, C). After each treatment, the embryos were transferred to a clean well where they were washed extensively to remove the drug (Figure 2.1 C). Time-lapses were acquired using wide-field microscope. We analysed the effect on somite length by drawing a line of interest (LOI) parallel to the notochord to measure the anteroposterior length of each segment post-treatment. The resulting distributions were normalised using the DMSO condition to obtain a ratio of how much larger or smaller the treatment-induced somite was (Figure 2.1 D).

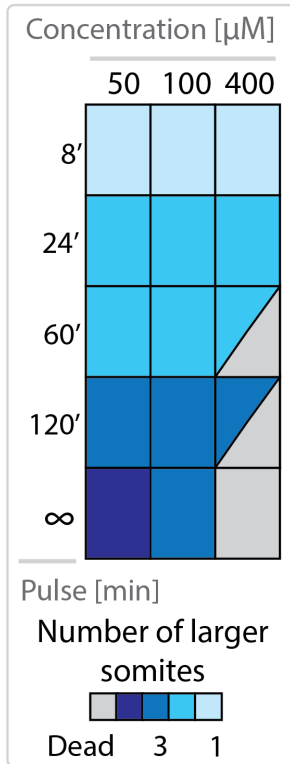
As mentioned above, when comparing somite lengths between embryos there is a certain distribution. Therefore, how do we distinguish between a longer somite due to the treatment versus a longer somite due to intrinsic variability of somite length? To do this, I collected all somite lengths in the DMSO-treated embryos and calculated the mean and standard deviations for each somite stage. Then, I calculated the coefficient of variation (COV), a unit-less measure of variation, producing distributions for each zebrafish line used (Figure 2.1 F). As a result, any variation greater than the standard deviation of these coefficient of variation distributions would be considered a longer somite. Based on the COV, the critical value was set at 10 %, meaning that any deviations in the ratios greater than 10 % were considered changes due to treatment (Figure 2.1 E).

Consistent with previous publications, the fifth somite after treatment (shown as a vertical pink line in Figure 2.2 A), was the first longest somite we observed (Sawada, Shinya, et al., 2001; Ishimatsu et al., 2018). No matter the strength or duration of the pulse, 4 normal somites formed before the longest somite. This 4-somite delay indicates the presence of a transition region in the PSM beyond which cells do not respond to

A Comparison of somite size ratio after SU5402 titration pulses



B Summary



C Comparison of standard deviations of somite sizes

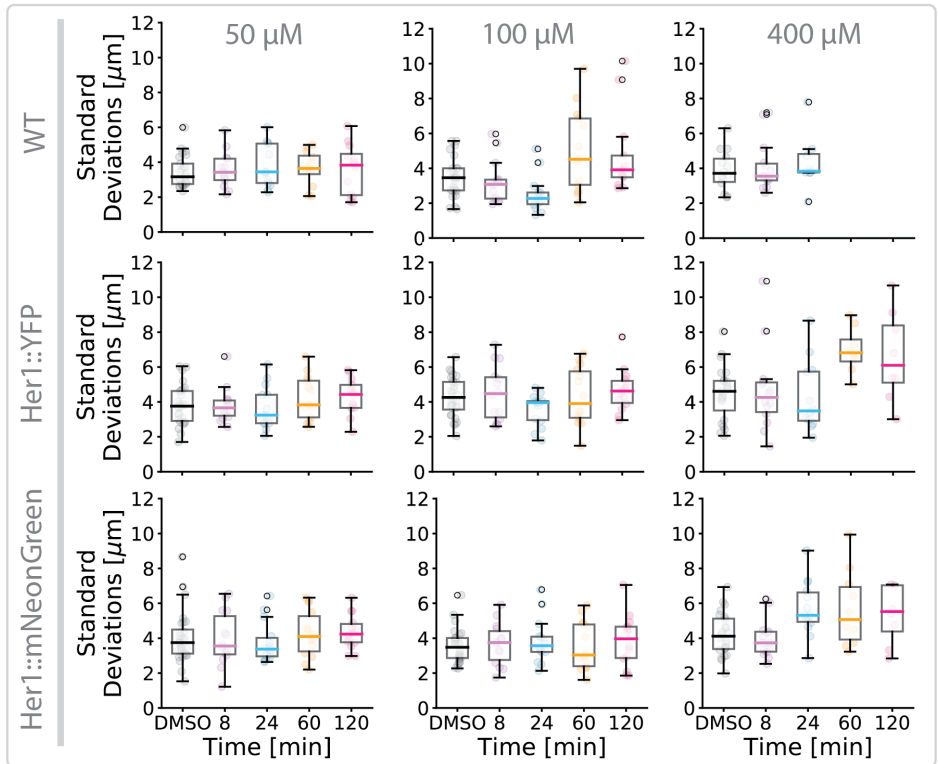


Figure 2.2: SU5402 Titration results - precision vs accuracy in somite boundary positioning.

Figure 2.2: (Previous page) Titration experiment was performed on wild-type (WT) and 2 transgenic lines (Her1::YFP and Her1::mNeonGreen). All experiments included 8-10 embryos per condition. Concentrations of 50 μ m, 100 μ m and 400 μ m were used to assess phenotype severity. In addition, pulses spanned 8 minutes, 24 minutes, 1 hour and 2 hours. **A.** The figures show the ratio of the mean somite length for that particular treatment and somite to the DMSO case. The pink line shows the 5th somite after the treatment. The dashed black line shows when the ratio is equal to 1 (meaning the same somite length for the SU5402 and DMSO treated cases). The shaded horizontal regions show a 10% increase or decrease of the ratio. **B.** Table showing the overall results of the SU5402 titration experiment. In blue, the maximum number of longer somites according to the chosen criterion. In grey, the cases in which cell death was observed. Partial or complete grey squares correspond to the level of cell death observed. **C.** Standard deviations from somite length for all the somites in from a given condition and experiment. Comparing the SU5402 treated conditions versus their corresponding DMSO gave rise to non-significant differences (Mann–Whitney U test).

FGF signal. This region could correspond to the distance from the anterior end of the PSM to the determination front, a point along the axis where FGF no longer participates in the delivery of spatiotemporal information (Dubrulle, McGrew, and Pourquié, 2001).

High concentrations and long exposure to the treatment resulted in high cell death in the tailbud and elongation problems. In addition, for all conditions, the overall increase in observed somite length was between 25-40 %, which at this stage corresponds to 12-20 μ m (somite length at 12ss \sim 50 μ m). Even when we increased SU5402 concentrations, passing the point of cell death and elongation problems, the change in somite length reached a limit. At concentrations without cell death and elongation problems, the largest change we observed was 30 %. These findings reinforce the idea that there might be other mechanisms, e.g. signalling gradients such as Wnt and RA, that act in combination with FGF (Stulberg et al., 2012). Thus, when FGF is being compromised by the inhibitor, Wnt and/or RA could act as backup mechanisms to avoid having an even longer somite.

Figure 2.2 B summarises our findings of the number of longer somites in each of the conditions of the titration experiment and whether cell death was observed. The periodicity of somites was analysed in all embryos, but no significant changes were observed, as expected (Simsek and Özbudak, 2018). However, the temporal resolution of the movies was 5 minutes, so a faster rate should be explored to avoid missing possible minor changes in the period. Assuming the period did not change, the expected effect was that the number of longer somites would be defined by the number of somite cycles affected given the duration of the treatment. Considering the period of somite formation (30 minutes at 24°C), we had expected that a 24-minute inhibition of FGF would result

in one longer somite, and a 2-hour pulse would result in 4 longer somites. We find that 24 and 60-minute inhibition of FGF result in 2 longer somites whereas 120-minute result in 3 (Figure 2.2 B). These results are not in agreement with what we expected. However, they are consistent with previous studies performing similar perturbations. In [Ishimatsu et al., 2018](#) they reported that longterm inhibition using SU5402 (but at low concentration, $16\mu\text{M}$) only resulted in one longer somite. However, [Cotterell, Robert-Moreno, and Sharpe, 2015](#) performed a long-term experiment in chick with a higher SU5402 concentration ($50\mu\text{M}$), and observed 3 longer somites. Thus, from our data and previously reported findings, the number of longer somites produced after adding SU5402 seems to be related to the duration and concentration of the pulse. However, the pulse duration does not correspond to the observed number of longer somites.

The average position of the somite boundary shifted more posterior during the SU5402 treatments, resulting in a change in accuracy (Figure 3 B). However, the precision did not change, e.g. the standard deviations when measuring somite length did not differ significantly (Figure 2.2 C). This is consistent with the results reported by [Sawada, Fritz, et al., 2000](#), where embryos treated with an 8-minute pulse of $675\mu\text{M}$ SU5402 had a similar somite length variation as of the DMSO-treated embryos. Therefore, the resulting longer somites are precisely formed.

2.1.2 dpERK spatial profile during longer somite formation

Next, we sought a closer look at the spatiotemporal pattern of the FGF signalling gradient in the WT case and during these transient inhibitions. We used dpERK antibody staining to observe how the spatial profile of dpERK changed during different SU5402 pulses since it allows us to compare with previous studies ([Sawada, Fritz, et al., 2000](#); [Akiyama et al., 2014](#)). We fixed embryos every 30 minutes from the 8-somite stage to the 15-somite stage. We then captured 3D tissue images using a wide-field microscope. Finally, we obtained a maximum projection and by drawing a line of interest (LOI) parallel to the notochord we were able to quantify the spatial dpERK distribution (Figure 2.3 A).

Figure 2.3 B shows a doubling of dpERK intensity during the formation of the 5 somites (8ss - 13ss) in the WT scenario. As observed, dpERK changes rapidly, while the somite length remains relatively constant in the first 4 somites formed ($50 - 55\mu\text{m}$). This suggests that the maximum intensity of the dpERK spatial profile is a poor readout of the somite boundary positioning. Along the same line, when we deliver an 8-minute SU5402 pulse (Figure 2.3 C), regardless of the concentration used we get a single large somite. If dpERK alone controlled boundary positioning, then for this set of treatments we would expect a profile in which ERK reactivation occurred in time to

correctly position the subsequent somites. However, in Figure 2.3 D, we can see that 30 minutes after the SU5402 pulse, the dpERK profile has not recovered in 100 and 400 μM SU5402 concentrations. Moreover, [Sawada, Shinya, et al., 2001](#) showed, using western-blot, that dpERK took 3 hours to fully recover after an 8-minute pulse of 675 μM SU5402. This again suggests that dpERK is not the direct readout of the wavefront and that other mechanisms are put in place to compensate for the FGF inhibition, like for example Wnt and RA.

RA is synthesised in the formed somites, thus every time a new somite is formed, a new source of RA is produced ([Swindell et al., 1999](#)). In chick embryos, the up-regulation of FGF represses the levels of *Raldh2*, the RA-synthesising enzyme ([Corral et al., 2003](#)). Moreover it was shown that embryos treated with Disulphiram, blocked RA production and smaller somites resulted from an FGF gain of function ([Vermot and Pourquié, 2005](#)). In *Xenopus* embryos treated with SU5402 (FGFr inhibitor), *Cyp26* expression was reduced ([Moreno and Kintner, 2004](#)). Although these studies provide evidence to support that RA could be acting as an antagonist mechanism when FGF is compromised, further experiments exploring RA expression during SU5402 treatments in zebrafish should be conducted.

[Stulberg et al., 2012](#) reported cross-regulation between FGF and Wnt in the zebrafish TB. They showed that SU5402 treatment leads to increased expression of *dkk1*, a Wnt inhibitor, suggesting FGF promotes Wnt signalling through the inhibition of Wnt antagonists. [Bajard et al., 2014](#) showed that by controlled activation of *dkk1* using heat-shock inducible transgene, the effects observed on the wavefront were not dependent on alterations to the FGF signalling. However, because perturbations on Wnt and FGF produce similar effects on somite lengths ([Aulehla, Wehrle, et al., 2003](#); [Sawada, Shinya, et al., 2001](#)) and similar delays on the appearance of the longest somite ([Bajard et al., 2014](#)), these two signalling gradients are likely to provide parallel inputs to the cells.

Further studies on the integration of Wnt, RA and FGF are needed to address the mechanisms underlying the precise positional information they provide to cells.

Models supporting dpERK spatial profile as readout for positional information

Given that manipulations of Wnt and FGF signalling gradients lead to changes in somite length ([Sawada, Fritz, et al., 2000](#); [Dubrulle, McGrew, and Pourquié, 2001](#); [Aulehla, Wehrle, et al., 2003](#)), it has been assumed that the somite boundary is established by a simple gradient threshold: the level of FGF and/or Wnt defining a position along the PSM that allows segmental determination of prospective somites ([Hubaud and Pourquié,](#)

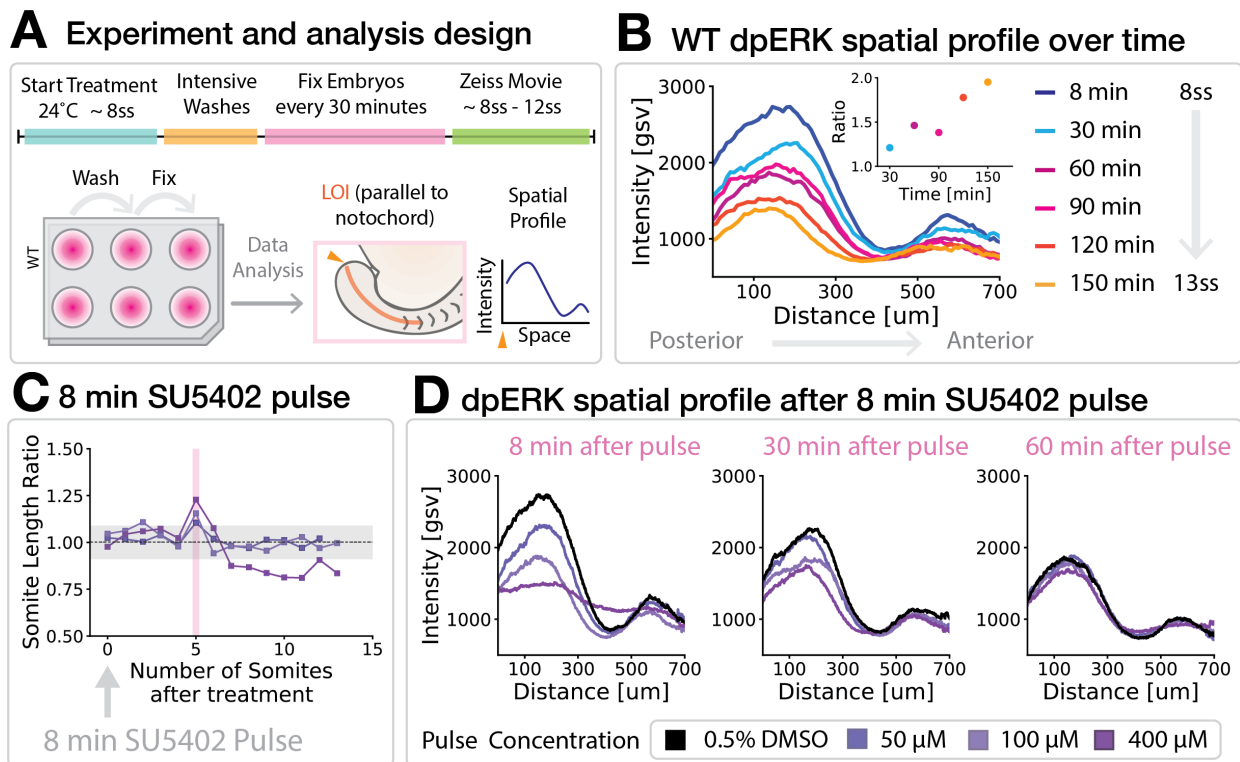


Figure 2.3: dpERK profile in WT embryos and during SU5402 transient inhibition. A. Experimental and analytical design. First (if necessary), SU5402 treatment and washout was performed starting at 8ss. Treated and untreated embryos were fixed every 30 minutes then stained for dpERK and DAPI. Finally, snapshots were acquired using a Zeiss wide field. To obtain the spatial profile of dpERK, we drew a LOI parallel to the notochord in a maximally projected snapshot. **B.** Spatial expression of WT dpERK by antibody staining in embryos from 8ss to 15ss. Curves show the mean spatial expression of 10 embryos per condition. Ratios were calculated using the 8ss dpERK curve as a reference. The ratio shows the reduction of the fold change compared to the 8ss curve. The time axis represents the fixation times that represents with the formation of each newly formed somite (at 24°C somites form every 30 minutes). **C.** Ratio of somite length for all the concentrations shown in Figure 2.2 A but clustering together all the 8-min pulses. **D.** Spatial profiles of dpERK antibody staining of embryos from 8ss. Embryos were treated with 8 min pulses of 50, 100 and 400 μM of SU5402 and 0.5% DMSO as control. After washout, the embryos were fixed at 8 min, 30 mins and 60 mins.

2014). How the FGF signalling gradient is read out to provide positional information has been proposed in several studies with the help of theoretical models.

Ishimatsu et al., 2018 proposed that somite boundaries are formed given a specific clock phase and a threshold of the gradient of FGF. The threshold is calculated as the location on the PSM where the relative intensity of dpERK profile crosses 50 % of the

maximum intensity (referred to as L50). [Naoki et al., 2019](#) proposed a model in which cells at a given threshold of dpERK suppress the activity of neighbour cells giving rise to a stepwise regression of the dpERK profile and positioning the somite boundary. [Simsek and Özbudak, 2018](#) proposed that positional information is delivered to cells by comparing a signal fold change (SFC) of dpERK. When the SFC exceeds a threshold, the presumptive somite boundary is placed. All of these models show different ways to read dpERK spatial profile to provide positional information. However, when we perform our transient FGF inhibition with high SU5402 concentration, 675 μM ([Sawada, Shinya, et al., 2001](#)), we obtain a flat dpERK profile (Figure 2.4 B). If the spatial profile of dpERK is the signal used by the cells to read positional information and thus locate a somite boundary, when the curve becomes flat, the cells would lose their spatial orientation.

Taken together, what we learned from this titration experiment was:

- Regardless of pulse duration or concentration, the fifth somite is always the longest. The number of consecutive longest somites depends on the SU5402 pulse duration and concentration but, does not correspond to the recovery time of the intensity of the spatial expression of dpERK. We suggest that dpERK is not the direct readout of the wavefront that positions somite boundaries or that it might act in convolution with other signals. Further experiments should be performed to fully understand why dpERK takes longer to recover the spatial profile (up to 3 hours, depending on the concentration and pulse duration). One possibility is that FGFRs are inactivated or degraded during the pulse and then it takes time to make new ones. It has been shown that SU5402 inhibits the tyrosine kinase activity of the FGFR which prevents the transmission of signals by sequential phosphorylation of downstream kinases ([Mohammadi et al., 1997](#)). SU5402 binds the ATP-binding domain of FGFRs through hydrogen bonds ([Liang et al., 2012](#)), strong dipole-dipole interactions. Thus, quantification of the FGFR during the treatments will provide more insight on how are the receptors affected by SU5402 during and after the treatment.
- The largest change in somite boundary positioning (at 8ss - 10ss) is 25-40 %, which corresponds to 12-20 μm or, in other words, 2-3 cells in diameter. In terms of tissue scale, this is a very small perturbation as the length of the PSM at 8ss is about 400 μm . We suggest that a redundant mechanism, such as another signalling gradient, is acting to prevent the formation of even longer somites as we increase FGF inhibition. One possibility is RA, which originates from the forming somite and antagonises the gradient of FGF ([Corral et al., 2003](#); [Vermot and Pourquié, 2005](#)). In addition, the parallel input provided to the cells by Wnt signalling could also mitigate the effects on somite length ([Bajard et al., 2014](#)).
- No somite boundary defects were observed, even at high concentrations and long

pulses. Additionally, overall variability of somite length between treated embryos remained constant, even when a longer somite was formed. Thus, FGF appears more involved in somite boundary positioning, i.e. accuracy, rather than driving the precision of boundary formation.

2.2 Changes in the clock and maturation during FGF signalling perturbations

The clock and wavefront mechanism translate the temporal information of an oscillator into a fixed periodic pattern in space (Cooke and Zeeman, 1976). As mentioned above, at the steady state, the length of each somite (S) can therefore be described as the product of the velocity of the wavefront (v) and the period of the clock (T), $S = vT$ (Oates, Morelli, and Ares, 2012). In the clock and wavefront model, a change in the velocity of the wavefront is given by a change in the timing gradient of maturation. In the following sections we explore how are the period of the clock and maturation affected during perturbations of the FGF signalling gradient.

2.2.1 The temporal dynamics of the clock gene *her1* are not affected in FGF perturbations

I have shown that, over a wide range duration and concentration of the perturbation to the FGF signalling gradient, somite boundary position can be shifted. Importantly, this shift is done precisely among all treated embryos. This suggests that FGF can affect the accuracy of the positioning of the boundary but not its precision. This change can be due to changes in the wavefront velocity or the periodicity of the clock. In this section we will explore whether the changes we observed are due to changes in the period of the clock. Sawada, Shinya, et al., 2001 suggested that the oscillator was unaffected, as posterior PSM *her1* expression patterns in SU5402 treated embryos at 2ss indicated cyclic expression. However, the clock has never been imaged live during an FGF perturbation experiment in zebrafish and in situ hybridisation cannot reveal the true dynamics.

To follow somitogenesis, we acquired movies of embryos carrying a Her1-mNeonGreen (Her1-mNG) transgene using wide-field imaging. These embryos were treated for 8 minutes starting at 8ss with 2 % DMSO and 675 μ M SU5402, resulting in a longer fifth somite (Figure 2.4 A). These are the same pulse duration and concentrations Sawada, Shinya, et al., 2001 used in their study. Additionally, dpERK antibody staining

Figure 2.4 B, showed that dpERK levels in these embryos went flat 8 minutes post-treatment then took 3 hours to recover, consistent with data in [Sawada, Shinya, et al., 2001](#).

To describe *her1* dynamics, we drew a line of interest parallel to the notochord for each time point to build a kymograph. Kymographs, Figure 2.4 C allow visualisation of Her1-mNG waves moving anteriorly through the PSM then arresting upon somite boundary formation. Using the kymograph of treated and control embryos, we determined the anterior and posterior periods of *her1* by calculating the time elapsed between two consecutive intensity peaks, as done in [Soroldoni, Jörg, et al., 2014](#). As a result, we found no change to periodicity during the course of the experiment. This suggests that the dynamics of *her1* are robust to variations in the FGF gradient, in line with the results of the titration experiment in the previous section, where the periodicity of somite formation was not affected.

We noticed that the spatial pattern of the Her1-mNG waves in the kymograph was different in the two embryos. To investigate this, I calculated the peak values at the anterior end, and then fitted a line (Figure 2.4 C, dashed white line) to get an idea of where the Her1-mNG waves stop relative to the posterior end. Comparing these two curves, we found that Her1-mNG waves in SU5402-treated embryos stop earlier, almost 40 μm more posterior than in control embryos. Although this arrest occurs in time with the appearance of the longest somite, it does not correspond spatially with the size of the longer somite. The 13th somite was 54 μm in the control embryo versus 76 μm in the SU5402-treated embryo. The difference in somite length is 22 μm , while the waves stop 40 μm earlier. This spatial mis-match between Her1-mNG wave arrest and somite boundary shift suggests that there may be other factors, such as elongation problems, at work in the SU5402 treated embryo. Since we are using the most posterior point as a reference, the wavefront velocity is not relative to the last boundary formed, but to the TB. This measure is convenient when there are no problems in elongation but now that there might be, elongation changes are convolved in this measure. Moreover, anterior maximum intensity of Her1-mNG is not a good proxy for somite boundary positioning. To better understand the contributions of earlier maturation and changes in elongation, in the next section we use the last formed somite to measure the size of the PSM and compare it with the size of the longest somite during SU5402 treatment.

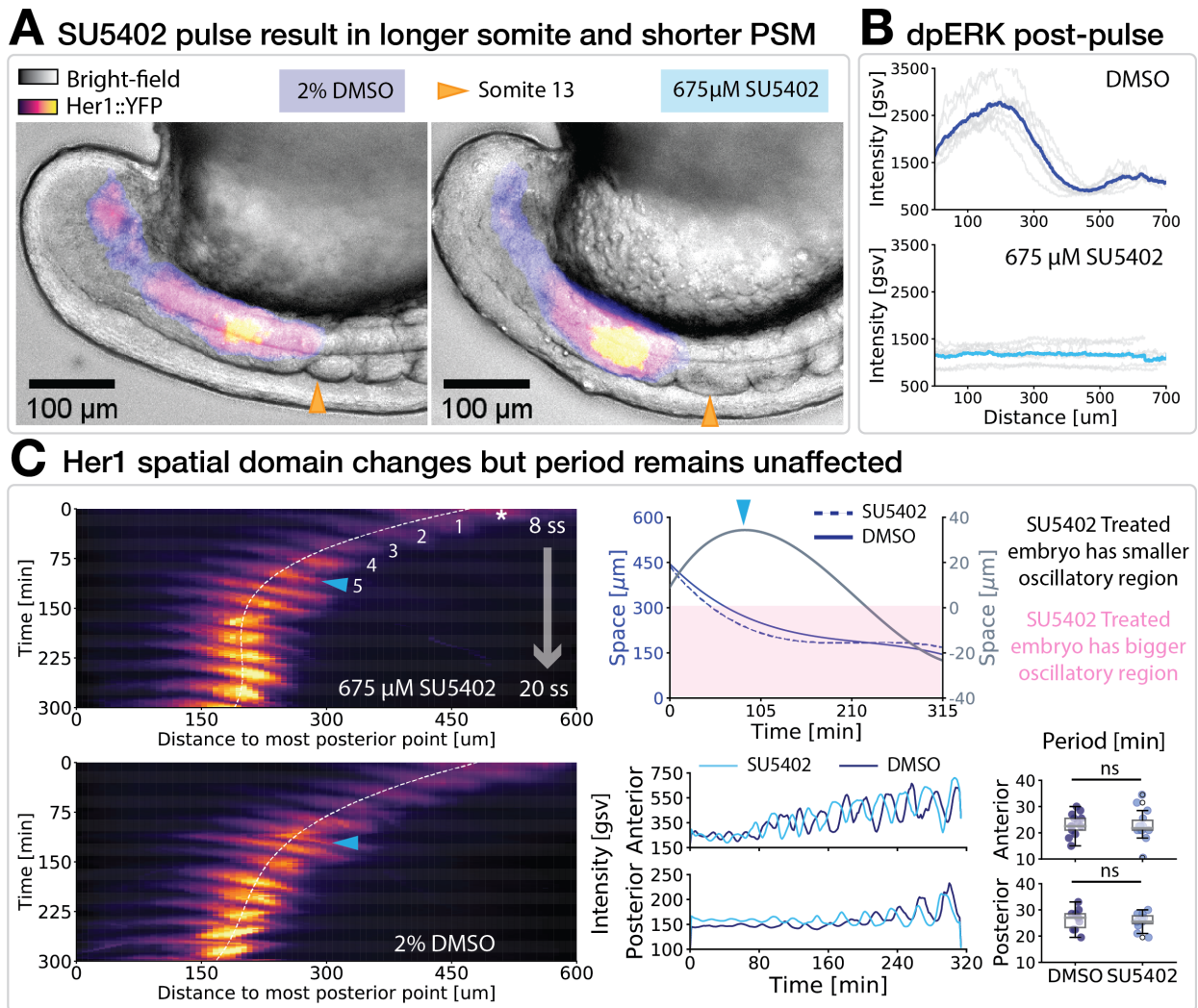


Figure 2.4: Her1-mNG dynamics during transient SU5402 inhibition. **A.** Snapshot of embryos treated with DMSO and SU5402 during the formation of the longer somite shown with an orange triangle (13ss, 5 somites post-treatment). **B.** In parallel, embryos after the 8 min treatment were washed and fixed. Staining with dpERK antibody was performed and the spatial profile was obtained as previously (N=10). In grey lines, each individual embryo and in blue the mean over space. **C.** Example kymograph of a light-sheet microscopy time-lapse of an embryo treated with 675 μ M of SU5402 (top panel) and with 2 % DMSO (lower panel). They were imaged in parallel starting from the 8ss until the 20ss. The asterisk (*) show the time of the treatment and the numbers are the somites formed before the longer one (the fifth, shown by a blue arrowhead). The dashed white line was fitted from the maximum Her1-mNG values over time in the kymograph. These two fitted lines were compared in the top right graph. The blue lines are the fitted lines for each condition and the grey line represents the difference of these lines over time (right axis, different scale). The white region shows maximum Her1-mNG

Figure 2.4: (Previous page) values in the anterior PSM. These lines are later compared in the graph on the right to show that in the SU5402 treated embryo, the oscillatory region is smaller (in the white area) but then becomes larger (in the pink area). From these fitted lines, the intensity was obtained for the anterior and then a straight vertical line was drawn in the posterior. The periodicity of the anterior and posterior oscillatory regions was compared (DMSO vs SU5402) and the differences were non-significant (ns).

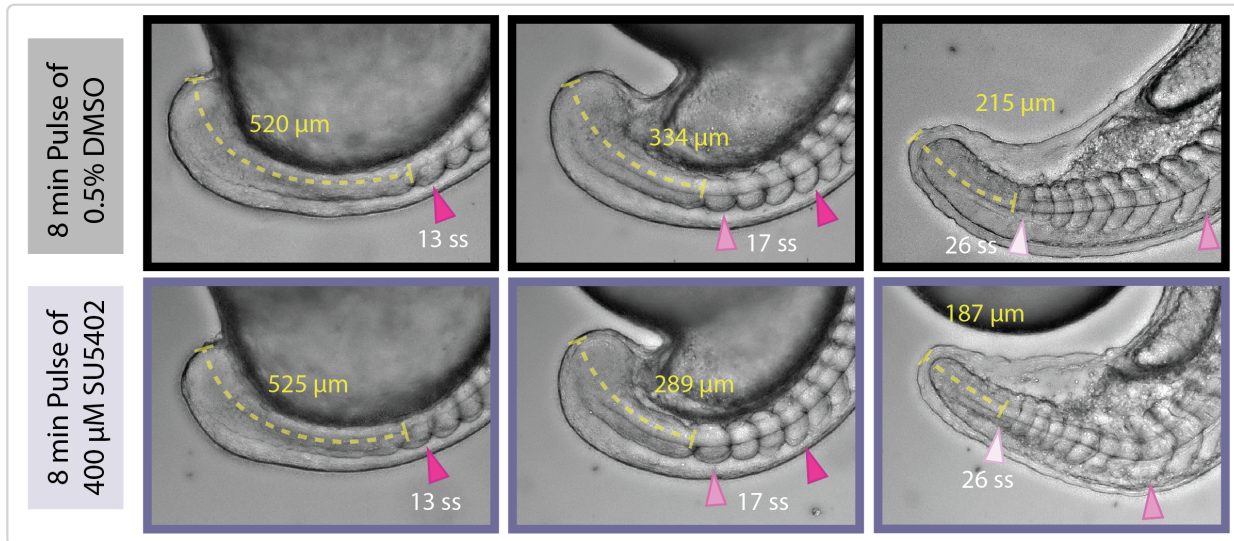
2.2.2 Elongation is affected in addition to maturation when FGF is highly reduced

Delfini et al., 2005 suggested that the posterior-to-anterior gradient of FGF/ERK controls cell motility in the PSM of chick embryos. Bénazéraf et al., 2010 blocked FGF signalling by electroporating a dominant-negative version of the FGF receptor (FGFR1dn) in PSM cells in chick embryos. As a result, they observed a shallower motility, a severe reduction of tissue convergence extension movements and a decrease in elongation rate. In addition, incubation of the embryos in SU5402 also resulted in a significant slowing of axis elongation.

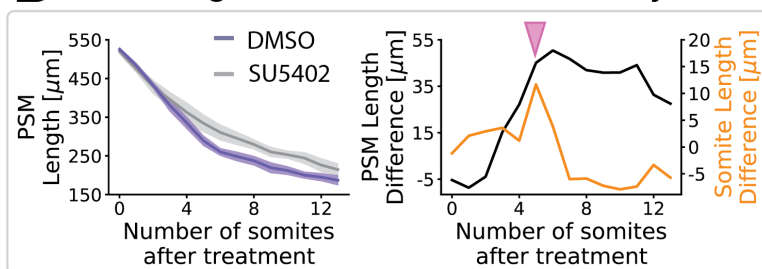
Figure 2.5 A shows a 12ss treated embryo with a 8-min pulse of 400 μM SU5402. Immediately after the treatment, the PSM is the same length in the DMSO and SU5402 treated embryos (519.85 μm , N=6 versus 480 μm , N=5, respectively) (Figure 2.5 A). The 5th somite after the treatment and thus the longest is 11.66 μm longer than the control (51.16 μm , N=10 versus 62.82 μm , N=10) (Figure 2.5 B). However, at this point the SU5402 treated embryo has a PSM shorter by 45 μm (334.26 μm versus 289.17 μm). Therefore, only changes in the wavefront which accelerate maturation and shift the position of the boundary more posterior are not enough to explain this shortage of the PSM (Figure 2.5 C). We propose that a combination of early maturation and problems in axis elongation result in the PSM size difference we observe in Figure 2.5. Thus, it is possible that the missing *her1* anterior stripe in Sawada, Shinya, et al., 2001 after 8-minute pulse of 675 μM SU5402 is a result of changes in both elongation and wavefront velocity.

Moreover, as the embryo develops, the notochord buckles at the position of the bigger somite, the tailbud becomes smaller and the somites also become smaller over time (as shown in Figure 2.2 C). This can be a consequence of axis elongation problems. Further experiments should be performed to understand what exactly causes these problems in elongation: the TB clearly reduced its size but we do not know whether cell density was also reduced or maybe less cells enter the TB. Fior et al., 2012 showed that in the absence of *msgn1*, the flux of cells from the TB to PSM is reduced and somites result abnormally small. Thus, careful analysis using a nuclear marker and tracking single cells should be conducted to inspect changes in cell density, division and motility. This way, a

A 8 min pulse of 400 μM SU5402 affect elongation and TB development



B PSM Length in DMSO vs SU5402 embryos



C Wavefront and elongation

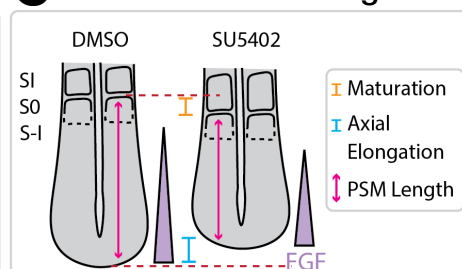


Figure 2.5: **SU5402 short pulse at high concentration affects PSM extension and TB development.** **A.** Example of a 8 min pulse of DMSO and a 400 μM of SU5402 treated embryos. First column corresponds to one somite after the treatment (which started at 12ss). Second column corresponds to the formation of the longest somite (5 somites after the treatment started). Last panel is at 26ss. Pink arrows show the formation of the somite written in white letters. Yellow dashed line are a representation of the LOI drawn parallel to the notochord to obtain the length of the PSM. Numbers shown in yellow are the average of N-DMSO=6 and N-SU5402=5 embryos. **B.** Left plot shows the mean and standard deviations of the length of the PSM (using the most recently formed somite, SI, as a reference). Purple and grey lines represent the DMSO and SU5402 treated embryos, respectively. The right panel shows in black the difference of the average of these two PSM length curves over time. The orange curve shows the difference in somite size for the same experiment (but with more embryos, N=10 for each condition). The pink arrowhead points the longest somite formed (the fifth). **C.** Illustration showing the consequences observed during treatment with SU5402. Changes in wavefront velocity accelerates maturation resulting in a longer somite. Early maturation and axis elongation problems contribute to the shorting of the PSM.

better picture can be obtained of what drives elongation problems in order to decouple them from the effects of changes in the wavefront.

2.3 S-IV does not have a constant position on the dpERK curve throughout segmentation

FGF signalling gradient aids global positioning of somite boundary and does so in concert with other signalling gradients such as Wnt and RA. So far I have shown the effects on clock dynamics, maturation and somite length when manipulating the FGF signalling gradient. However, it still remains unclear how, when and where the FGF signalling gradient provides positional information to the cells in the PSM. We next look at current models of how FGF signalling gradient provides positional information.

A long-standing hypothesis is that there is a region in the posterior PSM where somite determination occurs. It started with the heat shock experiments in the 1970s (Elsdale, Pearson, and Whitehead, 1976), where 5 normal somites were formed before a defective boundary was generated. It was already proposed in Cooke and Zeeman, 1976 as a “sudden change of cell behaviour”, although there was no experimental proof until more than 2 decades later. Surgical manipulation of the PSM to reverse different regions showed that there is one region that has already been determined, so it cannot adapt and gives rise to the reversed polarity (Dubrulle, McGrew, and Pourquié, 2001). This region at S-IV in the PSM was termed the "determination front". The evidence I present above highlights the constancy of a 5-somite delay after perturbation, consistent with an action of FGF on cells at S-IV in the PSM.

There is evidence to support multiple different hypotheses about how the clock information is translated into spatial information. Many of these hypotheses focus on the role of the signalling gradient of FGF at the S-IV location. A key idea is that there is some property of the gradient that is constant at S-IV, and this feature is used by cells to make the determination decision as they transit through the S-IV position. However, the mapping of the trajectory of cells through the S-IV position into the somite boundaries has not been accomplished in any species. Hence the validity of hypotheses that depend on the relationship of boundary cells to a determination front at S-IV remains uncertain.

In this section I will show that our results suggest an alternative scenario. With the help of single cell tracking and the ability to make long time-lapse movies, we back-tracked somite boundary cells through their S-IV position during different developmental stages. We compared their spatial dynamics with the temporal dynamics of *her1* and

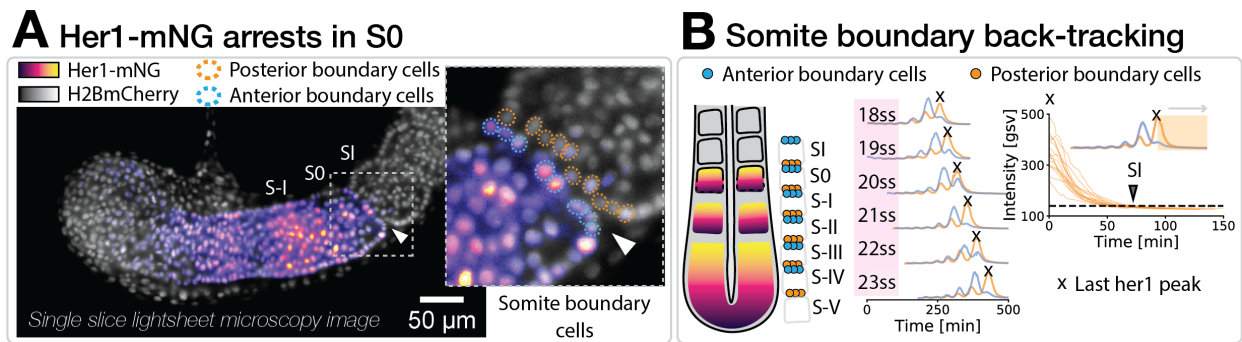


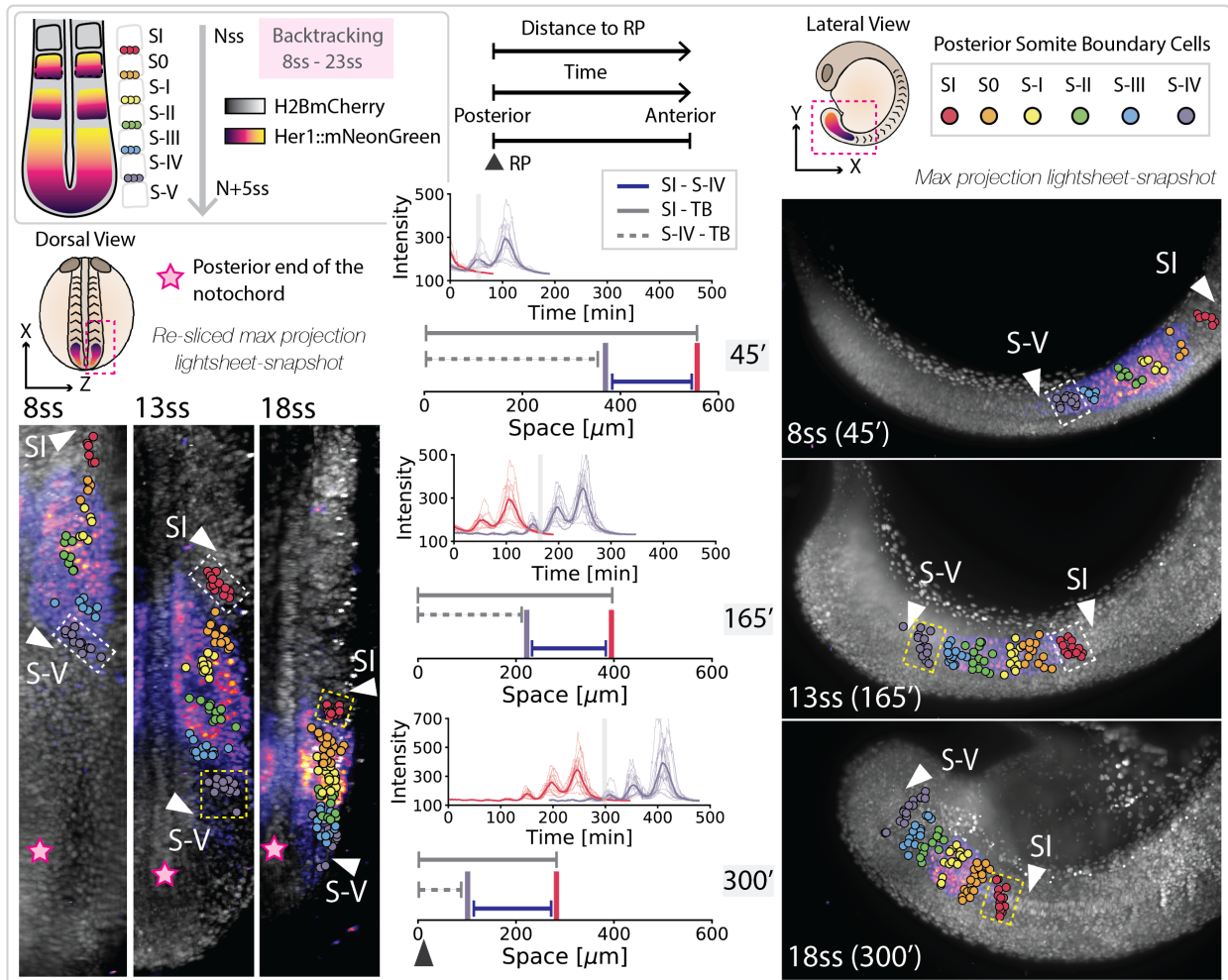
Figure 2.6: **Somite boundary cell tracking.** **A.** Single slice of a light-sheet microscopy snapshot. In orange, an example of posterior boundary cells and in blue, anterior boundary cells. **B.** Back tracking was performed starting at 8ss until 23ss from somite S-I, which was determined by visual inspection of the cells and using the offset of Her1-mNG as a reference. In blue and orange, example traces of the tracked cells from posterior and anterior somite boundaries, respectively (here we only show the traces from 18ss to 23ss, but the tracking started at 8ss).

the spatial distribution of dpERK. In contrast to the previously held view in the literature, we show that the position cells occupy when they are at S-IV does not scale with PSM length, with the length of the next somites to form or with the spatial profile of dpERK.

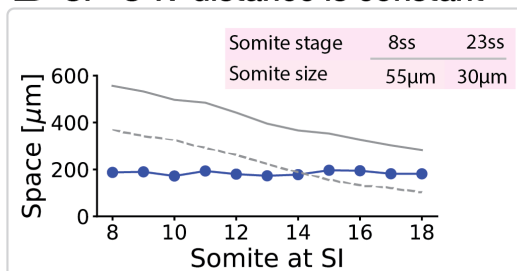
To get a map of where the cells are during somitogenesis, I back-tracked cells in the posterior and anterior somite boundaries from 8ss to 23ss (Figure 2.6). I used light-sheet microscopy to record an 8-hour time-lapse of the developing embryo carrying Her1::mNeonGreen and H2B::mCherry. Figure 2.6 B shows an example of the Her1-mNG dynamics in the tracked cells. We started back-tracking when the cells were in S-I, which is the stage when a somite first has an anterior and posterior boundary. This position can be identified unambiguously by observing the nuclei or using the Her1-mNG signal offset (Figure 2.6 A). The different presumptive somite locations (S-I, S-II...) can be pinpointed by counting the somites that are forming. For example, cells that will end up in somite 13 are identified in S-V exactly when somite 8 forms, and cells that will end up in somite 18 are identified in S-V exactly when somite 13 forms, etc.

Figure 2.7 A shows the back-tracking results. In this case, only the posterior boundary cells are shown for simplicity. Dorsal and lateral views of embryos and tracked cells are shown. In addition, cells are colour-coded according to their position on the spatial axis within the PSM (S-I to S-IV). The first thing to note is that already in S-IV the cells are spatially clustered (from 8 to 23ss), i.e. there is very little mixing of cells. Although at the tissue level, the system appears to be highly dynamic, e.g. tail elongation, embryo growth, in the PSM the cells maintain a relative position with respect to their neighbours.

A Her1 and S-IV relationship during different developmental stages



B SI - S-IV distance is constant



C Differences in dpERK levels in S-IV

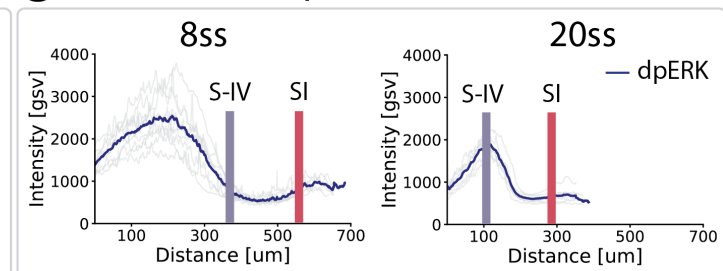


Figure 2.7: **Spatial expression of dpERK and S-IV position at different developmental stages.** **A.** Maximum projections of the dorsal (left) and lateral (right) views of light-sheet microscopy time-lapses of transgenic lines carrying H2B::mCherry and Her1::mNeonGreen. Posterior boundary tracked cells are shown and colour-coded according to their position relative to the newly formed somite (SI, S0, S-I, etc). In the centre, the temporal dynamics of Her1-mNG at different developmental stages at the SI (red) and S-IV (in purple) positions. The grey vertical lines show the time-points where the maximum projections have been taken (45, 165 and 300 minutes).

Figure 2.7: (Previous page) **B.** Distance measured from SI to TB (grey continuous line), from S-IV to TB (grey dashed line) and from S-V to SI (blue line). The pink box shows the size of the somites at 8ss (beginning of the analysis) and at 23ss (end of the analysis). **C.** dpERK staining of 8ss and 20ss embryos. In grey lines the individual spatial profiles of each embryo and in blue the mean. The purple and red vertical lines show the S-IV and SI positions obtained from cell tracking, respectively.

We looked closely at the location of S-IV at different somite stages (Figure 2.7 A). We observed that at 8ss, S-IV is in the PSM whereas at 18ss, it is in the TB (we use the end of the notochord to mark the arbitrary separation between PSM and TB). Not only is S-IV at different locations, at 8ss the cells are in their second-to-last Her1-mNG cycle while at 18ss they are in the third-to-last Her1 cycle. Importantly, comparison of where S-V sits within the dpERK signal profile at 8ss and 20ss shows a large difference. This finding suggests that mechanisms of comparing dpERK levels with neighbours, i.e. with the gradient fold change (Simsek and Özbudak, 2018), or with the bistable switch (Naoki et al., 2019), does not hold across the different developmental stages. Because S-IV is found in such different regions of the embryo during development, it appears to be an unrobust region for reading positional information directly from an FGF gradient.

Last but not least, we found that the distance from S-IV to the tailbud and the distance from SI to the tailbud decrease with time, which is consistent with previous observations that the PSM is getting shorter and shorter (Gomez et al., 2008; Schröter, Herrgen, et al., 2008). Previous work has assumed that the cells in the PSM contributing to each somite are distributed according to the final AP length of the somites that will form. Strikingly, however, when we look at the distance from S-IV to SI in Figure 2.7 B, it remained constant over time (200 μm).

This was unexpected, as the size of the somites varies substantially across developmental stages; namely 55 μm at 8ss and 30 μm at 23ss. This means that at 8ss, the region between S-IV to SI will expand in the AP direction in order to accommodate 5 somites of around 50 μm , while at 23ss it will compress. The deformations may be executed by tissue-scale convergence-extension movements, or by more local rearrangements. Thus, models that rely on the assumption of a distribution of cells along the AP axis of the PSM that matches the length of the somites they will form will be in error. Furthermore, models which assume that the S-IV position scales to the PSM length are also incorrect. Given this finding, we suggest that the final local precision and accuracy of somite formation could be established in the anterior PSM.

Summary Chapter 2

Overall, this chapter has revisited some of the previous experiments carried out to understand the role of FGF, but this time, with better spatiotemporal resolution thanks to new imaging and analysis tools. We find that FGF is involved in the global control of accurate somite boundary positioning, and confirm a universal 5-somite delay to the first-formed longer somite in all treatment variations. Furthermore, we have observed that FGF does not affect the precision of somite boundary positioning or the temporal dynamics of the *her1* clock gene. However, it does affect elongation of the axis and these changes in PSM length therefore need to be taken into account in future experiments with SU5402. We observed that the temporal evolution of the dpERK signal after perturbation was a poor predictor of the number of larger somites. Finally, we saw how the S-IV region does not correspond with the dpERK distribution over developmental time, suggesting that it does not seem feasible for dpERK to act alone as an instruction or readout of positional information. The role of dpERK in convolution with other signals needs to be explored. In particular, since the distance from SI to S-IV remains constant, whereas the distance from to the S-IV tailbud shortens continuously, a gradient acting from the anterior of the PSM might appear better-suited to instructing a determination front. Further experiments exploring the role of Wnt and RA in combination with FGF should be performed to better understand how signalling gradients play a role during somite boundary formation. In any case, the quantitative and dynamic evidence generated in this chapter call into doubt the existing models for instruction of PSM cell behaviour by an FGF signalling gradient, and raise the possibility that mechanisms other than extrinsic signals may be at work.

With this picture in mind, we turn to the next chapter, which investigates how intrinsic signals also play an important role during the segmental programme.

Chapter 3

Cell autonomous generation of the wave pattern

This chapter includes an updated version of [Rohde et al., 2021](#), entitled:

- Cell-intrinsic timing drives the vertebrate segmentation clock's wave pattern.

In this study, we compare clock dynamics in culture and in the embryo. We conclude that cells *in vitro* are able to oscillate, slow down and arrest the oscillation but more noisily than cells *in vivo*. This cell-intrinsic activity initiates during cell exit from the TB and runs down anteriorly towards the PSM. This work suggests that a noisy cell-intrinsic timer drives the slowing of the oscillations giving rise to observed tissue level wave pattern.

Title: Cell-intrinsic timing drives the vertebrate segmentation clock's wave pattern

Authors:

5 Laurel A. Rohde^{1,2,†}, **Arianne Bercowsky-Rama**^{1,†}, Jose Negrete Jr.^{1,3}, Guillaume Valentin⁴,
Sundar Ram Naganathan^{1,5}, Ravi A. Desai^{2,6}, Petr Strnad^{1,7}, Daniele Soroldoni^{1,2,8}, Frank
Jülicher³, and Andrew C. Oates^{1,2,5,*}

Affiliations:

¹Institute of Bioengineering, École Polytechnique Fédérale de Lausanne; Lausanne, CH

10 ²Department of Cell and Developmental Biology, University College London; London, UK

³Max Planck Institute for the Physics of Complex Systems; Dresden, DE

⁴Center of PhenoGenomics, École Polytechnique Fédérale de Lausanne; Lausanne, CH

⁵The Francis Crick Institute; London, UK

⁶Current address: Imperial College London; London, UK

15 ⁷Current address: Viventis Microscopy Sàrl; Lausanne, CH

⁸Current address: Vienna BioCenter Core Facilities GmbH; Vienna, AU

†Equal contribution

*Corresponding author. Email: andrew.oates@epfl.ch

20 Summary

Rhythmic and sequential segmentation of the growing vertebrate body relies on the segmentation clock, a multi-cellular oscillating genetic network (Oates et al., 2012). The clock is visible as tissue-level kinematic waves of gene expression that travel through the pre-somitic mesoderm (PSM) and arrest at the position of each forming segment (Aulehla et al., 2008; Delaune et al.,
25 2012; Masamizu et al., 2006; Palmeirim et al., 1997; Soroldoni et al., 2014). Here we test how this hallmark wave pattern is driven by culturing single maturing PSM cells. We compare their intrinsically-generated transient oscillatory and arrest dynamics to those we observe in the embryo at cellular resolution, finding remarkable agreement. This suggests that cell-extrinsic signals are

not used by the cells to instruct the developmental program underlying the wave pattern. In contrast, we show that a cell-intrinsic timing activity initiates during cell exit from the tailbud, then runs down in the anteriorward cell flow in the PSM, thereby using elapsed time to provide positional information to the clock. Exogenous FGF lengthens the duration of the cell-intrinsic timer, indicating extrinsic factors in the embryo may regulate the segmentation clock via the timer. Comparison of experimental data to a theoretical description of a clock driven by a timer identifies features within the timer that account for the observed differences in the clock's transient oscillatory dynamics. Our work suggests that a noisy cell-intrinsic timer drives the slowing and arrest of oscillations underlying the wave pattern, while extrinsic factors in the embryo tune this timer's duration and precision. This is a new insight into the balance of cell-intrinsic and -extrinsic mechanisms driving tissue patterning in development.

Main:

As the vertebrate embryo develops, a multi-cellular patterning system called the segmentation clock translates the rhythm of genetic oscillations into the successive and periodic formation of tissue segments. These segments, called somites, give rise to the metameric backbone, ribs and associated muscles of the adult body. The segmentation clock's dynamics are visible in the embryo as tissue-level waves of gene expression (Hubaud and Pourquié, 2014) that travel anteriorly through the presomitic mesoderm (PSM) until they arrest at the position of the newly forming somite (Aulehla et al., 2008; Delaune et al., 2012; Masamizu et al., 2006; Palmeirim et al., 1997; Soroldoni et al., 2014). Waves are produced by oscillations slowing as cells mature and flow anteriorly through the spatial reference frame of the PSM, creating a phase shift along the anteroposterior axis (Delaune et al., 2012; Morelli et al., 2009; Shih et al., 2015). Here we

investigate how the cellular-level transient dynamics and clock arrest are driven, in particular determining the balance of cell-intrinsic and -extrinsic factors in this patterning.

5 Previous work has implicated both cell-intrinsic mechanisms and extrinsic signals in driving the spatiotemporal segmentation clock pattern. These mechanisms include morphogen gradients across the PSM (Moreno and Kintner, 2004; Sawada et al., 2001; Simsek and Özbudak, 2018), the decay of signaling factors carried anteriorly by PSM cells (Aulehla et al., 2003; Dubrulle and Pourquié, 2004), the counting of oscillations (Palmeirim et al., 1997; Zákány et al., 2001), the comparison of oscillator phase within cells (Sonnen et al., 2018), neighboring cells comparing
10 oscillations (Boareto et al., 2021; Murray et al., 2011), and cell-cell signaling in an excitable system (Diaz-Cuadros et al., 2020; Hubaud et al., 2017). However, definitive evidence for these competing models is lacking, and even the relative balance of cell-intrinsic versus -extrinsic information remains an open question.

15 PSM cell culture systems facilitating deconstruction of the segmentation clock are increasingly playing a role in determining this balance. In particular, mammalian PSM *in vitro* segmentation clock models have been recently developed to overcome challenges of working in the embryo (van den Brink et al., 2020; Diaz-Cuadros et al., 2020; Hubaud et al., 2017; Lauschke et al., 2012; Matsuda et al., 2020a, 2020b; Matsumiya et al., 2018a; Tsiairis and Aulehla, 2016). Travelling
20 waves and cell maturation with spatiotemporal organization mimicking that in the embryo have been described in some of these multi-cellular cultures (van den Brink et al., 2020; Lauschke et al., 2012; Matsuda et al., 2020a, 2020b; Matsumiya et al., 2018b; Tsiairis and Aulehla, 2016). Isolated mammalian cells have been shown to oscillate in permissive conditions, yet transient

dynamics have not been reported (Diaz-Cuadros et al., 2020; Hubaud et al., 2017; Matsuda et al., 2020b). We have previously reported persistent oscillations in isolated zebrafish cells (Webb et al., 2016), however, after the removal of growth factors, serum and BSA from this culture, we observed transient clock oscillations and theoretically described this as regulated via clock gene production (Negrete JR et al., 2021). Here, by quantitative comparison of cell behavior in culture and in the intact zebrafish embryo, we ask whether the transient dynamics in isolated PSM cells reveal the existence of a cell-intrinsic program driving the wave pattern.

Cell-intrinsic transient dynamics in concert with PSM differentiation

To analyze transient dynamics from cells originating within a defined anteroposterior region of the PSM, we dissected out the posterior-most quarter of the PSM (PSM4) (Fig. 1a). Each PSM4 explant was separately dissociated and cultured (N=11 embryos) at low-density on protein A-coated glass in L15 medium without added signaling molecules, small molecule inhibitors, serum, or BSA. Oscillation and arrest dynamics were followed using Her1-YFP, a fluorescently-tagged core clock component, previously used to define the zebrafish clock's tissue-level wave pattern (Soroldoni et al., 2014), and a novel *Mesp-ba-mKate2* transgene, which marks the rostral half of the forming somite in the anterior PSM (Fig. 1a-c; Extended data Fig. 1), as expected (Cutty et al., 2012). *Mesp* expression has been used in multi-cellular segmentation clock cultures as a marker of differentiation upon clock arrest (Diaz-Cuadros et al., 2020; Lauschke et al., 2013; Matsuda et al., 2020a; Matsumiya et al., 2018b; Tsiairis and Aulehla, 2016). Analysis of Her1-YFP and *Mesp-ba-mKate2* intensity was carried out in single cells that survived over 5 hours post-dissociation, remained the only cell in the field of view, did not divide, and showed transient Her1-YFP dynamics (Extended data Fig. 2).

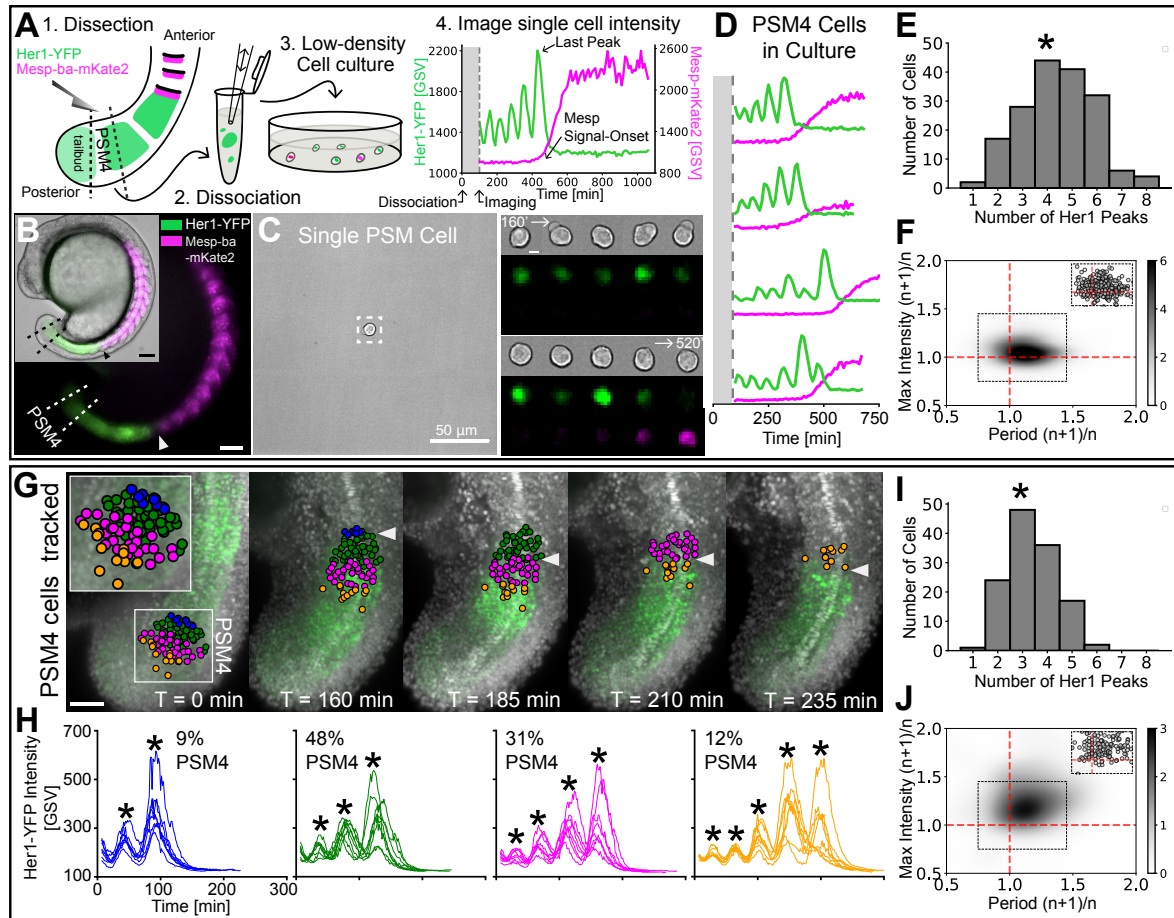


Fig. 1. Cell-intrinsic transient dynamics reproduce those underlying wave pattern.

(A) Experimental design: 1) posterior-PSM quarter (PSM4) dissection (dashed line) from a *Tg(her1-yfp;mesp-ba-mKate2)* 15 somite-stage embryo, 2) dissociation into single cells, 3) culture a low-density, and 4) Her1-YFP and Mesp-ba-mKate2 imaging over time. (B) Mesp-ba-mKate2 in a 15 somite-stage embryo *Tg(her1-yfp;mesp-ba-mKate2)* embryo (lateral view, brightfield inset). Arrowheads mark the recently formed somite (S1). Dissection lines surrounding PSM4. Scale bar 100 μm . (C) One cell per field of view imaged (scale bar 50 μm). Boxed region over time (scale bar 5 μm). Intensity trace shown in A. (D-F) PSM4 cells in culture (N=11 embryos, n=174 cells). (D) Representative intensity traces. (E-I) Her1-YFP peaks per cell (*mean \pm SD, 4.4 ± 1.6 peaks in culture, 3.4 ± 1.0 peaks in embryo). (F, J) Successive peak (maxima) intensity and period ratios. Upper right quadrant indicates successive intensity rise and oscillation slowing. (n=421 cycles, 55% cycles in upper-right quadrant in culture; n=179 cycles, 72% cycles in upper-right quadrant in embryo).

Single PSM4 cells in culture produced Her1-YFP oscillations with 1 to 8 peaks before arresting (N = 11 embryos, n = 174 cells; Fig. 1d-e; Extended Data Fig. 3). These oscillations typically slowed and increased amplitude, then abruptly arrested (Fig. 1d,f, Extended Data Fig 4.).

5 Oscillation arrest, marked by the Her1-YFP last peak, was also associated with *Mesp-ba-mKate2* signal-onset (Fig. 1a,d; Extended Data Fig. 5a), suggesting that arrest occurs in concert with differentiation as expected from the tissue-level pattern (Fig. 1b). These transient dynamics were independent of cell-survival time in culture (Extended Data Fig. 6), reproduced in cells isolated one-per-well (Extended Data Fig. 7) and did not require *Tg(mesp-ba-mKate2)* (Extended Data Fig.

10 8. Variation in arrest timing was not due to differences between individual embryos and experiments (Extended Data Fig. 9), limiting its source to heterogeneity within the starting PSM4 cell population and/or to the noise in an intrinsic process. Thus, PSM4 cells intrinsically slow oscillations and arrest the clock in concert with expression of a segmental marker.

15 **Intrinsic PSM transient dynamics mirror those in the embryo**

To see whether PSM4 cell-intrinsic clock dynamics in culture recapitulated those produced in cells in the embryo that originate from PSM4, then flow anteriorly until somite formation, we used light-sheet imaging and tracked cells as the embryo *Tg(Her-YFP;H2B-mCherry)* was freely-growing (Fig. 1g). Retaining their initial anteroposterior arrangement, these cells predominantly

20 contributed to two somites and differed by at most one Her1-YFP peak within a somite (N=2 embryos, n=133 cells; Fig. 1g,h; Extended Data Fig. 10). To normalize for a general slowing of developmental time observed in zebrafish culture (Extended Data Fig. 11) (Langenberg et al., 2003; Webb et al., 2016), we compared the number of peaks generated and the ratio of successive

periods and peak intensities, rather than absolute time. Cells in the embryo produced on average fewer peaks and showed decreased variability in the number of peaks compared to cells in culture (Fig 1e,i), indicating that the duration of intrinsic transient dynamics until arrest is longer in culture and more variable. Despite this difference, the key features of successive slowing and increased intensity are comparable in culture and in the embryo (Fig 1f,j, Extended Data Fig. 4)). Because the cells tracked in the embryo originated from the same starting population as those in culture, these results indicate that the greater variation in duration observed in culture is not due to initial heterogeneity within that cell population, but reflects an increase in the temporal variability of the intrinsic dynamics.

10

We next asked how the spatial precision of Her1-YFP arrest and Mesp-mKate2 signal-onset in the embryo compares to the timing of these events in culture. To systematically evaluate these events in the embryo, we backtracked all the cells in the recently formed somite (S1) (Extended data Fig. 12a-c). All cells in the somite expressed Her1-YFP and most produced a last peak in the prospective somite (S -1), creating a phase profile across the future rostral-caudal somite axis that reflected the tissue-level wave's arrival (N= 1 somite, n= 233 cells; Extended data Fig. 12d). Thus, in the embryo, arrest of all the cells that form one somite is tightly regulated in space and time. Mesp-ba-mKate2 was also tightly regulated within the forming somite (S0), appearing as a gradient with higher levels rostrally (Extended data Fig. 12e). We defined signal-onset times only within the rostral half, permitted by the high intensity signal in this region (Extended data Fig. 5b). The distribution of Mesp-ba-mKate2 intensity rise and percentage of cells with a clear signal-onset time in vivo was comparable to that seen within the population of PSM4 cells in culture (N = 2 somite, n= 190 and 217 cells; Extended data Fig. 5a,b), suggesting that there is no intrinsic default

20

state, i.e. on or off, for Mesp expression. To directly compare the relationship of Mesp-ba-mKate2 signal-onset and Her1-YFP arrest in individual cells, we backtracked from the most recently formed somite (S1) in *Tg(her1-YFP;mesp-mKate2)* dual-transgenic embryos. We found that Mesp-ba-mKate2 signal-onset only occurred after the last Her-YFP peak (Extended Data Fig 5c,d and 13). In culture, however, this relationship was not as precise, with Mesp-ba-mKate signal-onset spanning the last peak (N = 2 embryos, n = 41 cells, Extended Data Fig 5c,d), indicating a loss of precision in the relationship between arrest and segment polarization.

Together, our data suggests that the slowing and arrest of oscillations underlying the wave pattern in embryos is driven cell-intrinsically in maturing PSM cells. However, the longer-running and noisier dynamics in culture indicate that extrinsic signals present in the embryo may shorten and sharpen this program.

Cell-intrinsic timer independent of clock in embryo

We propose that a cell-intrinsic timing program in maturing PSM cells encodes positional information as cells flow anteriorly. This timer is likely independent of the clock, as we found the timing of Mesp-ba-mKate2 signal-onset in single cells with disabled clock oscillations comparable to that in cells with a functional clock (Extended Data Fig. 14 gullum).

We have previously provided a theoretical description of a noisy timer driving a genetic clock (Fig. 2a,b) (Negrete et al., 2021), and we next asked whether cells in the embryo can be described with the same model; and if so, which parameters of the timer would describe the differences in the dynamics observed above between culture and embryo cells. Fitting the model by comparing

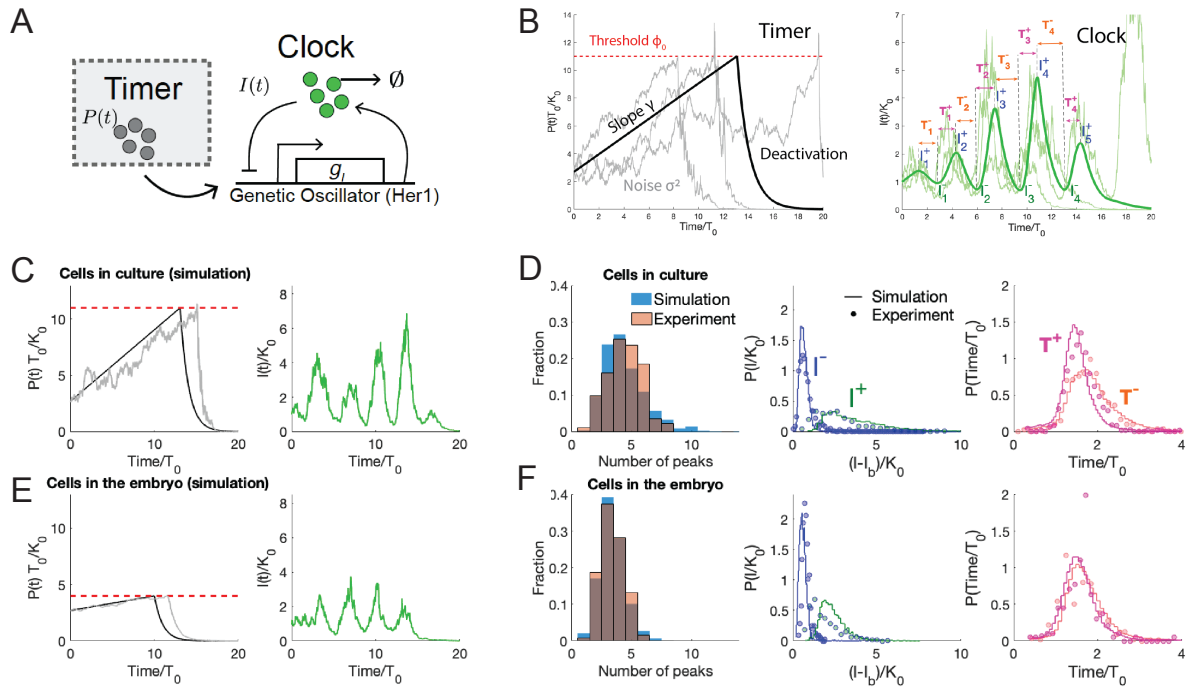


Fig. 2. Oscillatory profile reveals signature of cell-intrinsic timing mechanism in the embryo

(A) Schematic of timer-driven clock model. (B) Left panel, parameters of the timer: threshold, slope, noise and deactivation, deterministic time trace (black) illustrated together with representative traces from stochastic numerical simulations of intrinsic program (grey). A noisy ramp of production acts as the time-keeping factor for the clock. Right panel, observables of transient clock signal in Her1-YFP profile: peak (I^+) and trough (I^-) intensity; time-intervals of production (T^+) and degradation (T^-), deterministic time trace (green) illustrated together with representative traces from stochastic numerical simulations of intrinsic program as in left panel (light green). (C) Representative simulation of PSM4 cell in culture, showing deterministic and a noisy ramp that drives a resulting transient clock signal. (D) Comparison of distribution of number of peaks for experiment and simulations of model fitted to cultured PSM4 cell experimental data from Fig. 1D-E (left panel), and probability distributions of clock observables from experimental data and simulations. (E, F) As above in (C, D), but for PSM4 cells imaged in the embryo from Fig 1H-J.

simulated and experimental data of the peak and trough intensities and the rise and fall times of the oscillatory signal, and the distribution of number of peaks of the cultured cells gave a good agreement, as expected (Fig 2c,d, Supplementary Theory Text). We observed a similarly good fit to the oscillatory signal of the embryonic cells by changing only timer parameters: reducing the threshold, the slope, and the noise strength in the production (Fig. 2e,f). These results support the hypothesis that the dynamics in culture and in the embryo are underlain by the same cell-intrinsic timer, and suggest how modulation by the combination of the extrinsic signals present in the embryo may influence the clock via this timer, giving the clock fewer cycles and making it more precise.

10

FGF extends timer duration in cultured posterior PSM cells

We next explored how FGF, an extrinsic signal known to affect segmentation, interacts with the intrinsic timer by culturing PSM4 cells in the presence of FGF8. A gradient of FGF signaling has been shown to extend from the tailbud across the PSM and has been postulated to provide spatiotemporal information to the segmentation clock (Dubrulle et al., 2001; Sawada et al., 2001; Dubrulle et al. 2004; Akiyama et al., 2014; Sari et al., 2018). Previous experiments implanting FGF8-soaked beads adjacent to posterior PSM in the embryo resulted in an extension of clock/PSM activity such that somite boundary formation was delayed, yielding shorter segments (Dubrulle et al., 2001, Sawada et al., 2001). Consistent with this delay in vivo, we found that FGF in the culture medium extended transient dynamics in single PSM4 cells, such that more oscillations were produced (3.3 peaks in control cells, 6.7 + FGF) and the Her1-YFP last peak was later (269 min post-dissociation in control cells, 568 min post dissociation in cells with FGF) (Fig. 3a-d; Extended data Fig.15).

20

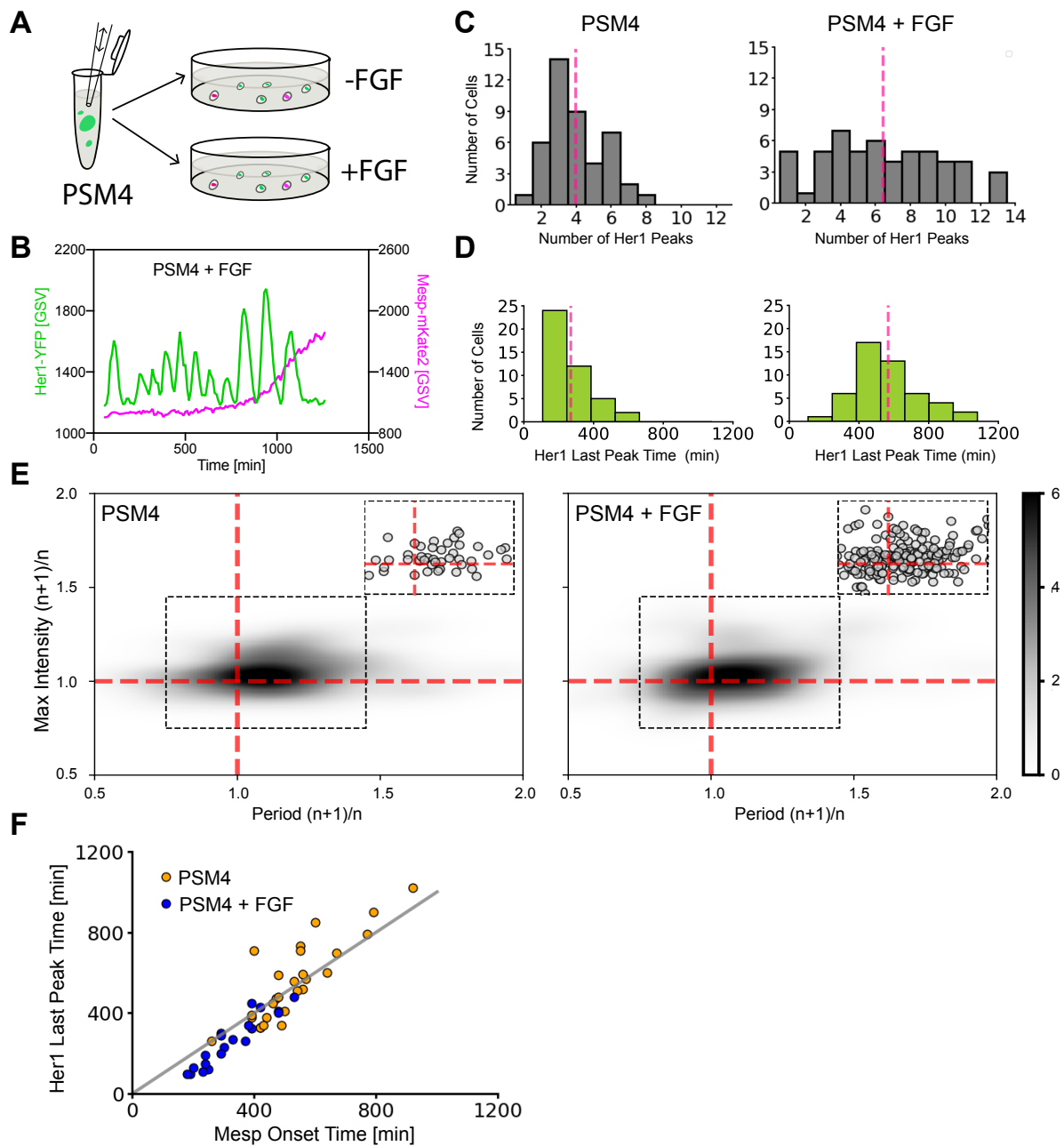


Fig. 3. FGF extends intrinsic timer / program duration in vitro

(A) A pool of dissociated PSM4 cells was split into a control well and one containing FGF-8b, then cultured ($N=4$; $n= 44$ PSM4 cells and $n= 54$ PSM4 cells with added FGF). (B) Representative Her1-YFP and Mesp-mKate2 traces in a PSM4 cell culture with added FGF. (C) Number of Her1-YFP Peaks produced per cell, with pink line at the mean. (D) Time of Her1-YFP last peak (min post-dissociation), with pink line at the mean. (E) Ratio of the intensity of successive Her1-YFP peaks versus that of successive periods. (F) Correlation of Her1-YFP last peak time and Mesp-bb-mKate2 signal-onset time.

Despite this extension of the intrinsic program, successive oscillations continued to slow and increase amplitude (Fig. 3e; Extended data fig. 16) This suggests that the role of FGF may be to tune the duration of the intrinsic program rather than directly specify the oscillatory dynamics.

5 Mesp signal-onset and the last peak of Her1 also retained their temporal association in the presence of FGF (Fig. 3f), although a subset of cells produced multiple Her1 cycles after the Mesp onset (Fig. 3f, Extended Data Figure 15). Mesp intensity distribution was not altered (Extended data Fig. 16). Notably, exogenous FGF did not improve precision of the timer, as cells showed a larger range in the number of oscillatory peaks (Fig 3c). Numerical simulations of the theoretical model showed

10 a good fit to the oscillatory signal of FGF-stimulated cells by modifying only timer parameters: increasing the threshold and noise strongly, with a weaker increase in production slope (Extended data Fig. 17). As in the case of the embryo, above, no changes were made to the clock's internal parameters. These changes to the timer increase both the average and range in the number of clock cycles, and suggest that FGF alters the intrinsic timer, causing a time-keeping factor to accumulate

15 to a higher level and with more range.

Together, our data shows that FGF extends the duration of the cell-intrinsic transient dynamics in a manner that could explain reported FGF activity in the embryo (Dubruelle et al., 2001, Sawada et al., 2001) and supports a hypothesis that extrinsic signals act upon the clock through the cell-

20 intrinsic timer. We propose that the alteration of segment length in the embryo observed by altering FGF activity corresponds to a change in duration of the intrinsic timer.

Timer initiates as cells exit the tailbud

If a cell-intrinsic timer provides positional information to the clock in the embryo, we predicted that cells located more anteriorly in the PSM will have less time remaining before arrest and differentiation. To test this, we followed oscillation and arrest dynamics in single cells cultured from tissue quarters extracted from different locations along the PSM (Fig. 4a). Consistent with a
5 timer running down in the embryo, PSM cells originating more anteriorly - PSM3 and PSM2 - tended to arrest Her1-YFP oscillations earlier (Fig. 4b,c), in concert with *Mesp-ba-mKate2* signal-onset (Fig. 4d).

To explore when this timer starts, we cultured cells from the tailbud (TB) (Fig. 4a), where Her1-
10 YFP oscillations are present (Soroldoni et al., 2014) and progenitor cells are thought to be maintained (Martin, 2016). Single TB cells in culture also oscillated with successive slowing, then arrested concurrent with *Mesp-ba-mKate2* signal-onset (Fig. 3b-d; Extended Data Fig 18). Moreover, TB and PSM4 dissected from the same embryo were found to arrest oscillations with similar timing, despite the more posterior origin of the TB cells (N=3 embryos; Fig 4c; Extended
15 Data Fig. 18a). These results suggest that experimental removal from the TB starts the timer such that its duration is equivalent to that of cells which have recently entered the PSM. We thus propose that TB cells express the intrinsic timing mechanism, but require a trigger associated with exit from the TB to start timing.

20 If the timer starts upon TB exit, then we expected that cells in the embryo initiate transient dynamics when they transition into the PSM. Cells within the TB are known to mix and remain for a range of times before joining the PSM (Mara et al., 2007). To compare the start of transient dynamics in TB cells that join the PSM at different times, we backtracked individual cells located

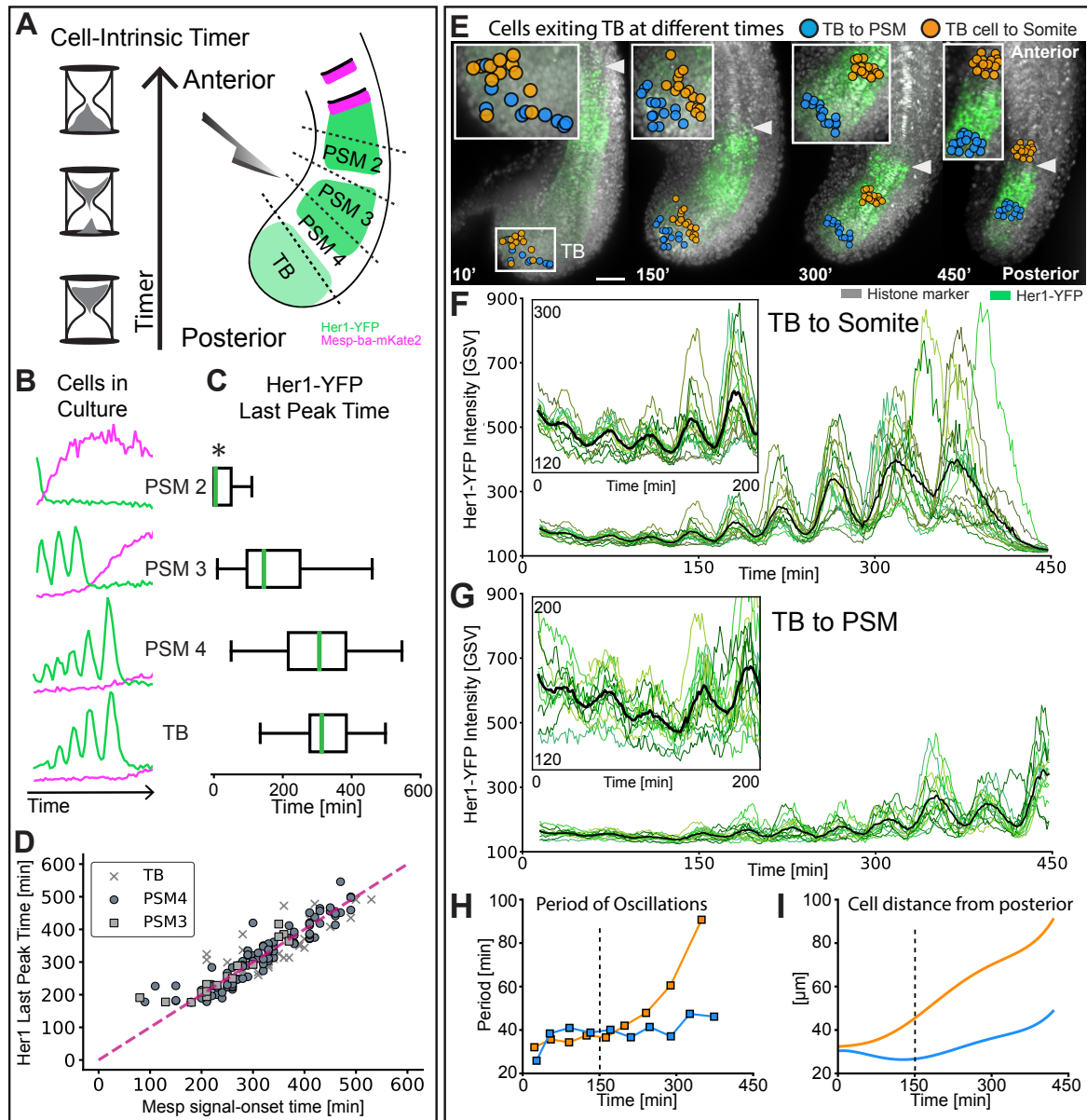


Fig. 4. Cell-intrinsic timer initiates upon TB exit and duration shortens in anterior cell flow.

(A) Experimental design: *Tg(her1-yfp;mesp-bb-mKate2)* PSM dissection into different anteroposterior quarters, dissociation, and culture. PSM4 was dissected and cultured in parallel from each embryo as an internal reference. (B) Representative intensity traces in cultured cells. (C) Her1-YFP last peak times as median (green line) with interquartile box and whiskers. Time given as post-dissociation. Data pooled by cell type (N=3 embryos, n=32 PSM2 and 32 PSM4 cells; N=3 embryos, n=65 PSM3 and 41 PSM4 cells; N=3 embryos, n=38 TB and 59 PSM4 cells). PSM2 last peaks that occurred prior to the start of imaging were set to acquisition start (*). (D) Correlation of Her1-YFP Last Peak and *Mesp-bb-mKate2* signal-onset time. (E) Cells backtracked from posterior-PSM (blue, n=17) and 28th somite (orange, n=15) to TB at 15 somite stage (N=2, 7.5 h imaging, *Tg(her1-yfp;h2b-mcherry)*). Arrowhead at recently formed somite boundary. (F, G) Her1-YFP intensity traces for individual cells (green) and mean intensity (black). Inset zoom of TB oscillations. (H) Mean period of Her1-YFP oscillations. (I) Cell distance from posterior tail tip.

either within PSM4 or the most recently formed somite at the end of a 450 min time-lapse movie (N= 3 embryos; Fig. 4e; Extended Data Fig. 19). We observed that while in the TB, individual cells from both groups showed low-intensity, noisy Her1-YFP oscillations (Fig. 4f,g). As the embryo developed, the group of cells that later reach the somite were the first to join the PSM, at which time their oscillations increased in peak intensity and slowed successively (Fig. 4h,i). These dynamics continued as cells flowed anteriorly then arrested during somite formation (Fig. 4f,h,i). In contrast, the group of cells backtracked from PSM4 exited the TB later and showed a corresponding delay in slowing, and intensity rise (Fig. 4g-i). This tight correlation of the initiation of transient dynamics in cells with their exit from the TB in the embryo, over substantial developmental time, supports the idea that exit from the tailbud starts the intrinsic timer.

Discussion

The population-level behavior of the oscillators of the segmentation clock is the hallmark wave pattern. The role of short-range cell-cell signaling through the Delta-Notch pathway in the local synchronization of the oscillators is well established (Venzin and Oates, 2020), providing local coherence to the wave pattern. However, the mechanism for the gradual slowing and stopping of the oscillators that creates the phase off-set required for waves at the tissue-level remains a topic of debate. Our results clearly implicate a cell-intrinsic program of slowing and stopping as the basis for the tissue-level wave-pattern in the zebrafish, and show that a universal picture of the vertebrate segmentation clock that is centered on persistent cellular oscillators instructed by extrinsic signals is inadequate. Rather, our work highlights the importance of transient dynamics driven by a cell-intrinsic timing mechanism.

How the balance of cell-intrinsic dynamics and extrinsic signaling plays out in other segmentation clock systems remains to be tested. However, the concept of a cell-intrinsic timer explains the long-known intrinsic properties of explanted PSM tissue from several species to segment with periodicity and AP directionality (Aulehla and Pourquié, 2006; Dubrulle et al., 2001; Henry et al., 2005; Lauschke et al., 2013; Maroto et al., 2005; Palmeirim et al., 1997, 1998). Indeed, the long-standing “Clock and Wavefront” model of the segmentation clock originally postulated an intracellular timing gradient as the mechanism behind the wavefront of cellular change interacting with the clock to determine somite position (Cooke and Zeeman, 1976). Here we show that the clock and wavefront are both captured in a single cell running an intrinsic program.

Nevertheless, the difference in duration and precision between cellular dynamics in the embryo and those in culture conditions distinguishes important roles of extrinsic signaling in the zebrafish segmentation clock. These roles are to shorten the transient dynamics and to increase their precision in the population, so that all cells contributing to a single somite in the embryo stop oscillating and express a differentiation marker together within the period of somite formation. If the variability of the cultured cells were to be mapped on to the embryonic axis, the program exit would be spread across multiple somites, with catastrophic results for segmentation. The ability of FGF to extend the duration of the program of cultured cells fits well with data from embryo experiments on changing segment lengths (Dubrulle et al., 2001, Sawada et al., 2001), but the very high variability observed implies that additional signals, or the temporal dynamics of the signals, are important for precision. Whether other candidate signals such as Wnt and RA (Aulehla

and Pourquie, 2010), or signal dynamics (Sonnen et al., 2018), integrate into the control of intrinsic cell behavior to explain the precision of embryonic segmentation can now be explored.

The intrinsic timer's identity and how it is tuned by extrinsic signals during development remain
5 intriguing questions. The molecular details of the timer are not constrained by our data here, and
could involve a number of plausible intermediates such as transcription factor or microRNA
cascades similar to those in timing of neuroblast differentiation or *C. elegans* molting (Ambros,
2011; Brody and Odenwald, 2000) or phospho-timers as found in the circadian clock (Diernfellner
and Brunner, 2020). The latter mechanism would provide an attractive link to extrinsic signalling
10 by FGF gradients in the PSM (Sawada et al., 2001; Simsek and Özbudak, 2018). The model of the
timer can be used to evaluate candidate molecules. The timer's proposed role in slowing and then
stopping oscillations via the rise and fall of Her1 production (Negrete JR et al., 2021) suggests that
molecules controlling *her1* transcription, such as Tbx proteins (Brend and Holley, 2009) and/or
Her1 translation (Dill and Amacher, 2005) are involved as time-keeping factors. In this light, the
15 activity of the Tbx-degrading factor Ripply (Wanglar et al., 2014) may play a role in the threshold
at which production falls, thereby rapidly stopping the oscillations. Whatever the identity, our
results indicate the timer ought to exert control over differentiation independent of the clock.

Organizing animal and plant tissues and microbial assemblies with oscillatory mechanisms in
20 naturally occurring and synthetic systems is a rapidly evolving field of interest (Chou et al., 2022;
De Simone et al., 2021; Ferenc et al., 2021; Perez-Garcia et al., 2022). This includes the
investigation of the segmentation clock through innovative 3D culture models (van den Brink et
al., 2020). Although patterns in multicellular contexts can emerge from extrinsic signaling

processes alone (Danino et al., 2010), understanding the cell-intrinsic potential within these various systems is vital to interpreting and directing population level behavior. Our work combining isolated primary cell culture and single-cell resolution imaging of the corresponding developing tissue, reveals that cell-intrinsic timing directs the tissue-level patterning of the clock, and offers new opportunities to study the balance of extrinsic and intrinsic control in oscillatory patterning systems.

References

- Ambros, V. (2011). MicroRNAs and developmental timing. *Current Opinion in Genetics & Development* 21, 511–517. <https://doi.org/10.1016/j.gde.2011.04.003>.
- Aulehla, A., and Pourquié, O. (2006). On periodicity and directionality of somitogenesis. *Brain Struct Funct* 211, 3–8. <https://doi.org/10.1007/s00429-006-0124-y>.
- Aulehla, A., and Pourquie, O. (2010). Signaling Gradients during Paraxial Mesoderm Development. *Cold Spring Harbor Perspectives in Biology* 2, a000869–a000869. <https://doi.org/10.1101/cshperspect.a000869>.
- Aulehla, A., Wehrle, C., Brand-Saberi, B., Kemler, R., Gossler, A., Kanzler, B., and Herrmann, B.G. (2003). Wnt3a Plays a Major Role in the Segmentation Clock Controlling Somitogenesis. *Developmental Cell* 4, 395–406. [https://doi.org/10.1016/S1534-5807\(03\)00055-8](https://doi.org/10.1016/S1534-5807(03)00055-8).
- Aulehla, A., Wiegraebe, W., Baubet, V., Wahl, M.B., Deng, C., Taketo, M., Lewandoski, M., and Pourquié, O. (2008). A β -catenin gradient links the clock and wavefront systems in mouse embryo segmentation. *Nature Cell Biology* 10, 186–193. <https://doi.org/10.1038/ncb1679>.
- Boareto, M., Tomka, T., and Iber, D. (2021). Positional information encoded in the dynamic differences between neighboring oscillators during vertebrate segmentation. *Cells & Development* 203737. <https://doi.org/10.1016/j.cdev.2021.203737>.
- Brend, T., and Holley, S.A. (2009). Expression of the oscillating gene *her1* is directly regulated by hairy/enhancer of split, T-box, and suppressor of hairless proteins in the zebrafish segmentation clock. *Developmental Dynamics* 238, 2745–2759. <https://doi.org/10.1002/dvdy.22100>.
- van den Brink, S.C., Alemany, A., van Batenburg, V., Moris, N., Blotenburg, M., Vivié, J., Baillie-Johnson, P., Nichols, J., Sonnen, K.F., Martinez Arias, A., et al. (2020). Single-cell and

spatial transcriptomics reveal somitogenesis in gastruloids. *Nature* 582, 405–409. <https://doi.org/10.1038/s41586-020-2024-3>.

Brody, T., and Odenwald, W.F. (2000). Programmed Transformations in Neuroblast Gene Expression during *Drosophila* CNS Lineage Development. *Developmental Biology* 226, 34–44. <https://doi.org/10.1006/dbio.2000.9829>.

Chou, K. T., Lee, D. D., Chiou, J. G., Galera-Laporta, L., Ly, S., Garcia-Ojalvo, J., & Süel, G. M. (2022). A segmentation clock patterns cellular differentiation in a bacterial biofilm. *Cell*, 185(1), 145–157.e13.

Cooke, J., and Zeeman, E.C. (1976). A clock and wavefront model for control of the number of repeated structures during animal morphogenesis. *Journal of Theoretical Biology* 58, 455–476. .

Cutty, S.J., Fior, R., Henriques, P.M., Saúde, L., and Wardle, F.C. (2012). Identification and expression analysis of two novel members of the *Mesp* family in zebrafish. *Int. J. Dev. Biol.* 56, 285–294. <https://doi.org/10.1387/ijdb.113447sc>.

Danino, T., Mondragón-Palomino, O., Tsimring, L., and Hasty, J. (2010). A synchronized quorum of genetic clocks. *Nature* 463, 326–330. <https://doi.org/10.1038/nature08753>.

De Simone, A., Evanitsky, M.N., Hayden, L., Cox, B.D., Wang, J., Tornini, V.A., Ou, J., Chao, A., Poss, K.D., and Di Talia, S. (2021). Control of osteoblast regeneration by a train of Erk activity waves. *Nature* 590, 129–133. <https://doi.org/10.1038/s41586-020-03085-8>.

Delaune, E.A., François, P., Shih, N.P., and Amacher, S.L. (2012). Single-Cell-Resolution Imaging of the Impact of Notch Signaling and Mitosis on Segmentation Clock Dynamics. *Developmental Cell* 23, 995–1005. <https://doi.org/10.1016/j.devcel.2012.09.009>.

Diaz-Cuadros, M., Wagner, D.E., Budjan, C., Hubaud, A., Tarazona, O.A., Donnelly, S., Michaut, A., Al Tanoury, Z., Yoshioka-Kobayashi, K., Niino, Y., et al. (2020). In vitro characterization of the human segmentation clock. *Nature* 580, 113–118. <https://doi.org/10.1038/s41586-019-1885-9>.

Diernfellner, A.C.R., and Brunner, M. (2020). Phosphorylation Timers in the *Neurospora crassa* Circadian Clock. *Journal of Molecular Biology* 432, 3449–3465. <https://doi.org/10.1016/j.jmb.2020.04.004>.

Dill, K.K., and Amacher, S.L. (2005). *tortuga* refines Notch pathway gene expression in the zebrafish presomitic mesoderm at the post-transcriptional level. *Developmental Biology* 287, 225–236. <https://doi.org/10.1016/j.ydbio.2005.07.032>.

Dubrulle, J., and Pourquié, O. (2004). *fgf8* mRNA decay establishes a gradient that couples axial elongation to patterning in the vertebrate embryo. *Nature* 427, 419–422. <https://doi.org/10.1038/nature02216>.

Dubrulle, J., McGrew, M.J., and Pourquié, O. (2001). FGF Signaling Controls Somite Boundary Position and Regulates Segmentation Clock Control of Spatiotemporal Hox Gene Activation. *Cell* 106, 219–232. [https://doi.org/10.1016/S0092-8674\(01\)00437-8](https://doi.org/10.1016/S0092-8674(01)00437-8).

Ferenc, J., Papasaikas, P., Ferralli, J., Nakamura, Y., Smallwood, S., and Tsiairis, C.D. (2021). Mechanical oscillations orchestrate axial patterning through Wnt activation in *Hydra*. *Sci. Adv.* 7, eabj6897. <https://doi.org/10.1126/sciadv.abj6897>.

Henry, C.A., Poage, C.T., McCarthy, M.B., Campos-Ortega, J., and Cooper, M.S. (2005). Regionally Autonomous Segmentation Within Zebrafish Presomitic Mesoderm. *Zebrafish* 2, 7–18. <https://doi.org/10.1089/zeb.2005.2.7>.

Hubaud, A., and Pourquié, O. (2014). Signalling dynamics in vertebrate segmentation. *Nature Reviews Molecular Cell Biology* 15, 709–721. <https://doi.org/10.1038/nrm3891>.

Hubaud, A., Regev, I., Mahadevan, L., and Pourquié, O. (2017). Excitable Dynamics and Yap-Dependent Mechanical Cues Drive the Segmentation Clock. *Cell* <https://doi.org/10.1016/j.cell.2017.08.043>.

Langenberg, T., Brand, M., and Cooper, M.S. (2003). Imaging brain development and organogenesis in zebrafish using immobilized embryonic explants. *Dev. Dyn.* 228, 464–474. <https://doi.org/10.1002/dvdy.10395>.

Lauschke, V.M., Tsiairis, C.D., François, P., and Aulehla, A. (2012). Scaling of embryonic patterning based on phase-gradient encoding. *Nature* 493, 101–105. <https://doi.org/10.1038/nature11804>.

Lauschke, V.M., Tsiairis, C.D., François, P., and Aulehla, A. (2013). Scaling of embryonic patterning based on phase-gradient encoding. *Nature* 493, 101–105. <https://doi.org/10.1038/nature11804>.

Mara, A., Schroeder, J., Chalouni, C., and Holley, S.A. (2007). Priming, initiation and synchronization of the segmentation clock by deltaD and deltaC. *Nature Cell Biology* 9, 523–530. <https://doi.org/10.1038/ncb1578>.

Maroto, M., Dale, J.K., Dequeant, M.-L., Petit, A.-C., and Pourquie, O. (2005). Synchronised cycling gene oscillations in presomitic mesoderm cells require cell-cell contact. *The International Journal of Developmental Biology* 49, 309–315. <https://doi.org/10.1387/ijdb.041958mm>.

Martin, B.L. (2016). Factors that coordinate mesoderm specification from neuromesodermal progenitors with segmentation during vertebrate axial extension. *Seminars in Cell & Developmental Biology* 49, 59–67. <https://doi.org/10.1016/j.semcdb.2015.11.014>.

Masamizu, Y., Ohtsuka, T., Takashima, Y., Nagahara, H., Takenaka, Y., Yoshikawa, K., Okamura, H., and Kageyama, R. (2006). Real-time imaging of the somite segmentation clock: revelation of unstable oscillators in the individual presomitic mesoderm cells. *Proceedings of the National Academy of Sciences* 103, 1313–1318. .

Matsuda, M., Yamanaka, Y., Uemura, M., Osawa, M., Saito, M.K., Nagahashi, A., Nishio, M., Guo, L., Ikegawa, S., Sakurai, S., et al. (2020a). Recapitulating the human segmentation clock with pluripotent stem cells. *Nature* 580, 124–129. <https://doi.org/10.1038/s41586-020-2144-9>.

Matsuda, M., Hayashi, H., Garcia-Ojalvo, J., Yoshioka-Kobayashi, K., Kageyama, R., Yamanaka, Y., Ikeya, M., Toguchida, J., Alev, C., and Ebisuya, M. (2020b). Species-specific segmentation clock periods are due to differential biochemical reaction speeds. *Science* 369, 1450–1455. <https://doi.org/10.1126/science.aba7668>.

Matsumiya, M., Tomita, T., Yoshioka-Kobayashi, K., Isomura, A., and Kageyama, R. (2018a). ES cell-derived presomitic mesoderm-like tissues for analysis of synchronized oscillations in the segmentation clock. *Development* 145, dev156836. <https://doi.org/10.1242/dev.156836>.

Matsumiya, M., Tomita, T., Yoshioka-Kobayashi, K., Isomura, A., and Kageyama, R. (2018b). ES cell-derived presomitic mesoderm-like tissues for analysis of synchronized oscillations in the segmentation clock. *Development* 145, dev156836. <https://doi.org/10.1242/dev.156836>.

Morelli, L.G., Ares, S., Herrgen, L., Schröter, C., Jülicher, F., and Oates, A.C. (2009). Delayed coupling theory of vertebrate segmentation. *HFSP Journal* 3, 55–66. <https://doi.org/10.2976/1.3027088>.

Moreno, T. a., and Kintner, C. (2004). Regulation of segmental patterning by retinoic acid signaling during *Xenopus* somitogenesis. *Developmental Cell* 6, 205–218. [https://doi.org/10.1016/S1534-5807\(04\)00026-7](https://doi.org/10.1016/S1534-5807(04)00026-7).

Murray, P.J., Maini, P.K., and Baker, R.E. (2011). The clock and wavefront model revisited. *Journal of Theoretical Biology* 283, 227–238. <https://doi.org/10.1016/j.jtbi.2011.05.004>.

Negrete JR, J., Lengyel, I.M., Rohde, L.A., Desai, R.A., Oates, A., and Jülicher, F. (2021). Theory of time delayed genetic oscillations with external noisy regulation. *New J. Phys.* <https://doi.org/10.1088/1367-2630/abd80b>.

Oates, A.C., Morelli, L.G., and Ares, S. (2012). Patterning embryos with oscillations: structure, function and dynamics of the vertebrate segmentation clock. *Development* 139, 625–639. <https://doi.org/10.1242/dev.063735>.

Palmeirim, I., Henrique, D., Ish-Horowicz, D., and Pourquié, O. (1997). Avian hairy gene expression identifies a molecular clock linked to vertebrate segmentation and somitogenesis. *Cell* 91, 639–648. [https://doi.org/10.1016/S0092-8674\(00\)80451-1](https://doi.org/10.1016/S0092-8674(00)80451-1).

Palmeirim, I., Dubrulle, J., Henrique, D., Ish-Horowicz, D., and Pourquié, O. (1998). Uncoupling segmentation and somitogenesis in the chick presomitic mesoderm. *Developmental Genetics* 23, 77–85. [https://doi.org/10.1002/\(SICI\)1520-6408\(1998\)23:1<77::AID-DVG8>3.0.CO;2-3](https://doi.org/10.1002/(SICI)1520-6408(1998)23:1<77::AID-DVG8>3.0.CO;2-3).

Perez-Garcia, P., Serrano-Ron, L., and Moreno-Risueno, M.A. (2022). The nature of the root clock at single cell resolution: Principles of communication and similarities with plant and

animal pulsatile and circadian mechanisms. *Current Opinion in Cell Biology* 77, 102102. <https://doi.org/10.1016/j.ceb.2022.102102>.

Sawada, A., Shinya, M., Jiang, Y.-J., Kawakami, A., Kuroiwa, A., and Takeda, H. (2001). Fgf/MAPK signalling is a crucial positional cue in somite boundary formation. *Development* 128, 4873–4880. .

Shih, N.P., Francois, P., Delaune, E.A., and Amacher, S.L. (2015). Dynamics of the slowing segmentation clock reveal alternating two-segment periodicity. *Development* 142, 1785–1793. <https://doi.org/10.1242/dev.119057>.

Simsek, M.F., and Özbudak, E.M. (2018). Spatial Fold Change of FGF Signaling Encodes Positional Information for Segmental Determination in Zebrafish. *Cell Reports* 24, 66–78.e8. <https://doi.org/10.1016/j.celrep.2018.06.023>.

Sonnen, K.F., Lauschke, V.M., Uraji, J., Falk, H.J., Petersen, Y., Funk, M.C., Beaupeux, M., François, P., Merten, C.A., and Aulehla, A. (2018). Modulation of Phase Shift between Wnt and Notch Signaling Oscillations Controls Mesoderm Segmentation. *Cell* 172, 1079–1090.e12. <https://doi.org/10.1016/j.cell.2018.01.026>.

Soroldoni, D., Jorg, D.J., Morelli, L.G., Richmond, D.L., Schindelin, J., Julicher, F., and Oates, A.C. (2014). A Doppler effect in embryonic pattern formation. *Science* 345, 222–225. <https://doi.org/10.1126/science.1253089>.

Tsiairis, C.D., and Aulehla, A. (2016). Self-Organization of Embryonic Genetic Oscillators into Spatiotemporal Wave Patterns. *Cell* 164, 656–667. <https://doi.org/10.1016/j.cell.2016.01.028>.

Venzin, O.F., and Oates, A.C. (2020). What are you synching about? Emerging complexity of Notch signaling in the segmentation clock. *Developmental Biology* 460, 40–54. <https://doi.org/10.1016/j.ydbio.2019.06.024>.

Wanglar, C., Takahashi, J., Yabe, T., and Takada, S. (2014). Tbx Protein Level Critical for Clock-Mediated Somite Positioning Is Regulated through Interaction between Tbx and Ripply. *PLoS ONE* 9, e107928. <https://doi.org/10.1371/journal.pone.0107928>.

Webb, A.B., Lengyel, I.M., Jörg, D.J., Valentin, G., Jülicher, F., Morelli, L.G., and Oates, A.C. (2016). Persistence, period and precision of autonomous cellular oscillators from the zebrafish segmentation clock. *ELife* 5, e08438. <https://doi.org/10.7554/eLife.08438>.

Zákány, J., Kmita, M., Alarcon, P., de la Pompa, J.-L., and Duboule, D. (2001). Localized and Transient Transcription of Hox Genes Suggests a Link between Patterning and the Segmentation Clock. *Cell* 106, 207–217. [https://doi.org/10.1016/S0092-8674\(01\)00436-6](https://doi.org/10.1016/S0092-8674(01)00436-6).

Acknowledgements: Our thanks to the following: A. Aulehla, M. Ebisuya, J. Garcia Ojalvo, M. Gonzalez-Gaitan, C-P Heisenberg, A. Martinez Arias, G. Mönke, L. Morelli, C. Mulas, B. Steventon, K. Uriu, and Oates lab members for comments on the manuscript; J-Y Tinevez and T. Pietzsch for Mastodon assistance; MPI-CBG, UCL, and EPFL fish facilities; D. Rohde for an X; U. Schulze and A. Boni for imaging help; and C. Jollivet and V. Sergy for technical and administrative support.

Funding:

École Polytechnique Fédérale de Lausanne (AO)

Francis Crick Institute (AO)

Max-Planck-Gesellschaft (AO and FJ)

SNSF Project funding division III 31003A_176037 (JN and AO)

Wellcome Trust Senior Research Fellowship in Basic Biomedical Science WT098025MA (AO)

MPIPKS Visitors Program (JN)

Long-Term HFSP postdoctoral fellowship LT000078/2016 (SRN)

Whitaker International Fellowship (RAD)

Author contributions:

Conceptualization: LAR, JN, ABR, ACO

Methodology: LAR, ABR, JN, GV, SRN, RAD, PS, DS

Investigation: LAR, ABR, JN, GV, SRN, RAD

Visualization: ABR, LAR, JN, ACO

Software: ABR, SRN, JN, PS

Funding acquisition: FJ, ACO

Supervision: FJ, ACO

Writing – Original Draft Preparation: LAR

Writing – Review & Editing: LAR, ABR, JN, ACO

Competing Interests: PS is a co-founder of Viventis Microscopy.

Data and materials availability: All data, code, and materials available upon request

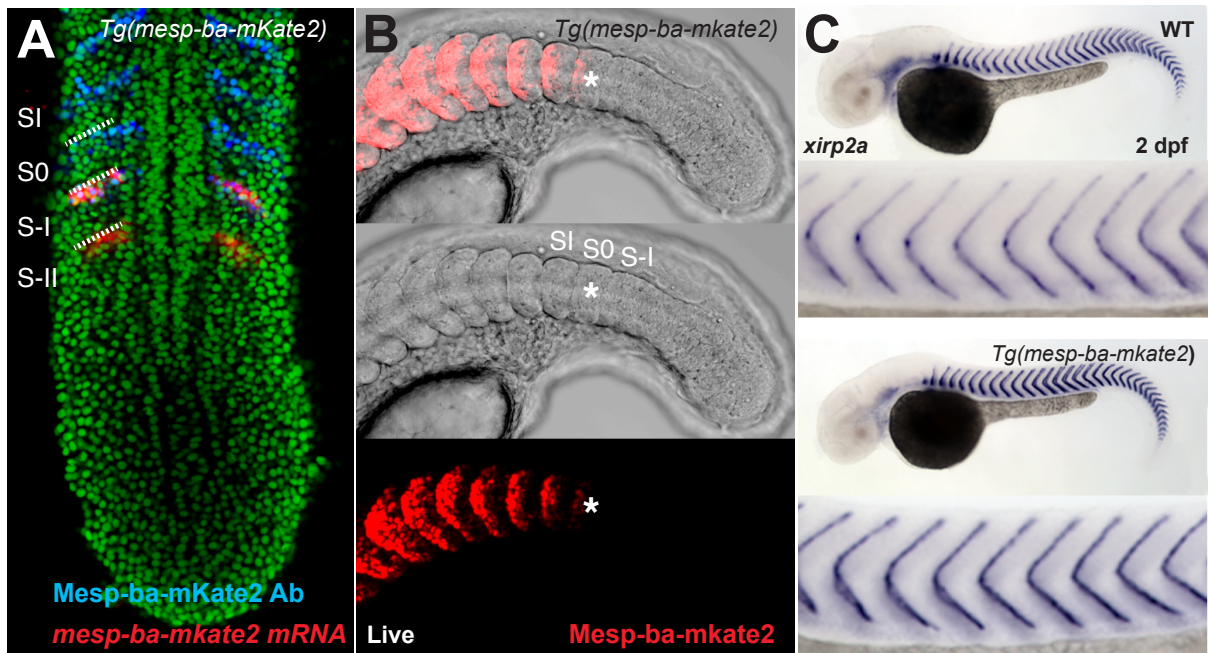
Supplementary Materials:

Materials and Methods

Supplementary Text 1

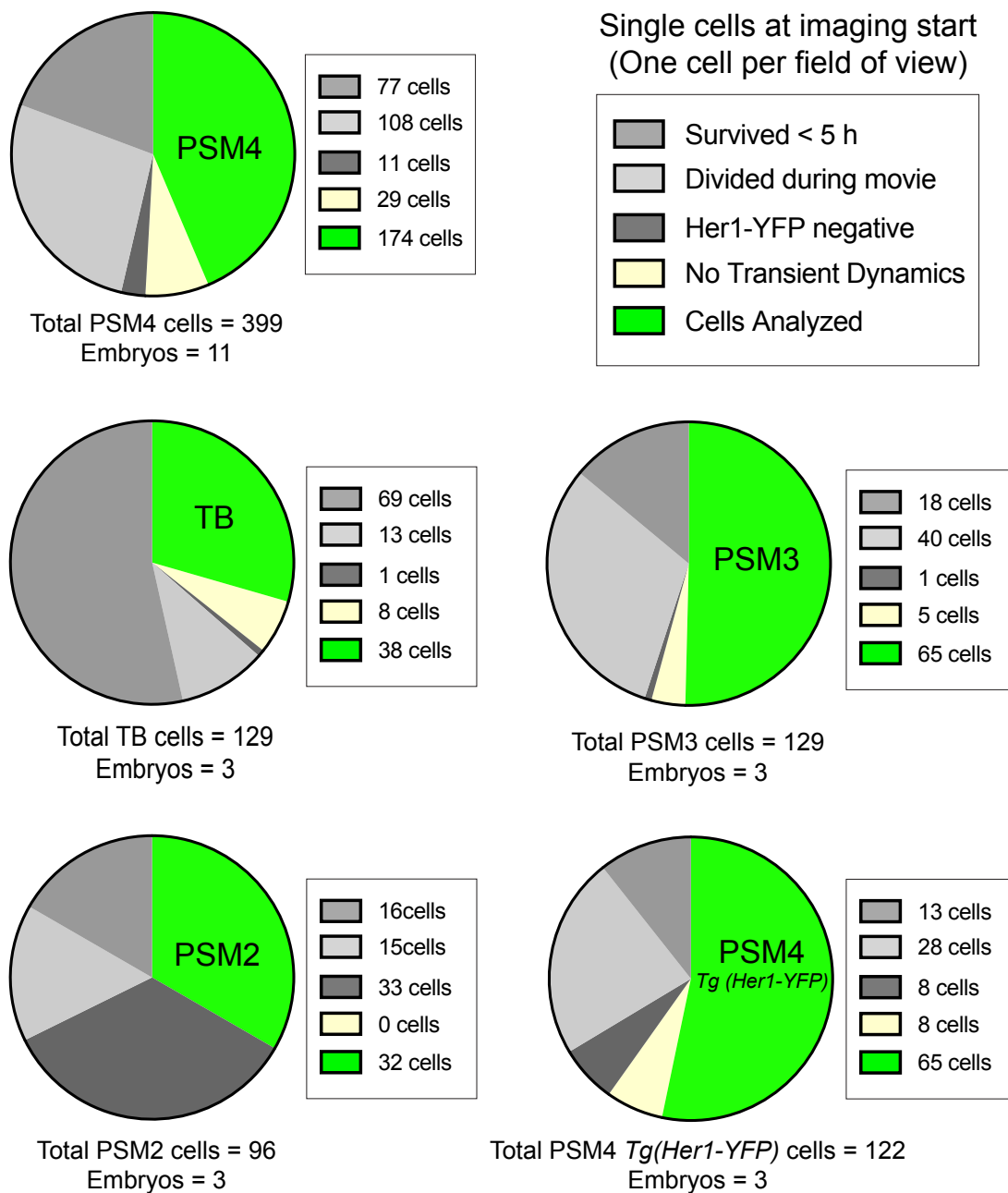
Figures S1 to S14

Table S1



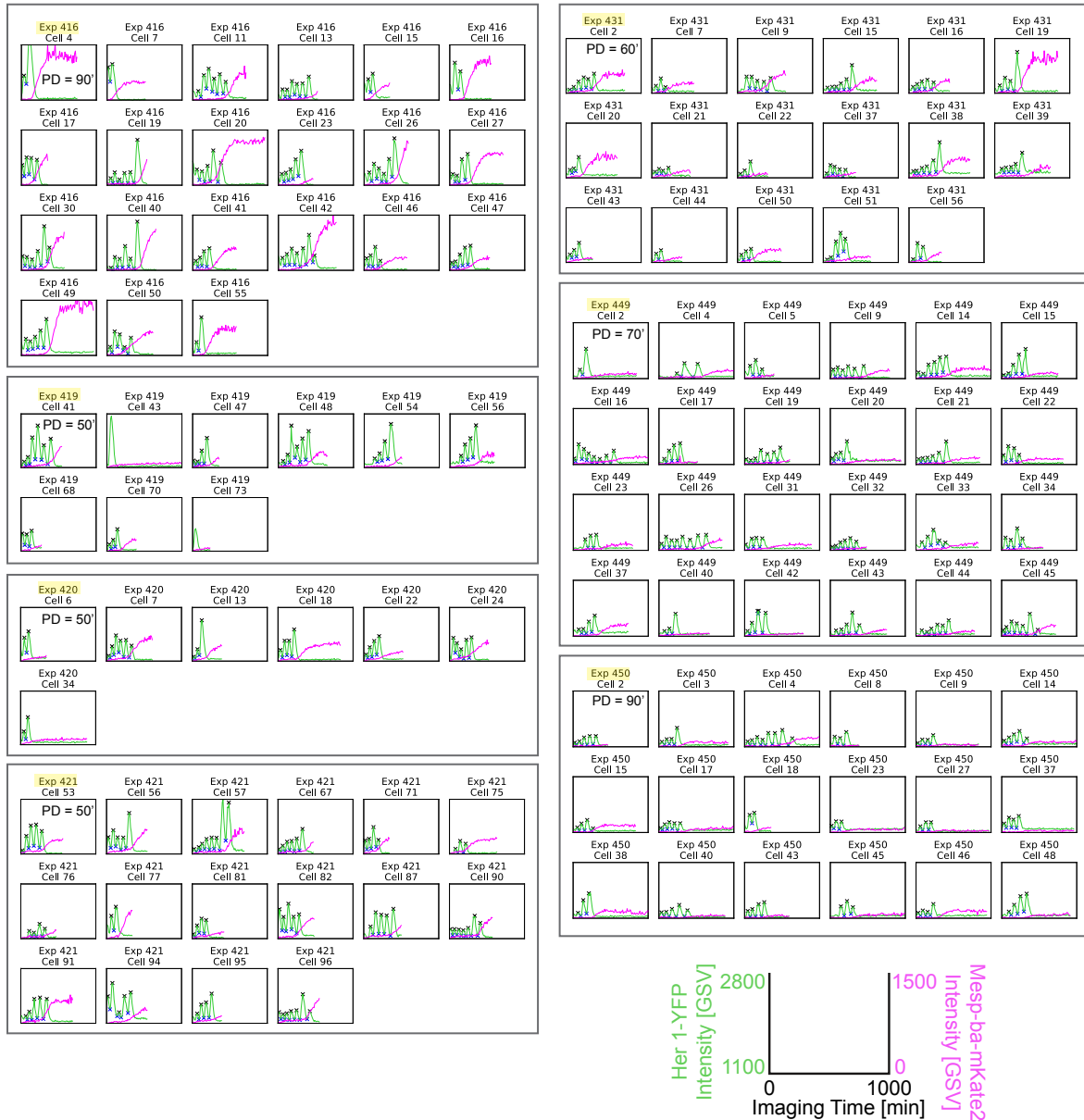
Extended Data Fig. 1. Mesp-ba-mKate2 transgenic expression and detection.

(A) Detection of *mesp-ba-mkate2* mRNA (red, in situ hybridization) and Mesp-ba-mKate2 (blue, anti-mKate2 antibody) in a fixed *Tg(mesp-ba:mesp-ba-mkate2)* 10 somite-staged embryo (nuclei labelled green). *mesp-ba-mkate2* was detected only in the rostral half of pre-segments (S-II and S-I) in the anterior PSM as expected from endogenous *mesp-ba* expression (Cutty et al., 2012). Mesp-ba-mKate2 was first detected by antibodies to mKate2 in the rostral half of S-I, where it persisted in the newly forming somite (S0) and formed somites (SI). (B) Mesp-ba-mKate2 signal was first detected in live *Tg(mesp-ba:mesp-ba-mkate2)* embryos within the rostral half of S0 (*), after which it remained in the rostral half of the formed somites (21-somite-stage embryo). (C) Boundary formation was normal as detected by in situ hybridization for the boundary marker *xirp2a* in *Tg(mesp-ba:mesp-ba-mkate2)* embryos compared to wildtype (WT) at 2 days post-fertilization (dpf).



Extended Data Fig 2. Cell culture analysis criteria.

Dissociated cells originating from different anteroposterior positions (TB and PSM 2, 3 and 4) in *Tg(her1-yfp;h2b-mcherry)* or *Tg(her1-yfp)* embryos. Analysis criteria was as follows: 1) Single cells alone in the field of view were selected at the start of imaging (Total cells); 2) Cells dying before 5 hours post-dissociation were excluded from analysis (Survived < 5 h); 3) Cells that survived > 5 h but divided during the movie were excluded (Divided during movie); 4) From the remaining cells, those not expressing Her1-YFP (Her1-YFP negative) or failing to arrest before cell death were excluded (No Transient Dynamics); 5) Transient Dynamics were then analyzed in the remaining cells. Note that PSM2 cells listed as Her1-YFP negative may have already arrested before imaging started.

A**Extended Data Fig. 3. Her1-YFP and Mesp-ba-mKate2 intensity traces.**

(A-D) Cells dissected, dissociated and cultured from 15 somite-staged *Tg(her1-yfp;h2b-mcherry)* embryos. Single oscillating cells that remained the only cell in the field of view, survived > 5h post-dissociation, did not divide, and showed transient dynamics were analyzed. Her1-YFP and Mesp-ba-mKate2 intensity traces from single cells with the maxima (peaks) and minima (troughs) marked (X). Traces are labelled by experiment number and cell position. The time post-dissociation (PD) at which imaging started is given for each experiment. (A) Posterior quarter of PSM (PSM4) (N=11, n=174 cells).

Extended Data Fig. 3 continues on the next page.



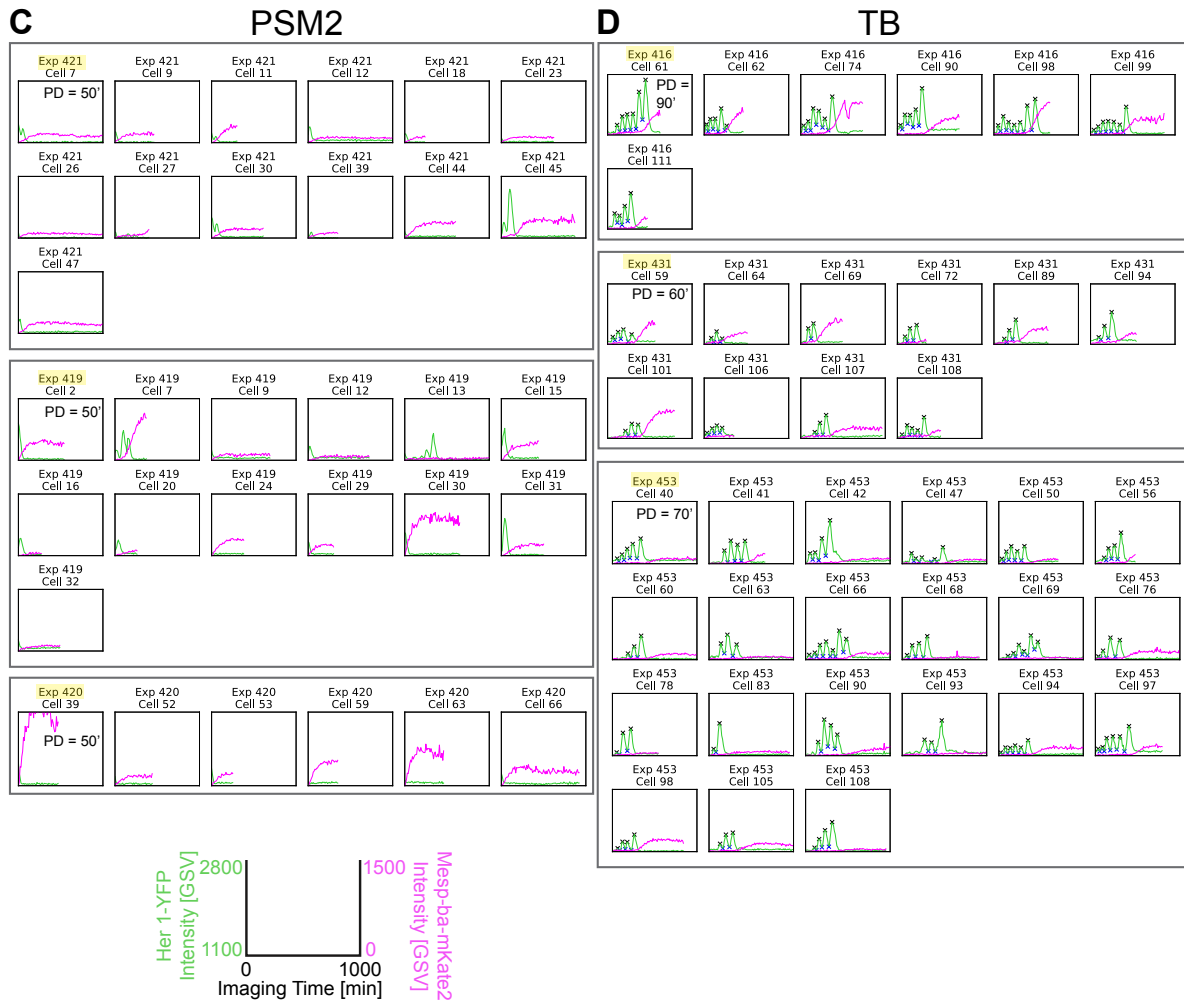
Extended Data Fig. 3. Her1-YFP and Mesp-ba-mKate2 intensity traces.

Continued from previous page.

(A) Intensity traces from posterior quarter of PSM (PSM4) (N=11 experiments, n=174 cells).

(B) Intensity traces from the third quarter of PSM (PSM3) (N=3 experimnets, n=65 cells)

Extended Data Fig. 3 continues on the next page.

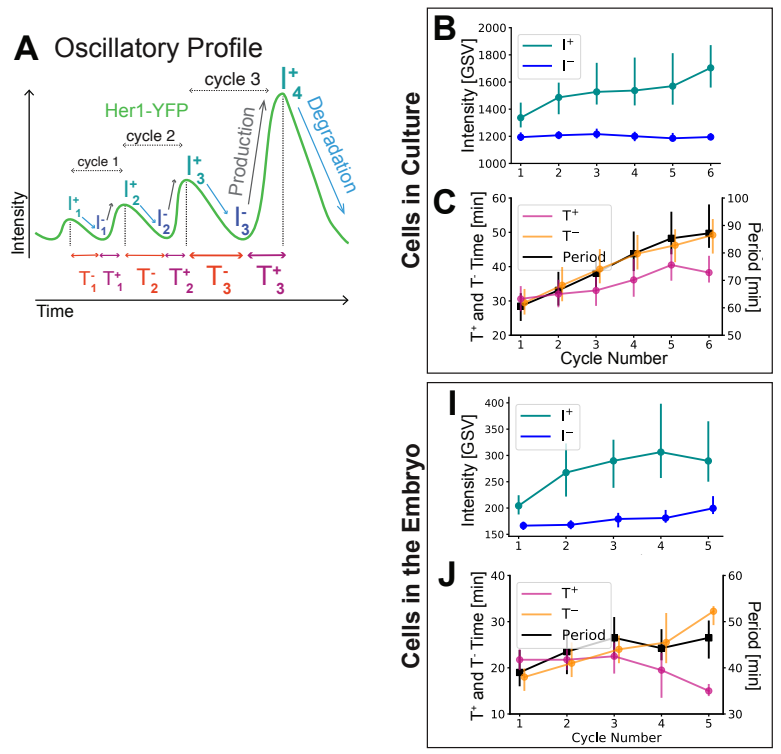


Extended Data Fig. 3. Her1-YFP and Mesp-ba-mKate2 intensity traces.

Continued from previous page.

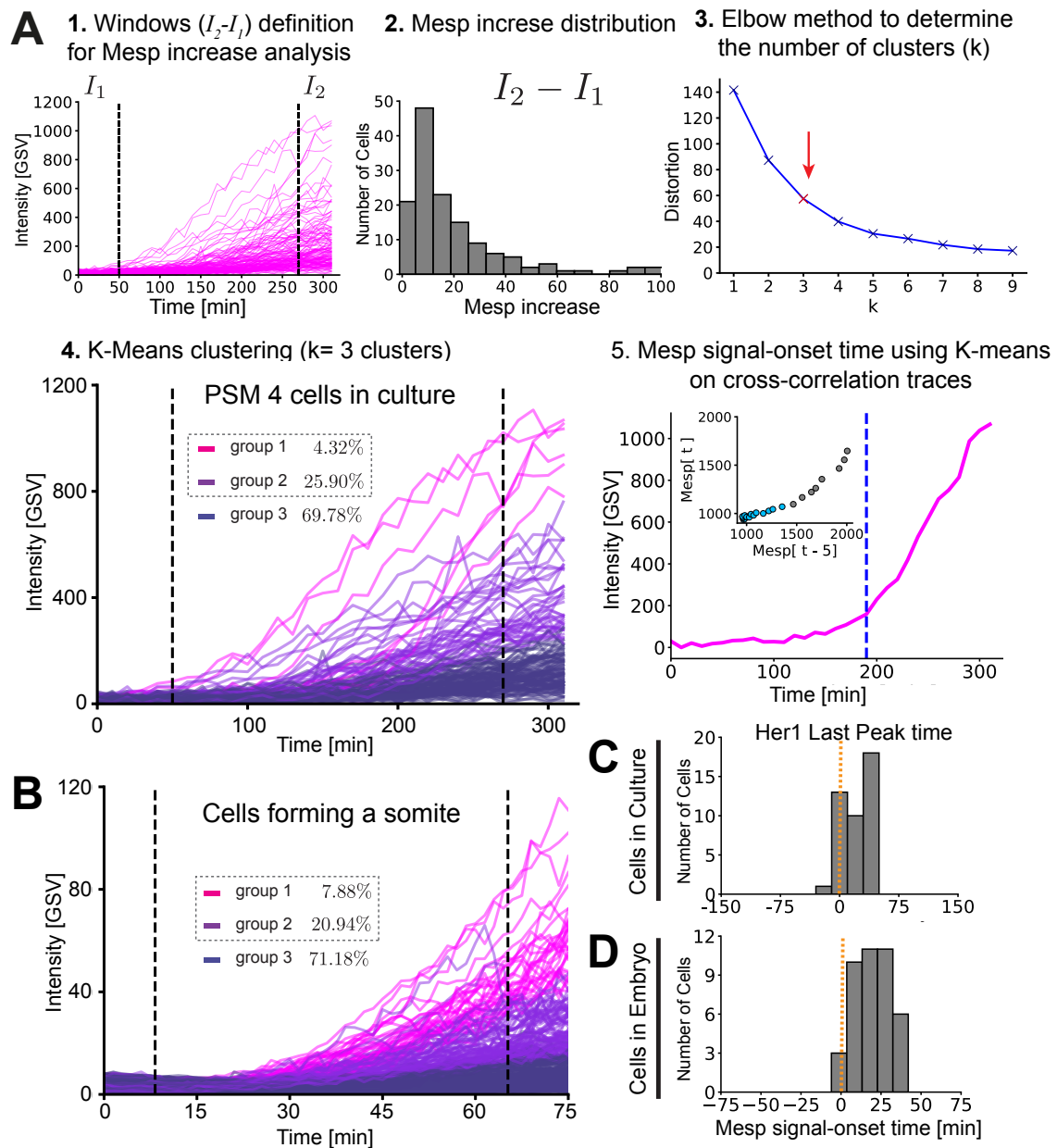
(C) Intensity traces from second quarter of PSM (PSM2) (N=3 experiments, n=32 cells).

(D) Intensity traces from Tailbud (TB) (N=3 experiments, n=38 cells).



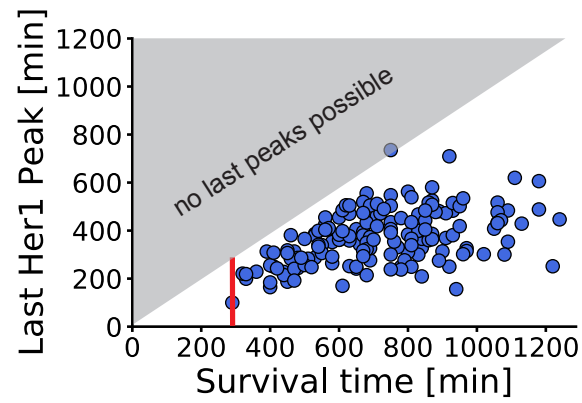
Extended Data Fig. 4. Her1-YFP Oscillatory Profile.

(A) Observables of Her1-YFP profile: peak (I^+) and trough (I^-) intensity; time-intervals of production (T^+) and degradation (T^-). (B, C) Cell-autonomous PSM4 observables aligned by first cycle. (I, J) Observables from PSM4 cells in embryo aligned by first cycle.



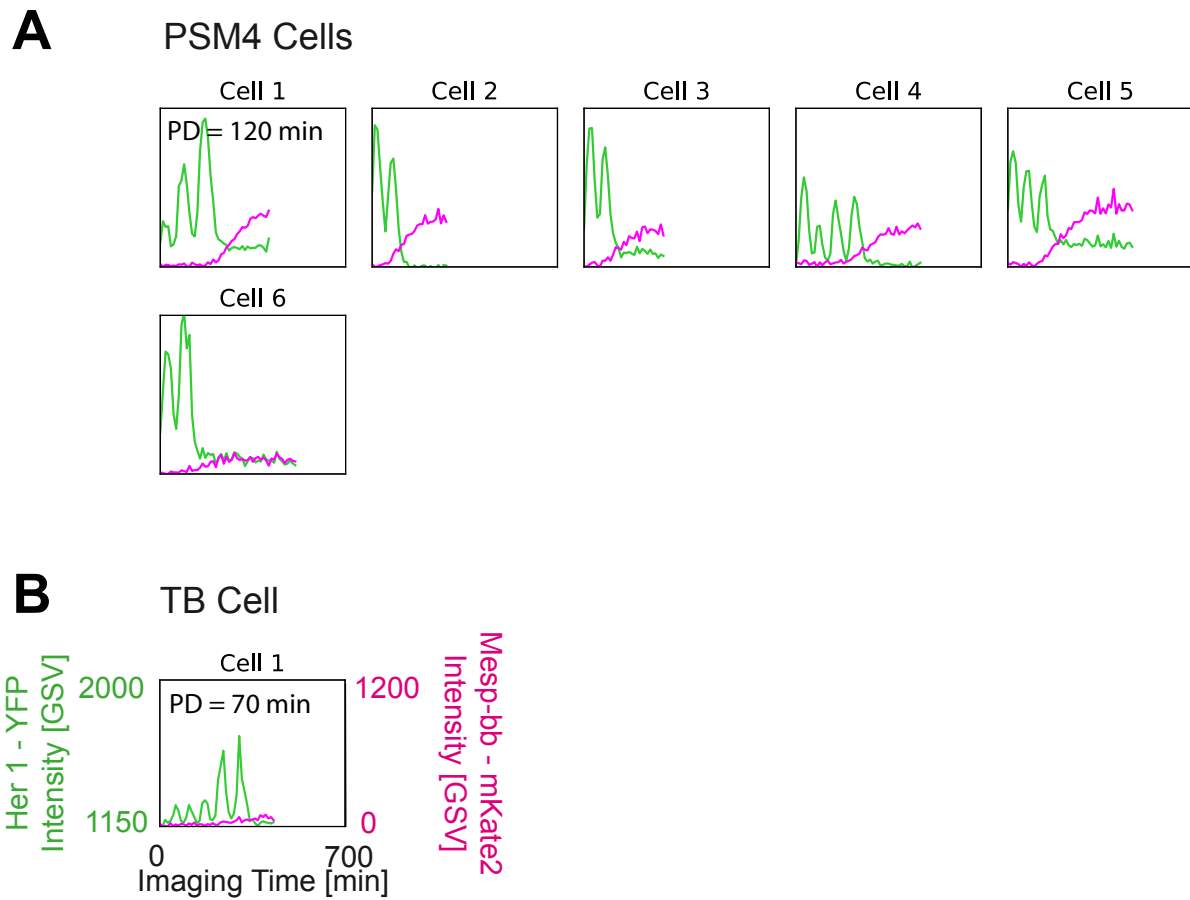
Extended Data Fig. 5. Mesp-ba-mKate2 Signal-Onset defined in individual intensity traces.

(A) Mesp-ba-mKate2 signal-onset time defined in intensity traces from single PSM4 cells in culture ($N = 11$ embryos, $n = 174$ cells). Steps to define signal-onset: 1) An arbitrary window was defined across the intensity traces, then average intensity within each window was calculated. 2) Mesp-ba-mKate2 increase was obtained by subtracting the first intensity window (I_1) from the second (I_2), shown as a distribution. 3) Because intensity trace profiles varied between cells, we used the elbow method to identify the number of clusters. 4) Mesp-ba-mKate2 increase for each cell was then used to perform K-Means clustering using $k=3$. Groups 1 and 2 are cells showing an obvious Mesp-ba-mKate2 signal-onset. 5) Signal-onset time was then determined in these groups using K-Means on a lag-plot of the intensity. (B) Mesp-ba-mKate2 signal-onset in cells forming a somite in the embryo ($n= 190$). (C, D) Time of Mesp signal-onset with respect to Her1-Last Peak in PSM 4 cells in culture (C) and to cells tracked in an embryo carrying *mesp-ba-mKate2* and *her1-YFP* transgenes ($n= 41$).



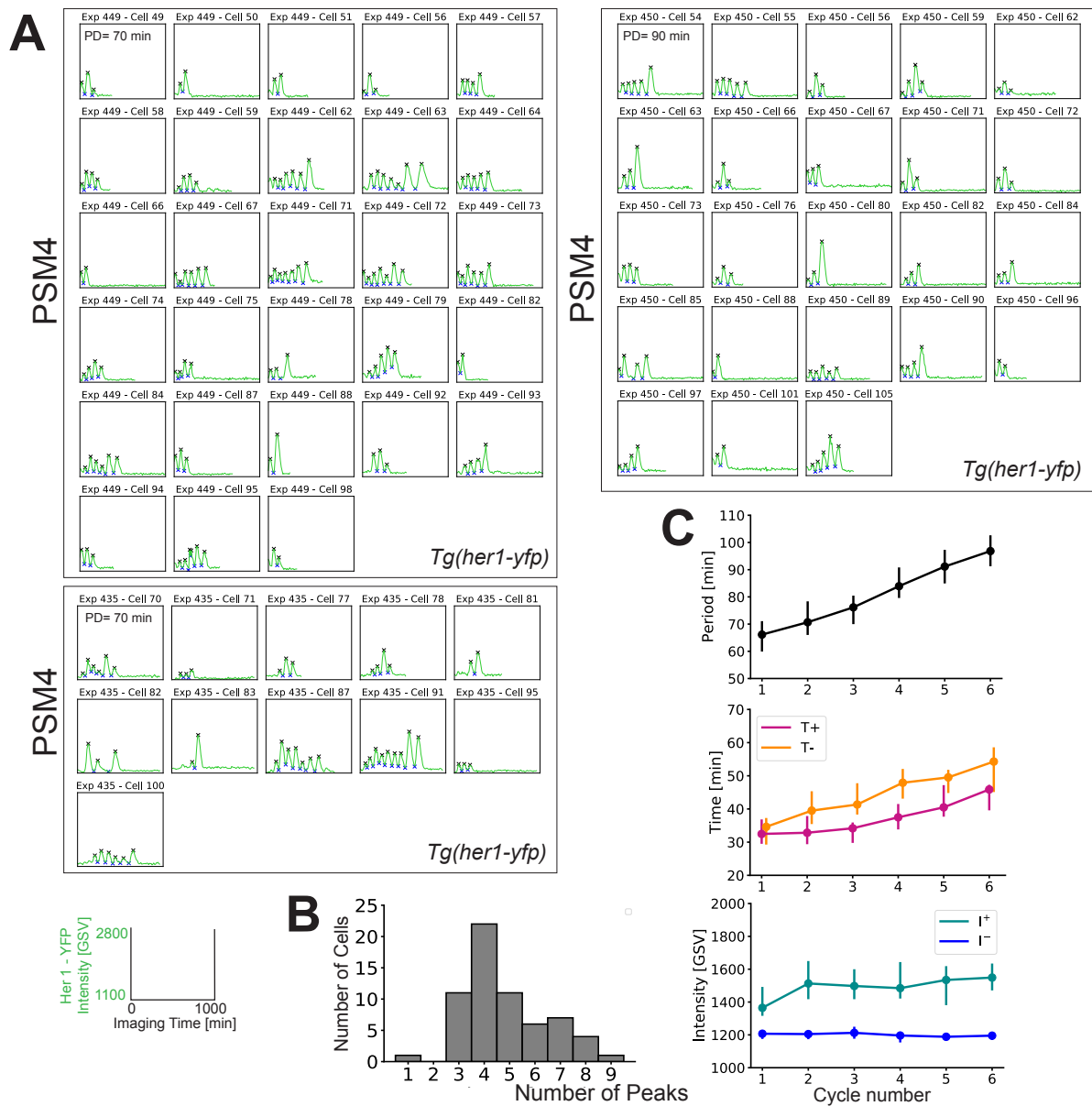
Extended Data Fig. 6. Time of cell death and oscillatory arrest in single cells.

Time of PSM4 cell death in culture and Her1-YFP last peak time in single cells (N = 11 embryos, n = 174 cells). Grey triangle marks region in which a last peak is not possible because cells are already dead. Cells that were alive at the end of imaging were not included in this plot (n=14). Mean cell survival time was 1293, SD \pm 319 minutes.



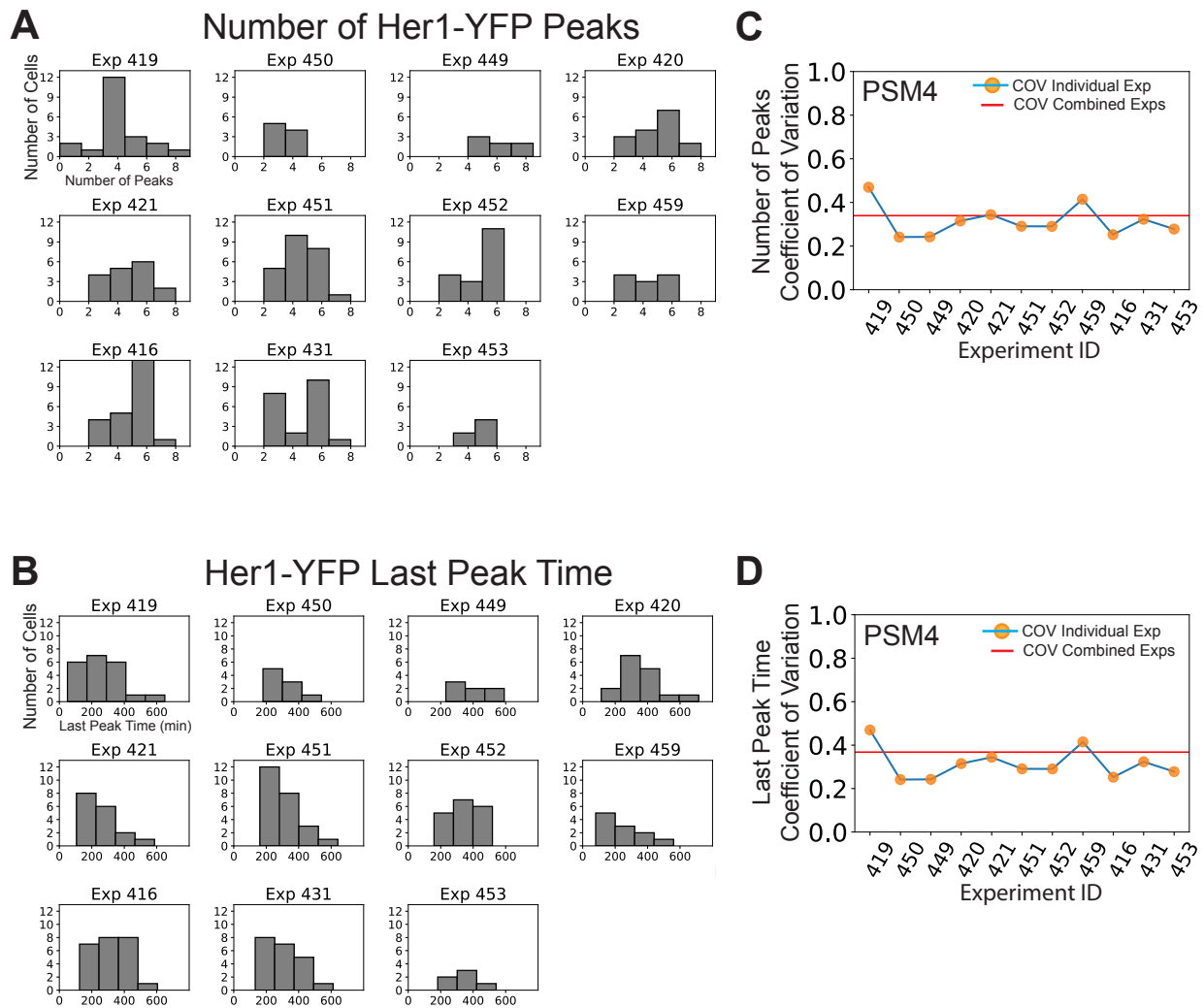
Extended Data Fig. 7. Cells isolated one-per-well reproduce autonomous behaviour seen in low-density culture.

(A, B) Mesp-ba-mKate2 and Her1YFP intensity traces in PSM4 (A) and TB (B) cells isolated one-per-well in a 24-well plate (N=3 embryos, n=6 PSM4 cells, n=1 TB cell). Time of imaging start post-dissociation (PD) given. Oscillations, intensity-increase and arrest in concert with Mesp-ba-mKate2 signal-onset in the isolated cells reproduces behaviour we describe in low-density culture (Fig. 1).



Extended Fig. 8. Autonomous Her1-YFP dynamics do not depend on *Tg(mesp-ba-mKate2)*

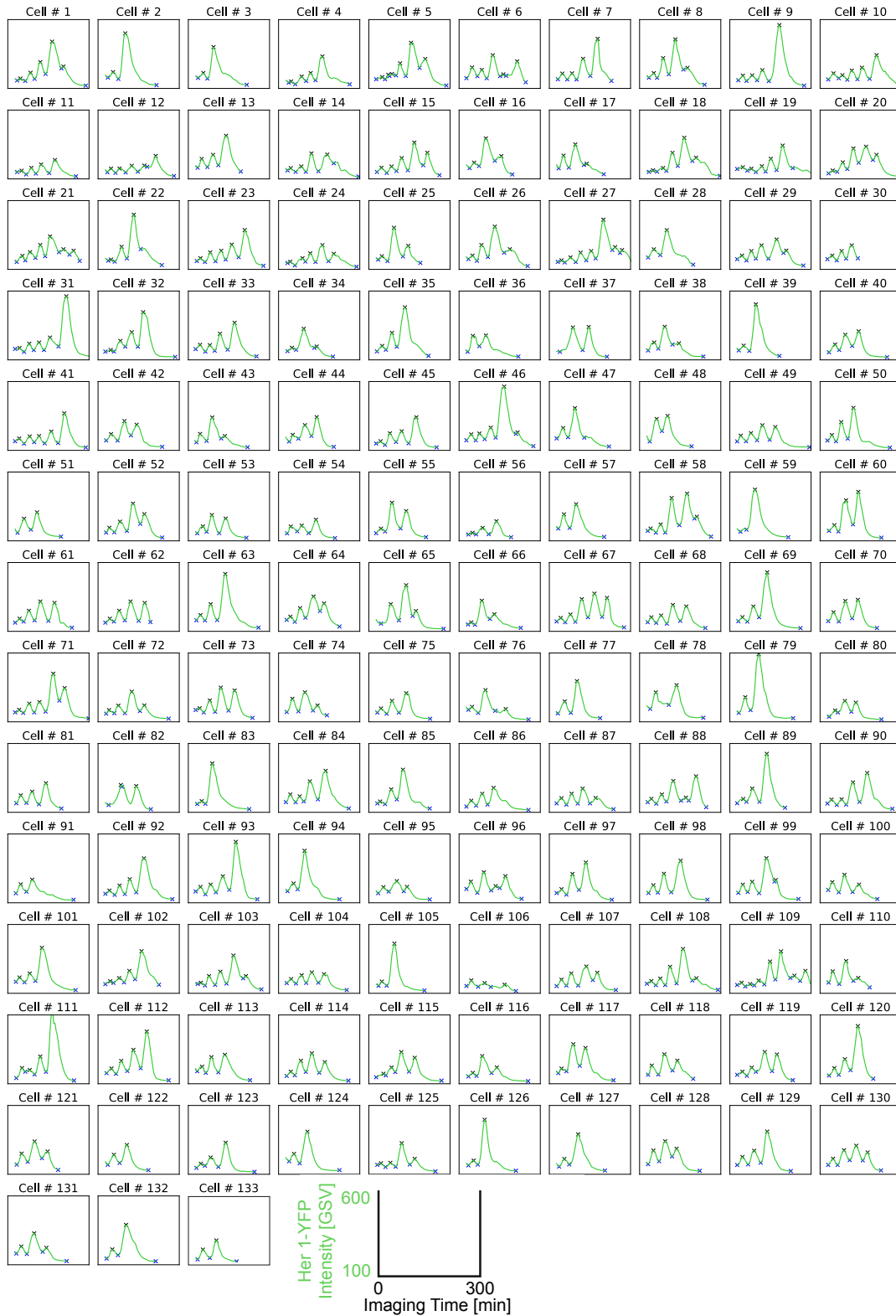
(A) Her1-YFP intensity traces in cultured PSM4 cells from embryos carrying only *Tg(her1-yfp)* (N=3 embryos; n= 63 cells) that were cultured in parallel to PSM4 from *Tg(her1-yfp; mesp-ba-mkate2)* embryos (experiments 449 and 450 in Fig. S4). Time imaging started post-dissociation (PD). (B) Number of peaks (compare to Fig 2 D). (C) Her1-YFP intensity trace observables without *Tg(mesp-ba-mkate2)* were similar to *Tg(her1-yfp; mesp-ba-mkate2)* cells (Fig. 4B,C,I,J), including: increasing period, increasing maxima (I+) and constant minima intensity (I-) over successive cycles; and, asymmetric production (T+) and degradation (T-) intervals.



Extended Data Figure Fig. 9. Variability in autonomous timing until oscillatory arrest is not due solely to inter-experimental differences.

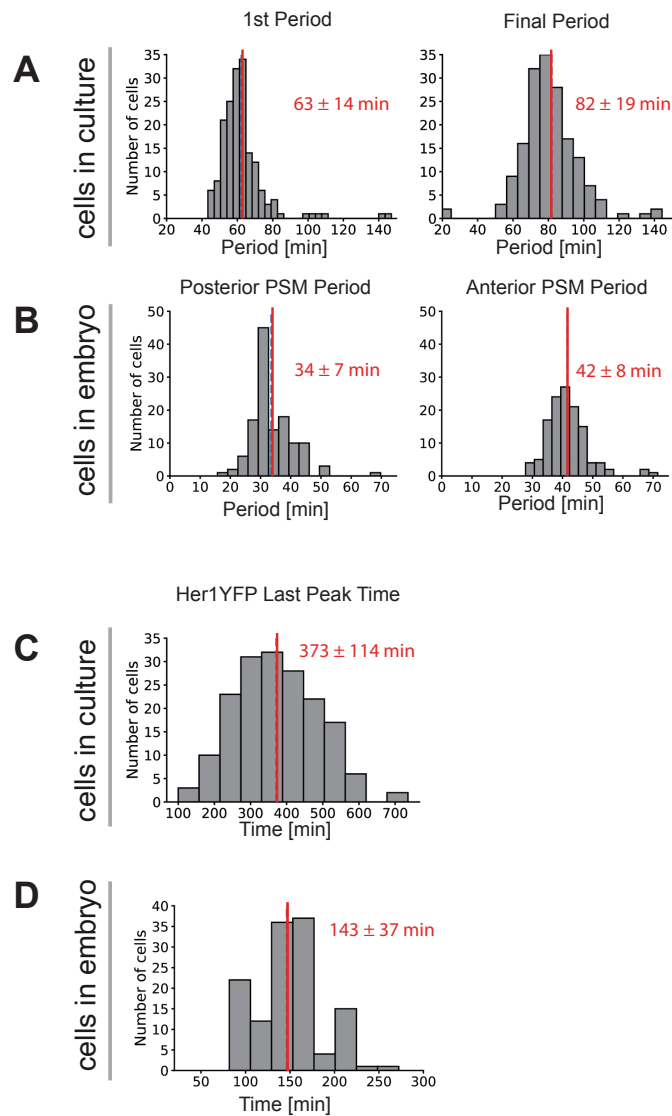
(A) PSM4 cell data was pooled from 11 different experiments, each with one embryo (Fig. 1). Distribution of the numbers of Her1-YFP peaks generated by individual cells shown for each experiment. (B) Distribution of the time of the Her1-YFP last peak in individual cells for each experiment. (C, D) Coefficient of Variation (COV) for each individual experiment (orange points, blue line) and COV for the combined set of experiments (red line) for both numbers of peaks (C) and last peak time (D).

PSM4 in the embryo



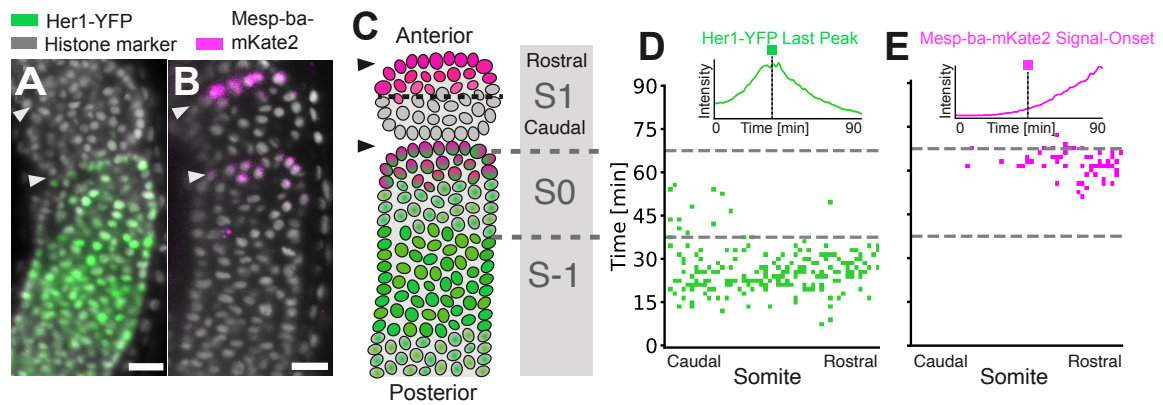
Extended Data Fig. 10. Her1-YFP intensity traces from PSM4 cells tracked in the embryo until somite formation.

Cells were selected within PSM4 of 15 somite-staged *Tg(her1-yfp; h2bmcherry)* embryos, then tracked until somite formation as shown in Fig. 1 (N=2 embryos, n=133 cells). Her1-YFP intensity traces with peaks and troughs (X).



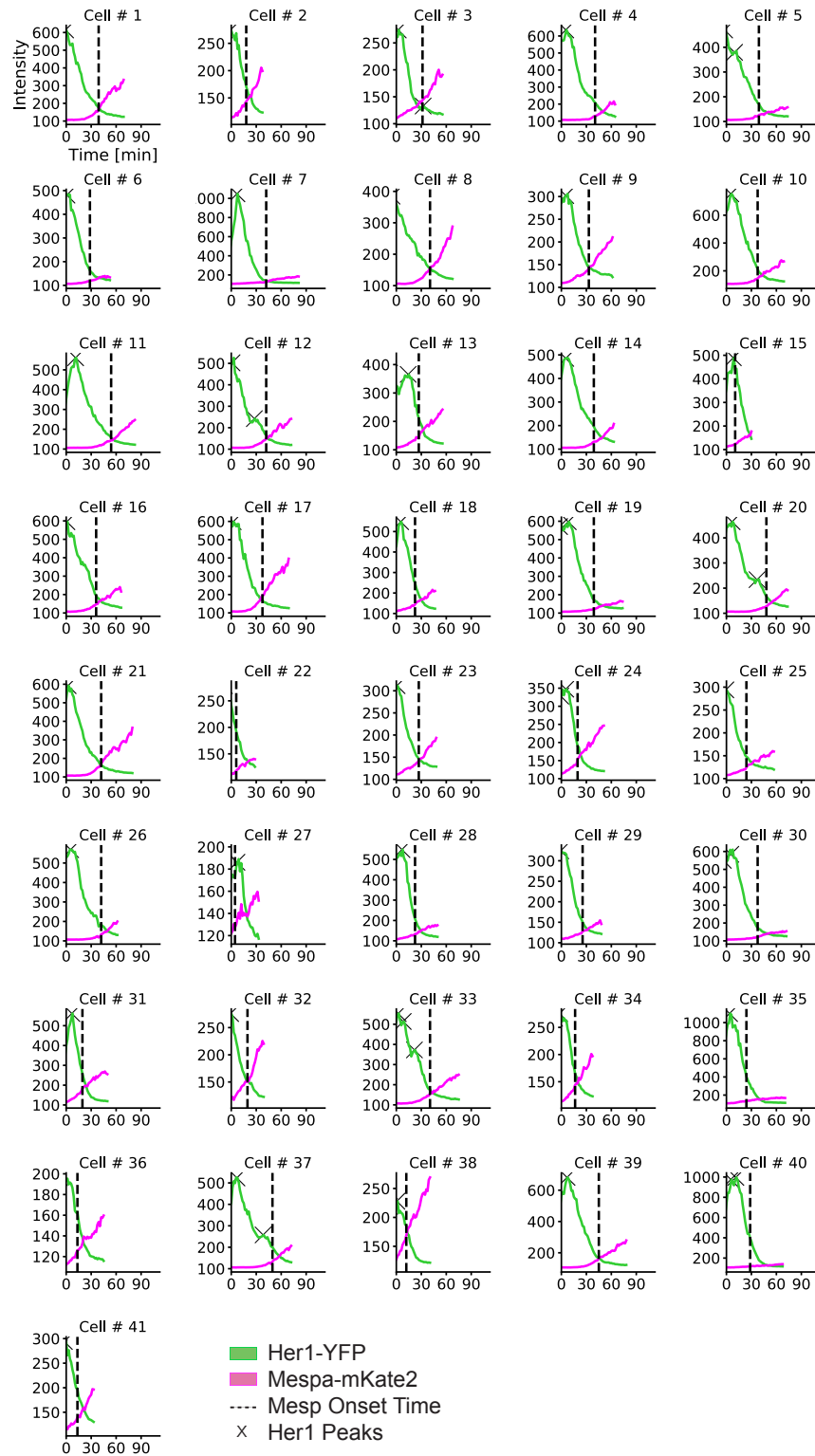
Extended Data Fig. 11. Lengthening of developmental time in culture.

(A) First and final periods (mean ± SD) of Her1-YFP oscillations in PSM4 cells in culture analyzed in Fig. 1A-F. (B) Posterior- and Anterior-most periods of Her1-YFP in PSM4 cells tracked in the embryo analyzed in Fig 1G-J. (C-D) Time of the Her1-YFP last peak in PSM4 cells in culture (C) and in the embryo (D). The mean of the last peak time in culture is more than double that in the embryo, indicating that the transient dynamics are skewed to comparatively longer times in culture.



Extended Data Fig. 12. Clock arrest and Mesp signal-onset within the forming somite.

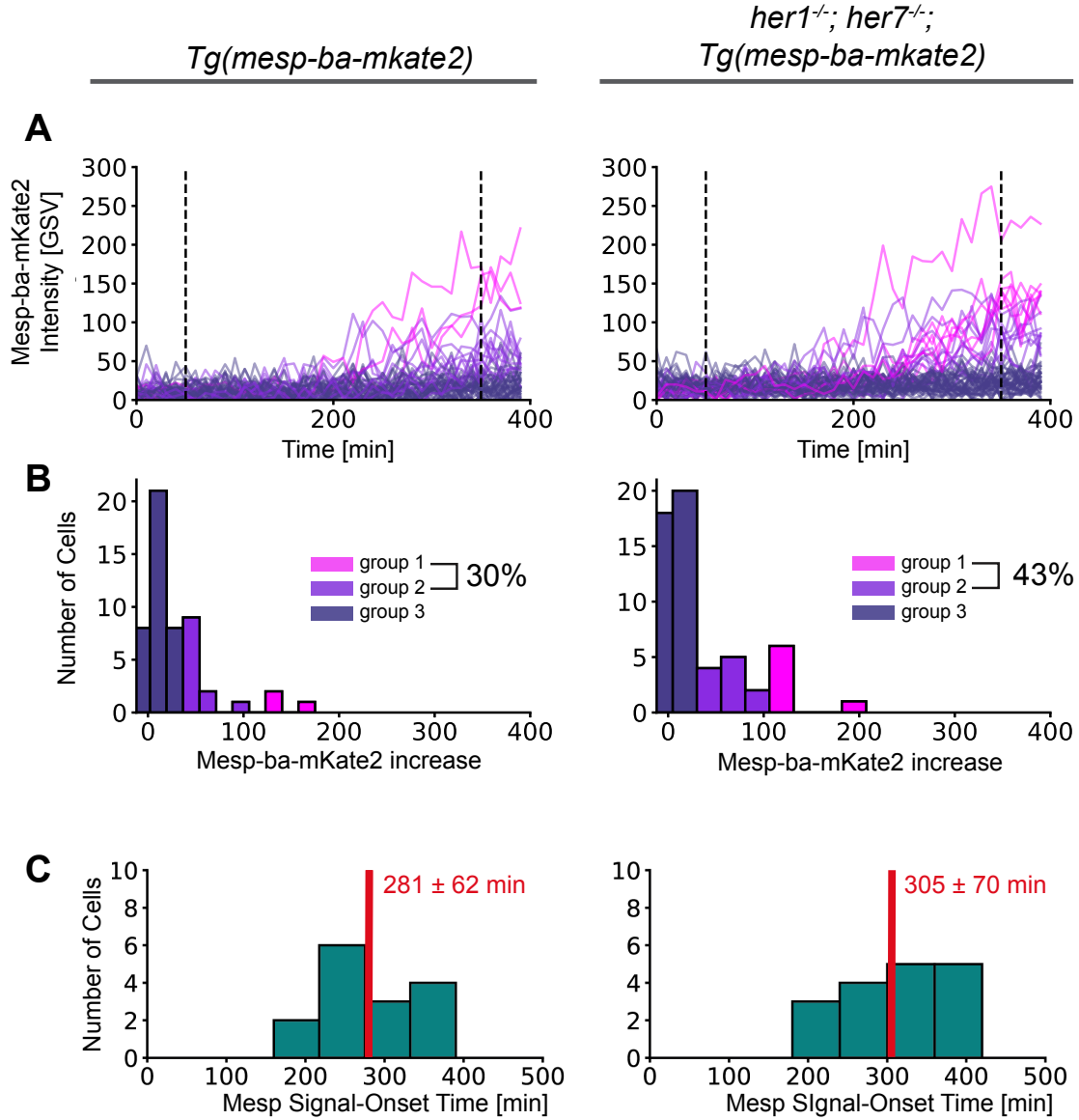
(A) Her1-YFP in a *Tg(her1-yfp;h2b-mcherry)* embryo (arrowheads at somite boundaries). (B) Mesp-ba-mKate2 in a *Tg(mesp-ba-mKate2a;h2a-gfp)* embryo. (C) Cartoon of the formed somite (S1), the forming somite (S0) and the prospective somite (S-1). (D, E) S1 backtracked in a *Tg(her1-yfp;h2b-mcherry)* embryo (233 cells) (D) and a *Tg(mesp-ba-mKate2a;h2a-gfp)* embryo (190 cells) (E). Kymograph of Her1-YFP last peak (D) and Mesp-ba-mKate2 signal-onset time (E) in cells relative to the rostral-caudal somite axis (inset with example traces). Dashed grey line at transitions S-1 to S0 and S0 to S-1.



Extended Data Fig. 13. Mesp-ba-mKate2 Signal-Onset defined in individual intensity traces.

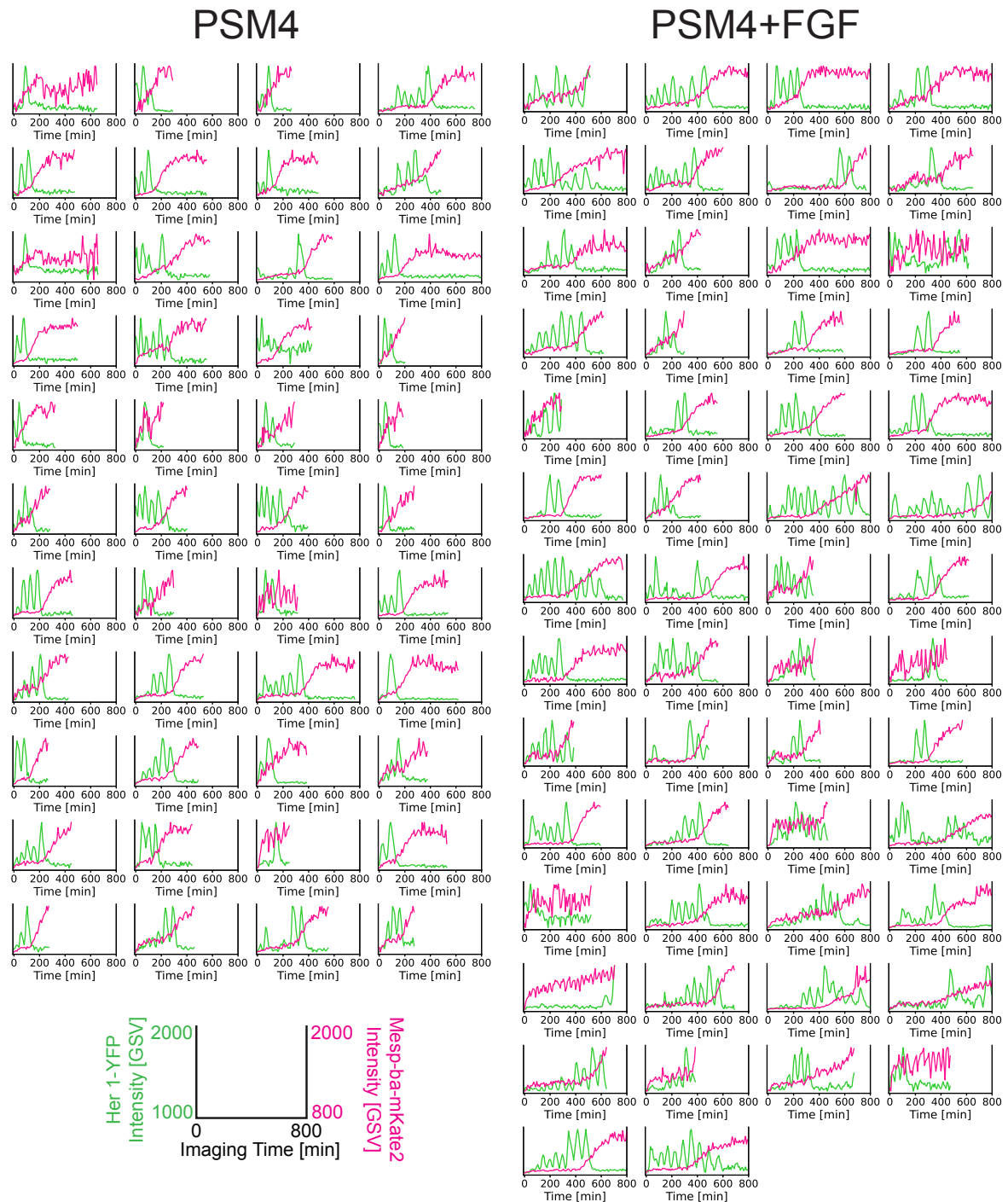
Intensity traces from cells tracked from S-I through to SI in *Tg(her1-yfp; mesp-ba-mKate2)* embryos used in to find relative timing of Mespba-mKate2 signal-onset and Her1-YFP last peak time.

PSM4 cells in culture



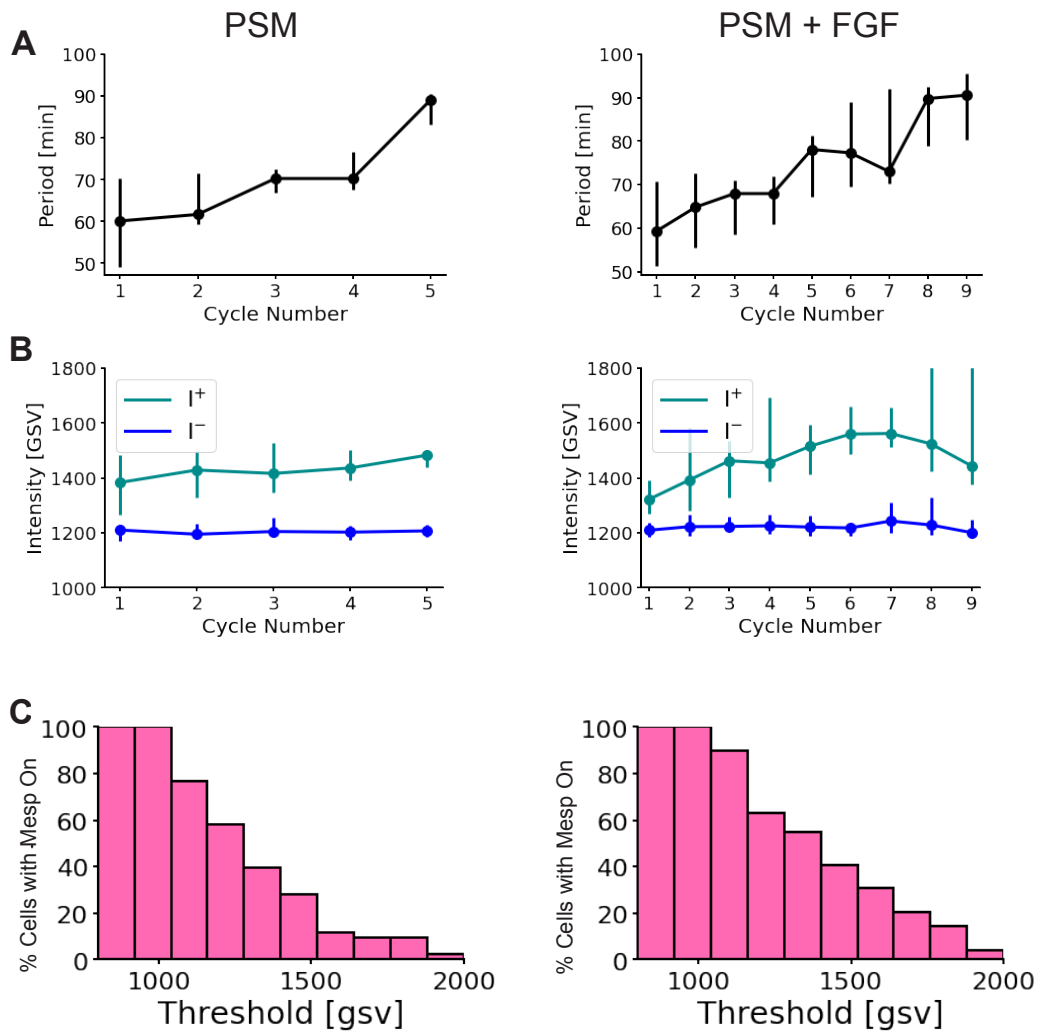
Extended Data Fig. 14. Mesp-ba-mKate2 signal-onset in *her1^{-/-};her7^{-/-}* cells with a disabled segmentation clock.

(A to C) PSM4 cells were cultured in parallel from *her1^{-/-};her7^{-/-}* mutant embryos carrying *Tg(mesp-ba-mKate2)* (N=2 embryos, n=72 cells), and control *Tg(mesp-ba-mKate2)* embryos (N=2 embryos, n=78 cells). (A) Mesp-ba-mKate2 intensity traces aligned by time. (B) Mesp-ba-mKate2 intensity-increase clustered into groups (as described in Extended data Fig. 4). Percentages of cells with a Mesp-ba-mKate2 signal-onset detected. (C) Mesp-ba-mKate2 signal-onset times (mean \pm SD).



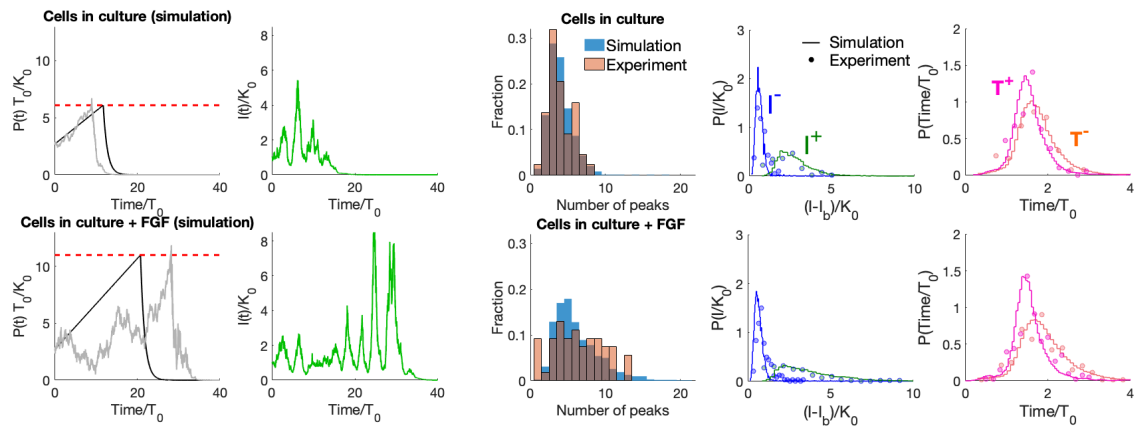
Extended Data Fig. 15 . Her1-YFP and Mesp-ba-mKate2 intensity traces.

(A-D) Cells were dissected from 15 somite-staged *Tg(her1-yfp;mesp-ba-mkate2)* embryos, then dissociated. For each experiment (N=4), dissociated cells from one to two embryos were split between two wells, then cultured +/- FGF-8b. Single oscillating cells that remained the only cell in the field of view, survived > 5h post-dissociation, did not divide, and showed transient dynamics were analyzed. Her1-YFP and Mesp-ba-mKate2 intensity traces from single cells shown (n= 44 control PSM4 cells, n= 54 PSM4 cells + FGF).



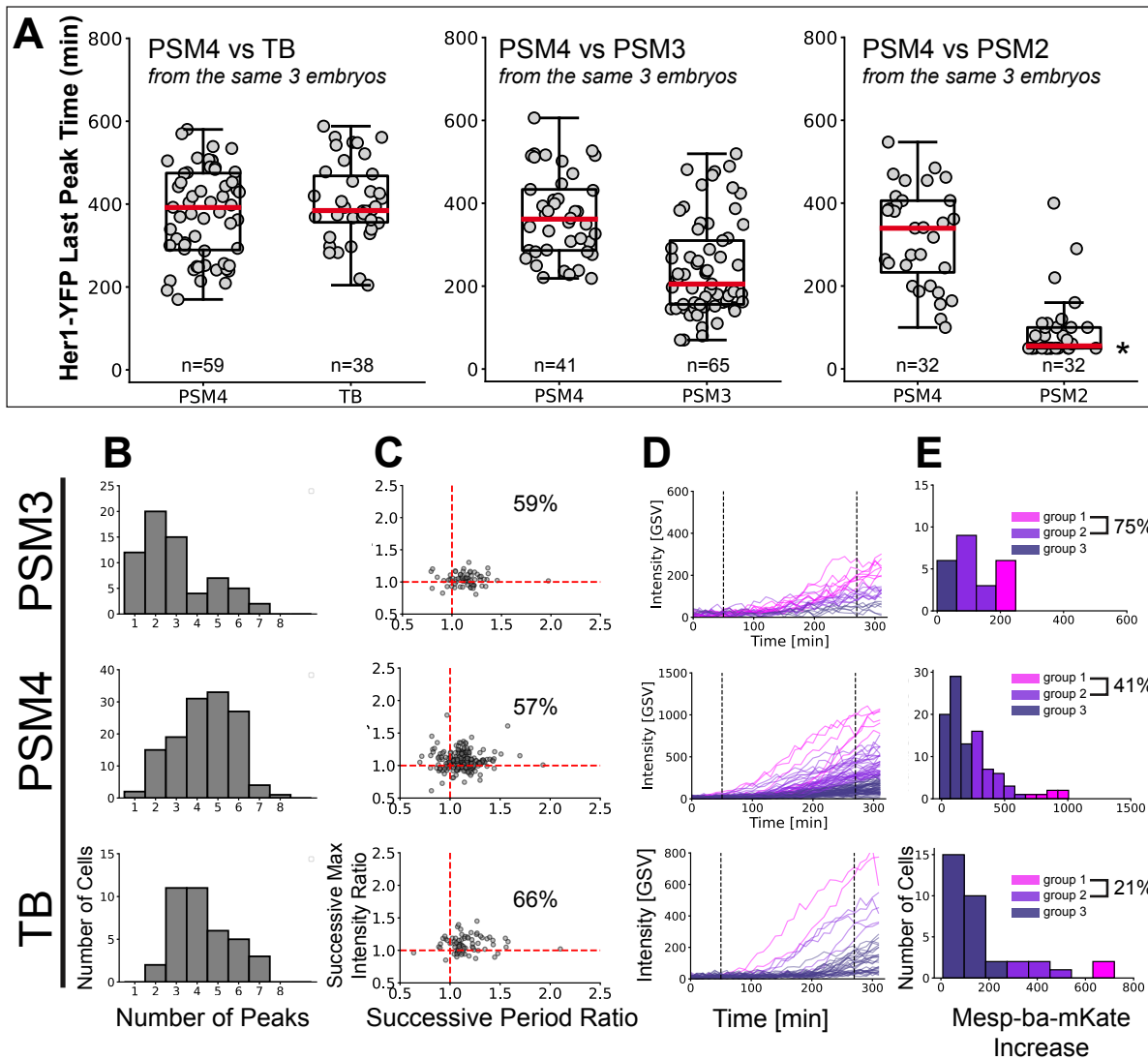
Extended Data Fig. 16. Her1-YFP Oscillatory Profile.

(A, B) Cell-autonomous PSM4 observables aligned by first cycle. Her1-YFP profile: Period (A) and peak (I+) and trough (I-) intensity (B). (C) Mesp-ba-mKate intensity shown by percent of cells reaching a range of intensity thresholds.



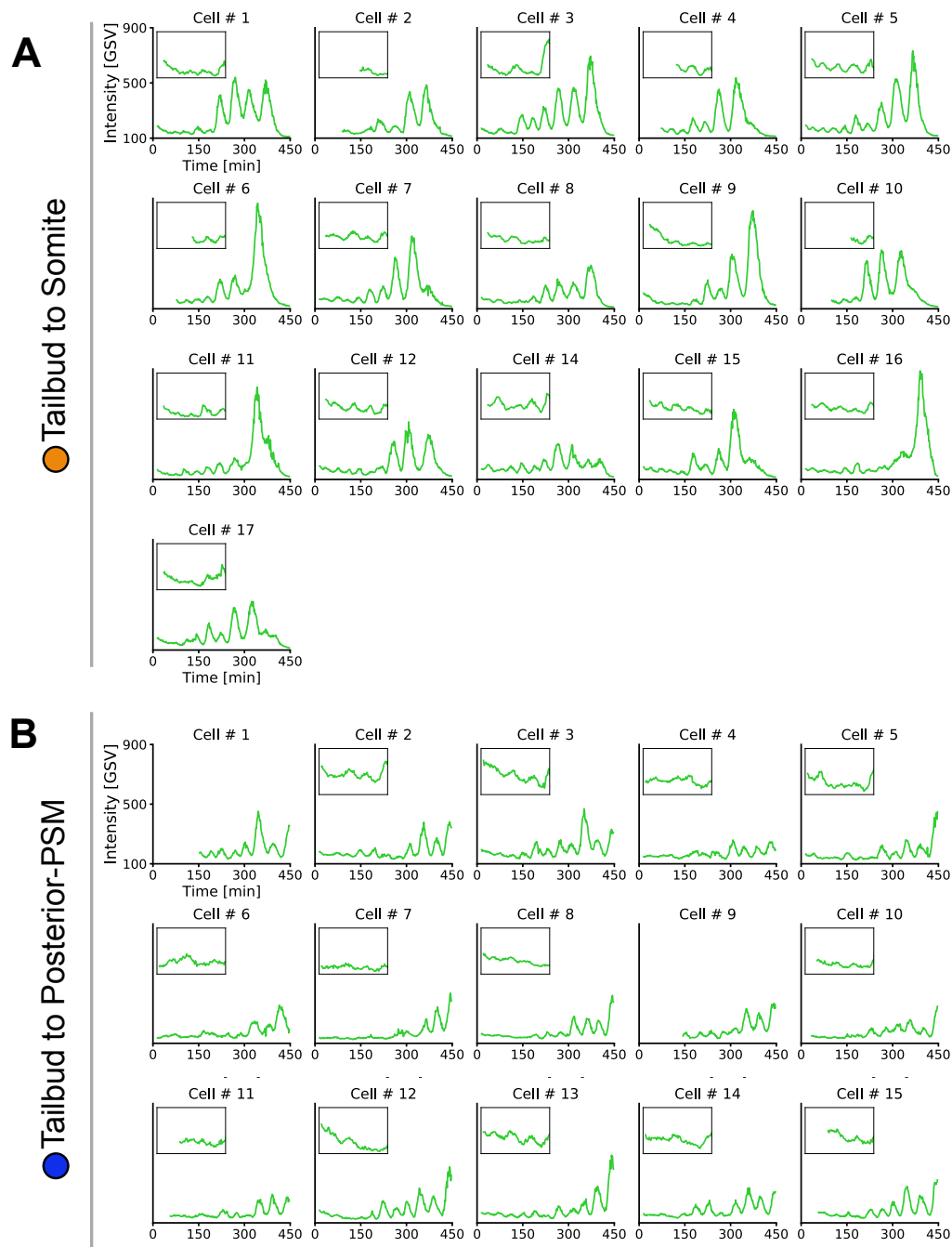
Extended Data Fig. 17. Oscillatory profile reveals FGF-induced changes to cell-intrinsic timing mechanism

(A) Representative simulation of control cultured PSM4 cell (no FGF) in culture, showing noisy ramp and resulting transient clock signal. (B) Comparison of distribution of number of peaks for experiment and simulations of model fitted to control cultured PSM4 cell (no FGF) experimental data from Fig. 3 (left panel), and probability distributions of clock observables from experimental data and simulations. (C, D) As above in (A, B), but for cultured PSM4 cells stimulated with FGF from Fig. 3.



Extended Data Fig. 14. Cell-autonomous Her1-YFP and Mesp-ba-mKate2 dynamics in cells dissected from different anteroposterior positions.

(A) Her1-YFP last peak times in cultured cells dissected from different anteroposterior positions (PSM2, PSM3, PSM4, and TB) in *Tg(her1-yfp;mesp-ba-mkate2)* embryos (Fig. 4). PSM4 was dissected and cultured in parallel to other anteroposterior positions from the same embryo (pooled data in Fig 2B and C). Median last peak time (red line) with interquartile box. Many PSM2 cells were in the degradation interval of the last peak when imaging initiated, thus the last peak time for such cells was set to time imaging started post-dissociation (*). (B) Number of Her1-YFP peaks. (C) Successive period and intensity ratios. Percentage of cycles slowing and increasing intensity. (D, E) Mesp-ba-mKate2 intensity-increase clustered into groups (see Extended Data Fig. 4).



Extended Data Fig. 19. TB to Somite segmentation clock transient dynamics at cellular-resolution in the embryo.

(A, B) Continuous multi-dimensional light-sheet imaging (stack acquired every 1.5 min over 7.5 h) and back tracking of individual cells from their final position in the posterior-PSM or the 28th somite in a *Tg(her1-yfp;h2b-mcherry)* embryo (n=15 posterior-PSM cells, n=17 somite cells). Intensity traces shown for each cell in Fig. 4. Inset is zoom of low-intensity oscillations.

Materials and Methods

Zebrafish and embryo care

Wildtype (WT) and transgenic (*Tg*) fish were maintained according to standard procedures in facilities at University College London (UCL, London, UK) and École polytechnique fédérale de Lausanne (EPFL, Lausanne, CH). *Tg* embryos were heterozygotes produced by natural pairwise spawning with WT (AB, TL) or another *Tg* line. The following lines used here have been described previously: *Tg(her1:her1-ypf)* (Soroldoni et al., 2014); *Tg(h2az2a:h2az2a-GFP)* (zfin ID: ZDB-TGCONSTRUCT-070117-39); *Tg(Xla.Eef1a1:H2BmCherry)* (Recher et al., 2013); *Def(Chr5:her1 zf2173/zf2173;her7 hu2526/hu2526)* (Lleras Forero et al., 2018). Embryos were incubated at 28.5°C in E3 without methylene blue (UCL) or facility water (EPFL) until shield stage then incubated at 19.5°C until the 8 to 10 somite stage when they were returned to 28.5°C. Embryos for experiments were then dechorionated manually and kept in agarose-coated petri-dishes.

mesp-ba-mKate2 transgenesis

Transgenesis was performed as described previously (Soroldoni et al., 2014). In short, *mKate2* was fused to the 3' end of *mesp-ba* so as to generate a C-terminal fusion protein, then the modified BAC was subcloned to obtain a 15 kb construct. The resulting BAC was co-injected with I-Sce Meganuclease (Roche) at a concentration of 100 ng/μl and a bolus size of 130 μm. Transient expression in F0 embryos was used as a proxy to confirm the functional expression of the *Mesp-ba-mKate2* fusion protein and all embryos were raised to adulthood. In total, 9 independent transgenic founders (out of 29 fish) were identified by whole-mount in situ hybridization using a probe to *mKate2*, yielding a transgenesis frequency of 30%. Based on the optimal signal to noise ratio, and the *mKate2* stripe pattern, a single founder was selected. Heterozygous and homozygous

Tg(mesp-ba:mesp-ba-mKate2) were viable, fertile, and stably expressed mKate2 through multiple generations over 10 years.

The following primers were used for tagging and subcloning:

5 Forward Primer Mesp-ba tagging:

TTTACGGAAAAA ACTTTGGCTATCATCTCGTTCCTCAGACTTACTGGAGAAGCTCAG
GAGGTAGCGGC

Reverse Primer Mesp-ba tagging:

ACACAATACAGTATCCGCCCTCAGTTTTTGGTGTGATGGAGATCTTTCCGCGTCAGT
10 CAGTACCGTTCG

Forward Primer shaving:

CCAAATTAGGTTAGATTAGTTACTCATCCTGGTAGCTGTACAAATAGATATAGGGAT
AACAGGGTAATTGCAC
TGAAATCTAGA

15 Reverse Primer shaving:

CCCTGCAGTACACTGAATCTACCATGACACCATATCTTATCTTTCCAGCCccgTAGGG
ATAACAGGGTAATTT

Light sheet time-lapse imaging of embryos

20 *In vivo* multi-position time-lapse imaging experiments (1.5 min/stack; up to 7.5 h) were conducted using a dual-illumination light sheet microscope (LS1 Live, Viventis Microscopy Sàrl, Switzerland and a custom-built version of the LS1 Live microscope of identical configuration). The microscope had the following configuration: Andor Zyla 4.2 sCOMS camera; 515 nm laser to image YFP; 561

nm laser to image mCherry or mKate2; CFI75 Apochromat 25X, NA 1.1 detection objective (Nikon); scanned gaussian beam light sheet with thickness (FWHM) of 2.2 μm . Tail and PSM regions of growing embryos were kept in the field of view by automatically tracking the mass of the Her1-YFP signal while acquiring the time-lapse and adjusting stage positions. 2 embryos were
5 imaged in parallel in each experiment. Stacks of YFP and mCherry or mKate2 (150 planes with 1.5 μm spacing) were acquired at each position every 90 seconds.

Prior to imaging, embryos were dechorionated and placed in facility water (EPFL) with 0.02% Tricaine to prevent muscle twitching. Multiple embryos were mounted at the bottom of a light
10 sheet microscope sample holder (Viventis Microscopy Sàrl, Switzerland) and orientated laterally in agarose depressions designed to hold the yolk of an embryo and allow unhindered extension of the body and tail (Herrgen L., Schröter C., Bajard L., Oates A.C., 2009). Temperature was maintained at 28.5°C using a recirculating air heating system (Cube 2, Life Imaging Services, Switzerland).

15

Image Processing

First, we defined the dataset by creating an XML file, which included all metadata and recorded transformations performed on the raw data, and saved the data in HDF5 file format (The HDF Group, 1997-2019). These two files were used in all subsequent steps. Second, to produce spatially
20 registered time-lapse movies, images were temporally registered with a linear transformation, with the first time point as a reference, using a Fiji plugin (Preibisch et al., 2014; Schindelin et al., 2012). Cellular nuclei were used as registration markers and all transformations were rigid, where the Euclidean distances between points were preserved. All of these transformations were saved

in the XML file, thus the data in the HDF5 file remained unaltered. In parallel to this registration process, the notochord was segmented for each time point using a custom FIJI script. This was used as a spatial reference in the embryo, and applied to create the kymograph.

5 Cell Tracking in the embryo

Using Mastodon – a large-scale tracking and track-editing framework for large, multi-view images (<https://github.com/mastodonsc/mastodon>) – each individual cell was segmented and tracked based on nuclear signal (*Tg(h2az2a:h2az2a-GFP)*, *Tg(Xla.Eef1a1:H2BmCherry)*). We performed a semi-automatic analysis, where cells of interest were manually selected then followed by automated tracking. All tracks were manually checked and corrected. The output was the intensity for each cell, in both channels, obtained from the segmented volume (in the 3 spatial dimensions). X,Y and Z coordinates were also obtained.

Data from forward tracking of PSM4 cells in a 15 somite-staged embryo (Fig. 1G-J) was only included for cells that did not divide to be comparable to our cell culture data. Backtracking of cells in Fig. 2E was performed by selecting cells within the posterior-PSM and within the most recently formed somite (28th somite) at the end of the movie. Backtracking of entire somites through to prospective somite -1 (fig. S11) was done in 15-20 somite-staged embryos. Cells that were backtracked across the S-1 to S0 transition in *Tg(her1-yfp;mesp-ba-mKate2)* embryos (fig. S4) were followed by first selecting rostral cells with nuclear Mesp-ba-mKate2 signal, then switching to the Her1-YFP signal in the anterior PSM.

Mesp-ba-mKate2 signal-onset

To systematically define Mesp-ba-mKate2 signal-onset and its timing in the intensity traces from cells in culture and in the embryo, the steps outlined in fig. S3 were applied.

Mesp-ba-mKate2 and Her1-YFP Kymograph

5 Using the segmented notochord as a spatial reference in the preliminary data set, the spatial coordinates of the cells were projected to the nearest point in the notochord using Euclidean distance. This produced a new coordinate system, where cells have a reference frame in the moving and growing embryo. Each notochord segment, corresponding to the area of projected tracked cells, was then aligned over time to create a kymograph (Extended Data Fig. 10) Using the X and
10 Y coordinates in the projected notochord, a matrix was built where the rows are each notochord segment over time going from posterior to anterior. The columns correspond to a binned spatial region of the cell projection. The color code used for the Her1-YFP Kymograph was the time and position of the last peak of the cells (green) (N= 1 somite, n= 233 cells). For Mesp-ba-mKate2, the signal-onset time and position (magenta) was used (N= 2 somites, n= 190 and 217 cells).

15

Cell culture

Individual 15 somite-staged embryos were dechorionated in E3 then transferred into DPBS(-CaCl₂, -MgCl₂), where cells of interest were dissected out within 5 minutes. Using a forcep (Dumont #5SF Forceps, straight, superfine, Fine Science Tools Item 11252-00) and microknife
20 (Needle Blade Microsurgical Knife Straight, Sharpoint, ref 78-6810), the skin and yolk were removed, leaving the trunk and tail intact. Holding the embryo in a lateral view, the TB was cut off at the level of the Kupffer's Vesicle (posterior to the notochord). The remaining AP axis up to the last formed somite boundary was quartered. PSM quarters from the desired AP level were then

oriented in cross-section view so that PSM could be cut free of lateral tissue, neural tube and notochord. Dissected tissue was moved with F-127 Pluronics-coated pipette tips into coated tubes containing 50 μ l DPBS(-CaCl₂, -MgCl₂), using care not to mix cell types from different axial levels or embryos. After a 5 min incubation in DPBS, the pieces were manually dissociated into single
5 cells by brief pipetting and then transferred into wells of a 24-well glass bottom plate (Greiner Bio-One, 662896) coated with Protein A from Staphylococcus aureus (Sigma P6031; 100 ng/ μ l PA) and containing 800 μ l culture media (Leibovitz's L15 Medium, no phenol red, Thermo Fisher 21083027; 50 ng/ μ l Protein A; 0.01% Methyl Cellulose, Sigma 274429). In experiments testing the influence of FGF, we added FGF8 (423-F8b R&D System; 100ng/ml) to the culture media.
10 Remaining clusters of cells were aspirated out of the culture well using a glass needle attached to a syringe. Embryos and cells were maintained around 28.5°C throughout dissection and dissociation.

Cells were allowed to settle in the well plate on the microscope stage at 28.5°C and imaging
15 positions were selected and focused in a 50 – 90 min period before imaging started (Fig. 1A). The time post-dissociation that imaging started was noted for each experiment so that Her1-YFP last peak and Mesp-ba-mKate2 signal-onset timing could be adjusted and compared relative to the time of dissociation rather than to the start of imaging.

20 Control or comparison cells were dissected and dissociated in parallel, cultured in separate adjacent wells, and imaged at the same time. To compare cells of different anteroposterior origins (Figure 4 and Extended data figure 18), PSM4 was dissected from each embryo alongside the other PSM quarter of interest or TB, then separately cultured and imaged. This provided an internal

reference for arrest timing differences along the anteroposterior axis. In experiments comparing control and FGF-treated results (Figure 4, Extended data figures 16, 17), a starting set of dissociated cells from was split into two wells (\pm FGF).

5 Comparison of cell-autonomous *Mesp-ba-mKate2* signal-onset timing in PSM4 cells from embryos that have a disabled clock (*her1*^{-/-}; *her7*^{-/-}; *Tg(mesp-ba-mKate2)*), with PSM4 cells from control (*Tg(mesp-ba-mKate2)*) embryos was also carried out simultaneously in different wells. We selected the *her1*^{-/-}; *her7*^{-/-} line because multiple studies have shown that the segmentation clock is critically crippled by the removal of two or more Hes family members from the core clock
10 mechanism (Henry, 2002; Lleras Forero et al., 2018; Oates and Ho, 2002; Sari et al., 2018; Schröter et al., 2012; Zinani et al., 2021).

Our criteria for continued analysis of cells in culture was as follows: 1) alive > 5 hours post-dissociation; 2) one cell in the field of view; 3) undivided; and 4) expressed and arrested Her1-
15 YFP. See Extended data figure 2) for numbers and percentages of cells in these categories.

Cell culture imaging

Cells were imaged on a Nikon Eclipse Ti (inverted) equipped with a 40x NA0.95 objective, Andor iXon897 Ultra EMCCD (512 x 512 with 16 μ m pixels), Lumencor SpectraX, and hardware
20 autofocus. Her1-YFP was detected using a Chroma 49003 filter, and *Mesp-ba-mKate2* with Chroma 49008. Imaging parameters were as follows: YFP at 400 ms exposure, 4x4 binning, 1 MHz (16-bit) read-out mode, EM Gain =50, Conversion Gain=1, 510 nm LED at 20% intensity; *mKate2* at 1000 ms exposure, 4x4 binning, 1 MHz (16-bit) read-out mode, EM Gain=50,

Conversion Gain=1, 586 nm LED at 3% intensity; Bright field at arbitrary exposure time, no binning, 1 MHz (16-bit) read-out mode, EM Gain=50, Conversion Gain =1. Up to 120 positions per experiment were selected at the start of imaging that had only one cell in the field of view. A single plane of bright field, YFP and mKate2 were captured at 10 min intervals for over 16 h.

5 Because the cells remained in the center of the field of view (FOV), there was no re-positioning throughout the movie. Temperature was controlled at $28.5 (\pm 0.3^\circ\text{C})$ using a stage-top incubator (Bold line, Okolab), and a light-blocking incubation chamber set to 28.0°C around the microscope (Solent Scientific).

10 Cell culture image processing

Bright field images were passed through a custom MATLAB code for segmenting single cells.

Contrast of the grayscale image of the first frame was enhanced using the `adapthisteq` built-in algorithm, then filtered using a guided filter (`imguidedfilter`, neighbourhood=3 by 3 pixels and degree of smoothing=0.001) to preserve cell edges (regions of high variance in pixel intensity)

15 while filtering out noise. Next, a gradient image was generated by subtracting an eroded image (`imerode`, disk structuring element=2 pixels) from a dilated (`imdilate`, disk structuring element=2 pixels) image, providing a rough outline of potential cells. Otsu's thresholding was applied to this,

resulting in a binary image with several white regions (termed blobs) that represented potential cells. Given that cells were positioned approximately at the center of each image, the largest blob

20 at the center of the image was segmented and pixel intensities in the rest of the image were set to zero (black). This served as a mask for further processing. The built-in `activecontour` algorithm (300 iterations, Chan-Vese method, smooth factor=1, contraction bias=0.1) was then applied on the gradient image with the mask serving as the initial state of the algorithm. The boundaries of

the object region in the mask (in white) define the initial contour position used for contour evolution that ultimately segments the cell. Output from the algorithm represented the segmented cell. Fluorescent intensities from the segmented region were then determined for further analysis. Segmentation of each frame was confirmed manually and corrected when necessary.

5

Her1-YFP intensity trace observables

Cells in culture: The high signal to noise of the traces allowed the oscillatory region to be determined by visual inspection. Within this region, the MATLAB command findpeaks, which is a local peak finder algorithm, was used to determine the position of each peak (maxima). To find
10 the troughs (minima), the time trace was multiplied by -1 so that the local peaks correspond to the minima. The same algorithm and parameters were applied to all traces. Because the sampling rate from the intensity traces in culture was coarse (10 min intervals), an extra step was performed to determine the magnitude and the time point of each maxima and minima after the initial detection. Two neighbouring time points were used to fit a second order polynomial using least squares
15 minimization. This enabled us to find the maximum of the second order polynomial and record its corresponding time point. Oscillatory cycles were defined as the time intervals between maxima, and within each cycle we further defined the following: a production interval (time from a given cycle's minima to maxima, T+); a degradation interval (time from a given cycle's maxima to minima, T-); change in intensity between the minima and maxima in a given cycle (I+); and change
20 in intensity between maxima and minima in a given cycle (I-).

Cells in the embryo: Peaks (maxima) and troughs (minima) were defined using the entire intensity trace of Her1-YFP. The peaks and troughs of these oscillations were then calculated using the

Scientific Python library's peak finder (`scipy.signal.find_peaks`) (SciPy 1.0 Contributors et al., 2020). A single set of parameters (width, distance and prominence) were chosen for peak identification in all intensity traces. Oscillatory cycles, degradation and production intervals were calculated following the same method used for the cells in culture.

5

Data analysis, model simulation and parameter fitting

Normalized histograms of $(I^\pm - I_b)/K_0$ and T^\pm/T_0 were generated using the Freedman-Diaconis rule, which determines the bin size that minimizes the difference between the histogram created and the probability distribution function (pdf) behind the stochastic process that generates these values. An automatic and stochastic parameter search was performed to determine the scaling parameters $\{I_b, K_0, T_0\}$, as well a set of basis parameters to fit the mathematical model of the clock and timer. During this parameter search we used the cultured PSM4 cells data set (Figure 1A-F, Extended data figure 3A) as a reference and we determined the basis parameters using a criterion based on the coefficient of determination. For each experimental condition (PSM4 in the embryo Fig. 1G-J, or treated with FGF Fig. 3) the parameters were further refined using the probability distribution $(I^\pm - I_b)/K_0$ and the histograms of number (N) of observed Her1-YFP cycles. This refinement was guided by theoretical observations on the dependence for the pdf of $(I^+ - I_b)/K_0$ on the timer's threshold ϕ_0 , while the mean and variance of N depend on the timer's threshold ϕ_0 , slope γ and noise σ_p^2 . Details of the model, simulation and parameter fitting are given in supplementary text 1.

10

15

20

Summary Chapter 3

This chapter shows that the clock and wavefront are both captured in a single cell running an intrinsic program. By performing quantitative comparison of cell behaviour in culture and in the embryo, we revealed the existence of a cell-intrinsic program driving the wave pattern. The longer and noisier dynamics in culture cells indicate that extrinsic signals present in the embryo may shorten and sharpen the program. The ability of FGF to extend the duration of the program of cultured cells fits well with data from embryo experiments on changing somite lengths (Dubrulle, McGrew, and Pourquié, 2001; Sawada, Shinya, et al., 2001), and the results presented in Chapter 2. But, the higher variability observed implies that additional signals, or the temporal dynamics of the signals, are important for precision. Moreover, we propose that TB cells express the intrinsic timing mechanism, but require a trigger associated with exit from the TB to start timing. The intrinsic timer's identity and how it is tuned by extrinsic signals during development remain intriguing questions.

With these results, we turn to the last chapter, which investigates molecular candidates for the timer mechanism.

Chapter 4

Clock, wavefront and timer model

The clock and wavefront model originally postulated an intracellular timing gradient of development as the mechanism behind the wavefront of cellular change interacting with the clock to determine somite position. In Chapter 3 we showed that the clock and wavefront are both captured in a single cell running an intrinsic program. Our PSM *in vitro* data shows that PSM cells themselves have intrinsic information that allows them to temporally recapitulate a cell's behaviour along the spatial AP axis of the PSM *in vivo*. This suggests that PSM cells use internal time as a spatial reference in segmentation clock dynamics. What is the intrinsic timer mechanism in the PSM and how does it link to extrinsic spatiotemporal information, the segmentation clock and cell maturation? The mechanism of this timer is unknown but as we speculated in the introduction it may be controlled by negative feedback between *tbx6* and *rippy1/2*. Here, I focus on testing these genes as components of the intrinsic timer and testing how does external spatiotemporal information link to the timer.

In this chapter I will focus on the following questions:

1. What are good molecular candidates for the intrinsic timer? We speculate that *tbx6* and *rippy1/2* might act as a time-keeping mechanism due to previous studies and our model predictions.
2. Can the candidate timer be influenced by extrinsic signals? We have seen that, *in vitro*, when FGF is added to cells, differentiation and subsequent programme arrest are prolonged and become noisier. Therefore, the intrinsic timer must be able to respond to the FGF signalling gradient.
3. How does the timer modulate the clock? We believe that this intrinsic timer is re-

sponsible for stopping the programme, but how does it affect the clock? In Rohde et al., 2021 we showed that the timer mechanism affects the clock and differentiation but it does so in independent ways.

4. How does the timer information translate into the formation of somite boundaries? We have preliminary results on how the accuracy of the somite boundary positioning could be controlled by the intrinsic mechanism of the timer.

To answer these questions we will use a combination of antibody staining for Tbx6, the *fss* mutant and a new transgene generated in the lab, Tbx6-mNeonGreen (Tbx6-mNG). Together with tissue-level analysis and cell tracking, we show that *tbx6* can be part of the time-keeping mechanism suggested in Chapter 3.

4.1 *tbx6* and *rippy1/2* are good molecular candidates for a timer mechanism

One of the first zebrafish mutants related to somitogenesis to be observed was *fused somites* (*fss*) (Van Eeden et al., 1996b). Ever since, it has been a widely studied mutant due to the absence of somite furrows. This mutant encodes the T-box transcription factor Tbx6 (Nikaido et al., 2002). Tbx6 expression is maintained by transcriptional auto-regulation in the anterior PSM (Ban et al., 2019) and it is then degraded at the protein level by the Ripply proteins (Kawamura et al., 2005). Similarly, when the *rippy* genes are knocked out, somite furrows are also not formed.

Previous work has viewed the Tbx6-Ripply interaction as a vital part of the regulatory mechanism stopping the clock down-stream of signalling gradients. With our discovery of a cell autonomous timing program in PSM cells, we argue that this existing view requires re-evaluation. There are several reasons why we believe *tbx6* and *rippy* work together as a critical part of the time-keeping mechanism of the future somite cells:

- In the absence of *tbx6*, the last *her1* stripe is missing due to maturation defects (Sawada, Shinya, et al., 2001; Holley, Geisler, and Nüsslein-Volhard, 2000). It has been speculated, but never experimentally proved, that the clock is still oscillating in an *fss* mutant. In addition, anterior somite polarity genes such as *mesp* and *papc* are lost, although posterior polarity genes such as *myoD* are still present (Oates, Rohde, and Ho, 2005).

- In the absence of *rippy1/2*, we observe the opposite effect: the clock does not stop in the anterior but continues to be ectopically expressed in the region where somites would form. In addition, polarity genes are also expressed but expanded in the anterior (Kawamura et al., 2005).
- *tbx6* and *rippy1/2* zebrafish mutants are the only ones that do not show somite boundaries. Even in the absence of the clock itself, somite boundaries form but with defects and polarity markers like *mesp* are also expressed even though they lose their polarity (Forero et al., 2018).
- *tbx6* is the anterior-most T-box gene and can bind to the anterior PSM enhancer of the *her1* gene (Brend and Holley, 2009a), meaning it is potentially the last input given to *her1* and it indirectly activates its own degradation by driving the expression of *rippy1/2* (Kawamura et al., 2005).
- Tbx6 and Ripply are both nuclear proteins and their interaction does not require any extrinsic signals. Thus, they are biochemically well-suited to comprise a cell-autonomous timing mechanism.

4.2 Can Tbx6 be influenced by FGF in the embryo?

In Chapter 3 we showed how FGF can prolong the duration of oscillations and the onset of differentiation in culture. Therefore, for Tbx6-Ripply to act as a timing mechanism, they need to be able to respond to FGF.

Wanglar et al., 2014 performed an 8-minute 400 μ M pulse of SU5402 in 2ss embryos. As a result, they reported a posterior shift of the anterior domain of Tbx6 protein and of the anterior border of the posterior-most band of *rippy1* mRNA. Together, they suggested that FGF is required for the suppression of *rippy1* expression in the PSM. They concluded that the somite boundary appears with high levels of Tbx6 and low levels of FGF, which is required for *rippy1/2* expression.

In the mouse, the combination of oscillating changes in Notch and FGF signalling determine the onset of *Mesp2* in the anterior PSM (Niwa et al., 2011; Oginuma et al., 2008). Similar than before, Niwa et al., 2011 observed that *Mesp2* expression occurred prematurely (in S-II instead of in S-I like in control embryos) in SU5402 treated embryos. Activation of Ripply1/2 expression and subsequent definition of the Tbx6 protein boundary is *Mesp2*-dependent. Therefore, it is hypothesised that the *Mesp2*-Ripply-

Tbx6-mediated machinery converts oscillation into somite boundary positioning (Takahashi et al., 2010).

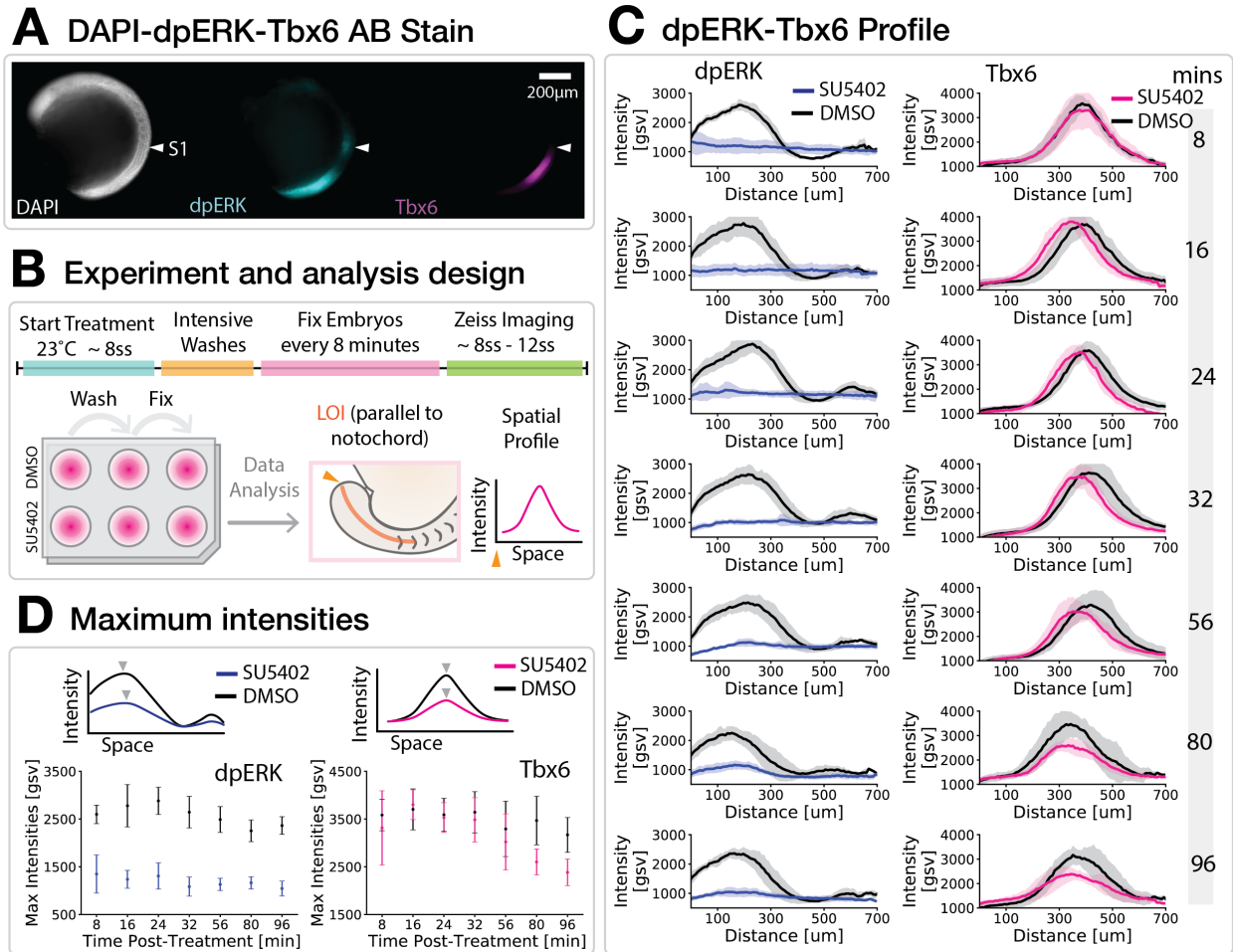


Figure 4.1: Tbx6 is responsive to FGF. **A.** Images of a 8ss WT embryo stained with DAPI, dpERK and Tbx6. White triangles mark the position of SI. **B.** Embryos were treated with an 8 min, 675 μ M SU5402 pulse (like in Sawada, Shinya, et al., 2001). Then they were washed and fixed every 8 minutes. To quantify the spatial expression of dpERK and Tbx6, a line of interest (LOI) was drawn using the tailbud as reference point (shown as an orange triangle). **C.** Example of the spatial distributions for DMSO and SU5402 treated embryos. Solid lines are the mean (N=8-10 embryos per condition) and in lighter colour the standard deviation is shown. **D.** Maximum intensities of the spatial profiles shown as mean and standard deviations over different fixation times.

To explore whether *tbx6* can be influenced by FGF, we used the same pulse duration (8 minutes) and concentration (675 μ M) of SU5402 from Sawada, Shinya, et al., 2001 as this is the combination that results in the longest somite and thus, the biggest change in the wavefront. In Chapter 2, I showed how an 8-minute 400 μ M pulse of SU5402 results in slower elongation (Figure 2.5). Therefore, we need to take this into account to

decouple the posterior regression of gene expression and elongation problems when interpreting the results. The experiment consisted of using antibody staining for dpERK, Tbx6 and counter-staining of the nuclei in the PSM with DAPI (Figure 4.1 A). Embryos were treated with SU5402 or DMSO, washed and fixed every 8 minutes (Figure 4.1 B). A line of interest parallel to the notochord was used to obtain the spatial distributions of Tbx6 and dpERK in the DMSO and SU5402-treated embryos (Figure 4.1 B). As expected, we saw the distribution of dpERK drop to a flat base-line immediately after SU5402 treatment (Figure 4.1 C). We observed a slight posterior regression of the Tbx6 peak starting 16 minutes after treatment. This is consistent with the report of [Kawamura et al., 2005](#), but it is likely that regression in Tbx6 distribution at 56 minutes is the result of the SU5402-induced changes in elongation. Interestingly, we observed a down-regulation of Tbx6 expression levels starting after 56 min post-treatment (Figure 4.1 C-D). From Chapter 2 and from the literature ([Sawada, Shinya, et al., 2001](#)) we know that the fifth somite after the treatment is the longest. Thus, if we record the appearance of the longest somite when it reaches SI, during SU5402 treatment, the cells forming this somite were in S-IV. Changes in Tbx6 intensity were observed from minute 56 and we report them until minute 96. During this time, the cells which would give rise to the longest somite are between S-II and S-I, at which point these cells no longer express Tbx6. Furthermore, we observed no difference in intensity before the 32 minutes post-treatment. Together, these data shows that *tbx6* can respond to perturbations in the FGF signalling gradient, as observed *in vitro* in Chapter 3. However, it argues against expression level playing a mayor role in mediating FGF changes in somite boundary formation.

One way to explain the appearance of the longest somite in SU5402 treatment is by the posterior regression of all factors such as Tbx6 and Ripply, which in turn would arrest the clock earlier ([Kawamura et al., 2005](#)). This could be explained by cells switching on the timer mechanism earlier because FGF levels decreased, simulating a situation where the cells exit the TB. Further experiments should be conducted where the expression patterns of Tbx6 and Ripply are drawn using the last formed somite as a reference to avoid including contributions on axial elongation problems.

4.3 Tbx6 modulates the maximal expression of the clock gene *her1* in a relative dosage form

In the previous section, I showed that Tbx6 levels can be modulated by inhibition of FGF in the embryo. To see the consequence on the clock of altering Tbx6 levels, in this section I explore the interactions between *tbx6* and *her1* at tissue and single cell levels. The

zebrafish *fused somites* (*fss*) mutant has a non-segmented paraxial mesoderm (Figure 4.2 A) and lacks the last *her1* stripe. The clock gene *her1* has a binding site for Tbx6 (Brend and Holley, 2009a). It has been suggested that clock dynamics are maintained in the posterior PSM of *fss*, but do not deliver clock information in the anterior PSM (Van Eeden et al., 1996b; Holley, Geisler, and Nüsslein-Volhard, 2000; Nikaido et al., 2002). However, the live characterisation of this mutant, which would help us to understand how *tbx6* interacts with the clock, is lacking.

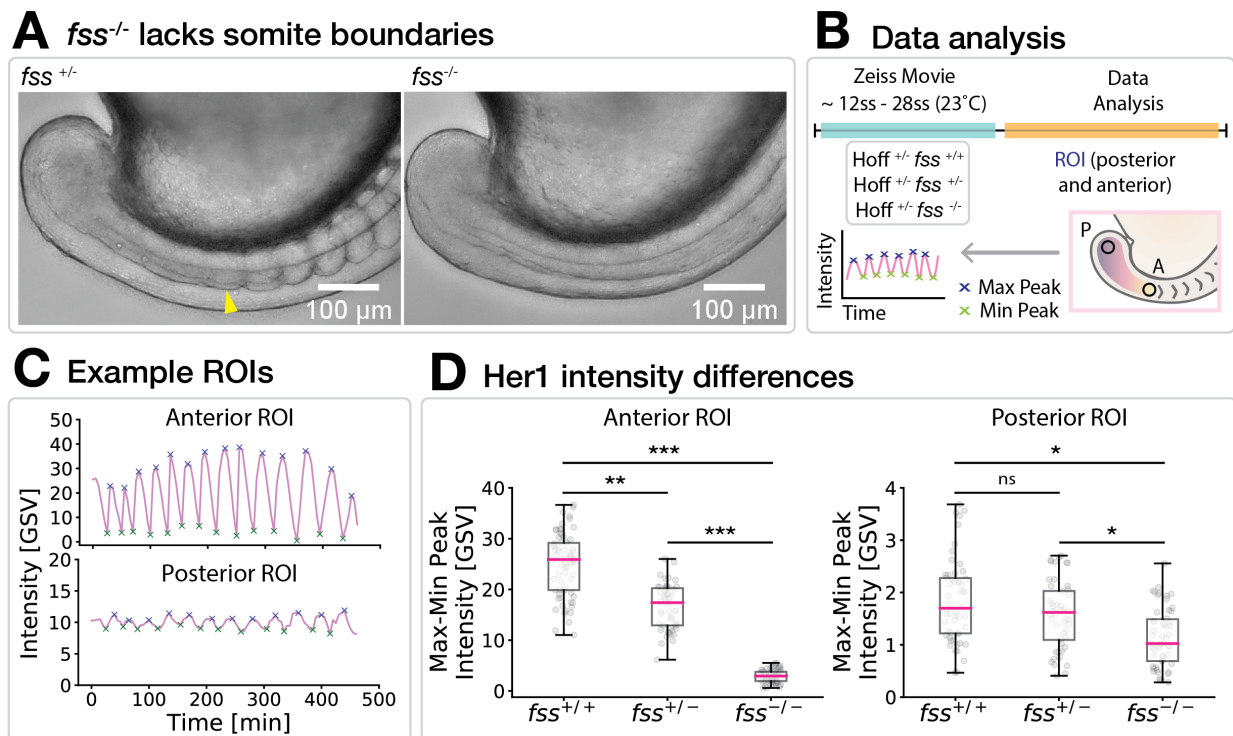


Figure 4.2: Her1-mNG intensity in the anterior PSM is dependent on Tbx6 copy number. **A.** Images of a 12ss *fss*-heterozygous and its homozygous sibling. **B.** Wide-field movies were acquired between 12 and 28ss of WT, *fss*^{+/-} and *fss*^{-/-} lines carrying Her1::mNeonGreen. Regions of interest (ROIs) were placed in the anterior and posterior of the PSM over time. The resulting oscillatory profile was used to calculate the maximum and minimum peaks. **C.** Example of the Her1-mNG dynamics from the ROI in the anterior and the posterior of a WT embryo. **D.** Difference in intensity between the maximum and minimum peaks. Pink lines show the median and stars reflect the level of significance (*P-value < 0.05, **P-value < 0.005 and ***P-value < 0.0005, using Mann-Whitney U test).

To understand how *tbx6* affects *her1* levels, we took wide-field time-lapses of WT, *fss*-heterozygous and homozygous *her1*::mNeonGreen carriers. To quantify Her1-mNeonGreen (Her1-mNG) intensity, I measured the average signal intensity in a region of interest (ROI) in the posterior and anterior PSM using tail-bud and Her1-mNG inten-

	$fss^{+/+}$	$fss^{+/-}$	$fss^{-/-}$
Anterior	31.03 ± 7.6 min	30.29 ± 7.7 min	31.50 ± 6.95 min
Posterior	25.80 ± 10.90 min	26.53 ± 11.09 min	26.54 ± 11.48 min

Table 4.1: Period of anterior and posterior PSM oscillations from Figure 4.2 measured as peak-to-peak interval.

sity as a reference, respectively (Figure 4.2 B). Note that the location of the anterior ROI in *fss* homozygous mutants is more posterior than in WT controls (see below). Figure 4.2 C shows an example of the temporal dynamics of the ROI for the anterior and posterior in a WT embryo.

The *fss*-homozygote shows a lower magnitude of Her1-mNG peak to trough intensity difference (max – min intensity) both in the anterior and in the posterior (Figure 4.2 D). The reduction of Her1-mNG in the posterior was not expected, as *Tbx6* has not been reported to be expressed in the tail bud. It was also a surprise to observe that *fss*-heterozygous mutants also showed a reduction of the Her1-mNG intensity in the anterior, since the heterozygote forms apparently normal somite boundaries. This is consistent with our previous result where we showed that *Tbx6* levels do not play a major role when FGF is inhibited (Figure 4.1 C). In addition, the period of the oscillations remained the same in the three cases both in the posterior and in the anterior (Table 4.1). Taken together, these results suggest that *Tbx6* activates *her1* in the anterior in a dose dependent manner. Similarly, it had been shown that relative gene dosage between *rippy1/2* and *tbx6* plays a role in somite formation (Kinoshita et al., 2018). Thus, it appears that *tbx6-rippy-her1* gene network in the anterior requires a tight control in order to arrest the oscillations in the anterior PSM.

The next question is whether the clock's spatial dynamics change in the *fss* mutants. To study this, I acquired time-lapse movies from light-sheet microscopy to study Her1-mNG dynamics at the tissue and single-cell level (Figure 4.3 A). Using the maximum projections of the time-lapse movies and a line of interest (LOI) parallel to the notochord, I calculate a kymograph (see method for obtaining the kymograph in Figure 5.10). As expected, the Her1-mNG wave arrests more posteriorly in homozygous mutant (Figure 4.3 B). At the beginning of the movie, at 12ss, the difference is $54 \mu\text{m}$ and at the end of the movie, at 28ss, the difference is $30 \mu\text{m}$ more posterior than WT. These differences coincide with the length of the somite at each of these developmental stages. Thus, in *fss*-homozygotes, *her1* gene expression arrests one somite length more posteriorly. This result explains the lack of the anterior *her1* stripe previously reported in fixed samples

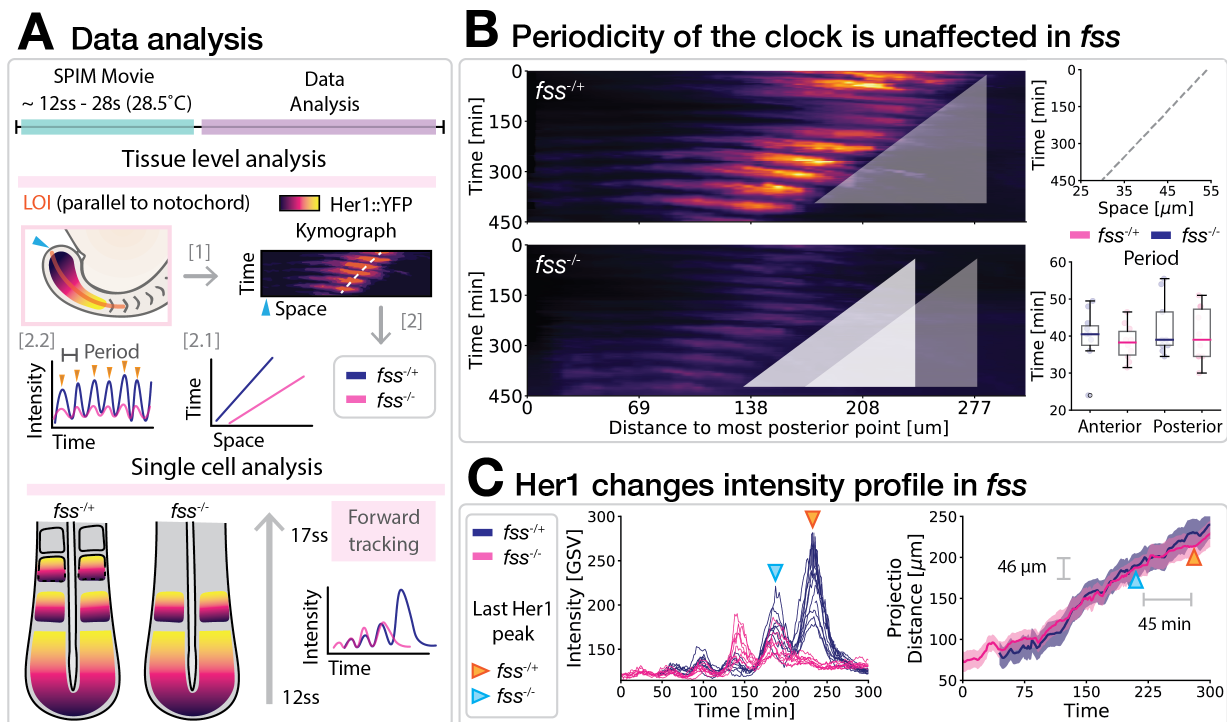


Figure 4.3: **Her1-mNG temporal dynamics are affected in fss .** **A.** fss -heterozygous and homozygous carrying Her1::mNeonGreen were imaged starting at 12ss using the light-sheet microscopy. Two levels of analysis were performed: (1) Tissue level analysis: Lines of interest (LOI) were drawn parallel to the notochord to obtain a kymograph. I then fitted a line (dashed white line) to the maximum intensity of the kymograph (which corresponds to the anterior Her1-mNG wave), and we draw a vertical line at the beginning of the kymograph (which corresponds to the TB region). These two Her1-mNG intensity measurements over time were used to obtain periodicity of the anterior and posterior regions, respectively. In addition, the anterior fitted line was used to quantify the position of the wave arrest in the anterior. (2) Single cell analysis: the cells were tracked in each case from 12ss to 17ss. **B.** Resulting kymographs with the same intensity scale to appreciate the differences in Her1-mNG expression. Grey dashed line shows the difference in wave arrest in the anterior (depicted as white triangles in the kymograph). Box-plots show the periodicity for each mutant at the anterior and posterior regions. **C.** Single cell tracks ($fss^{+/-}$ N = 12 and $fss^{-/-}$ N = 23). Intensities over time (left panel) and projection distance using the tailbud as reference (right panel). Orange and blue triangle show the position in space and time of the last $fss^{+/-}$ and $fss^{-/-}$ Her1-mNG peaks, respectively

(Holley, Geisler, and Nüsslein-Volhard, 2000). Although the position of the *her1* wave arrest changed, the periodicity remains the same (Figure 4.3 B).

To better understand the early arrest of the clock pattern in the fss PSM, I then

checked how the single cells behave. For this, I tracked cells in a *fss* heterozygous and homozygous mutants carrying Her1-mNG. Because the homozygous mutant does not form somite boundaries, the cells' alignment was done using their trajectory in space with the tailbud as a reference point (Figure 4.3 C). The *fss* homozygous cells arrested oscillations earlier in time (45 minutes) and in space (46 μm), in accordance with the more-posterior arrest of the tissue-level wave. We asked whether the *fss* homozygote profile is a simple truncation of the WT pattern, or whether there is a distinct profile. We observed that the second-to-last and the last peak of *fss* homozygous mutants are almost at the same intensity level, whereas in the heterozygote the past peak is higher than the second to last. In addition, the second-to-last Her1-mNG peak is higher intensity than the corresponding cycle in the heterozygous. Thus, the temporal profile of the individual cells reveals that the clock shows a distinct profile in the homozygous mutant.

The oscillatory profile remaining in the *fss* homozygote may be the result of other Tbx proteins acting to activate *her1* expression, and the distribution of *tbx6L* and *tbx16* expression as gradients from the tailbud is a plausible source (Morrow et al., 2017; Amacher et al., 2002). The finding of a Her1-mNG peak that is higher in the homozygous mutant is not expected in the simplest scenario, in which the transcriptional input from Tbx6 at the *her1* regulatory region is missing. Apart from Tbx6, the only other activating factor known to bind to the *her1* regulatory region in the anterior PSM is Suppressor of Hairless, Su(H) (Brend and Holley, 2009a), a DNA-binding transcription factor component of the Notch signalling pathway (Bray and Furiols, 2001). However, the expression of Notch is known to be lost in the anterior PSM in the *fss* homozygote (Oates, Rohde, and Ho, 2005). Thus, an alternative possibility is the up-regulation of an entirely novel factor acting on *her1* expression.

Combined, these findings show that oscillations of the clock terminate early in the absence of Tbx6, as is expected for a component of a timing mechanism. The effect of Tbx6 on the peak intensities of *her1* further reveals its action as a transcriptional activator in the mechanism.

4.4 How is the timer information translated into somite boundary formation?

It has been shown that the Tbx6 anterior border is regulated by Ripply at the protein level in both zebrafish and mouse (Oginuma et al., 2008; Wanglar et al., 2014; Zhao et al., 2015). However, this has mainly been studied using fixed and young embryos

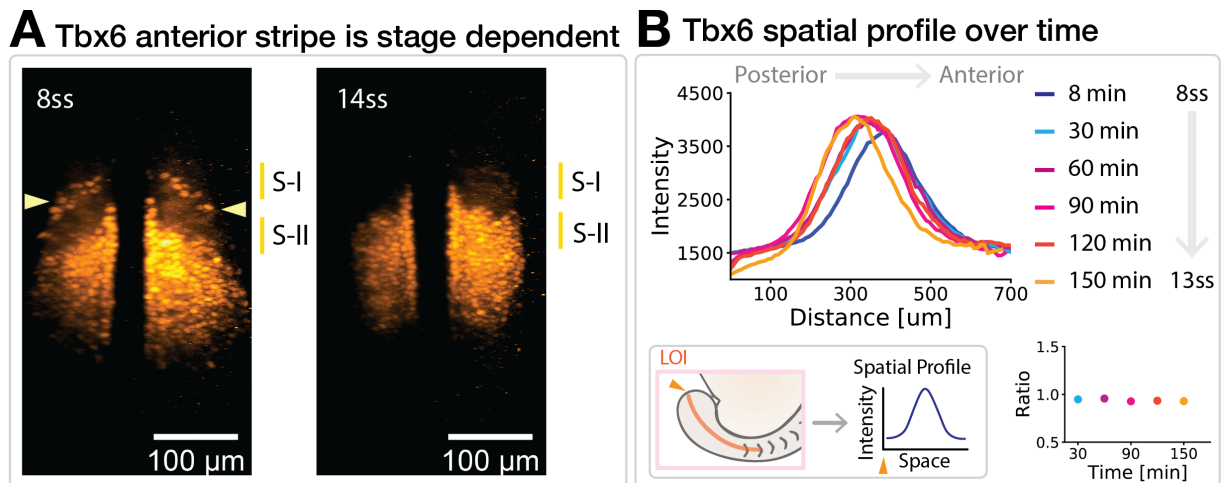


Figure 4.4: **Tbx6 spatial pattern.** **A.** Tbx6 antibody staining at 8ss and 14ss. Images were acquired with a light-sheet microscope. Maximum projections of the dorsal view are shown. S-I and S-II regions are specified using DAPI (not shown) to locate the formation of the last somite boundary. **B.** Tbx6 antibody staining from 8ss to 13ss (embryos were fixed every 30 minutes at 24°C). Images were acquired with wide-field microscopy. Maximum projections of the lateral view were obtained and a line of interest (LOI) parallel to the notochord was drawn to obtain the spatial profile of Tbx6. Ratios were calculated using the 8ss Tbx6 profile as reference. The ratio shows the reduction of the fold change compare to the reference curve. Time axis represents the fixation times with correspond to the formation of a new somite.

(around 10ss in zebrafish). By comparing the spatial expression of Tbx6 in fixed 8ss and 14ss embryos, we realised that the pattern was changed. At early stages, a stripe has been reported in the most anterior region of the Tbx6 spatial domain. However, in the later stages this stripe was gone and the expression was similar to that in the mouse (Oginuma et al., 2008; Zhao et al., 2015) (Figure 4.4 A). This may have been overlooked, because most previous work has been done in earlier stages since it is easier to de-yolk and flat-mount fixed samples for imaging. Although the spatial expression changes, the levels of expression remain constant (Figure 4.4 B), in contrast to the relatively rapid changes observed in dpERK distributions in Chapter 2 (Figure 2.3 B).

The thin anterior stripe of Tbx6 protein features in models of its function during the specification of the boundary (Wanglar et al., 2014). However, our result indicates that the anterior stripe observed at early stages is not necessary for orderly somite segmentation, at least of the posterior body, and raises the possibility that it is not required at all, as is the case in mouse (Oginuma et al., 2008). Experimental manipulations that delete the anterior protein stripe and leave the main domain intact during early somitogenesis would be needed to test this idea.

Ban et al., 2019 speculated that *tbx6* transcription is differentially regulated during somite segmentation. They showed that deletion of one of the Tbx6 auto-regulatory binding sites (T1) led to an abnormal expression pattern of segmentation genes, but only at early stages (up to 12ss). The basic molecular mechanisms of clock and wavefront may be differently regulated along the axis (Holley, 2006), consistent with our previous results on the dpERK spatial expression (Chapter 2, Figure 2.7 C). There are differences between how the trunk and tail regions are regulated (Griffin et al., 1998). In addition, different temporal regulation of certain genes could reflect different phenotypes observed. However, *fss* mutant phenotype is the same along the axis thus any difference we observe in Tbx6 expression is not obviously relevant. Nevertheless, knock-down of *her7*, a clock gene in zebrafish, shows regional disruption of the 8th to 17th somite segments. On the other hand, *her1* mutants show defects at all three anterior-most somite borders (Choorapoikayil et al., 2012). Thus, maybe the difference in *tbx6* regulation comes across when the clock is compromised. In any case, it is of great importance that live reporters and mutant analysis are performed to cover the different developmental stages.

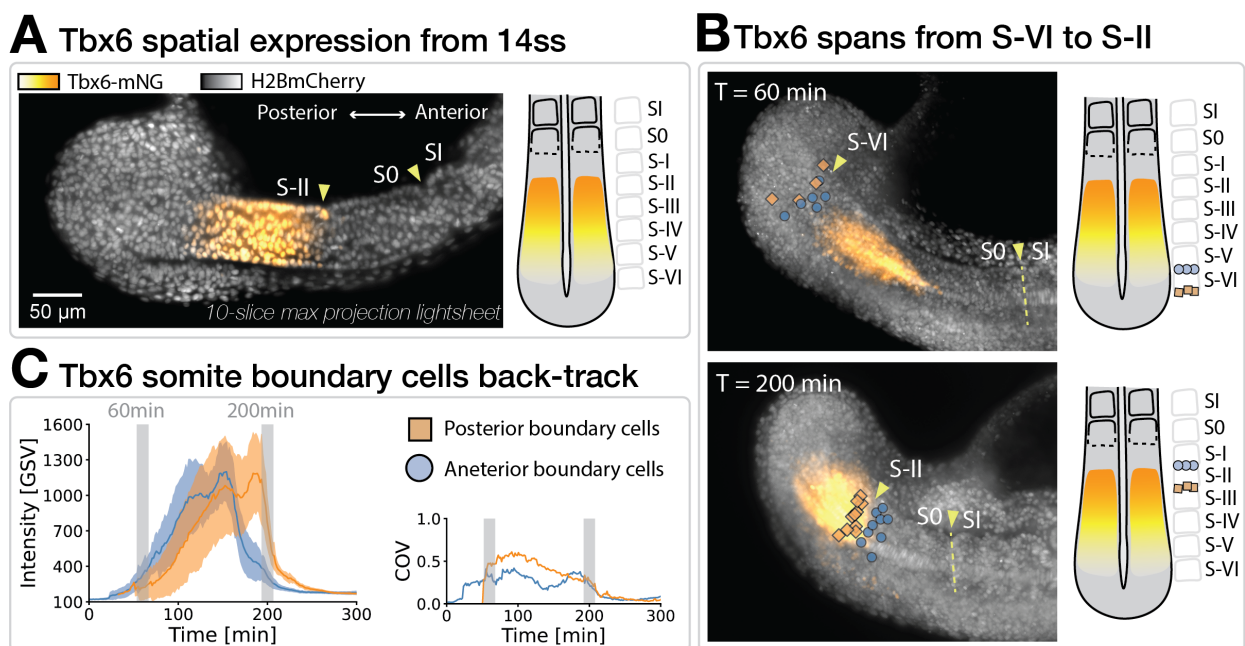


Figure 4.5: **Tbx6 spans S-VI to S-II and shows a rapid arrest at the cellular level. A.** Light-sheet microscopy max projection of 10-slices of a 14ss embryo carrying Tbx6-mNG. **B.** Images of the tracked cells at the onset of Tbx6 expression at S-VI (upper panel) and at the offset at S-II (lower panel). Yellow dashed line marks the somite boundary. **C.** Anterior and posterior somite boundary cells back-tracked from the same somite (22nd). Solid lines represent the means and lighter bands represent the standard deviation over time (N = 15 anterior cells and N = 21 posterior cells). The grey lines show the times the cells are at the S-VI and the S-II in the PSM. The coefficient of variation was also calculated over time.

Recently, a transgenic line reporting the expression of a Tbx6-mNeonGreen (mNG) fusion protein was generated in the lab (Figure 4.5 A). This was constructed by inserting an in-frame mNeonGreen coding sequence into the stop codon of *tbx6* in a BAC containing the endogenous genomic region. The resulting fusion protein is nuclear-localised and the transgenic line does not interfere with normal somitogenesis. In combination with light-sheet microscopy and modern analysis tools we can now obtain a better picture of the spatiotemporal dynamics of Tbx6.

With the use of cell tracking, we observed that Tbx6 starts to rise in S-VI at 14ss and falls at S-II (Figure 4.5 B). The position of the anterior Tbx6 boundary is consistent with previous studies even in younger somite stages (Wanglar et al., 2014; Windner et al., 2015; Ban et al., 2019). However, the posterior domain of Tbx6 was not explored before. We observed that at these stages, already in the posterior PSM, cells start to express Tbx6. If Tbx6 is part of the time-keeping mechanism, this could be one of the reasons why when cells from the posterior PSM (PSM4) are cultured, they already have their timer running.

It has previously been shown that the anterior domain of Tbx6 is a sharp boundary, which led to the idea that it could be providing crucial positional information for the positioning of the somite boundary (Oginuma et al., 2008; Wanglar et al., 2014; Zhao et al., 2015). Looking at the cellular level, we observed that the offset of Tbx6 occurs in the order of few minutes and in a very precise way (the coefficient of variation is reduced) (Figure 4.5 C). This is consistent with the observed steep anterior Tbx6 boundary at the tissue level and with the fast protein degradation by Ripply (Kawamura et al., 2005). Comparing the rise and fall of Tbx6 at the cellular level reminded us of the spatial precision shown by Hunchback in *Drosophila* (Houchmandzadeh, Wieschaus, and Leibler, 2002). The rise of Tbx6 is variable but the offset occurs in a rapid and precise manner.

In both mouse and zebrafish, it has been shown that the anterior border of Tbx6 coincides with the *Mesp2* and *mesp-b/a* expression domains, respectively (Oginuma et al., 2008; Zhao et al., 2015; Wanglar et al., 2014). Thus, it has been speculated that the anterior border of Tbx6 retreats in a stepwise manner with an interval of one somite length towards the posterior region of the PSM. This has been inferred using fixed samples. To study the spatiotemporal dynamics of Tbx6, I performed time-lapse imaging using the light-sheet microscope of Tbx6-mNG embryos starting at 12ss (Figure 4.6 A). As previously shown, we calculate the kymograph of Tbx6 using the posterior of the embryo as the reference point. Each horizontal line in the kymograph contains the spatial profile recorded with the LOI. Figure 4.6 C shows two of these lines to observe how the profile has regressed posteriorly and also how it became narrower over the 7 hours of development from 14 to 22 somite stage. Computing the peak of these curves

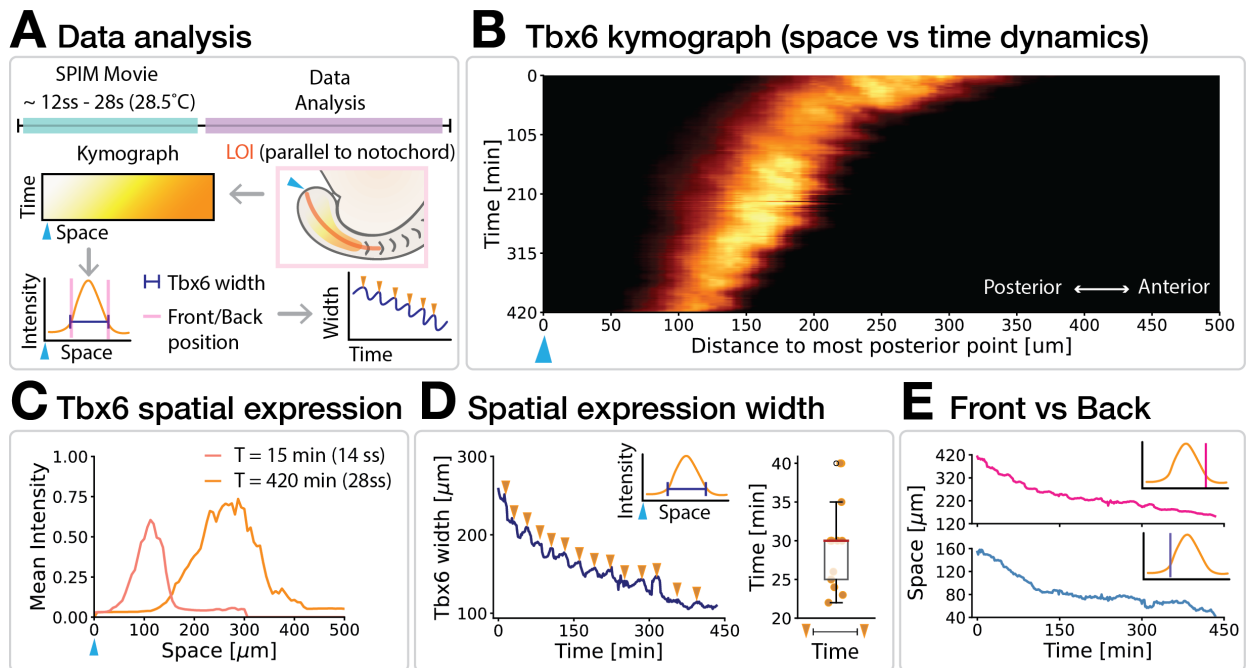


Figure 4.6: Tbx6 velocity front matches the periodicity of somite boundary formation. **A.** A light-sheet microscopy time-lapse was acquired at 12ss from an embryo carrying Tbx6::mNeonGreen. Maximum intensity projections were used to draw a line of interest (LOI) and obtain a kymograph. By taking the vertical lines of the kymograph, we can obtain the spatial expression of Tbx6 over time. These expression curves were quantified by detecting the peaks, widths and velocity of the front and back positions of the curve. **B.** Resulting kymograph of Tbx6 using the tip of the tailbud as reference point (blue triangle). **C.** Examples of the spatial expression of Tbx6 at two different somite stages. **D.** Width of Tbx6 over time. The periodicity of these dynamics match that of somite formation. **E.** Position of the front (pink) and back (purple) over time.

over time, we can then obtain the width of the curve using a relative distance (80%) of the peak's height and prominence. As a result, we obtain the width dynamics of Tbx6 protein as shown in Figure 4.6 D.

The width of the Tbx6-mNG distribution appears to oscillate, and the periodicity of this matches that of somite boundary formation. To determine whether this periodic regression is a result of the back (posterior) or front (anterior) point in the Tbx6-mNG spatial profile, we evaluated their separate dynamics over time (Figure 4.6 E). We observed that it is the front, i.e. the anterior position of the curve which provides the oscillatory regression of the width. Moreover, if we calculate the velocity of front and back positions, we observe that the velocity of the back position is steady and low whereas the velocity of the front is changing over time and is higher (Figure 4.7 A). Thus, the Tbx6 protein domain reduces its width over developmental time by regressing faster at the front than

the back.

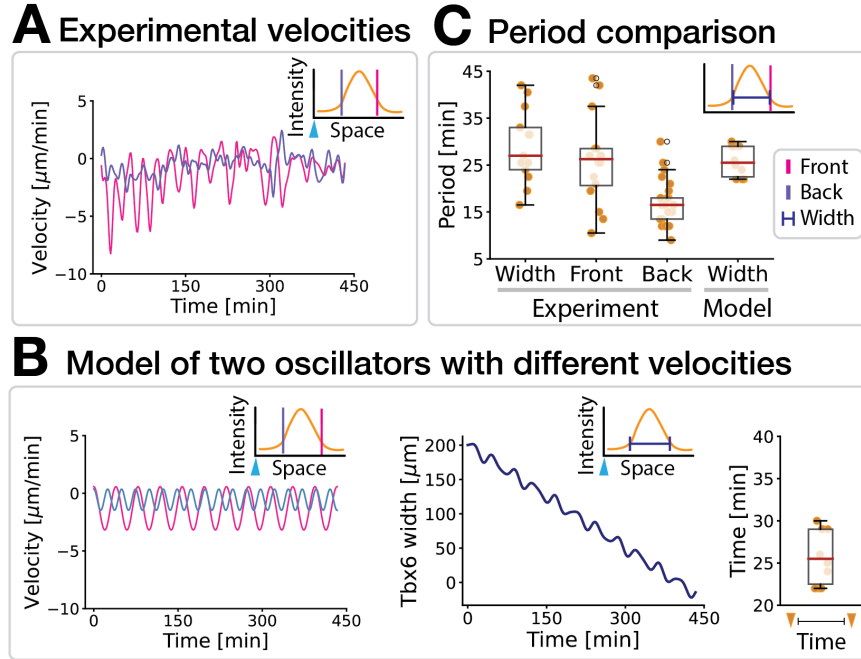


Figure 4.7: **Tbx6 spatial domain front and back velocities are different.** **A.** Velocities of the front (pink) and back (purple) positions of the Tbx6 width. The blue arrowhead marks the reference point which is in the posterior of the TB (see Figure 4.6 A). **B.** With the resulting velocities (equation 4.2) we can reconstruct the width of the Tbx6 distribution and calculate the period of the Tbx6 width dynamics in the model. **C.** Comparison of the periods of the experimental Tbx6 width, front and back positions with the obtained model width. Each dot represents the period (peak-to-peak difference) of the width, front and back expressions.

Using the average velocities of the front and back positions (equation 4.1), we can construct a simple model of a regressing distribution (equation 4.2). By allowing either the front or the back to move in an oscillatory manner, we can ask which situation best fits to the experimental data. We observed that the model with the oscillatory front reproduced a similar behaviour to the experimental situation (Figure 4.7 B), confirming that the front position of the Tbx6 width is the one leading the oscillatory behaviour (Figure 4.7 C). Taken together, these results are the first live observation of Tbx6 step-wise regression, previously inferred from fixed samples.

$$\begin{aligned}
 V_F &= \frac{dx_F}{dt} \rightarrow V_F \text{ is the experimental velocity and } x_F \text{ experimental position} \\
 V_B &= \frac{dx_B}{dt} \rightarrow V_B \text{ is the experimental velocity and } x_B \text{ experimental position}
 \end{aligned}
 \tag{4.1}$$

$$\begin{aligned}
v_F &= \cos(2\pi x_F f_F t) \times \sigma(V_F) + \mu(V_F) \rightarrow v_F \text{ is the modeled velocity} \\
v_B &= \cos(2\pi x_B f_B t) \times \sigma(V_B) + \mu(V_B) \rightarrow v_B \text{ is the modeled velocity}
\end{aligned}
\tag{4.2}$$

We have shown above that the Tbx6 domain regresses in a step-wise manner towards the posterior with a periodicity that matches somite formation, and we have also shown that individual cells have a relatively variable and gradual Tbx6 accumulation starting in S-VI and a sharp and sudden decrease in Tbx6 levels in S-II. We next wanted to understand the relationship between the sudden decrease and the step-wise regression. In particular, we wanted to determine what unit of cells were degrading Tbx6 together. Previous work from mouse and zebrafish using fixed samples has proposed that the unit of cells that degrade Tbx6 at the same time would be the prospective somite (Wanglar et al., 2014; Oginuma et al., 2008), and the posterior limit of this domain of coordinated degradation marks and determines the position of the next segment boundary.

To investigate this hypothesis, we back-tracked cells from SI, where the boundaries of the somite and their constituent cells are unambiguous, all the way to S-VI to cover the entire Tbx6 region in transgenic embryos carrying Tbx6-mNG (Figure 4.8 A). The dynamics of the boundary cells were reproducible between somite boundaries 18 through to 22 (Figure 4.8 B) and the offsets matched periodicity of somite formation (every ~ 30 minutes). Similar to the spatial profiles obtained in Figure 4.4 B from 8ss to 15ss. This contrasts with the relatively rapid change in dpERK distribution that we previously observed in Chapter 2 (Figure 2.3 B). We also followed Tbx6-mNG signal in the cells from the interior of the somites, i.e. those that do not contribute to either of the boundaries.

We compared the average Tbx6 dynamics of the cells of the posterior boundary, the anterior boundary, and the internal cells of the somite for somites 19 and 20 (Figure 4.8 C). The average signal for posterior boundary cells exhibited two peaks of Tbx6-mNG, and then a smooth and rapid decline in signal. Anterior boundary cells of the same somite shared a similar profile, but off-set in time such that their second peak was coincident with the posterior boundary cells' first peak. The rapid degradation phase of Tbx6-mNG signal for anterior boundary cells featured a small shoulder at low intensity coincident with the posterior cells' second peak. Internal somitic cells displayed a profile more similar to the posterior cells, with a shared timing of the first peak, a degradation phase with pronounced shoulder at high intensity, and a rapid decline in signal in concert with that of posterior cells. Remarkably, the posterior boundary cells of one somite, e.g. somite 19 arrested at the same time as the anterior boundary cells of the next somite, e.g. somite 20.

These results mean that the dynamics of Tbx6-mNG signal offset are not grouped as expected if the entire somite n lost Tbx6 at the same time, namely [anterior $_n$ -internal $_n$ -

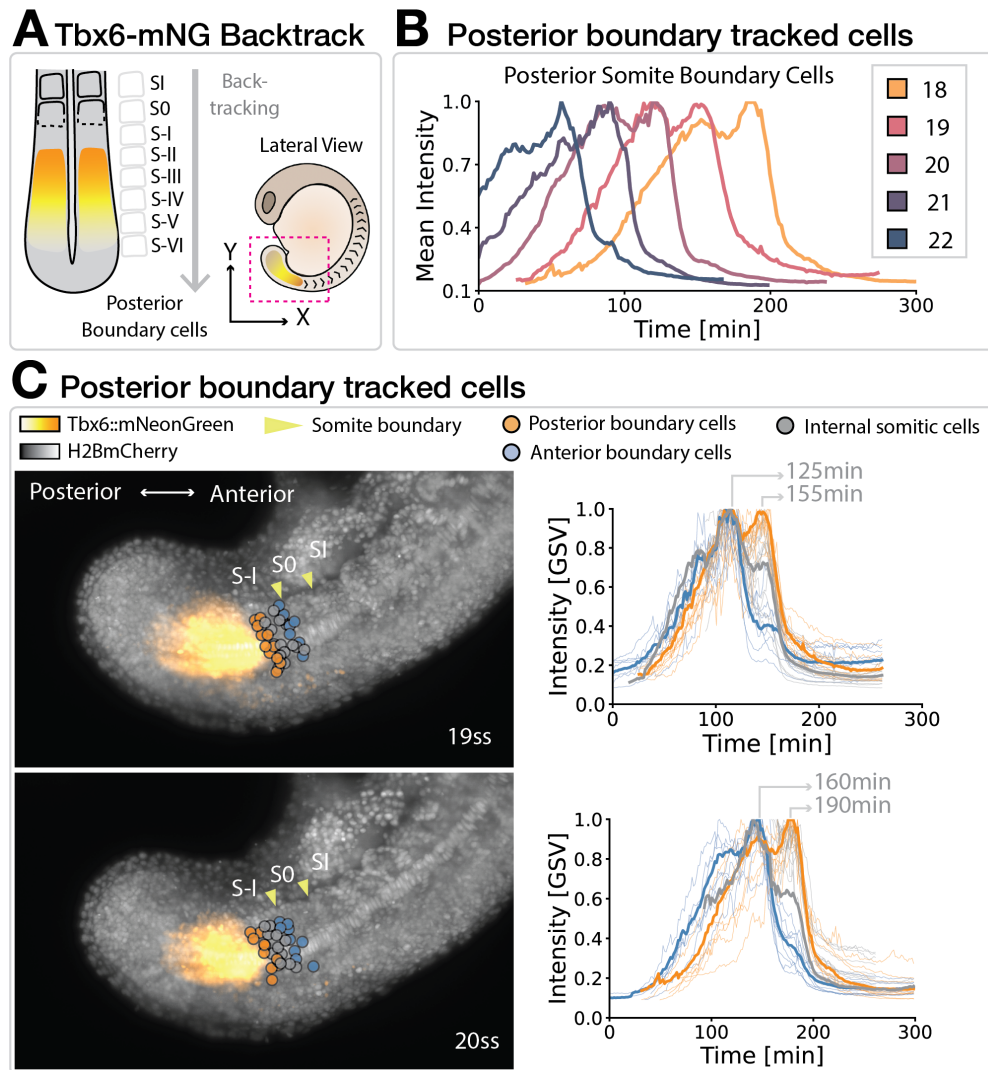


Figure 4.8: **Tbx6 single cell tracking reveals stepwise dynamics.** **A.** Cartoon showing the Tbx6 domain and the back tracking performed. **B.** Posterior boundary cells from somites 18 to 22. Lines show are averages of tens of cells. **C.** Example of two consecutive somites in which cells in the same somite are tracked. On the right, these tracks are colour coded according to their position in the anterior-posterior boundary or in the interior of the somite.

posterior_n] (Figure 4.9 A). Rather, Tbx6-mNG signal offsets are temporally organised across the future somite boundary furrow, namely [internal_n-posterior_n-anterior_{n+1}] (Figure 4.9 B). This organisation implies that the segmental unit specified by the clock and wavefront is not, strictly speaking, the somite, but rather the boundary. Consistent with this, it has been recognised for decades that the first sign of segmentation of the zebrafish mesoderm is not somite 1, but rather the boundary between the future somite 1 and future somite 2 (Wood and Thorogood, 1994; Kimmel et al., 1995). Whether this

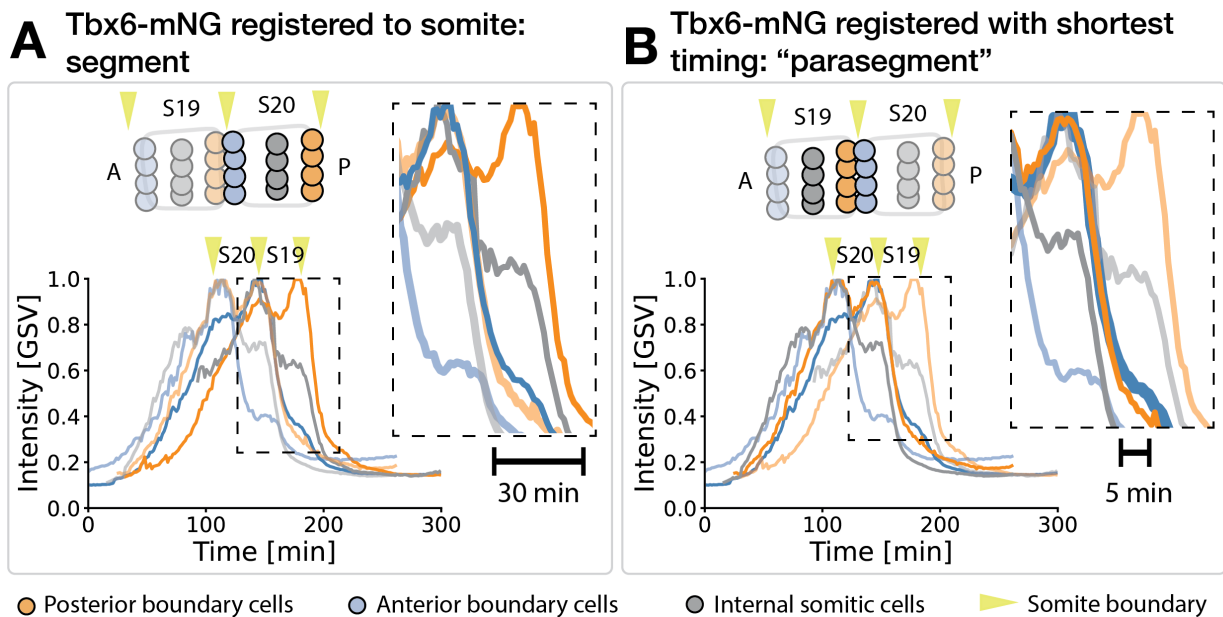


Figure 4.9: Natural clustering that minimises the Tbx6-mNG offset time between cell locations. Cartoons shows two consecutive somites (19 and 20) where left is anterior and right is posterior. Yellow arrowheads represent somite boundaries. Opaque versus lighter lines represent the clustering that results as a **A.** segment and as a **B.** "parasegment".

trans-boundary grouping is the case in other vertebrates remains an open question, as studies using appropriate transgenics and imaged at sufficient spatiotemporal resolution are lacking. Nevertheless, imaging at single cell resolution in chick embryo revealed the simultaneous formation of posterior_n and anterior_{n+1} boundaries, rather than the formation of the complete somite (Kulesa and Fraser, 2002), in line with our findings from the zebrafish.

The initial pattern of somite boundaries is also not the final segmental morphology in vertebrates. As noted by Remak in 1855, the bone-forming cells of the sclerotomes undergo a process called *resegmentation*, in which the posterior half of one sclerotome and the anterior half of the next fuse to form the vertebral bodies of the axial skeleton (Bagnall, Higgins, and Sanders, 1988). This ensures that the muscles and tendons generated from the myotome in each somite, and which retain their initial spatial relationship to the somite boundary, span adjoining vertebral bodies, a geometry critical for the coordination of movement.

At much greater evolutionary distance, the existence of a genetic segment of specification that is out-of-phase with the subsequent morphological segment is most well-known as the para-segment of *Drosophila melanogaster* (Martinez-Arias and Peter A Lawrence, 1985). In the embryonic parasegments of insects, the initial repeated pat-

tern is defined by a developmental compartment, which prevents cell mixing, and this compartment boundary is determined through mutual signalling by Hedgehog from the anterior cells and Wingless from the posterior cells. Hedgehog is initially driven by the Engrailed transcription factor, which is induced by Wingless. Later, as the morphological body segments form to provide the larva with repeated belts of denticles for locomotion, the engrailed and Hh expressing cells are located at the very posterior of the true segment. However, none of these genes are thought to be involved in the segmentation of vertebrates, and while cell mixing is limited in the anterior PSM, initial periodic specification does not appear to behave as a compartment.

Thus, whether there are deeper evolutionary connections between the two systems is unknown, but the uncoupling of the genetic specification of a repeated pre-pattern and the phase of the subsequent morphological pattern appears to be a strategy explored by evolution multiple times.

Summary Chapter 4

Overall, this chapter has shown the experiments performed to better understand our molecular candidates for the timer mechanism. We believe *tbx6-rippy* work together as a critical part of the time-keeping mechanism of future somite cells, given the literature and our discovery of autonomous timing programme of PSM cells. We showed that Tbx6 modulates the maximal intensity of *her1* in a dose-dependent manner using homozygous and heterozygous *fss* mutants. Furthermore, at the single-cell level, *fss* homozygous showed a distinct temporal profile than heterozygous, suggesting that other T-box proteins act to activate *her1* or an up-regulation of an entirely new factor. In addition, using a novel reporter line, Tbx6-mNG, we quantified changes in spatial expression time and found that the Tbx6 protein domain reduces its width over developmental time, with the front of the domain regressing faster than the back of the domain. Finally, by inspecting this phenomena at the cellular level, we saw that Tbx6-mNG offset occurs in the order of few minutes in a precise manner and is organised temporally across the future somite boundary furrow. This implied that the segmental unit specified by the clock and wavefront is not, strictly speaking, the somite but rather the boundary. Further experiments exploring the role of Ripply in conjunction with Tbx6 should be performed to better understand how the timer mechanism works during somite boundary formation. In sum, the live imaging and analysis of mutant *fss* and transgene Tbx6-mNG in this chapter showed evidence of a candidate for the time-keeping mechanism and raised the possibility that together with signaling gradients, control the precise and accurate positioning of somite boundaries.

Outlook

This report shows the work done during my four years of PhD studies. I have guided you through my working model of how somite boundaries are precisely and accurately positioned during somitogenesis in zebrafish. This model is based on the idea of an underlying cellular intrinsic timer that is regulated by external spatiotemporal signals. An important element of my work was the creation of a basis for the analysis of PSM dynamics at the cellular level. To date there is limited description of the cellular-level PSM pattern and its inherent precision. I have made preliminary progress on this front using a relatively long image pre-processing pipeline (3 days per time-lapse) and semi-automated single cell tracking. Thanks to the pipeline and tools presented in Chapter 1, we were able to image clock dynamics during FGF inhibition and show the exact position of the S-IV, the presumed determination front, by tracking cells at the boundaries of consecutive somites in Chapter 2. Furthermore, in Chapter 3 we showed single cell TB clock oscillations and constructed a map of clock dynamics from TB to somites in the embryo. Finally, in Chapter 4, we observed clock dynamics in *fss* mutants and *tbx6* dynamics in a new transgenic line, suggesting Tbx6 is part of the timer mechanism. These proof-of-principle data were sufficient to reveal new elements of the PSM dynamic pattern. However, improvements in speed and automation are needed to perform experiments requiring controls and replicates. Therefore, an important part of future work is to develop faster and more automated image analysis tools. Ultimately, these open source tools that I have created will serve the wider community and open the doors to those imaging model systems that feature rapid cellular rearrangements and molecular dynamics.

Materials and Methods

5.1 Antibody Staining

5.1.1 Reagents used

Primary antibodies:

- **dpERK:** Mouse monoclonal IgG2 (Sigma, M9692). Concentration used was 1:1000
- **Tbx6:** Mouse monoclonal IgG2b (A66). Concentration used was 1:1000

Secondary antibodies:

- **488 GFP:** Mouse anti-IgG1 from Goat (Thermofisher, A21121). Concentration used was 1:1000
- **633 farRFP:** Mouse Anti-IgG2b from Goat (Thermofisher, A21146). Concentration used was 1:1000
- **568 RFP:** F(ab)₂ from Goat Anti-rabbit IgG (H+L) (Thermofisher, A21069). Concentration used was 1:1000

5.2 Zeiss Movies

5.2.1 Acquisition

Time-lapse movies and images on the Zeiss wide-field were always acquired using the 20x objective and in the case of live imaging a constant temperature of 28°C was

maintained and recorded using a probe.

5.2.2 Analysis

Max Projections for visualisation

Zeiss time-lapse images used for visualisation purposes where all processed under the same steps:

1. Split the channels using the `split channels` command from Fiji in order to have the stack over time for each channel separately (since we process them differently).
2. On bright-field channel:
 - 2.1 Stack Focuser Fiji plugin: choose the slices you want to include in the process. The result is a 32-bit float copy of the original image. This is a focused image from the stack of images corresponding to different focal planes. (<https://imagej.nih.gov/ij/plugins/stack-focuser.html>)
 - 2.2 Use unsharp mask filter in order to increase the contrast along the edges of the image. This way, somite boundaries will be emphasised.
 - 2.3 Convert back to a 16-bit image.
3. On the fluorescent channel(s):
 - 3.1 Max projection of all the slices of interest.
 - 3.2 Gaussian blur filter with small σ size (around 2).
4. Merge the resulting channels using the `merge channels` command from Fiji.
5. Add scale bars and if movies, use time-stamper.

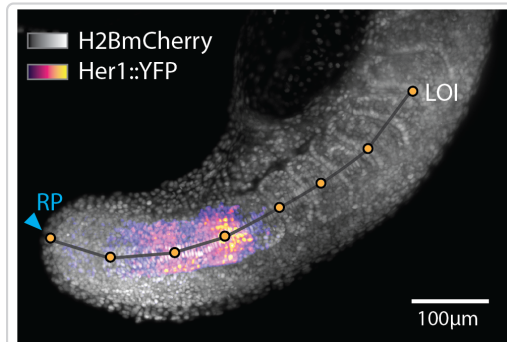
5.3 Image Analysis

5.3.1 SPIM Movies

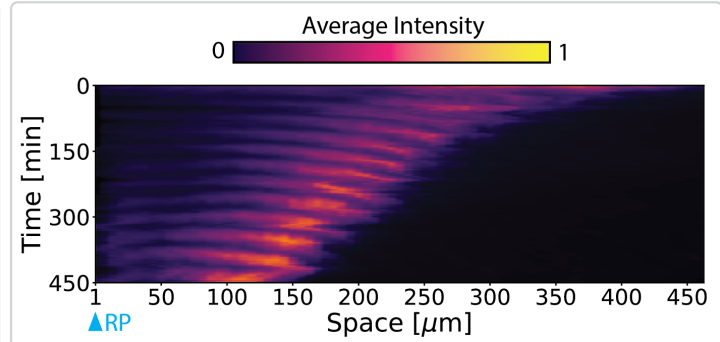
Kymographs

1. Reference spatial frame: Manually segment the Notochord over time in order to use it as the reference frame (Figure 5.10A).
 - 1.1 Use the `segmented line` command from Fiji and draw always the same number of points on each of the desired timepoints
 - 1.2 Depending on the temporal resolution, draw segmented lines every N time points. For instance, with 90 second time step, we draw segmented lines every 10 frames.
 - 1.3 Once the segmented lines are recorded using the ROI Manager from Fiji, use the Macro: **MacroInterpolateLinesRois.ijm** to interpolate lines between the frames without segmented lines.
 - 1.4 Save the .roi files in a folder as a SetRoi.zip file.
2. Python code to generate the Kymograph:
 - 2.1 Figure 5.10B, shows an overview of how the Python code. The lines shown are the segmented lines saved as ROIs in the previous steps. For this step, the maximum projection of the signal of interested will be used in order to obtain the desired intensities over space and time.
 - 2.2 As a result, you obtain a kymograph of the desired signal (Figure 5.10C). In the example, the waves of Her1 can be observed and the arrest coincides with the formation of a newly formed somite.

A Line of interest (LOI)

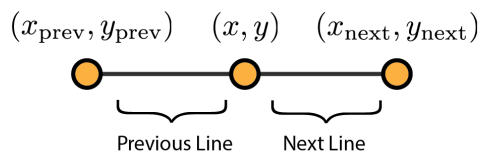


C Example Kymograph



B Steps to make a Kymograph

1. Find the slope of the Previous and Next lines.

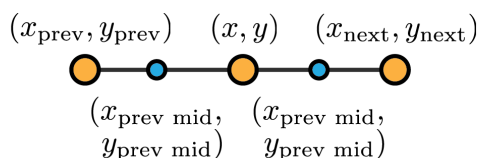


2. Any perpendicular line to the Previous and of the Next lines is equal to the inverse of that slope multiplied by (-1).

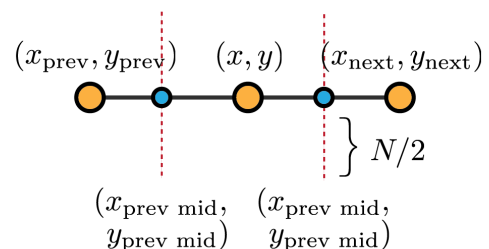
$$\text{Slope}_{\text{prev}} = \frac{y - y_{\text{prev}}}{x - x_{\text{prev}}} \quad \text{Slope}_{\text{next}} = \frac{y - y_{\text{next}}}{x - x_{\text{next}}}$$

$$\text{Slope}_{\text{prev}\perp} = \frac{-1}{\text{Slope}_{\text{prev}}} \quad \text{Slope}_{\text{next}\perp} = \frac{-1}{\text{Slope}_{\text{next}}}$$

3. Find the intermediate points between the previous and the next points with respect to the one in the center.



4. Draw a perpendicular line using these middle points as a reference and make these perpendicular lines be N pixels long.



5. Create a 2D polygon and all the points inside this polygon will be projected into the point x,y.

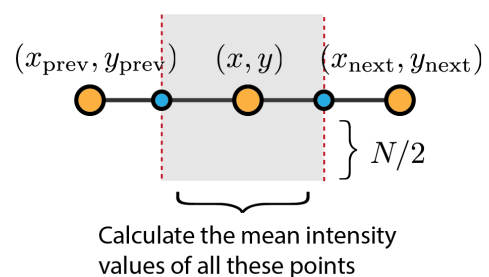
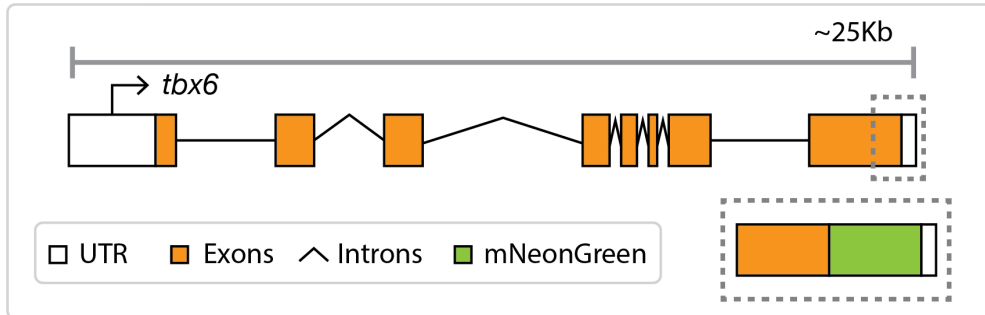


Figure 5.10: Kymograph Generation. **A.** Following the Notochord as a reference, use the segmented line tool from Fiji to obtain the same number of points starting from the TB (which is used as the reference point (RP)). **B.** Details of the steps followed in order to obtain the values surrounding the segmented line to calculate the average intensities. The width of the expansion of the segmented line (N) is defined by the user. **C.** Example of how a Kymograph looks like from a 14ss Looping embryo over a period of 7.5 hours.

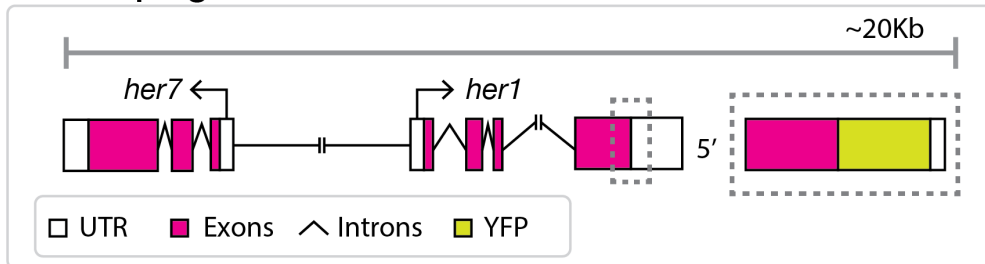
5.4 Transgenic lines

These are the main lines used during this thesis and generated in our lab. Benchmarking for Hoff and Hulk included antibody staining to compare endogenous versus transgene spatial patterns, in situ hybridisation with *xirp2a* to check for boundary defects, rescue experiments with mutants and live imaging to quantify somite formation period. Figure 5.11 A show Tbx6-mNeonGreen (Hulk). This line was created and benchmarked by Chloé Jollivet. Rescue experiments were conducted with *fss* mutants where 12 out of 27 were showing small boundary defects. Moreover, 50 % of the Tbx6-mNG embryos show some level of defect at the first 14 somites formed. Figure 5.11 B show Her1-mNeonGreen (Looping) from Soroldoni and Oates, 2011. Figure 5.11 C Her1-mNeonGreen, Her1-mKate (Hoff). This line was created by Daniele Soroldoni and benchmarked by Chloé Jollivet and Olivier F. Venzin. Rescue experiments were conducted with a *her1*, *her7* double mutant where at least the first 4 somites were rescued. No somite defects were observed and the period and number of somite was almost identical (16 somites counted from the anus instead of 17 as the WT).

A Hulk, *tbx6:Tbx6-mNeonGreen*



B Looping - *her1:Her1-YFP*



C Hoff - *her:Her1-mNeonGreen, Her7:mKate*

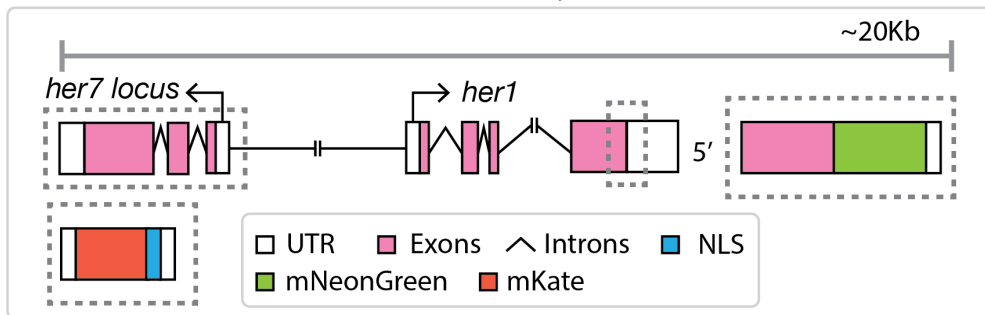


Figure 5.11: Zebrafish transgenic lines. **A.** *Tbx6-mNeonGreen* (Hulk). **B.** *Her1-YFP* (Looping) from Soroldoni and Oates, 2011. **C.** *Her1-mNeonGreen, Her1-mKate* (Hoff).

Bibliography

- Akiyama, Ryutaro, Miwa Masuda, Shoichiro Tsuge, Yasumasa Bessho, and Takaaki Matsui (2014). “An anterior limit of FGF/Erk signal activity marks the earliest future somite boundary in zebrafish”. In: *Development* 141.5, pp. 1104–1109.
- Amacher, Sharon L, Bruce W Draper, Brian R Summers, and Charles B Kimmel (2002). “The zebrafish T-box genes no tail and spadetail are required for development of trunk and tail mesoderm and medial floor plate”. In:
- Aulehla, Alexander and Randy L Johnson (1999). “Dynamic Expression of lunatic fringe Suggests a Link between notch Signaling and an Autonomous Cellular Oscillator Driving Somite Segmentation”. In: *Developmental biology* 207.1, pp. 49–61.
- Aulehla, Alexander and Olivier Pourquié (2010). “Signaling gradients during paraxial mesoderm development”. In: *Cold Spring Harbor perspectives in biology* 2.2, a000869.
- Aulehla, Alexander, Christian Wehrle, Beate Brand-Saberi, Rolf Kemler, Achim Gossler, Benoit Kanzler, and Bernhard G Herrmann (2003). “Wnt3a plays a major role in the segmentation clock controlling somitogenesis”. In: *Developmental cell* 4.3, pp. 395–406.
- Aulehla, Alexander, Winfried Wiegraebe, Valerie Baubet, Matthias B Wahl, Chuxia Deng, Makoto Taketo, Mark Lewandoski, and Olivier Pourquié (2008). “A β -catenin gradient links the clock and wavefront systems in mouse embryo segmentation”. In: *Nature cell biology* 10.2, pp. 186–193.
- Bagnall, KM, SJ Higgins, and EJ Sanders (1988). “The contribution made by a single somite to the vertebral column: experimental evidence in support of resegmentation using the chick-quail chimaera model”. In: *Development* 103.1, pp. 69–85.
- Bajard, Lola, Luis G Morelli, Saúl Ares, Jacques Pécréaux, Frank Jülicher, and Andrew C Oates (2014). “Wnt-regulated dynamics of positional information in zebrafish somitogenesis”. In: *Development* 141.6, pp. 1381–1391.
- Ban, Hiroyuki, Daisuke Yokota, Shiori Ootosaka, Morimichi Kikuchi, Hirofumi Kinoshita, Yuuri Fujino, Taijiro Yabe, Hiroki Ovara, Ayaka Izuka, Kagari Akama, et al. (2019). “Transcriptional autoregulation of zebrafish *tbx6* is required for somite segmentation”. In: *Development* 146.18, dev177063.

- Bénazéraf, Bertrand, Paul Francois, Ruth E Baker, Nicolas Denans, Charles D Little, and Olivier Pourquié (2010). “A random cell motility gradient downstream of FGF controls elongation of an amniote embryo”. In: *Nature* 466.7303, pp. 248–252.
- Bessho, Yasumasa and Ryoichiro Kageyama (2003). “Oscillations, clocks and segmentation”. In: *Current opinion in genetics & development* 13.4, pp. 379–384.
- Boareto, Marcelo, Tomas Tomka, and Dagmar Iber (2021). “Positional information encoded in the dynamic differences between neighboring oscillators during vertebrate segmentation”. In: *Cells & Development*, p. 203737.
- Bokman, Stephen H and William W Ward (1981). “Renaturation of Aequorea green-fluorescent protein”. In: *Biochemical and biophysical research communications* 101.4, pp. 1372–1380.
- Bradbury, Jane (2004). “Small fish, big science”. In: *PLoS biology* 2.5, e148.
- Bray, Sarah and Marc Furriols (2001). “Notch pathway: making sense of suppressor of hairless”. In: *Current Biology* 11.6, R217–R221.
- Brend, Tim and Scott A Holley (2009a). “Expression of the oscillating gene *her1* is directly regulated by hairy/enhancer of split, T-box, and suppressor of hairless proteins in the zebrafish segmentation clock”. In: *Developmental dynamics: an official publication of the American Association of Anatomists* 238.11, pp. 2745–2759.
- (2009b). “Zebrafish whole mount high-resolution double fluorescent in situ hybridization”. In: *JoVE (Journal of Visualized Experiments)* 25, e1229.
- Campos-Ortega, Jose A (1988). “Cellular interactions during early neurogenesis of *Drosophila melanogaster*”. In: *Trends in neurosciences* 11.9, pp. 400–405.
- Chalfie, Martin, Yuan Tu, Ghia Euskirchen, William W Ward, and Douglas C Prasher (1994). “Green fluorescent protein as a marker for gene expression”. In: *Science* 263.5148, pp. 802–805.
- Chapman, Deborah L and Virginia E Papaioannou (1998). “Three neural tubes in mouse embryos with mutations in the T-box gene *Tbx6*”. In: *Nature* 391.6668, pp. 695–697.
- Choorapoikayil, Suma, Bernd Willems, Peter Ströhle, and Martin Gajewski (2012). “Analysis of *her1* and *her7* mutants reveals a spatio temporal separation of the somite clock module”. In: *PloS one* 7.6, e39073.
- Chudakov, Dmitriy M, Mikhail V Matz, Sergey Lukyanov, and Konstantin A Lukyanov (2010). “Fluorescent proteins and their applications in imaging living cells and tissues”. In: *Physiological reviews* 90.3, pp. 1103–1163.
- Coffman, Clark, William Harris, and Chris Kintner (1990). “Xotch, the *Xenopus* homolog of *Drosophila notch*”. In: *Science* 249.4975, pp. 1438–1441.
- Conlon, Ronald A, Andrew G Reaume, and Janet Rossant (1995). “Notch1 is required for the coordinate segmentation of somites”. In: *Development* 121.5, pp. 1533–1545.
- Cooke, Jonathan (1975). “Control of somite number during morphogenesis of a vertebrate, *Xenopus laevis*”. In: *Nature* 254.5497, pp. 196–199.

- Cooke and Erik Christopher Zeeman (1976). “A clock and wavefront model for control of the number of repeated structures during animal morphogenesis”. In: *Journal of theoretical biology* 58.2, pp. 455–476.
- Corral, Ruth Diez del, Isabel Olivera-Martinez, Anne Goriely, Emily Gale, Malcolm Maden, and Kate Storey (2003). “Opposing FGF and retinoid pathways control ventral neural pattern, neuronal differentiation, and segmentation during body axis extension”. In: *Neuron* 40.1, pp. 65–79.
- Cotterell, James, Alexandre Robert-Moreno, and James Sharpe (2015). “A local, self-organizing reaction-diffusion model can explain somite patterning in embryos”. In: *Cell systems* 1.4, pp. 257–269.
- Dale, Kim J and Olivier Pourquié (2000). “A clock-work somite”. In: *Bioessays* 22.1, pp. 72–83.
- Delaune, Emilie A, Paul François, Nathan P Shih, and Sharon L Amacher (2012). “Single-cell-resolution imaging of the impact of Notch signaling and mitosis on segmentation clock dynamics”. In: *Developmental cell* 23.5, pp. 995–1005.
- Delfini, Marie-Claire, Julien Dubrulle, Pascale Malapert, Jérôme Chal, and Olivier Pourquié (2005). “Control of the segmentation process by graded MAPK/ERK activation in the chick embryo”. In: *Proceedings of the National Academy of Sciences* 102.32, pp. 11343–11348.
- Denk, Winfried, David W Piston, and Watt W Webb (1995). “Two-photon molecular excitation in laser-scanning microscopy”. In: *Handbook of biological confocal microscopy*. Springer, pp. 445–458.
- Dequéant, Mary-Lee, Earl Glynn, Karin Gaudenz, Matthias Wahl, Jie Chen, Arcady Mushegian, and Olivier Pourquié (2006). “A complex oscillating network of signaling genes underlies the mouse segmentation clock”. In: *science* 314.5805, pp. 1595–1598.
- Dubrulle, Julien, Michael J McGrew, and Olivier Pourquié (2001). “FGF signaling controls somite boundary position and regulates segmentation clock control of spatiotemporal Hox gene activation”. In: *Cell* 106.2, pp. 219–232.
- Dubrulle, Julien and Olivier Pourquié (2004). “fgf8 mRNA decay establishes a gradient that couples axial elongation to patterning in the vertebrate embryo”. In: *Nature* 427.6973, pp. 419–422.
- Durbin, Lindsey, Paolo Sordino, Arantza Barrios, Martin Gering, Christine Thisse, Bernard Thisse, Caroline Brennan, Anthony Green, Stephen Wilson, and Nigel Holder (2000). “Anteroposterior patterning is required within segments for somite boundary formation in developing zebrafish”. In: *Development* 127.8, pp. 1703–1713.
- Elsdale, Tom, Murray Pearson, and Margaret Whitehead (1976). “Abnormalities in somite segmentation following heat shock to *Xenopus* embryos”. In:
- Fior, Rita, Adrienne A Maxwell, Taylur P Ma, Annalisa Vezzaro, Cecilia B Moens, Sharon L Amacher, Julian Lewis, and Leonor Saúde (2012). “The differentiation and move-

- ment of presomitic mesoderm progenitor cells are controlled by Mesogenin 1". In: *Development* 139.24, pp. 4656–4665.
- Forero, Laura Lleras, Rachna Narayanan, Leonie FA Huitema, Maaïke VanBergen, Alexander Apschner, Josi Peterson-Maduro, Ive Logister, Guillaume Valentin, Luis G Morelli, Andrew C Oates, et al. (2018). "Segmentation of the zebrafish axial skeleton relies on notochord sheath cells and not on the segmentation clock". In: *Elife* 7, e33843.
- Garnett, Aaron T, Tina M Han, Michael J Gilchrist, James C Smith, Michael B Eisen, Fiona C Wardle, and Sharon L Amacher (2009). "Identification of direct T-box target genes in the developing zebrafish mesoderm". In:
- Gierer, Alfred and Hans Meinhardt (1972). "A theory of biological pattern formation". In: *Kybernetik* 12.1, pp. 30–39.
- Goering, Lisa M, Kazuyuki Hoshijima, Barbara Hug, Brent Bisgrove, Andreas Kispert, and David Jonah Grunwald (2003). "An interacting network of T-box genes directs gene expression and fate in the zebrafish mesoderm". In: *Proceedings of the National Academy of Sciences* 100.16, pp. 9410–9415.
- Goldman, D, M Hankin, Z Li, X Dai, and J Ding (2001). "Transgenic zebrafish for studying nervous system development and regeneration". In: *Transgenic research* 10.1, pp. 21–33.
- Gomez, Céline, Ertuğrul M Özbudak, Joshua Wunderlich, Diana Baumann, Julian Lewis, and Olivier Pourquié (2008). "Control of segment number in vertebrate embryos". In: *Nature* 454.7202, pp. 335–339.
- Göppert, M (1931). "Über die wahrscheinlichkeit des Zusammenwirkens zweier Lichtquanten in einem elementarakt. *Naturwissenschaften*, 1929, 17, 932-932;(b) Göppert-Mayer, M. Über elementarakte mit zwei quatenstrüßen". In: *Ann. Phys* 401, pp. 273–294.
- Gotoh, Yukiko and Eisuke Nishida (1996). "Signals for mesoderm induction. Roles of fibroblast growth factor (FGF)/mitogen-activated protein kinase (MAPK) pathway". In: *Biochimica et Biophysica Acta (BBA)-Reviews on Cancer* 1288.1, F1–F7.
- Greco, Tamara L, Shinji Takada, Matthew M Newhouse, Jill A McMahon, Andrew P McMahon, and Sally A Camper (1996). "Analysis of the vestigial tail mutation demonstrates that Wnt-3a gene dosage regulates mouse axial development." In: *Genes & development* 10.3, pp. 313–324.
- Gregor, Thomas, David W Tank, Eric F Wieschaus, and William Bialek (2007). "Probing the limits to positional information". In: *Cell* 130.1, pp. 153–164.
- Griffin, KJ, Sharon L Amacher, Charles B Kimmel, and David Kimelman (1998). "Molecular identification of spadetail: regulation of zebrafish trunk and tail mesoderm formation by T-box genes". In: *Development* 125.17, pp. 3379–3388.
- Guo, Long, Shiro Ikegawa, and Chisa Shukunami (2018). "Emergence of Zebrafish as a Model System for Understanding Human Scoliosis". In: *Zebrafish, Medaka, and Other Small Fishes*. Springer, pp. 217–234.

- Harima, Yukiko, Yoshiki Takashima, Yuriko Ueda, Toshiyuki Ohtsuka, and Ryoichiro Kageyama (2013). “Accelerating the tempo of the segmentation clock by reducing the number of introns in the *Hes7* gene”. In: *Cell reports* 3.1, pp. 1–7.
- He, Zhisong, Ashley Maynard, Akanksha Jain, Tobias Gerber, Rebecca Petri, Hsiu-Chuan Lin, Malgorzata Santel, Kevin Ly, Jean-Samuel Dupré, Leila Sidow, et al. (2022). “Lineage recording in human cerebral organoids”. In: *Nature methods* 19.1, pp. 90–99.
- Henry, Clarissa A, Michael K Urban, Kariena K Dill, John P Merlie, Michelle F Page, Charles B Kimmel, and Sharon L Amacher (2002). “Two linked hairy/Enhancer of split-related zebrafish genes, *her1* and *her7*, function together to refine alternating somite boundaries”. In:
- Herrgen, Leah, Saúl Ares, Luis G Morelli, Christian Schröter, Frank Jülicher, and Andrew C Oates (2010). “Intercellular coupling regulates the period of the segmentation clock”. In: *Current Biology* 20.14, pp. 1244–1253.
- Herrmann, Bernhard G, Siegfried Labeit, Annemarie Poustka, Thomas R King, and Hans Lehrach (1990). “Cloning of the *T* gene required in mesoderm formation in the mouse”. In: *Nature* 343.6259, pp. 617–622.
- Hirata, Hiromi, Shigeki Yoshiura, Toshiyuki Ohtsuka, Yasumasa Bessho, Takahiro Harada, Kenichi Yoshikawa, and Ryoichiro Kageyama (2002). “Oscillatory expression of the bHLH factor *Hes1* regulated by a negative feedback loop”. In: *Science* 298.5594, pp. 840–843.
- Holley, Scott A (2006). “Anterior–posterior differences in vertebrate segments: specification of trunk and tail somites in the zebrafish blastula”. In: *Genes & development* 20.14, pp. 1831–1837.
- Holley, Scott A, Robert Geisler, and Christiane Nüsslein-Volhard (2000). “Control of *her1* expression during zebrafish somitogenesis by a delta-dependent oscillator and an independent wave-front activity”. In: *Genes & development* 14.13, pp. 1678–1690.
- Houchmandzadeh, Bahram, Eric Wieschaus, and Stanislas Leibler (2002). “Establishment of developmental precision and proportions in the early *Drosophila* embryo”. In: *Nature* 415.6873, pp. 798–802.
- Hubaud, Alexis and Olivier Pourquié (2014). “Signalling dynamics in vertebrate segmentation”. In: *Nature reviews Molecular cell biology* 15.11, pp. 709–721.
- Hubaud, Alexis, Ido Regev, Lakshminarayanan Mahadevan, and Olivier Pourquie (2017). “Excitable dynamics and Yap-dependent mechanical cues drive the segmentation clock”. In: *Cell* 171.3, pp. 668–682.
- Huisken, Jan, Jim Swoger, Filippo Del Bene, Joachim Wittbrodt, and Ernst HK Stelzer (2004). “Optical sectioning deep inside live embryos by selective plane illumination microscopy”. In: *Science* 305.5686, pp. 1007–1009.
- Ishimatsu, Kana, Tom W Hiscock, Zach M Collins, Dini Wahyu Kartika Sari, Kenny Lischer, David L Richmond, Yasumasa Bessho, Takaaki Matsui, and Sean G Megason

- (2018). “Size-reduced embryos reveal a gradient scaling-based mechanism for zebrafish somite formation”. In: *Development* 145.11, dev161257.
- Jiang, Yun-Jin, Birgit L Aerne, Lucy Smithers, Catherine Haddon, David Ish-Horowicz, and Julian Lewis (2000). “Notch signalling and the synchronization of the somite segmentation clock”. In: *Nature* 408.6811, pp. 475–479.
- Kawamura, Akinori, Sumito Koshida, Hiroko Hijikata, Akiko Ohbayashi, Hisato Kondoh, and Shinji Takada (2005). “Groucho-associated transcriptional repressor ripply1 is required for proper transition from the presomitic mesoderm to somites”. In: *Developmental cell* 9.6, pp. 735–744.
- Keller, Philipp J, Annette D Schmidt, Joachim Wittbrodt, and Ernst HK Stelzer (2008). “Reconstruction of zebrafish early embryonic development by scanned light sheet microscopy”. In: *science* 322.5904, pp. 1065–1069.
- Keynes, Roger J and Claudio D Stern (1984). “Segmentation in the vertebrate nervous system”. In: *Nature* 310.5980, pp. 786–789.
- Kim, Woong, Takaaki Matsui, Masataka Yamao, Makoto Ishibashi, Kota Tamada, Toru Takumi, Kenji Kohno, Shigeyuki Oba, Shin Ishii, Yuichi Sakumura, et al. (2011). “The period of the somite segmentation clock is sensitive to Notch activity”. In: *Molecular biology of the cell* 22.18, pp. 3541–3549.
- Kimelman, DAVID and ADOLF Maas (1992). “Induction of dorsal and ventral mesoderm by ectopically expressed Xenopus basic fibroblast growth factor”. In: *Development* 114.1, pp. 261–269.
- Kimmel, Charles B (1989). “Genetics and early development of zebrafish”. In: *Trends in Genetics* 5, pp. 283–288.
- Kimmel, Charles B, William W Ballard, Seth R Kimmel, Bonnie Ullmann, and Thomas F Schilling (1995). “Stages of embryonic development of the zebrafish”. In: *Developmental dynamics* 203.3, pp. 253–310.
- Kinoshita, Hirofumi, Nanae Ohgane, Yuuri Fujino, Taijiro Yabe, Hiroki Ovara, Daisuke Yokota, Ayaka Izuka, Daichi Kage, Kyo Yamasu, Shinji Takada, et al. (2018). “Functional roles of the Ripply-mediated suppression of segmentation gene expression at the anterior presomitic mesoderm in zebrafish”. In: *Mechanisms of Development* 152, pp. 21–31.
- Krzic, Uros, Stefan Gunther, Timothy E Saunders, Sebastian J Streichan, and Lars Hufnagel (2012). “Multiview light-sheet microscope for rapid in toto imaging”. In: *Nature methods* 9.7, pp. 730–733.
- Kulesa, Paul M and Scott E Fraser (2002). “Cell dynamics during somite boundary formation revealed by time-lapse analysis”. In: *Science* 298.5595, pp. 991–995.
- Lauschke, Volker M, Charisios D Tsiarris, Paul François, and Alexander Aulehla (2013). “Scaling of embryonic patterning based on phase-gradient encoding”. In: *Nature* 493.7430, pp. 101–105.

- Lawrence, Peter Anthony (1992). *The making of a flythe genetics of animal design*. 595.774 L38.
- Lawson, Nathan D and Brant M Weinstein (2002). “In vivo imaging of embryonic vascular development using transgenic zebrafish”. In: *Developmental biology* 248.2, pp. 307–318.
- Lewis, Julian (2003). “Autoinhibition with transcriptional delay: a simple mechanism for the zebrafish somitogenesis oscillator”. In: *Current Biology* 13.16, pp. 1398–1408.
- Liang, Guang, Zhiguo Liu, Jianzhang Wu, Yuepiao Cai, and Xiaokun Li (2012). “Anticancer molecules targeting fibroblast growth factor receptors”. In: *Trends in pharmacological sciences* 33.10, pp. 531–541.
- Liao, Bo-Kai, David J Jörg, and Andrew C Oates (2016). “Faster embryonic segmentation through elevated Delta-Notch signalling”. In: *Nature Communications* 7.1, pp. 1–12.
- Maden, Malcolm, Edwin Sonneveld, Paul T van der Saag, and Emily Gale (1998). “The distribution of endogenous retinoic acid in the chick embryo: implications for developmental mechanisms”. In: *Development* 125.21, pp. 4133–4144.
- Martinez-Arias, Alfonso and Peter A Lawrence (1985). “Parasegments and compartments in the *Drosophila* embryo”. In: *Nature* 313.6004, pp. 639–642.
- Masamizu, Yoshito, Toshiyuki Ohtsuka, Yoshiki Takashima, Hiroki Nagahara, Yoshiko Takenaka, Kenichi Yoshikawa, Hitoshi Okamura, and Ryoichiro Kageyama (2006). “Real-time imaging of the somite segmentation clock: revelation of unstable oscillators in the individual presomitic mesoderm cells”. In: *Proceedings of the National Academy of Sciences* 103.5, pp. 1313–1318.
- Matz, Mikhail V, Arkady F Fradkov, Yulii A Labas, Aleksandr P Savitsky, Andrey G Zarskiy, Mikhail L Markelov, and Sergey A Lukyanov (1999). “Fluorescent proteins from non-bioluminescent Anthozoa species”. In: *Nature biotechnology* 17.10, pp. 969–973.
- McGrew, Michael J, J Kim Dale, Sandrine Fraboulet, and Olivier Pourquié (1998). “The lunatic fringe gene is a target of the molecular clock linked to somite segmentation in avian embryos”. In: *Current Biology* 8.17, pp. 979–982.
- Medeiros, Gustavo de, Raphael Ortiz, Petr Strnad, Andrea Boni, Francisca Maurer, and Prisca Liberali (2021). “Multiscale light-sheet organoid imaging framework”. In: *bioRxiv*.
- Mohammadi, Moosa, Gerald McMahon, Li Sun, Cho Tang, Peter Hirth, Brian K Yeh, Stevan R Hubbard, and Joseph Schlessinger (1997). “Structures of the tyrosine kinase domain of fibroblast growth factor receptor in complex with inhibitors”. In: *Science* 276.5314, pp. 955–960.
- Mollring, Friedrich Karl (1965). “Methods of optical adaptation of the movie camera to the microscope”. In: *BioScience* 15.12, pp. 773–776.
- Moreno, Tanya A, Roberto Jappelli, Juan Carlos Izpisua Belmonte, and Chris Kintner (2008). “Retinoic acid regulation of the Mesp–Ripply feedback loop during vertebrate segmental patterning”. In: *Developmental biology* 315.2, pp. 317–330.

- Moreno, Tanya A and Chris Kintner (2004). “Regulation of segmental patterning by retinoic acid signaling during *Xenopus* somitogenesis”. In: *Developmental cell* 6.2, pp. 205–218.
- Morrow, Zachary T, Adrienne M Maxwell, Kazuyuki Hoshijima, Jared C Talbot, David J Grunwald, and Sharon L Amacher (2017). “*tbx6l* and *tbx16* are redundantly required for posterior paraxial mesoderm formation during zebrafish embryogenesis”. In: *Developmental Dynamics* 246.10, pp. 759–769.
- Morton de Lachapelle, Aitana and Sven Bergmann (2010). “Precision and scaling in morphogen gradient read-out”. In: *Molecular systems biology* 6.1, p. 351.
- Mueller, Rachel Lockridge, Cheng Huang, and Robert K Ho (2010). “Spatio-temporal regulation of Wnt and retinoic acid signaling by *tbx16*/*spadetail* during zebrafish mesoderm differentiation”. In: *BMC genomics* 11.1, pp. 1–16.
- Muller, Mv v, E v Weizsacker, and JA Campos-Ortega (1996). “Expression domains of a zebrafish homologue of the *Drosophila* pair-rule gene *hairy* correspond to primordia of alternating somites”. In: *Development* 122.7, pp. 2071–2078.
- Naoki, Honda, Ryutaro Akiyama, Dini Wahyu Kartika Sari, Shin Ishii, Yasumasa Bessho, and Takaaki Matsui (2019). “Noise-resistant developmental reproducibility in vertebrate somite formation”. In: *PLoS computational biology* 15.2, e1006579.
- Nikaido, Masataka, Atsushi Kawakami, Atsushi Sawada, Makoto Furutani-Seiki, Hiroyuki Takeda, and Kazuo Araki (2002). “*Tbx24*, encoding a T-box protein, is mutated in the zebrafish somite-segmentation mutant *fused somites*”. In: *Nature genetics* 31.2, pp. 195–199.
- Niwa, Yasutaka, Hiromi Shimojo, Akihiro Isomura, Aitor González, Hitoshi Miyachi, and Ryoichiro Kageyama (2011). “Different types of oscillations in Notch and Fgf signaling regulate the spatiotemporal periodicity of somitogenesis”. In: *Genes & development* 25.11, pp. 1115–1120.
- Nowotschin, Sonja and Anna-Katerina Hadjantonakis (2014). “Live imaging mouse embryonic development: seeing is believing and revealing”. In: *Mouse Molecular Embryology*, pp. 405–420.
- Nüsslein-Volhard, Christiane and Eric Wieschaus (1980). “Mutations affecting segment number and polarity in *Drosophila*”. In: *Nature* 287.5785, pp. 795–801.
- Oates, Andrew C and Robert K Ho (2002). “*Hairy/E (spl)*-related (*Her*) genes are central components of the segmentation oscillator and display redundancy with the *Delta/Notch* signaling pathway in the formation of anterior segmental boundaries in the zebrafish”. In:
- Oates, Andrew C, Luis G Morelli, and Saúl Ares (2012). “Patterning embryos with oscillations: structure, function and dynamics of the vertebrate segmentation clock”. In: *Development* 139.4, pp. 625–639.

- Oates, Andrew C, Laurel A Rohde, and Robert K Ho (2005). “Generation of segment polarity in the paraxial mesoderm of the zebrafish through a T-box-dependent inductive event”. In: *Developmental biology* 283.1, pp. 204–214.
- Oginuma, Masayuki, Yasutaka Niwa, Deborah L Chapman, and Yumiko Saga (2008). “Mesp2 and Tbx6 cooperatively create periodic patterns coupled with the clock machinery during mouse somitogenesis”. In:
- Okubo, Yusuke, Takeshi Sugawara, Natsumi Abe-Koduka, Jun Kanno, Akatsuki Kimura, and Yumiko Saga (2012). “Lfng regulates the synchronized oscillation of the mouse segmentation clock via trans-repression of Notch signalling”. In: *Nature communications* 3.1, pp. 1–9.
- Ordahl, CP and NM Le Douarin (1992). “Two myogenic lineages within the developing somite”. In: *Development* 114.2, pp. 339–353.
- Özbudak, Ertuğrul M and Julian Lewis (2008). “Notch signalling synchronizes the zebrafish segmentation clock but is not needed to create somite boundaries”. In: *PLoS genetics* 4.2, e15.
- Palmeirim, Isabel, Domingos Henrique, David Ish-Horowicz, and Olivier Pourquié (1997). “Avian hairy gene expression identifies a molecular clock linked to vertebrate segmentation and somitogenesis”. In: *Cell* 91.5, pp. 639–648.
- Pitrone, Peter G, Johannes Schindelin, Luke Stuyvenberg, Stephan Preibisch, Michael Weber, Kevin W Eliceiri, Jan Huisken, and Pavel Tomancak (2013). “OpenSPIM: an open-access light-sheet microscopy platform”. In: *nature methods* 10.7, pp. 598–599.
- Pourquié, Olivier (2003). “The segmentation clock: converting embryonic time into spatial pattern”. In: *Science* 301.5631, pp. 328–330.
- (2022). “A brief history of the segmentation clock”. In: *Developmental biology*, S0012–1606.
- Pourquié, Olivier and Patrick PL Tam (2001). “A nomenclature for prospective somites and phases of cyclic gene expression in the presomitic mesoderm”. In: *Developmental cell* 1.5, pp. 619–620.
- Preibisch, Stephan, Fernando Amat, Evangelia Stamataki, Mihail Sarov, Robert H Singer, Eugene Myers, and Pavel Tomancak (2014). “Efficient Bayesian-based multiview deconvolution”. In: *Nature methods* 11.6, pp. 645–648.
- Preibisch, Stephan, Stephan Saalfeld, Johannes Schindelin, and Pavel Tomancak (2010). “Software for bead-based registration of selective plane illumination microscopy data”. In: *Nature methods* 7.6, pp. 418–419.
- Primmatt, DR, CD Stern, and RJ Keynes (1988). “Heat shock causes repeated segmental anomalies in the chick embryo”. In: *Development* 104.2, pp. 331–339.
- Reaume, Andrew G, Ronald A Conlon, Ralph Zirngibl, Terry P Yamaguchi, and Janet Rossant (1992). “Expression analysis of a Notch homologue in the mouse embryo”. In: *Developmental biology* 154.2, pp. 377–387.

- Riedel-Kruse, Ingmar H, Claudia Muller, and Andrew C Oates (2007). “Synchrony dynamics during initiation, failure, and rescue of the segmentation clock”. In: *Science* 317.5846, pp. 1911–1915.
- Rohde, Laurel A, Arianne Bercowsky-Rama, Jose Negrete, Guillaume Valentin, Sundar Ram Naganathan, Ravi A Desai, Petr Strnad, Daniele Soroldoni, Frank Jülicher, and Andrew C Oates (2021). “Cell-autonomous generation of the wave pattern within the vertebrate segmentation clock”. In: *bioRxiv*.
- Sari, Dini Wahyu Kartika, Ryutaro Akiyama, Honda Naoki, Hannosuke Ishijima, Yasumasa Bessho, and Takaaki Matsui (2018). “Time-lapse observation of stepwise regression of Erk activity in zebrafish presomitic mesoderm”. In: *Scientific reports* 8.1, pp. 1–10.
- Sawada, Atsushi, Andreas Fritz, Y Jiang, Akihito Yamamoto, Kyo Yamasu, Atsushi Kuroiwa, Yumiko Saga, and Hiroyuki Takeda (2000). “Zebrafish Mesp family genes, mesp-a and mesp-b are segmentally expressed in the presomitic mesoderm, and Mesp-b confers the anterior identity to the developing somites”. In: *Development* 127.8, pp. 1691–1702.
- Sawada, Atsushi, Minori Shinya, Yun-Jin Jiang, Atsushi Kawakami, Atsushi Kuroiwa, and Hiroyuki Takeda (2001). “Fgf/MAPK signalling is a crucial positional cue in somite boundary formation”. In:
- Schindelin, Johannes, Ignacio Arganda-Carreras, Erwin Frise, Verena Kaynig, Mark Longair, Tobias Pietzsch, Stephan Preibisch, Curtis Rueden, Stephan Saalfeld, Benjamin Schmid, et al. (2012). “Fiji: an open-source platform for biological-image analysis”. In: *Nature methods* 9.7, pp. 676–682.
- Schröter, Christian, Saúl Ares, Luis G Morelli, Alina Isakova, Korneel Hens, Daniele Soroldoni, Martin Gajewski, Frank Jülicher, Sebastian J Maerkl, Bart Deplancke, et al. (2012). “Topology and dynamics of the zebrafish segmentation clock core circuit”. In: *PLoS biology* 10.7, e1001364.
- Schröter, Christian, Leah Herrgen, Albert Cardona, Gary J Brouhard, Benjamin Feldman, and Andrew C Oates (2008). “Dynamics of zebrafish somitogenesis”. In: *Developmental dynamics: an official publication of the American Association of Anatomists* 237.3, pp. 545–553.
- Schröter, Christian and Andrew C Oates (2010). “Segment number and axial identity in a segmentation clock period mutant”. In: *Current Biology* 20.14, pp. 1254–1258.
- Schulte-Merker, S, FJ Van Eeden, M El Halpern, CB Kimmel, and C Nusslein-Volhard (1994). “no tail (ntl) is the zebrafish homologue of the mouse T (Brachyury) gene”. In: *Development* 120.4, pp. 1009–1015.
- Shaner, Nathan C, Robert E Campbell, Paul A Steinbach, Ben NG Giepmans, Amy E Palmer, and Roger Y Tsien (2004). “Improved monomeric red, orange and yellow fluorescent proteins derived from *Discosoma* sp. red fluorescent protein”. In: *Nature biotechnology* 22.12, pp. 1567–1572.

- Shih, Nathan P, Paul François, Emilie A Delaune, and Sharon L Amacher (2015). “Dynamics of the slowing segmentation clock reveal alternating two-segment periodicity”. In: *Development* 142.10, pp. 1785–1793.
- Shimomura, Osamu, Frank H Johnson, and Yo Saiga (1962). “Extraction, purification and properties of aequorin, a bioluminescent protein from the luminous hydromedusan, *Aequorea*”. In: *Journal of cellular and comparative physiology* 59.3, pp. 223–239.
- Simsek, M Fethullah and Ertuğrul M Özbudak (2018). “Spatial fold change of FGF signaling encodes positional information for segmental determination in zebrafish”. In: *Cell reports* 24.1, pp. 66–78.
- Smithers, Lucy, Catherine Haddon, Yun-Jin Jiang, and Julian Lewis (2000). “Sequence and embryonic expression of deltaC in the zebrafish”. In: *Mechanisms of development* 90.1, pp. 119–123.
- Solnica-Krezel, Lilianna, Derek L Stemple, Eliza Mountcastle-Shah, Zehava Rangini, SC Neuhauss, Jarema Malicki, Alexander F Schier, DY Stainier, Fried Zwartkruis, Salim Abdelilah, et al. (1996). “Mutations affecting cell fates and cellular rearrangements during gastrulation in zebrafish”. In: *Development* 123.1, pp. 67–80.
- Soroldoni, Daniele, David J Jörg, Luis G Morelli, David L Richmond, Johannes Schindelin, Frank Jülicher, and Andrew C Oates (2014). “A Doppler effect in embryonic pattern formation”. In: *Science* 345.6193, pp. 222–225.
- Soroldoni, Daniele and Andrew C Oates (2011). “Live transgenic reporters of the vertebrate embryo’s Segmentation Clock”. In: *Current opinion in genetics & development* 21.5, pp. 600–605.
- Sparrow, DB, G Chapman, MA Wouters, NV Whittock, S Ellard, D Fatkin, PD Turnpenny, K Kusumi, D Sillence, and SL Dunwoodie (2006). “Mutation of the LUNATIC FRINGE gene in humans causes spondylocostal dysostosis with a severe vertebral phenotype”. In: *The American Journal of Human Genetics* 78.1, pp. 28–37.
- Stulberg, Michael J, Aiping Lin, Hongyu Zhao, and Scott A Holley (2012). “Crosstalk between Fgf and Wnt signaling in the zebrafish tailbud”. In: *Developmental biology* 369.2, pp. 298–307.
- Swindell, Eric C, Christina Thaller, Shanthini Sockanathan, Martin Petkovich, Thomas M Jessell, and Gregor Eichele (1999). “Complementary domains of retinoic acid production and degradation in the early chick embryo”. In: *Developmental biology* 216.1, pp. 282–296.
- Takahashi, Jun, Akiko Ohbayashi, Masayuki Oginuma, Daisuke Saito, Atsushi Mochizuki, Yumiko Saga, and Shinji Takada (2010). “Analysis of Ripply1/2-deficient mouse embryos reveals a mechanism underlying the rostro-caudal patterning within a somite”. In: *Developmental biology* 342.2, pp. 134–145.
- Tinevez, Jean-Yves, Nick Perry, Johannes Schindelin, Genevieve M Hoopes, Gregory D Reynolds, Emmanuel Laplantine, Sebastian Y Bednarek, Spencer L Shorte, and Kevin

- W Eliceiri (2017). “TrackMate: An open and extensible platform for single-particle tracking”. In: *Methods* 115, pp. 80–90.
- Trofka, Anna, Jamie Schwendinger-Schreck, Tim Brend, William Pontius, Thierry Emonet, and Scott A Holley (2012). “The Her7 node modulates the network topology of the zebrafish segmentation clock via sequestration of the Hes6 hub”. In: *Development* 139.5, pp. 940–947.
- Turing, Alan Mathison (1952). “The chemical basis of morphogenesis”. In: *Bulletin of mathematical biology* 52.1, pp. 153–197.
- Turnpenny, Peter D, Ben Alman, Alberto S Cornier, Philip F Giampietro, Amaka Offiah, Olivier Tassy, Olivier Pourquié, Kenro Kusumi, and Sally Dunwoodie (2007). “Abnormal vertebral segmentation and the notch signaling pathway in man”. In: *Developmental dynamics: an official publication of the American Association of Anatomists* 236.6, pp. 1456–1474.
- Van Eeden, FJ, Michael Granato, Ursula Schach, Michael Brand, Makoto Furutani-Seiki, Pascal Haffter, Matthias Hammerschmidt, Carl-Philipp Heisenberg, Yun-Jin Jiang, Donald A Kane, et al. (1996a). “Genetic analysis of fin formation in the zebrafish, *Danio rerio*”. In: *Development* 123.1, pp. 255–262.
- (1996b). “Mutations affecting somite formation and patterning in the zebrafish, *Danio rerio*”. In: *Development* 123.1, pp. 153–164.
- Vasiliauskas, Daniel and Claudio D Stern (2001). “Patterning the embryonic axis: FGF signaling and how vertebrate embryos measure time”. In: *Cell* 106.2, pp. 133–136.
- Venzin, Olivier F and Andrew C Oates (2020). “What are you synching about? Emerging complexity of Notch signaling in the segmentation clock”. In: *Developmental biology* 460.1, pp. 40–54.
- Vermot, Julien and Olivier Pourquié (2005). “Retinoic acid coordinates somitogenesis and left–right patterning in vertebrate embryos”. In: *Nature* 435.7039, pp. 215–220.
- Verveer, Peter J, Jim Swoger, Francesco Pampaloni, Klaus Greger, Marco Marcello, and Ernst HK Stelzer (2007). “High-resolution three-dimensional imaging of large specimens with light sheet–based microscopy”. In: *Nature methods* 4.4, pp. 311–313.
- Voie, Arne H, DH Burns, and FA Spelman (1993). “Orthogonal-plane fluorescence optical sectioning: Three-dimensional imaging of macroscopic biological specimens”. In: *Journal of microscopy* 170.3, pp. 229–236.
- Wang, Shengxian and Tulle Hazelrigg (1994). “Implications for bcd mRNA localization from spatial distribution of exu protein in *Drosophila* oogenesis”. In: *Nature* 369.6479, pp. 400–403.
- Wanglar, Chimwar, Jun Takahashi, Taijiro Yabe, and Shinji Takada (2014). “Tbx protein level critical for clock-mediated somite positioning is regulated through interaction between Tbx and Ripply”. In: *PLoS One* 9.9, e107928.

- Warga, Rachel M, Rachel L Mueller, Robert K Ho, and Donald A Kane (2013). “Zebrafish Tbx16 regulates intermediate mesoderm cell fate by attenuating Fgf activity”. In: *Developmental biology* 383.1, pp. 75–89.
- Webb, Alexis B, Iván M Lengyel, David J Jörg, Guillaume Valentin, Frank Jülicher, Luis G Morelli, and Andrew C Oates (2016). “Persistence, period and precision of autonomous cellular oscillators from the zebrafish segmentation clock”. In: *Elife* 5, e08438.
- Wilke, V (1985). “Optical scanning microscopy—the laser scan microscope”. In: *Scanning* 7.2, pp. 88–96.
- Windner, Stefanie E, Rosemarie A Doris, Chantal M Ferguson, Andrew C Nelson, Guillaume Valentin, Haihan Tan, Andrew C Oates, Fiona C Wardle, and Stephen H Devoto (2015). “Tbx6, Mesp-b and Ripply1 regulate the onset of skeletal myogenesis in zebrafish”. In: *Development* 142.6, pp. 1159–1168.
- Wolff, Carsten, Jean-Yves Tinevez, Tobias Pietzsch, Evangelia Stamatakis, Benjamin Harich, Léo Guignard, Stephan Preibisch, Spencer Shorte, Philipp J Keller, Pavel Tomancak, et al. (2018). “Multi-view light-sheet imaging and tracking with the MaMuT software reveals the cell lineage of a direct developing arthropod limb”. In: *Elife* 7, e34410.
- Wollman, Adam JM, Richard Nudd, Erik G Hedlund, and Mark C Leake (2015). “From Animaculum to single molecules: 300 years of the light microscope”. In: *Open biology* 5.4, p. 150019.
- Wong, Kah-Loon, Ryutaro Akiyama, Yasumasa Bessho, and Takaaki Matsui (2018). “ERK activity dynamics during zebrafish embryonic development”. In: *International Journal of Molecular Sciences* 20.1, p. 109.
- Wood, Andrew and Peter Thorogood (1994). “Patterns of cell behaviour underlying somitogenesis and notochord formation in intact vertebrate embryos”. In: *Developmental dynamics* 201.2, pp. 151–167.
- Yamaguchi, Terry P, Ronald A Conlon, and Janet Rossant (1992). “Expression of the fibroblast growth factor receptor FGFR-1/flg during gastrulation and segmentation in the mouse embryo”. In: *Developmental biology* 152.1, pp. 75–88.
- Yamamoto, Akihito, Sharon L Amacher, Sung-Hyun Kim, Douglas Geissert, Charles B Kimmel, and EM De Robertis (1998). “Zebrafish paraxial protocadherin is a downstream target of spadetail involved in morphogenesis of gastrula mesoderm”. In: *Development* 125.17, pp. 3389–3397.
- Yoshioka-Kobayashi, Kumiko, Marina Matsumiya, Yusuke Niino, Akihiro Isomura, Hiroshi Kori, Atsushi Miyawaki, and Ryoichiro Kageyama (2020). “Coupling delay controls synchronized oscillation in the segmentation clock”. In: *Nature* 580.7801, pp. 119–123.

Zhao, Wei, Rieko Ajima, Youichirou Ninomiya, and Yumiko Saga (2015). “Segmental border is defined by Ripply2-mediated Tbx6 repression independent of Mesp2”. In: *Developmental biology* 400.1, pp. 105–117.

Arianne Bercowsky Rama

Oates Lab, EPFL, SV
arianne.bercowskyrama@epfl.ch

Date of birth: May 18, 1995
Spanish-Venezuelan citizen
B Permit in Switzerland

EDUCATION

PhD student at the Oates Lab, École Polytechnique Fédérale de Lausanne, Switzerland (2018 – 2022)

Master in Multidisciplinary Research in Experimental Sciences, Pompeu Fabra University and Barcelona Institute of Technology, Spain (2017 – 2018)

BA in Biomedical Engineering at Pompeu Fabra University, Spain (2013 – 2017)

RESEARCH EXPERIENCE

PhD Thesis – *Precision in biological timers in somitogenesis*

- Zebrafish embryology, experimentation and imaging
- Light Sheet Microscopy
- Image and data analysis using Python and Fiji
- Construction of big-data pipelines from scope to analysis
- Development of python package for data analysis - <https://github.com/bercowsky/paleontologist>

Supervised by Professor Andrew C. Oates

École Polytechnique Fédérale de Lausanne, Switzerland (2018 – 2022)

Master Thesis - *“Free-form modelling of single-cell dynamical data”* - How MAP kinases communicate at the single cell level? Using image analysis and reverse engineering to obtain the biochemical structure of the system.

Supervised by Professor Jordi García Ojalvo and Federico Sánchez Nieto (IFAE) Pompeu Fabra University, Spain (September 2017 - July 2018)

BA Thesis - *“Understanding signalling pathways in early development using mouse embryonic stem cells aggregates, Gastruloids”*

Supervised by Jordi García Ojalvo and Alfonso Martinez Arias

Cambridge University, United Kingdom (January 2017 – July 2017)

Research assistant - *Theoretical & Experimental mechano-regulation of Bone Marrow Stromal Cells (BMSC) differentiation.*

Supervised by Professor Jérôme Noailly

DTIC, Pompeu Fabra University, Spain (December 2015 – March 2016)

iGEM synthetic Biology Competition - Bronze medal

Supervised by Jordi García Ojalvo

PRBB with the support of DCEXS, CRG and Pompeu Fabra University, Spain (September 2015 – October 2016)

Research assistant - *Molecular mechanisms on lung cancer and chronic obstructive pulmonary disease (COPD)* - Looking for biomarkers in order to find correlations between COPD and lung cancer patients.

Supervised by Professor Esther Barreiro Portela.

IMIM in the PRBB, Spain (July 2015 – September 2015)

TEACHING AND ADVISING

Teaching assistant in Cell and developmental biology for engineers at EPFL

Course by Professors Pierre Gönczy and Andrew C. Oates (2018)

Teaching assistant in Image processing I at EPFL

Course by Professors Michaël Unser and Dimitri Van De Ville (2019 – 2022)

Teaching assistant in Image processing II at EPFL

Course by Professors Michaël Unser, Dimitri Van De Ville, Daniel Sage and Michael Liebling (2019 – 2022)

Image Analysis Breakfasts (EPFL) – Part of the team of experts to help solve image analysis problems shown during the monthly sessions (2020 – 2022)

NEUBIAS Training School for Facility Staff (TS13) – Programme organizer and trainer on “Python data analysis and plotting”, Porto (2019)

NEUBIAS Training School for Bioimage Analysts (TS15) – Trainer on “Python data analysis and plotting”, Bordeaux (2020)

Member of the LS2 Microscopy intersection and organizing committee – Switzerland (2021-2022)

EPFL Centre of Imaging (Summer school) – Trainer on “Machine learning”, Montreux, Switzerland (2022)

Switzerland's Image and Data Analysis School (ZIDAS) – Trainer on “Python – data handling and plotting”, Lausanne, Switzerland (2022)

MA student supervisor - *Imaging centrioles during muscle development in the embryo*, Summer internship (2021)

BA student supervisor - *Imaging centrioles during muscle development in the embryo – Project continuation*, Summer internship (2022)

BA student supervisor – *Interactive Python widget to visualize cellular dynamics in a grid*, Summer internship (2022)

MA student supervisor – *Adaxial cell tracking and analysis*, Summer internship (2021)

TRAINING

Short Term Scientific Mission (STSM) - *Harnessing cell-lineaging in the zebrafish embryo in the context of very large images*
Institut Pasteur with Jean-Yves Tinevez (2018)

NEUBIAS School for Biominage analysis (TS11) in Luxembourg - Trainee (2019)

Learnathon in Dresden – Trainee (2019)

SCHOLARSHIPS AND AWARDS

COST Action CA15124 (NEUBIAS) for the STSM in Institut Pasteur – 1050 €

Erasmus plus – 1200 €

Master program fellowship to outstanding candidates - 8.420€

Poster prize in the conference *Synthetic Morphogenesis: From gene circuits to tissue architecture* (2019)

PUBLICATIONS

Book Chapter

Python: Data handling, analysis and plotting, (2022) **Arianne Bercowsky-Rama**, in *Bioimage Analysis Components and Workflows* (2022) ed. Natasa Sladoje & Kota Miura, Springer. In press.

Scripts

Gastruloid Intensity Profiler (2020) Zenodo. Stefano Vianello, Paul Sanchez, Arianne Bercowsky-Rama, Mathias Lutolf.

First author papers

Cell-Intrinsic generation of the wave pattern within the Vertebrate Segmentation Clock (2021) bioRxiv. Laurel A. Rohde*, **Arianne Bercowsky-Rama***, Jose Negrete Jr., Guillaume Valentin, Sundar Naganathan, Ravi Desai, Petr Strnad, Daniele Soroldoni, Frank Jülicher, and Andrew C. Oates - ***Shared first authorship.**

But, what are the cells doing? Image Analysis pipeline to follow single cells in the zebrafish embryo (2022) **Arianne Bercowsky-Rama**, Olivier F. Venzin, Laurel A. Rohde, Nicolas Chiaruttini, Andrew C. Oates. In preparation for submission.

Paleontologist – Modular python package for spatiotemporal analysis of single cell tracks (2022) **Arianne Bercowsky-Rama** and Andrew C. Oates. In preparation for submission.

Peer review

Open Access per review – *Bleach correction ImageJ plugin for compensating the photobleaching of time-lapse sequences* (2021), Kota Miura, F1000 Research. <https://doi.org/10.5256/f1000research.30015.r76514>

MEETINGS

NEUBIAS Conference - Luxembourg 2019	Oral Presentation
Synthetic Morphogenesis – EMBL Heidelberg 2019	Poster
LS2 Microscopy Webinar – Switzerland 2021	Oral Presentation
Swiss Zebrafish Meeting – Switzerland 2021	Oral Presentation
Synthetic Morphogenesis – EMBL Heidelberg 2021	Poster
Biological Time Keeping – CSHL 2021	Poster
Biological oscillators – EMBL Heidelberg 2022	Oral Presentation
LS2 Microscopy Webinar – Switzerland 2022	Oral Presentation